Environmental
Studies
Research
Funds

076 Operational Test of Wave-Forecasting Models During the Canadian Atlantic Storms Program *(CASP)*

Canada

August 1987

The Environmental Studies Research Funds are financed from special levies on the oil and gas industry and administered by the Canada Oil and Gas Lands Administration for the Minister of Energy, Mines and Resources, and by the Northern Affairs Program for the Minister of Indian Affairs and Northern Development.

Environmental Studies Research Funds

Report No. 076

August, 1987

OPERATIONAL TEST OF WAVE-FORECASTING MODELS DURING THE CANADIAN ATLANTIC STORMS PROGRAM (CASP)

By: Bassem M. Eid and Vince J. Cardone

MacLaren Plansearch Limited
Suite 701, Purdy's Wharf Tower
1959 Upper Water Street
Halifax, Nova Scotia

Scientific Advisor: V. Swail

The correct citation for this report is:

Eid, B.M. and V.J. Cardone. 1987. Operational test of wave-forecasting models during the Canadian Atlantic Storms Program (CASP). Environmental Studies Research Funds, Report Series No. 076. Ottawa, 111 p. + Appendices.

Published under the auspices
of the Environmental Studies
Research Funds
ISBN 0-920783-75-9

TABLE OF CONTENTS

TABLE OF CONTENTS (Cont'd)

LIST OF TABLES

LIST OF FIGURES

ACKNOWLEDGEMENTS

We wish to express our gratitude for support from the Environmental Studies Research Funds (ESRF) for this interesting study. Special thanks to the Scientific adviser Val Swail, of the Atmospheric Environment Services, for his assistance and guidance during the course of the study. We would also like to record with gratitude the assistance of Carl Anderson, Fred Dobson, Peter Smith, Will Perrie, and particularly Bechara Toulany of Bedford Institute of Oceanography for providing the shallow-water wave data and minimet winds, special thanks to Messrs. R.S. Hone and G. Verner of the Canadian Meteorological Centre for providing the CMC operational wind fields. Also, the contributions and collaborations of the CASP organizers at the Atmospheric Environment Services, Maritimes Weather Centre, Bedford, are gratefully acknowledged. We wish to record with gratitude the east coast offshore operators: Petro-Canada, Shell Canada Resources, and Husky-Bow Valley, for permitting us to use their MANMAR and Waverider buoy data in the present study.

This study was carried out jointly with Oceanweather Inc., Cos Cob, Connecticut. MacLaren Plansearch acknowledges with gratitude the outstanding efforts of Dr. Cardone and his co-workers for providing the wave forecasts "in real-time" from the first day to the last day of CASP, despite the enormous problems in obtaining the Canadian Meteorological Centre (CMC) operational winds.

ACRONYMS

AES:	Atmospheric Environment Services
ESRF:	Environmental Studies Research funds
CMC:	The Canadian Meteorological Centre, also used to refer to the operational NWP Spectral model of the Canadian Meteorological Centre.
NWP:	Numerical Weather Prediction
CASP:	Canadian Atlantic Storm Program
GALE:	Genesis of Atlantic Lows Experiment
METOC:	Meteorological and Oceanographic Centre of the Canadian Arm Forces, Department of National Defence (DND), Halifax, N.S.
ODGP:	Ocean Data Gathering Program
CASP-OC:	CASP Oceanographic Component
BIO:	Bedford Institute of Oceanography
NOAA	National Oceanographic and Atmospheric Administration
LFM:	NOAA Limited - Area Finite Mesh NWP Model
NGM:	NOAA Nested Grid Model
SOWM:	Spectral Ocean Wave Model of the U.S. Navy
RMSE:	Root Mean Square Error
FLSC:	Fetch-Limited Spectral Contribution Method
JONSWAP:	Joint North Sea Wave Analysis Project
NMC:	National Meteorological Centre (NOAA)
MPBL:	Marine Planetary Boundary Layer Model
NODC:	National Oceanographic Data Centre

SUMMARY

This report describes the work funded by the Environmental Studies Research Funds (ESRF) to set-up and test a regional spectral ocean wave model for providing real-time wave forecasting during the Canadian Atlantic Storms Program (CASP), 15 January - 15 March, 1986. The ODGP spectral Ocean Wave Model was selected for this test. The model is a fully-directional spectral model which resolves the spectra into 24 directional bands and 15 frequencies. A modified version of the ODGP was developed to include shallow-water equations describing wave propagation in the CASP-OC area.

The model was driven by wind fields obtained from the CMC spectral operational weather prediction model. The CMC winds were extracted at 0.998 sigma-level, which is approximately 16 m above the ocean surface in standard atmosphere. This version of the wave model refered to as ODGP-CMC. In addition, the results from the operational version of the ODGP (i.e. ODGP-OPR which was running in real-time as part of MacLaren Plansearch/Oceanweather forecasting service) were obtained and compared to those provided by the ODGP-CMC. The ODGP-OPR version is identical to the ODGP-CMC deep-water model, but driven by winds produced from reanalysis of the NOAA LFM/NGM pressure fields in a man-machine forecast system. Also the results from the two models were compared against the METOC wave height predictions.

A large amount of field measurements (both wind and wave) was collected from a number of locations on the U.S. east coast, Georges Bank, Scotian Shelf and the Grand Banks of Newfoundland. These data sets were used for the evaluation of both wind and wave predictions.

This study provided a comprehensive evaluation and statistical measures of the accuracy of the operational wave model when driven by two different wind fields (CMC and OPR). The CMC provided winds with a large positive bias, which grew with forecast projection time. This in turn, contributed to the large errors in wave height predictions from the ODGP-CMC model. The winds obtained from a man-machine mix procedure has shown to be superior.

In addition, a 1-D shallow-water wave model was tested within the CASP-OC area. The accuracy of this model is a function of input spectra (obtained from the deep-water model) at the end of the 1-D array, treatment of local winds (particularly offshore winds), and shallow-water propagation algorithm. When excluding the periods when the input deep-water spectra were incorrect (i.e. the last two weeks of January), the model predicted the wave height with reasonable skill.

RESUMÉ

Le présent rapport décrit le travail financé par les Fonds Recherche pour l'Étude de l'Environnement (FREE), afin de mettre sur pied et de tester un modèle spectral et régional des vagues de la mer, pour fournir des prévisions en temps réel dans le cadre du Canadian Atlantic Storms Project (CASP), entre le 15 janvier et le 15 mars 1986. On a choisi, pour cet essai, le modèle spectral de vagues ODGP, qui comprend toutes les directions et décompose le spectre en 24 bandes directionnelles et 15 fréquences. Une version modifiée du modèle a été élaborée, afin d'inclure des equations d'eau peu profonde, décrivant la propagation des vagues dans la zone du CASP-OC.

Ce modèle A ÉTÉ développé à partir des champs de vents obtenus du modèle spectral et opérationnel CMC de prévisions atmosphériques. Les vents du CMC étaient extraits au niveau de sigma 0,998, ce qui représente approximativement 16 m au-dessus de la surface de la mer, dans une atmosphère standard. Cette version du modèle de vagues est connue sous le nom d'ODGP-CMC. Aussi, les résultats de la version opérationnelle de l'ODGP (c'est-à-dire l'ODGP-OPR qui fonctionnait en temps réel pour le service de prévisions de MacLaren/Oceanweather) ont été obtenus et comparés aux résultats fournis par l'ODGP-CMC. La version de l'ODGP-OPR est identique au modéle d'eau profonde ODGP-CMC, mais elle utilise des vents produits à partir d'une nouvelle analyse des champs de pression NOAA LFM/NGM, dans un système de prévisions homme-ordinateur. De plus, les résultats des deux modèles ont été comparés aux prévisions de hauteurs de vagues du METOC.

Un grand nombre de mesures sur place (à la fois de vents et de vagues) ont été relevées à certains endroits sur la côte est des États-Unis, le banc Georges, de Nouvelle-Ecosse pour et le Grand-Banc de Terre neuve. On a utilisé ces donness l'évaluation des prévisions de vents et de vagues.

Cette étude a fourni des mesures statistiques et des évaluations détaillées de l'exactitude du modèle de vagues opérationnel, lorsqu'il est développé à partir de deux champs de vents différents (CMC et OPR). Le CMC a fourni des vents avec une forte déviation positive, qui a augmenté avec le temps de projections des prévisions. Ce qui, en retour, a contribué au grand nombre d'erreurs dans les prévisions de hauteurs de vagues par le modéle ODGP-CMC. Les vents obtenus à partir d'un système mixte homme-ordinateur ont donné des résultats plus précis.

De plus, on a testé un modèle unidimensionnel pour vagues d'eau peu profonde. L'exactitude de ce modèle est fonction des spectres de données (obtenus à partir du modèle en eau profonde) à la limite de la matrice unidimensionnelle, ainsi que du traitement des vents locaux (plus particulièrement des vents du large) et de l'algorithme de propagation en eau peu profonde. Lorsqu'on exclut les périodes où les spectres d'eau profonde n'étaient pas exacts (c'est-à-dire durant les deux dernières semaines de janvier), le modéle a prédit la hauteur des vagues avec une précision satisfaisante.

1. INTRODUCTION

Intensive field work for the Canadian Atlantic Storms Program (CASP) was carried out from 15 January to 15 March, 1986, off the east coast of Canada. The CASP field experiment was scheduled to coincide with its counterpart American experiment, the Genesis of Atlantic Lows Experiment (GALE), to study the mesoscale structure and evolution of many of the winter storms which ultimately affect Atlantic Canada (Figure 1). The CASP, therefore, is aimed at better understanding and forecasting of east coast winter storms. In addition, the CASP has provided a unique data base for numerical modelling studies for storm evolution and meteorological and sea state predictions. This program is the most comprehensive study of storm systems ever conducted in Canada.

One of the objectives of the CASP is the improvement of existing forecasting techniques, including wave forecasts. This study was funded by the Environmental Studies Research Funds (ESRF) to produce and evaluate real-time wave forecasts from a regional spectral wave model which includes shallow water effects, for the duration of the CASP field experiment.

The main objectives of this study were:

- to identify wind and wave forecasting procedures, i.e., identify the appropriate spectral ocean wave model to be run in real time during the CASP period, the availability of real-time data required as input to the wave model, and wave products required to meet operational needs;

- to provide real-time wave forecasting during the CASP field experiment; and

- to assess the model predictions under different storm conditions.

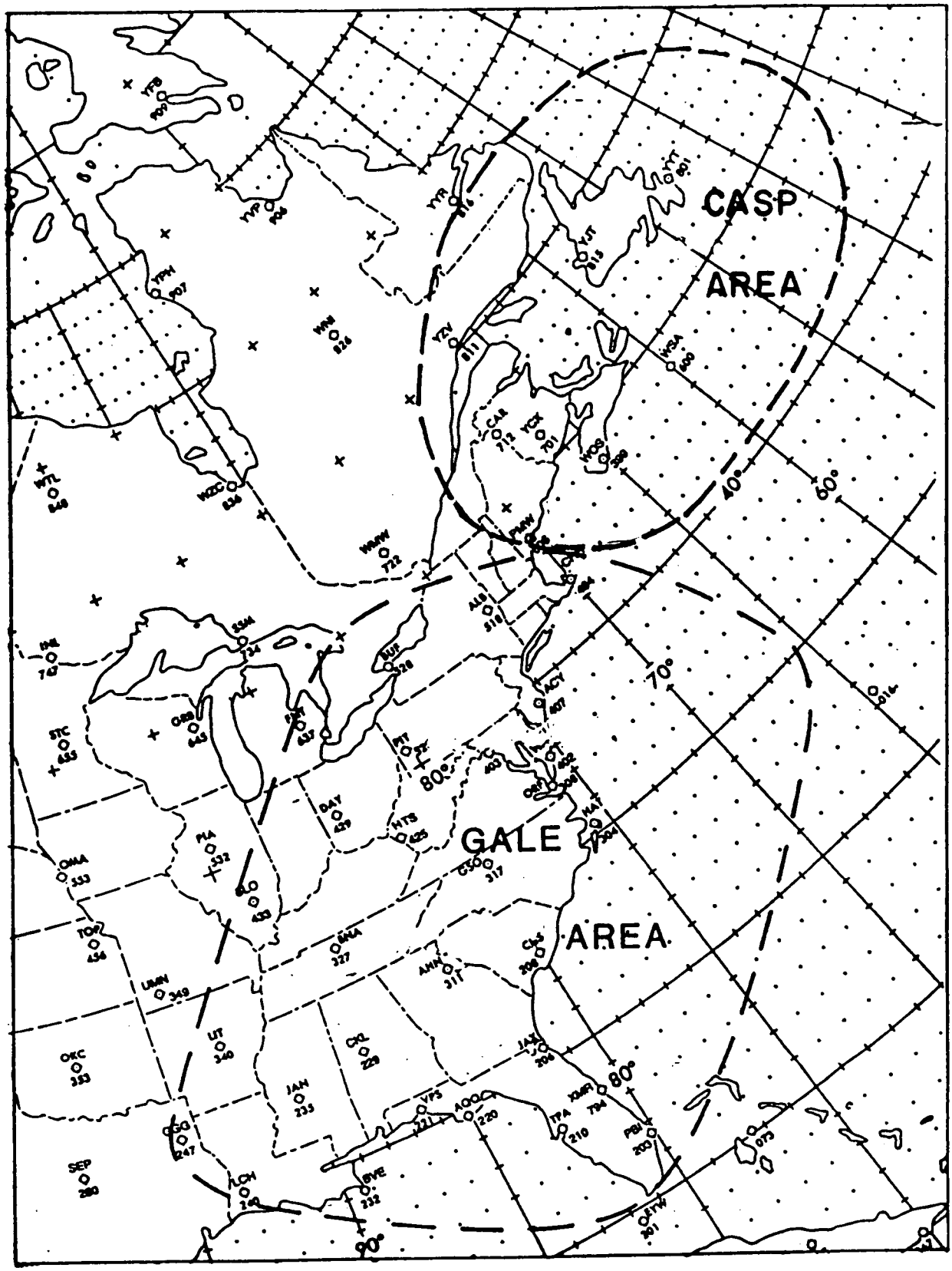

Figure 1. The CASP and GALE areas.

The study consisted of three phases. The first phase involved setting up the wave-forecasting procedure through the acquisition of real-time wind fields from the Numerical Weather Prediction (NWP) operational model of the Canadian Meteorological Centre (CMC) suitable for input to the wave forecast model. The Ocean Data Gathering Program (ODGP) Spectral Ocean Wave Model was selected for this test. A modified version of the model which includes shallow water equations describing wave propagation in the CASP Oceanographic Component (CASP-OC) area, was run on the Contractor's computer VAX 11/750. This phase also included arrangements to access the CMC Operational Spectral Model wind fields, extraction of wind vectors at all wave model grid points, and data transmission into the Contractor's computer to drive the wave model. The CMC winds (given at sigma 0.998 level) were used directly without modification as input to the ODGP wave model.

The next phase was to run a real-time test of the wave model during the CASP field project period for operational use and to evaluate the model contribution to improving the wave forecasting in Canadian waters.

The third phase involved the evaluation of the model performance by comparing model results with measured data collected during the CASP field experiment and wave predictions from other sources, such as the Meteorological and Oceanographic Centre (METOC) and the ODGP operational wave model which is driven by different winds in a man-machine forecasting system. The latter model has been running in real time as part of MacLaren Plansearch/Oceanweather Inc. operational forecasting system. A large amount of data on marine environment was collected during the CASP duration including measurements of winds and waves. These data were collected, checked, quality controlled, and used for verification of both wind and wave predictions. Field data were collected from several sources, of which some were directly involved in the CASP program and others were indirectly collecting the data for other operational purposes. These

sources were: Bedford Institute of Oceanography (BIO), Atmospheric Environment Service (AES), Shell Canada Limited, Petro-Canada, Huskey-Bow Valley, MacLaren Plansearch, and the National Oceanographic and Atmospheric Administration (NOAA) buoy data from National Oceanographic Data Centre.

2. FORECAST PROCEDURE SET-UP

2.1 BACKGROUND INTRODUCTION

The model selected for the CASP wave-forecasting test is the Ocean Data Gathering Program (ODGP) which has been operational at Ocean- weather Inc./MacLaren Plansearch since mid-September 1983. The model is a fully directional, spectral, deep-water wave model.

The ODGP wave model has been adopted for use in an operational wave analysis and forecast system, on the grid system shown in Figure 2. A nested grid (fine grid), in which the grid spacing is half that of the coarse, extends over the Scotian Shelf and the Grand Banks of Newfoundland.

The ODGP wave hindcast model evolved from the Spectral Ocean Wave Model of the U.S. Navy (SOWM) about a decade ago. Details of both the ODGP and SOWM models are given in MacLaren Plansearch Limited (1985). The ODGP model has since been tested against a broader range of wave regimes than any other existing model. This model incorporates a relatively simple representation of the source terms in the spectral energy balance equation compared to more recent formulations. The calibration of these parameterizations has remained stable over this period, unlike most contemporary models, which appear to undergo continuous tuning.

Before 1983, the ODGP model has been exercised mainly in hindcast studies of extreme wave regimes, albeit of many different types (e.g., winter cyclones, typhoons, hurricanes, and monsoon surges). Reece and Cardone (1982) summarized this extensive model experience and reported a record of hindcast skill unequalled by alternate models. The model, when driven by wind fields of accuracy about ± 2 m/s in speed, $\pm 20°$ in direction, provided unbiased specifications of significant wave height and peak frequency with a scatter of about 10%, which, incidently, is comparable to the scatter in estimates of these quantities from measured 20-min wave

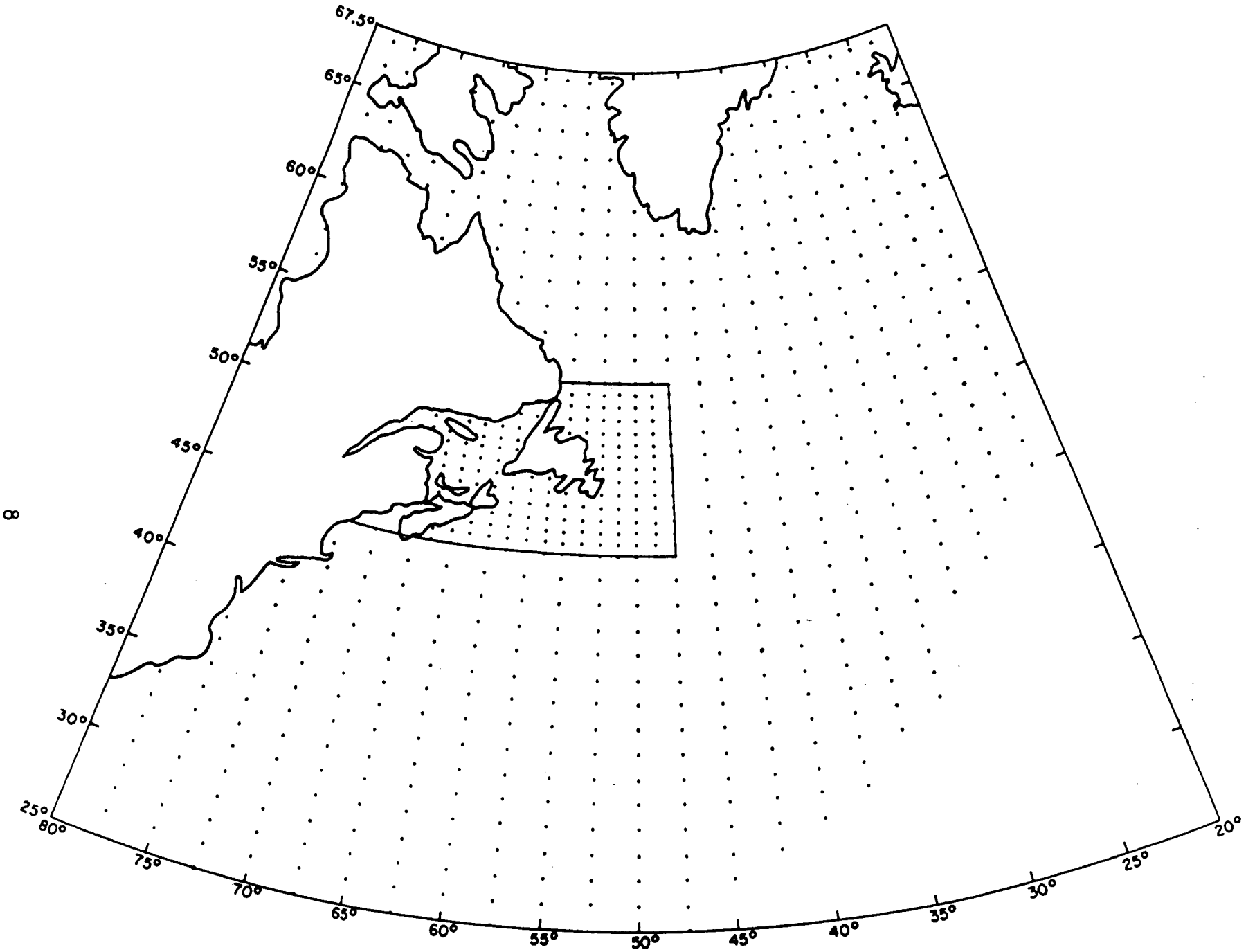

Figure 2. Operational ODGP wave forecast model grid.

records. Wherever possible, hindcast frequency and directional spectra have also compared and agreed. The model exhibits conspicuous skill in the specification of the complicated directional mix of local sea, and propagation swell excited by the moving, quasi-circular wind fields of migratory extratropical and tropical storms. For these reasons the ODGP appears to be a suitable model for the present CASP test.

We regard the general problem of wave climate specification in Canadian east coast waters as basically a three-scale problem. The largest scale requires a grid of about 100-km spacing covering most of the North Atlantic Ocean (e.g., the ODGP coarse grid). The second scale requires a grid of no more than about 50-km spacing (e.g., the ODGP fine grid) to resolve large islands and capes and irregular shoreline geometry, large-scale ice cover effects, and smaller scale features in the windfield. Given that the typical shelf width offshore (to depths of 50 m) in Canadian east coast waters of interest is in the order of 50 km, or one grid spacing on the fine grid, it is appropriate that the coarse and fine grid scales be treated as deep water. The third scale should resolve the shallow shelf width explicitly on a grid in the order of 1-2 km spacing (e.g., ODGP ultra-fine CASP grid).

While the time step in a wave model on the larger two scales is 1-3 h, the time step required in current shallow-water wave models for a 1- km grid is typically less than 60 s. Clearly the specification of a wave climate in shallow-water, using a wave model with shallow water physics is a computing intensive activity to be pursued only on a regional basis as required. However, the proposed deep-water model is invaluable in that it can provide the deep-water spectra which the shallow water models require as input.

For this study, therefore, the ODGP discrete spectral model (which based on deep-water physics) is applied on a two-dimensional, nested-grid system to account for the large and fine scales (see Figure 2), and on a

one-dimensional, spatial grid extending to a 100-m contour which covers the CASP-OC measurement sites with shallow-water propagation and transformation processes modelled.

Two versions of the deep-water ODGP model were used in the present study:

- ODGP-CMC: ODGP model driven by the CMC operational spectral model winds (at Sigma 0.998 level); and

- ODGP-OPR: the operational version of ODGP (which is running in real-time at MacLaren Plansearch/Oceanweather) driven by winds obtained from the NOAA Limited-area Finite Mesh/Nested Grid Model (LFM/NGM) numerical weather prediction model (NWP) surface pressure charts and a man-machine analysis.

The results from these two models (which are essentially same model driven by two differet wind fields) will provide an excellent evaluation of the CMC winds. The results of the ODGP-CMC at the end of the ultra-fine grid are used to run the shallow-water model as described in the following sections.

Model predictions (ODGP-CMC, ODGP-OPR, and ODGP-CASP shallow-water model) are evaluated against field observations at several locations within CASP study area as described in Sections 4 and 5. In addition, predictions of wave height obtained from METOC wave charts are also compared with these model results.

2.2 ODGP DEEP-WATER MODEL ALGORITHM

Only a brief summary is presented here. For detailed description of the model, the reader is referred to Cardone et al. (1976) and MacLaren Plansearch Limited (1985). The general energy-balance equation for wave evolution is given by:

$$\frac{\partial}{\partial t} S(f,\theta;x,t) + Cg \cdot \nabla S = F(f,\theta;x,t) \qquad (1)$$

Where:

$S=S(f,\theta;x,t)$ is the two-dimensional wave spectrum as a function of frequency (f) and direction (θ) at a given location (x) and time (t);

$C_g=C_g(f,\theta)$ is the deep-water group velocity;

$F(f,\theta;x,t)$ is the source function which represents all physical processes that transfer energy from or to the spectrum.

The source function may be expressed as a sum of three terms:

$$F = F_{in} + F_{nl} + F_{ds}$$

Where: F_{in} = energy input function by wind,
F_{nl} = non-linear transfer by wave-wave interaction,
F_{ds} = energy dissipation term.

The input source function (F_{in}) is represented in ODGP as a function of wind speed and frequency according to the linear equation:

$$F_{in} = A + B.S$$

The A term in this equation $=A(f_i,u)$ is a function of frequency (f) and wind speed (u). This term represents Phillips' external turbulent pressure forcing. The B·S term corresponds to Miles' linear feedback mechanism. The term $B(f_i,u*)$ is expressed in ODGP as a function of frequency and the friction velocity (u*).

The energy transfer associated with the non-linear, wave-wave interaction is not explicitly included in ODGP.

In general, hindcast models work by applying alternate steps to model the effects of propagation and growth. In the propagation step, the frequency bands of the model are totally uncoupled, and the directional bands are weakly coupled by convergence of meridians on a spherical earth. In the growth step, the grid points are totally uncoupled; the frequency and direction bins at one grid point are coupled because of the treatment of the source and sink terms in the spectral energy-balance equation.

Most propagation schemes have been devised to represent faithfully monochromatic wave propagation on a grid system with minimum dispersion. Such methods have employed higher-order advective differencing schemes, discontinuous schemes which jump energy from point to point and explicit representation of wave ray paths along characteristic curves. However, wave models represent the spectrum (or at least the swell part) as an array of frequency-direction components of finite frequency and direction bandwidth. Because of angular spreading and the variation of group velocity of individual wave components within a band, there is a natural dispersion of wave energy. Greenwood and Cardone (1977) were the first to observe that the error incident to even a crude gradient scheme is in the order of $N^{1/2}$, where N is the number of time steps, whereas the error inherent in neglecting bandwidth is in the order of N and is the dominant error for long propagation distances. There is, therefore, little point in selecting an advective scheme for a discrete wave model that minimizes dispersion. Advective operators that are consistent with the natural dispersion of finite bandwidth spectral components have not been developed, but the consistency requirements of such an operator have been described in SWAMP (1985).

The propagation scheme used in the ODGP operational model was constructed for use with a spherical earth, and combines elements of jump and interpolatory propagation. When an ocean basin is mapped on a plane by an arbitrary projection, and a rectangular or triangular grid overlaid, the

distance from each point to its neighbours, and thus the coefficients in the propagation formula, are functions of both latitude and longitude. Coefficients dependent on latitude alone arise when one set of grid lines consists of meridians equally spaced, and the other set consists of parallels at any convenient spacing. The present model grid (see Figure 2) is that used in the North Atlantic wave hindcast/forecast model referred to above. The grid consists of a coarse grid of spacing 1.25° latitude and 2.5° longitude, extending from 25°N to 67.5°N and from 20°W to 80°W, and a nested grid in which the grid size is half that of the coarse. The time step of the model is 3 hours, each of which consists of a full time step of propagation between two half time steps of growth. The present model has 24 directional bands spaced 15 degrees apart and 15 frequency bands spaced as shown in Table 4.4 (in Chapter 4).

The ODGP growth algorithm developed by Cardone et al. (1976), is a part of the family of Pierson, Tick and Baer (PTB) discrete-type spectral models described by Pierson et al. (1966). Although the ODGP spectral growth/dissipation algorithm is of the PTB type, significant differences between it and the U.S. Navy SOWM model (also a PTB type) evolved in the application and verification of the ODGP model against measured wave spectra in hurricanes. An important difference is in the calculation of the wave growth as a function of the angle between the wave direction and wind direction. In the SOWM, the energy in a given frequency component summed within $\pm$90 degrees of the local wind is the quantity subjected to growth. The incremental growth is then spread out over the same components.

In the ODGP model, each downwind spectral component is grown separately, and after computation of growth for all components within $\pm$90 degrees of the local wind direction, energy is redistributed over angles. This algorithm leads to slower growth of wave height with time in a turning wind than in a wind of constant direction. A more detailed description of the growth algorithm is given in Appendix A taken from MacLaren Plansearch Limited (1985).

The modelling of directional processes in the ODGP model is apparently sufficient to provide reasonably skilled simulation of the integrated properties of the directional spectrum of peak sea states in storms characterized by stationary, or moving, circular wind fields. In more than 60 individual comparisons in 19 different storms, Reece and Cardone (1982) found that the model exhibited negligible bias and root mean square (rms) errors of less than 1 m in significant wave heights and 1 s in peak spectral period. Comparisons of hindcast and measured directional wave properties are more limited. Forrestall et al. (1978, 1980) shows comparisons in two Gulf of Mexico tropical cyclones. The directional spectrum was estimated from measurements of surface elevation and orbital velocity. Directional properties were expressed in terms of the mean direction and spread as a function of frequency. Good agreement was found in both storms.

The performance of the ODGP/OPR model as operated in real-time off the east cost of North America has been reported by MacLaren Plansearch Limited (1985), Eid et al. (1985), and Cardone and Szabo (1985).

2.3 SHALLOW-WATER WAVE MODEL

2.1 CASP Extension of ODGP Wave Model

In recent years, two new concepts have been introduced to describe shallow-water wave transformations. The first concept follows from the theoretical finding that non-linear, wave-wave interactions, which are now generally believed to play an important role in the deep-water spectral-energy balance, are greatly enhanced in shallow water. Over a sloping bottom these interactions, though intrinsically energy-conserving, effectively act to cause attenuation of wave height, as energy transferred from the vicinity of the spectral peak to higher frequencies is lost

through waves breaking in the so-called saturation range of the spectrum. The second new concept is turbulent bottom friction, which depends sensitively on bottom sediment properties and on sediment transport processes. These newer bottom friction theories, for which there is increasing experimental support, predict much higher friction coefficients than do molecular viscosity theories.

These concepts have led to the introduction of a number of new, shallow-water, wave-prediction models, but the properties of these models vary widely and a number controversial issues that affect the quantitative performance of these models in storm situations have yet to be resolved. This controversy had led to a number of intercomparison studies involving alternate models. Several such studies are underway in the United States, Canada and Europe, and a much clearer picture of the relevant physics for shallow-water transformation should emerge in about one year. One of the seeming consequences of the dominance of one or both of these source terms in the process of shallow-water transformations (over the classical effects of shoaling and refraction which, except in highly inhomogeneous bottom conditions, are relatively slight in comparison) is the recent finding that wind-wave spectra in shallow water follow a self-similar form that can be described by the so-called TMA spectrum (Bouws et al. (1984)).

The TMA spectrum, which has been shown to fit well literally thousands of measured spectra from the North Sea and Atlantic continental shelf, has been interpreted by Bouws et al. (1984) as an upper limit to finite depth spectra in wind seas propagating through sloping bottoms typical of those over which the TMA spectrum was defined.

A second apparent source term of importance, especially for wave components of longer period than that of the spectral peak, is bottom friction resulting from bottom sediment properties, ripple formations, and sediment transport to be modelled.

The shallow-water model used in the CASP appliction, called SHALLOW3, was developed at Oceanweather beginning in December 1984. The model is basicly an extension of ODGP deep-water propagation and spectral growth algorithms to include the shallow water processes of refraction, shoaling, bottom friction, and wave-number scaling. Refraction and shoaling are modelled within the propagation step, whereas bottom friction and wave-number scaling are modelled within the growth step.

The calculation of a table of propagation coefficients in SHALLOW3 is greatly simplified by the assumption of straight, equally spaced bottom contours, parallel to the beach. The principal modifications of the growth subroutine are:

- transformation of the fully developed Pierson-Moskowitz (1964) form to shallow water;

- calculation of an explicit attenuation associated with bottom friction, which is modelled after the comprehensive treatment of Grant and Madsen (1982);

- calculation of the exponential growth rate using the shallow-water celerity; and

- use of wave-number scaling of the high-frequency saturation range of the spectrum, with the equilibrium range coefficient, α, taken as a function of the stage of wave development. Some more detailed descriptions of these aspects of SHALLOW3 are given in the next section.

2.3.2 Mechanisms Modelled

In the present study, the propagation code rests on a one-dimensional, refraction-and-shoaling table that takes waves in along a plane bottom of arbitrary slope (straight contour lines, parallel to the beach, and equally spaced) with stations at depths from 100 m to 7.5 m at intervals of 7.5 m. With this geometry, the turning angle and shoaling coefficient in moving from one station to the next are functions of the depths at the two stations and of the incident wave number. They are not explicit functions of the slope; the effect of slope is factored in by using a time step proportional to the horizontal distance between stations (in SHALLOW3, 2.205 km). The incident wave number is conveniently indexed by the frequency and the angle of incidence. This table has been used in tests of hypothetical seas at bottom slopes of 1/100, 1/1000, and 1/10000; and in hindcasts offshore Nigeria, approximating the shelf by a slope of 1 in 200.

The growth code, called CMPE28A, algorithm can be explained by starting with the original CMPE24 algorithm used in the deep-water hindcast and forecast (see Appendix A). Nine changes were made to the algorithm of CMPE24 to yield that of CMPE28A.

1. The reference spectrum is computed as Pierson-Moskowitz without an ω^{-4} range. Several traditional approximations in the numerics combine to yield $\alpha = 8.18559 \times 10^{-3}$.

2. The Pierson-Moskowitz peak frequency is computed from the wind speed:

$$\hat{\omega} = 0.8790132g/U_{19.5}.$$

where $U_{19.5}$ is wind speed at 19.5 m above mean sea level. This numeric implies that the constant β in the P-M spectral formula, nominally 0.74, is here taken as 0.7462625. The corresponding shallow-water wave number (k) is obtained as:

$$\hat{k} \tanh \hat{k}d = \hat{\omega}^2/g,$$

and the fully-developed shallow-water total variance as:

$$E_{tot} = 0.2 \times 8.18559 \times 10^{-3} \times \hat{k}^{-2}. \qquad (2)$$

3. At the beginning of each time step, the rms bottom excursions and rms bottom velocity are computed from:

$$a^2_{rms} = \sum s(i)/\sinh^2 k_i d,$$

$$U^2_{rms} = \sum s(i)\omega^2_i/\sinh^2 k_i d,$$

where s(i) is the variance component (not the spectral density), integrated over all directions, in frequency bin i; ω_i is the nominal radian frequency ($2\pi f$) in that bin; d is water depth (in feet in the code used; but the combination kd is dimensionless); and k_i is the scalar wave number computed from the shallow-water dispersion relation

$$\omega^2/g = k \tanh kd.$$

4. The α used in computing the tail of the spectrum is allowed to float according to Resio (1981) correlation:

$$\alpha = \alpha_o \ (E/E_{pm})^{-.23},$$

where: $\alpha_o = 8.18559 \times 10^{-3}$ and $E_{pm} = 0.2\alpha_o g^2 \hat{\omega}^{-4}$.

5. A bottom-friction factor (FW) is computed, following Grant and Madsen (1982), as the greatest of three tentative factors:

a) a smooth-flow friction factor depending on the Reynolds number

$$Re = 2.005^2 U_{rms} a_{rms}/\nu$$

where ν is the kinematic viscosity of sea water (a_{rms} is rms value of bottom excursion and U_{rms} is bottom orbital velocity). (For very small values of bottom excursion, the code in SHALLOW3 yields an unphysically high value of FW).

b) a skin friction factor, depending on the ratio of bottom excursion to sand-grain diameter (a sand-grain diameter of 0.2 mm was assumed throughout).

c) a friction factor reflecting the ability of the bottom velocity to raise ripples; it is a non-dimensional function of bottom excursion, bottom velocity, gravity, sand-grain diameter, and excess of the density of sand over the density of water.

6. For each frequency band the rate of dissipation, with dimension T^{-1}, is computed as

$$-FW \times U_{rms} \times \sinh^2 k_i / g\omega_i^2.$$

7. The A-term (linear growth) is computed as in CMPE24; the B-term (exponential growth) is a function of $u*/c$, where c is now the shallow-water celerity

$$c = (g/\omega)\tanh(\omega d/c).$$

8. For each frequency-direction bin the algebraic sum of B-term and dissipation is taken: this can be positive, negative, or zero. (The case where growth exactly balances bottom friction must be regarded to prevent division by zero.) Positive net growth is applied to the function $T(\theta_i)$ (see equation A.10 of Appendix A); negative net growth is applied to the variance component directly. Because the growth rate can be arbitrarily close to zero, the function

$$\exp(B\Delta t) - 1$$

naturally occurring in the integral of Equation A.10, is used in the floating-point computational form

$$\exp(B\Delta t)-1 = 2\exp(B\Delta t/2)\sinh(B\Delta t/2).$$

9. After upwind components are dissipated, as in CMPE24, the total variance (E) is computed by summing over 360 frequency-directional bins. The floating α is recomputed from

$$\alpha = 8.18559 \times 10^{-3}(E/E_{tot})^{-.23}$$

where E_{tot} was defined in equation (2) above. The bands to the right of the P-M peak are now computed to the k-scaled tail density

$$dS/dk = 1/2\ \alpha\ k^{-3};$$

frequency-direction bins (in downwind directions) that exceed the integral of this density spread into directions according to the SWOP (Coté et al. (1984)) distribution are cut back.

2.3.3 Model Implementation

The shallow-water model is adapted on a one-dimensional (1-D) array of grid points laid out along the CASP shallow-water measurement array, so-called ultrafine grid, as shown in Figure 3. The (1-D) array extends from 44°16'N, 62°55'W to shore in the direction 337.5°, normal to the bottom contours, which are taken as straight lines parallel to coastline. Sounding data and contour lines shown on Canadian Hydrographic Service chart L/C 4320 were used to approximate the bottom slope as constant in the

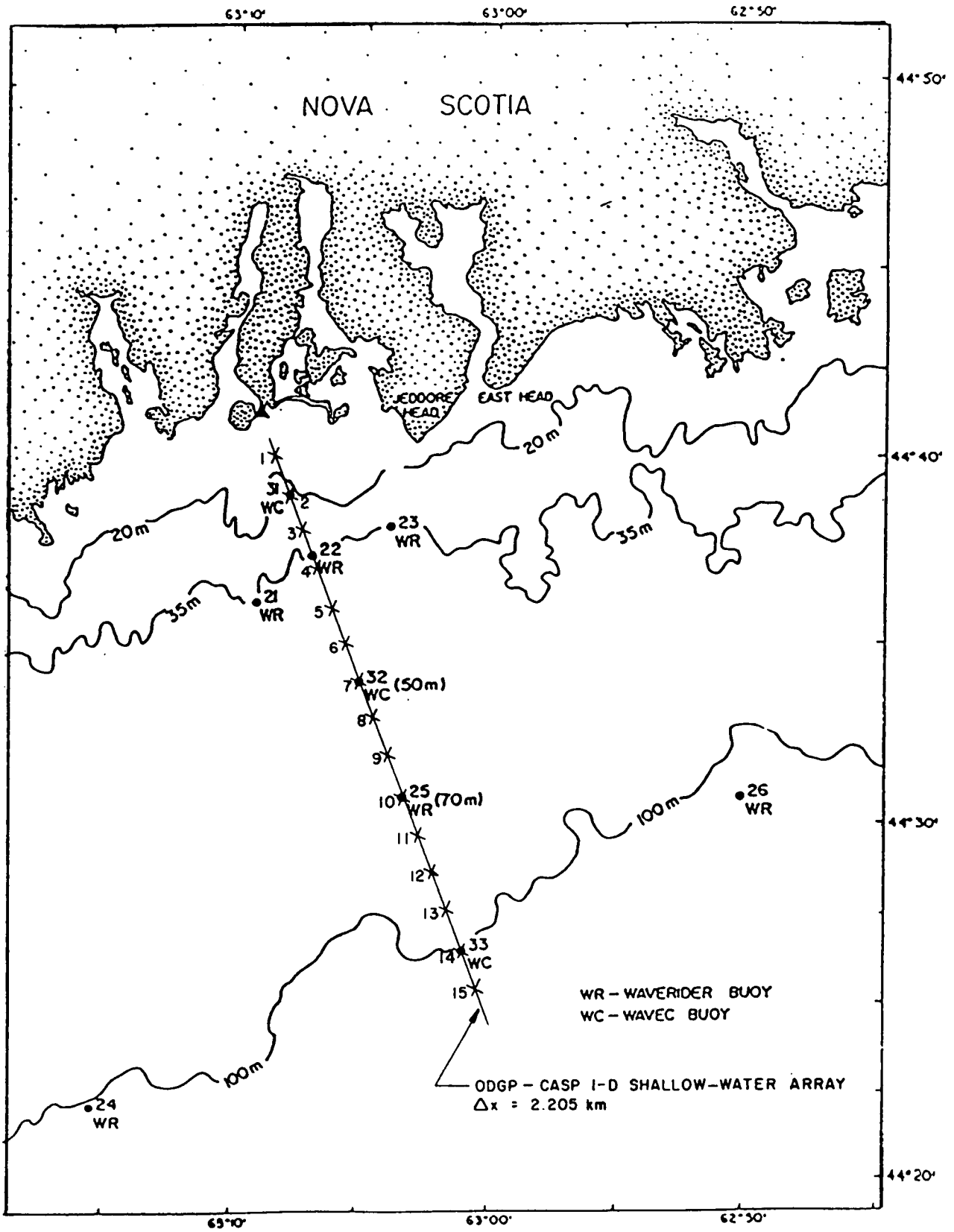

Figure 3. The CASP shallow-water, one-dimensional model grid.

ratio 1:294, between depths of 187.5 m and 15.0 m. Over this range of depths, grid points were spaced at depth intervals of 7.5 m, yielding a grid spacing of 2.205 km between 50.715 km and 4.410 km from shore.

Immediately following each CMC deep-water wave model run, the 1-D shallow-water model was executed separately nine times to provide wave analyses and forecasts on the 1-D, shallow-water grid at six-hourly intervals between forecast projection times of 0 and 48 hours. The 1-D model is initialized from the two-dimensional wave spectrum and wind speed and direction specified at the ODGP fine-grid point #1032, located at 44°22.5'N, 62°30'W.

At the deep-water end of the 1-D array, the full 2-D spectrum contains 12 direction bands that propagate onshore and 12 direction bands that propagate offshore. Within 50 km of shore, it can be expected that the wave energy in offshore-propagating spectral components is determined by the local wind field and by a fetch that is limited by the nearby coastline. The first step in the shallow-water model is to calculate a fetch-limited spectrum pertaining to all frequency bands in the 12 offshore propagating components, consistent with the local wind speed and direction, using a parametric model known as the fetch-limited spectral contribution (FLSC) method.

In the FLSC method, a directional spectrum is adopted whose properties (such as total energy, peak frequency, peak enhancement, and directional spreading) vary with fetch and wind speed in a prescribed fashion. At the hindcast location of interest within a restricted basin, the fetch is prescribed as a function of direction. The wind duration is assumed to be sufficient to allow development of strictly fetch-limited seas at the site for all directions. The hindcast directional spectrum at the location of interest is then the sume of spectral contributions computed separately for each discrete direction band and frequency according to a directional

spectrum appropriate to the direction-dependent fetch. In the present application, the model is used to specify spectral variances in the offshore propagating directional bands. The coastline is assumed to be straight and normal to the 1-D array of shallow-water grid points.

Seymour (1977) described an FLSC model based upon the JONSWAP spectrum and a $\cos^2\phi$, angular spreading law. The JONSWAP spectrum is basically a Pierson-Moskowitz (1964) spectrum with peak enhancement added. The form of peak enhancement adopted by JONSWAP is awkward to use because it can only be integrated numerically. The model used a more convenient, peak-enhanced, Pierson-Moskowitz spectrum:

$$S(\omega) = \alpha g^2 \omega^{-5} \left[0.2 \exp\left(-1.25\omega^4\hat{\omega}^{-4}\right) + \delta \exp\left(-1.25\omega^{20}\hat{\omega}^{-20}\right)\right]$$

with spectral density

$$\frac{dS}{d\omega} = \alpha g^2 \hat{\omega}^{-4}\omega^{-1} \left\{\Omega^{-5}\exp(-1.25\Omega^{-4}) + 21\delta\Omega^{-20}\exp(-1.05\Omega^{-20})\right\}$$

where ω is radian frequency; $\hat{\omega}$ is peak frequency, $\Omega=\omega/\hat{\omega}$; g is the acceleration of gravity; α is the so-called equilibrium range "constant"; and the coefficient δ is chosen to match a prescribed peak enhancement γ, defined as the ratio of the spectral density at $\hat{\omega}$ to the peak density of a Pierson-Moskowitz spectrum with the same $\hat{\omega}$. Following JONSWAP, α, the non-dimensional peak frequency $\hat{\omega}U_{10}/g$, and the non-dimensional total energy $\varepsilon = Eg^2U_{10}^{-4}$, are taken as universal functions of the non-dimensional fetch

$$\xi = xg/U_{10}^2,$$

where x is fetch and U_{10} is wind speed at 10 m.

The relevant forms are:

$$\hat{\omega}U_{10}/g = 17.84\xi^{-.30}; \quad \alpha = .0662\xi^{-.20}; \quad \varepsilon = 1.6077321\times10^{-7}\xi.$$

The adopted value $\delta = 0.046$ yields a peak enhancement

$$\gamma = 2.179875,$$

a value consistent with these relations and with the invariance of normalized spectral shape with fetch proposed in JONSWAP. The directional spreading form is taken from Mitsuyasu et al. (1975) and is modified to be rigorously zero for $\phi \geq \frac{1}{4}\pi$. For a class of peak-enhanced spectra including and generalizing these values, see Whalen and Ochi (1978).

The spectra computed are stored to serve as an upper limit to growth of offshore propagating seas. After the FLSC calculation, the shallow-water model is applied on the 1-D grid as follows. First, beginning from flat-calm conditions at each grid point shallower than 180 m, the entire spectrum is subjected to duration growth for 6 h, which serves mainly to spin up the equilibrium range part of the spectrum. Then, onshore propagating components undergo 3 h of growth, and propagation. Offshore propagating components underdo 3 h of growth, after which the spectral energy in each such band is set to the lesser of the result of that duration growth and the energy specified by the FLSC calculation.

2.4 INPUT WINDS

As described previously, two wind sources were used to provide surface wind fields required as input to the ODGP wave model:

- the CMC operational (spectral) model output, so called ODGP-CMC winds; and

- the sea-level pressure charts from the NOAA LFM/NGM numerical weather-prediction models for the analysis and forecast times are used in a man-machine procedure using a Marine Planetary Boundary Layer Model (MPBLM) (Cardone 1969) to specify the surface winds at the 19.5-m level. This wind will be referred to as ODGP-OPR winds.

These wind fields were obtained in real-time or near real-time twice a day to present 0000 and 1200 GMT analysis and forecast fields as described later.

2.4.1 ODGP-CMC Winds

The use of ocean wave models in an operational sense is dependent on the timing of the output from the NWP models as well as on the speed with which one can turn a spectral fore-cast into an operational forecast useful for real-time offshore operational needs.

The CMC operational spectral forecast model output wind was used to run the ODGP wave model. The CMC vector winds used in this study are the surface winds or so called the CMC boundary layer U, V (BLUV), which are the grid wind components in the lowest active layer of the CMC model. Most recently, after being installed on the CRAY supercomputer at the Canadian Meteorological Centre in Dorval, Quebec, the CMC NWP model has been refined to provide the surface winds at 0.998 sigma level (σ= pressure at a given level divided by surface pressure) on a 254-km grid. (The version now executing has a triangular truncation at 59 waves with 15 levels in the vertical; see Daley et al. (1976) and Delage (1985)).

For typical oceanic variations in surface pressure and air density, the sigma level of 0.998 is believed to represent 16 m $\pm$ 10 m above water surface. Because of this uncertainty, and as the CMC surface winds already contain some boundary layer physics, any further reduction to a required

wave model reference height, i.e., 19.5 m used in ODGP, or inclusion of thermal stability effects may duplicate physical structure. Therefore, the CMC wind was used directly as input to the wave model without modification. These use also was necessary to intercompare other operational models which were applied during the CASP using same winds (e.g., AES parametric wave model, and Resio's WAVAD model).

It must be noted that the 00-h analysis (or forecast) refers to the zero-time prognosis field generated by the CMC spectral model which is initialized through an objective analysis of observations as described by Creswick (1983). This should not be confused with the CMC analysis winds.

2.4.2 ODGP-OPR Winds

Winds are provided to the wave model from sea-level pressure analysis and forecast fields which are derived in a man-machine procedure from NOAA National Meteorological Centre (NMC) facsimile products. A Marine Planetary Boundary Layer model (MPBL) is used to specify the winds from sea-level pressure gradients.

The basis of the sea-level pressure analyses, which are used to generate the wave analysis in the real-time hindcast/update part of each forecast cycle, is the NMC North Atlantic surface pressure map distributed over the DIFAX (digital facsimile) network at six-hourly intervals. This map is a section of a Northern Hemisphere Polar Stereographic projection of scale 1:10,000,000 on which are shown computer-plotted land and surface ship reports and hand-analysed isobars drawn at 4-mb intervals. Positions of lows, highs, and fronts are also indicated.

This chart has a data cut-off of about 1 h and the maps are received about 4 h after nominal map time (0000, 0600, 1200, 1800 GMT). At NMC, a so-called Final Analysis is performed about 5 h after map time but these analyses are not distributed in real time.

At Oceanweather, there is sufficient time before the LFM forecast products are received to add ship reports transmitted over the GTS up to about 9 h after map time for 0600 GMT and 1800 GMT and about 3 h after map time for the 0000 GMT and 1200 GMT analyses. Such reports are plotted manually directly onto the DIFAX maps and the isobaric pattern is redrawn where the late data support modification of the NMC analysis.

The pressure fields are then digitized over the domain of the wave model using a digitizing table. The procedure involves digitization of locations of centres of action and their central pressures and of each isobar. An objective analysis program then recovers pressures on a regular grid of points spaced 0.625° in latitude and 1.250° in longitude.

Forecast wind fields are specified at 12-hourly intervals between t_0 (analysis time) +12 h through t_0 + 48 h, from 12-hourly surface pressure fields provided by the NOAA LFM numerical forecast model as transmitted on the DIFAX circuit. After 7 February, 1986, the LFM was replaced by the Nested Grid Model (NGM). Before the pressure fields are digitized, however, the isobaric patterns are modified through forecaster intervention in an attempt to remove systematic errors in specification of cyclone and anticyclone central pressures and corresponding pressure gradients. Initialization and persistence errors are also accounted for at this step. Wind fields are calculated from the modified pressure fields, using the same MPBL applied to the analysis pressure fields.

The MPBL model applied is an improved and updated version of the model proposed by Cardone (1969). The model has been found by numerous investigators to link effectively the external factors governing the MPBL to the near-surface wind structure. Those external factors, in a steady-state, horizontally homogeneous MPBL, may be listed as follows:

- latitude (or Coriolis parameter, f)
- surface roughness parameter, z_o
- air-sea temperature difference, $T_a - T_s$
- geostrophic wind vector, V_g
- horizontal temperature gradient, ∇T_a.

The model considers the MPBL as consisting of two layers. In the lower layer, the wind and temperature variation with height is governed by the effective roughness of the surface and the heat flux across the air-sea interface. The similarity theory of Monin-Obukov is applied there to provide a framework for the description of the mean wind profile. The theory is quasi-empirical in that general expressions are formulated from dimensional considerations and constants that appear in the expressions are derived from experimental data. Variations in the mean wind with height (Z) in the layer are related to wind speed (u), roughness length (z_o), and to the Monin-Obukov length (L) which is a function of both u and the heat flux. A more detailed description of the MPBL can be found in Cardone (1978) and MacLaren Plansearch Limited (1985).

3. REAL-TIME IMPLEMENTATION DURING THE CASP

3.1 ACCESSING CMC COMPUTER IN REAL-TIME

As mentioned previously, the main objective of this study was to set-up and test a regional spectral ocean wave model, which covers CASP project area, using wind fields obtained from the CMC operational model in real-time. This objective includes establishing an access to the CMC computers (CRAY-CYBER) and transmitting the surface wind vectors to our computer as soon as the CMC model output is available. Several problems had to be overcome:

- obtaining CMC wind field in real-time or near-real-time as soon as the files are available on the front-end computer (CYBER);

- establishing reliable communication means between CMC computer and the contractor's computer;

- devising an automatic procedure on CMC computer to update the wind files following each run of the CMC model and transmitting the files before new run is executed; and

- running the wave model and transmitting the forecast to CASP desk (via a telecopier) as soon as possible.

Implementation of the ODGP-CMC model followed closely the timelines used for the ODGP-operational model. Basically, the model was executed twice daily in a hindcast/forecast cycle from 0000 GMT and 1200 GMT (tau 0) initial states. In each run the tau minus six hours (T-6) and T-0 hours states are generated from the corresponding T-6 and 00-h analysis wind fields. It should be realized that the 00-h analysis refers to the time-zero prognostic field generated by the CMC model, not to be confused with

the other CMC analysis wind products. Values at T-6 were not immediately available from the CMC model output, instead T+6 prog values from the 12-h previous run were used.

Each run is continued forward 48 h, driven by CMC forecast winds for T+6, T+12.....T+48. This procedure is schematically presented in Figure 4. Usually, to spin-up the wave field, the model requires at least 24 h "warming-up" or spin-up time. It is, therefore, important to runthe model continuously to avoid a break in continuity of the wave analysis.

Each run of the wave model produced time histories of the full, two-dimensional spectrum and derived quantities (significant wave height, peak period, mean direction, and direction of maximum wave energy) at all analysis and forecast six-hourly intervals at a selected number of grid points at which wave measurements were taken as described in Section 4.

As mentioned previously, the degree of success in using an ocean wave model in an operational sense is dependent on the timing of the output from the numerical weather prediction model, as well as on the speed of running the wave model and providing forecast useful for real-time operational needs. Ideally, it was estimated that the CMC model results would be available for transmission at T+4 h, plus 1 h for communications and preparing the wind fields ready for input to the wave model, plus an additional 1.0 to 1.5 h to run the deep-water wave model and to provide the results. The wave model (deep) results may be available, at best, 6 h (T+6) after the analysis time (see figure 4). In addition, a 1.0 to 1.5-h period is required to run the shallow-water wave model and to transmit its results to the end user (e.g., CASP desk). However, because of several problems encountered during CASP operation, particularly the delays in accessing the CMC computer and in transmitting the results onto our computer, this time had been exceeded by several hours; we almost lost wind files several times as a result of failing to access the CMC computer before the wind files were updated with the new wind fields.

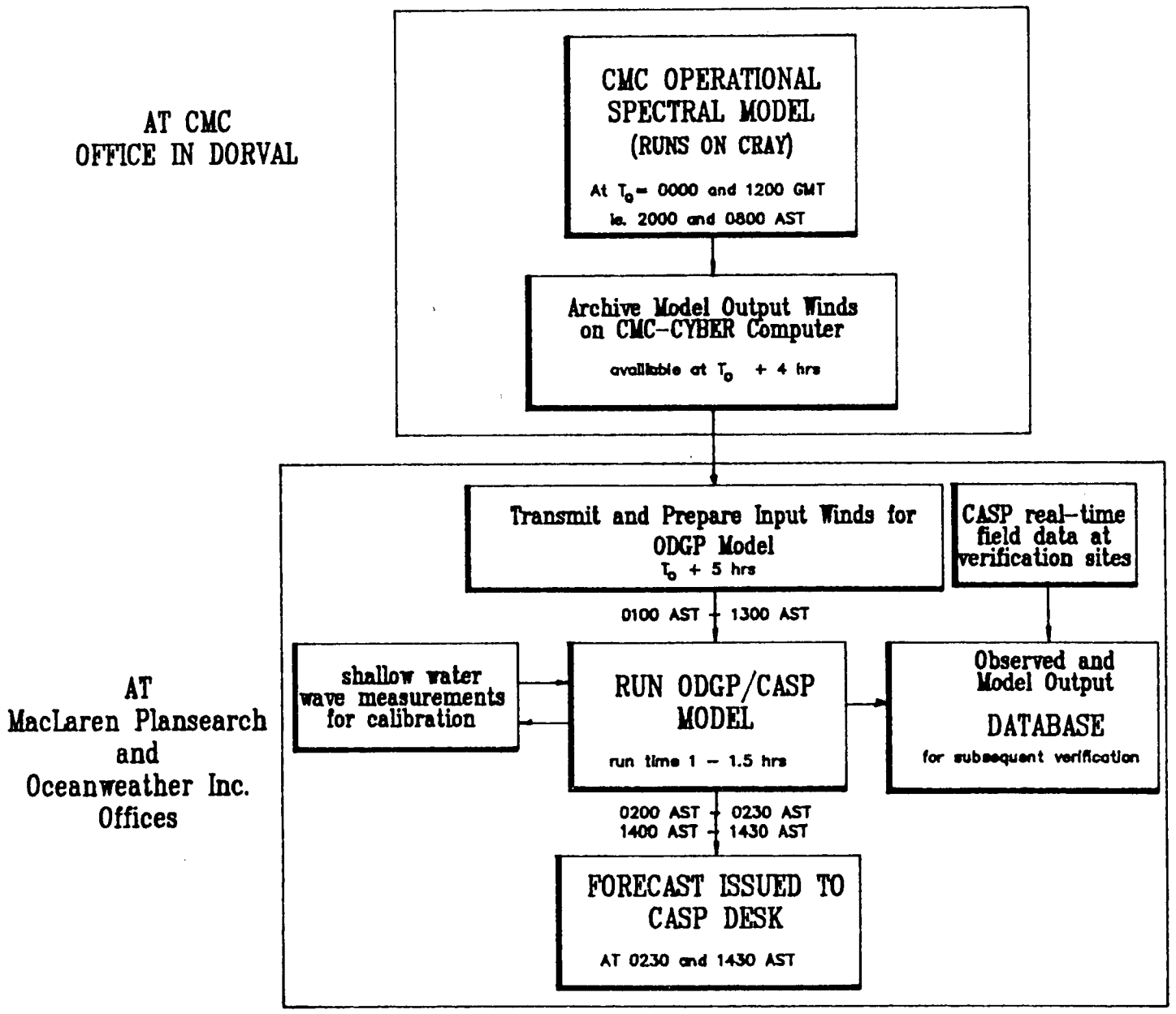

Figure 4. Operational ODGP-CMC wave forecast system for the CASP field experiment.

3.2 RECEIVING CMC WIND DATA

With the use of today's microcomputers moving files from one computer to another can be easily automated with a high degree of success. There are two major steps to perform a file transfer; dial/logon procedure and use of a file transfer protocol.

Dial/logon procedure. A desirable method of file transfer with a microcomputer is to use available packet switching technology such as Datapac 3101 service. Using this network whether public dial-up or a dedicated service, a user can establish a link to the host computer and can initiate a file transfer manually or automatically.

This transfer can be automated easily with the use of autodial/auto-answer modems. The microcomputer must establish a link by dialing a public dial-up port followed by establishing a Datapac link to the host computer. If a full automation of the logon procedure is desired, the microcomputer can run a custom program which will establish a link, will logon to the host computer, and will initiate the transfer. With the use of a hardware clock in the microcomputer, this task can be carried out automatically at specified times during the day.

File transfer protocol. Many file transfer protocols exist for transfering files from one computer to another such as Xmodem, Kermit, RMF, RJE, and HASP. A file protocol is required to ensure all the data within the file are transmitted correctly. A file could be copied to the microcomputer disk by a direct copy to the host computer terminal port, but there is no way of ensuring that no errors in a transmission may have occurred. With the use of a protocol, data is sent in packets and checked for errors, if an error should occur the packet is automatically retransmitted. In this case, it is required that both the host computer and the microcomputer must run a program that supports the protocol.

For this application, the most economical protocol to use was the Remote Micro Facility (RMF). This package is supported by CDC and is available on CYBER and most microcomputers.

Asynchronous data communication is relatively slow, and in operations in which file transfers are performed routinely, it is beneficial to optimize the file transfer by reformatting the file to be transmitted to contain only essential data (i.e., remove spaces, decimal points, and so on. The required CMC data files were reformatted and compacted reducing the size from 192k bytes to 60k bytes, this resulted in a reduction in transmission time, at 1200 baud, from 33 min to 10 min.

In the CASP experiment, surface wind files (at $\sigma = 0.998$) were created on the front-end Cyber computer at CMC using internal procedure software called PGSN. The PGSN provided the gridded wind U and V components on the ODGP coarse and fine grids using a processing program developed at CMC for this application.

The CASP wind files were packed and transmitted via DATAPAC/TYMNET to an IBM PC compatible computer followed by transmission to a VAX 11/750 where the ODGP wave model resides. Subsequently, these files were unpacked and were used to drive the wave model.

3.3 OPERATIONAL DIFFICULTIES

The operational CASP wave forecast system functioned nominally for about 70% of the runs made between 1200 GMT on 15 January, and 0000 GMT on 15 March. The remaining 30% of the runs were afflicted by one or more anomalies, which in the least caused delay in the transmission of the forecast to the CASP desk, and in the most extreme caused a total interruption of the analysis-forecast cycle, thereby requiring the system be restored.

Table 1 provides a concise summary of the occurrence of anomalies of various kinds. The most common difficulty was the receipt of the wind field so late in the cycle that the OGDP-OPR run was made first, thereby causing a delay of at least 3 h in the CASP run. The most common cause of late access to the wind file was simply the difficulty often encountered in gaining access to the CMC computer system. Transmission difficulties were surprisingly rare.

A particularly troublesome condition was the failure to obtain the CMC wind file before it was overwritten at CMC by the files created in the succeeding analysis-forecast cycle. In most such instances it was possible to maintain continuity of the wave analysis file at least by substituting appropriate forecast wind fields from previous runs for needed analysis fields. Where several successive CMC wind files failed to be accessed, however, a complete restart of the analysis from flat-calm initial conditions are necessary.

TABLE 1

Log of conditions encountered in the CASP operational forecasting

Month	Run Day	Hour	Condition* 1	2	3	4	5	6	7	8
JAN	15	1200	X							
	16	0000	X							
		1200	X							
	17	0000		X			X			
		1200					X			
	18	0000					X			
		1200					X			
	19	0000					X			
		1200					X			
	20	0000	X							
		1200	X							
	21	0000		X			X			
		1200					X			
	22	0000					X			
		1200					X			
	23	0000	X							
		1200	X							
	24	0000			X		X			
		1200	X							
	25	0000	X							
		1200	X							
	26	0000	X							
		1200	X							
	27	0000	X							
		1200	X							
	28	0000	X							
		1200	X							
	29	0000	X							
		1200	X							
	30	0000	X							
		1200				X	X			
	31	0000	X							
		1200		X			X			
FEB	1	0000	X							
		1200	X							
	2	0000					X			
		1200			X		X			
	3	0000	X							
		1200	X							
	4	0000	X							
		1200	X							
	5	0000	X							
		1200	X							

Table 1 continued

Run			Condition*							
Month	Day	Hour	1	2	3	4	5	6	7	8
	6	0000	X							
		1200	X							
	7	0000	X							
		1200	X							
FEB	8	0000	X							
		1200	X							
	9	0000	X							
		1200	X							
	10	0000	X							
		1200					X			
	11	0000	X							
		1200		X			X			
	12	0000	X							
		1200	X							
	13	0000	X							
		1200	X							
	14	0000	X							
		1200	X							
	15	0000	X							
		1200	X							
	16	0000	X							
		1200	X							
	17	0000	X							
		1200	X							
	18	0000	X							
		1200	X							
	19	0000			X		X			
		1200		X			X			
	20	0000	X							
		1200					X			
	21	0000		X			X			
		1200					X			
	22	0000	X							
		1200	X							
	23	0000	X							
		1200		X				X	X	
	24	0000		X				X	X	
		1200		X			X			
	25	0000		X			X			
		1200		X			X			
	26	0000	X							
		1200	X							
	27	0000	X							
		1200	X							
	28	0000	X							
		1200	X							

Table 1 Continued

Month	Run Day	Hour	Condition* 1	2	3	4	5	6	7	8
MAR	1	0000	X							
		1200				X			X	
	2	0000						X	X	
		1200					X			
	3	0000	X							
		1200	X							
	4	0000	X							
		1200	X							
	5	0000	X							
		1200	X							
	6	0000	X							
		1200	X							
	7	0000	X							
		1200	X							
	8	0000	X							
		1200						X		
	9	0000						X		
		1200					X			X
	10	0000	X							
		1200					X			
	11	0000		X			X			
		1200					X			
	12	0000		X			X			
		1200					X			
	13	0000	X							
		1200	X							
	14	0000	X							
		1200	X							
	15	0000	X							

*Conditions:
1 - Nominal.
2 - Difficulty logging on CMC system.
3 - Late wind file creation at CMC.
4 - Difficulty in transmission of wind file.
5 - Late receipt of wind file - run ODGP/OPR first.
6 - Computer failed to access CMC wind file.
7 - Synthesize CMC analysis file from previous forecast field.
8 - Failed to receive wind files on successive basis and started wave model from zero initial wave state.

4. DATA GATHERING AND PROCESSING

4.1 DATA SOURCES

The particular parameters considered are wind speed and direction, air and sea temperatures, significant wave height, peak period, wave direction, and wave spectra. The model was run with two different input winds, as described in Section 2, and the model products, as well as the input winds, are compared with observed data for various locations off the Canadian and U.S. east coasts. The significant wave heights obtained from the METOC wave charts are added for additional comparison.

A large amount of data was collected during the CASP field experiment. Field data were collected from several sources and different organizations, some of which were directly involved in the CASP (e.g., BIO) and others have indirectly gathered data for other operational purposes (e.g., offshore operators). Data used in this study were obtained from four sources.

1. Offshore drilling rigs: Marine observations (MANMAR Logs) and Waverider buoy measurements obtained from Shell Canada Resources (Sedco 709 and John Shaw rigs on the Scotian Shelf), Petro-Canada (Rowan Gorilla at Cohasset on the Scotian Shelf and SDS Vinland at Terra Nova on the Grand Banks) and Husky Bow Valley (Bowdrill 2 at Whiterose and Sedco 710 at North Ben Nevis on the Grand Banks).

2. NOAA buoy data: Meteorological and spectral wave data were obtained from the National Oceanographic and Atmospheric Administration, National Oceanographic Data Centre (NODC), Washington, D.C., which includes data from NOAA buoys 44004 and 44011 off the east coast of the USA.

3. BIO CASP-OC data: include 3 directional (WAVEC) and 6 waverider (heave) buoys and a meteorological (Minimet) buoy at the end of CASP-OC wave array.

4. METOC wave charts: The manually drawn charts of significant wave height produced at the METOC Centre, Halifax, N.S., were obtained and subsequently the wave heights at the evaluation sites were picked-up from these charts. The charts are produced using SMB type techniques as well as analyses of observed wave heights at T=0 (Morgan (1971)).

The above data were provided in different formats on different computers. Therefore, an extensive amount of data processing, quality checks and reformatting was required to create a unified data base that could easily be accessed and implemented as described in the following sections. This data base contains data files (observed or model results) written in same "standard" format, so called "MASTER DATA FILE" format (see Appendix B).

4.2 THE STUDY AREA

The study was conducted over a large area including portions of Georges Bank, the Scotian Shelf, and the Grand Banks of Newfoundland during the period 15 January to 15 March, 1986. Figure 5 depicts the study area and shows the relative positions of model grid points and evaluation sites selected for the study.

Region 1 is off the U.S. east coast with one of the sites on Georges Bank. Region 2 is on the Scotian Shelf near Sable Island. Region 3 is on the Grand Banks east of Newfoundland. Region 4 (CASP-OC area) consists of three nearshore locations at which the ODGP-CMC shallow- water model results were compared with BIO wave measurements. Complete descriptions of the various sites within each region are given in succeeding sections.

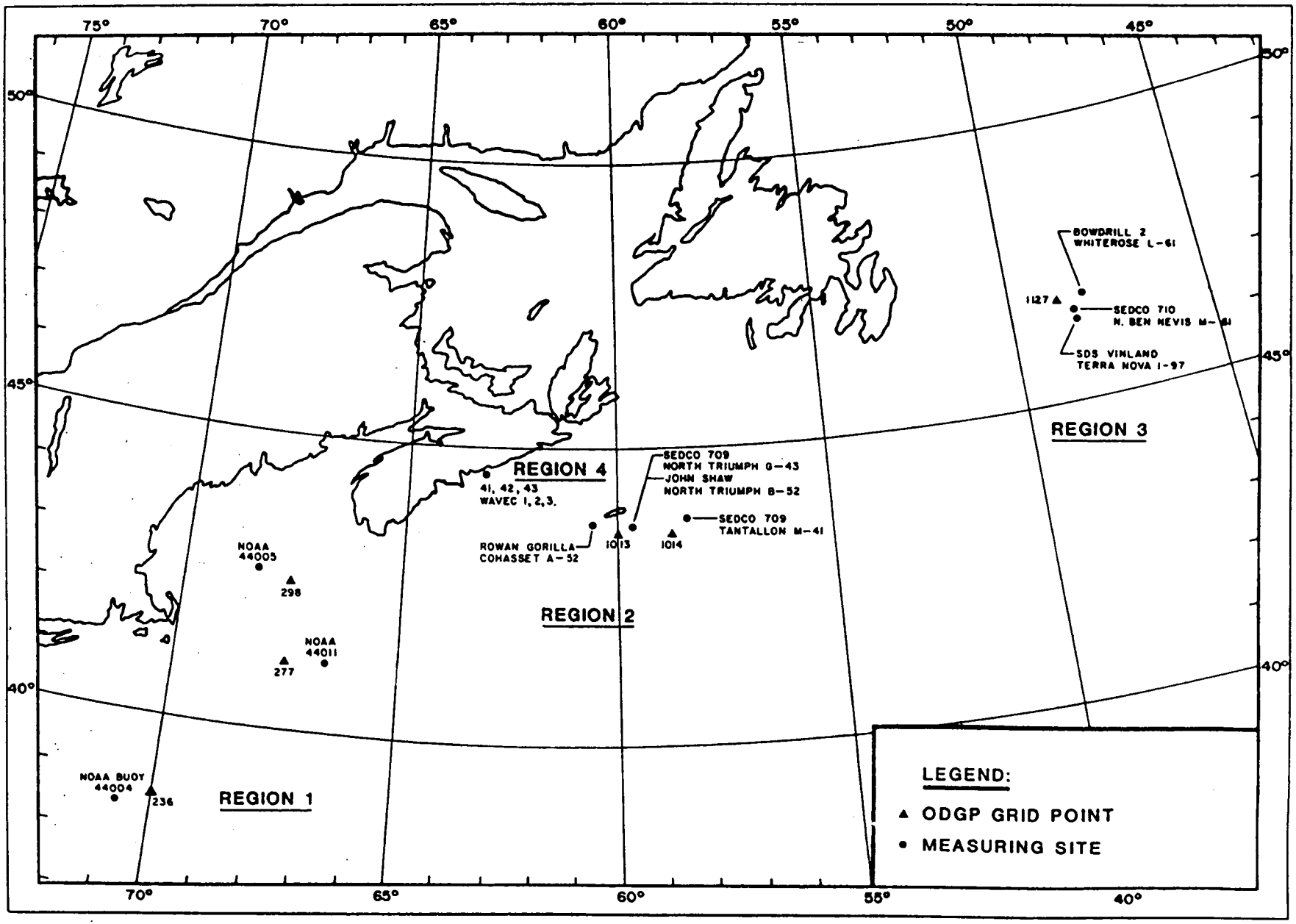

Figure 5. The CASP Study Area

4.3 FIELD MEASUREMENTS - DATA BASE

Many measured wind and wave data were obtained from various sources which are described in the subsections below. The locations of the data sites are depicted in Figure 5; the time periods over which the data are available are summarized in Table 2; and a description of each data site is given in Table 3.

4.3.1 MANMAR Data

Wind speed and direction, air and surface water temperatures, and significant wave height records were obtained from various rigs observation (MANMAR) logs at the Scotian Shelf and Grand Banks sites. The data were recorded every 3 h during the periods indicated in Table 2. Winds were measured at anemometer heights given in Table 4.

4.3.2 Waverider Buoy Data

Wave parameters were measured by waverider buoys moored in the vicinity of the particular rigs at those sites indicated in Table 2. Data from each waverider buoy were telemetered to a digital waverider receiver located on a particular rig and were subsequently analysed to produce significant wave height, peak period, and spectral density values. The data were telemetered every 3 h on or near the synoptic hour (i.e. 0000, 0300, 0600, ..., 2100 GMT) or every 20 min if wave height exceeded 4 m or if wind exceeded 34 knots, or both. The spectral density values extend from 0.055 Hz to 0.500 Hz in equal increments of 0.005 Hz.

The Waverider data from site 31b were not incorporated into the time series, scatter plots, or statistics. On the one hand, the data were received after this work has been completed. On the other hand, comparison of the waverider data, in time series forms with MANMAR observations, shows

TABLE 2
Model Output and Wind-Wave Evaluation Data

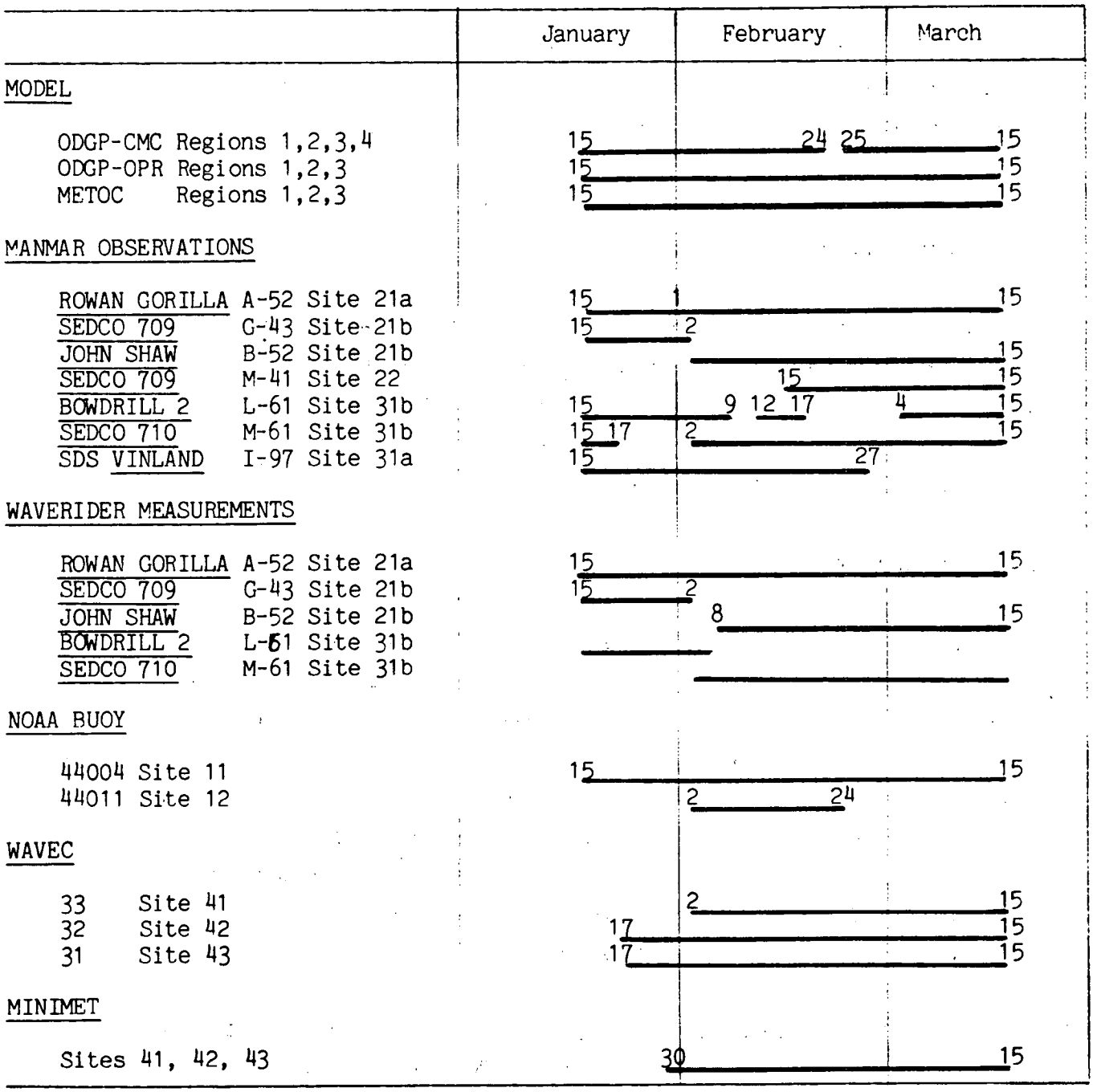

TABLE 3
Evaluation Sites

Site (m)	Location	Water Depth	ODGP Grid Point	Available Parameters	Data Source No.
11	38°31'N 70°42'W	2834	236	Wind, wave spectra, air & sea temp.	NOAA 44004
12	41°04'N 66°34'W	85	277	Wind, wave spectra, air & sea temp.	NOAA 44011
21a	43°51'N 60°38'W	40	1013	Wind, wave spectra, air & sea temp.	MANMAR/Waverider: R. GORILLA at Cohasset A-52.
21b	43°41'N 59°53'W	105	1013	Wind, wave spectra, air & sea temp.	MANMAR/Waverider: SEDCO 709 and JOHN SHAW at N. Triumph B-52
22	43°51'N 58°22'W	1516	1014	Wind, wave spectra, air & sea temp.	MANMAR: SEDCO 709 at Tantallon M-41
31a	46°27'N 48°29'W	97	1127	Wind, wave spectra, air & sea temp.	MANMAR: SDS VINLAND at Terra Nova I-97
31b	46 41'N 48°25'W 46°51'N 48°10'W	98 117	1127	Wind, wave spectra, air & sea temp.	MANMAR: SEDCO 710 at N. Ben Nevis M-61 BOWDRILL 2 at Whiterose L-61
41	44°27'N 63°01'W	100	SW14	2-D spectra, wind speed, direction	WAVEC #33/Minimet[a]
42	44°34'N 63°05'W	50	SW 7	2-D spectra, wind speed, direction	WAVEC #32/Minimet
43	44°39'N 63°08'W	25	SW 2	2-D spectra, wind speed, direction	WAVEC #31/Minimet

[a] One MINIMET buoy was deployed at 44°28'N, 63°00' W.

TABLE 4

Anemometer Heights

Site No.	Data Source	Anemometer Height (m)
11	NOAA BUOY 44004	10
12	NOAA BUOY 44011	10
21a	ROWAN GORILLA	88
21b	SEDCO 709	17
	JOHN SHAW	73
22	SEDCO 709	17
31a	SDS VINLAND	83
31b	BOWDRILL 2	82
	SEDCO 710	78
41	MINIMET	3

that there is no significant difference between the two sets of values. This result is to be expected because it is the usual practice of observers on rigs to incorporate available waverider data directly into the MANMAR logs.

4.3.3 NOAA Buoy Data

The wind and wave records were obtained from two NOAA buoys deployed off the U.S. east coast, one (44004) in deep water off the continental shelf and the other (44011) on Georges Bank. Both meteorological data and wave parameters were recorded at 1-h intervals over the periods indicated in Table 2. Meteorological data includes wind speed and direction, air temperature, and sea surface temperature. Wave parameters include significant wave height, peak period, and spectral density values. Spectral density values are provided in 48 bands extending from 0.03 Hz to 0.5 Hz in equal increments of 0.01 Hz.

4.3.4 BIO Data

WAVEC buoy data. Three WAVEC Buoys, which provide directional wave parameters, were deployed in a line nearshore, as depicted in Figure 6. In addition, six waverider (heave) buoys were deployed in CASP-OC area (see Figure 6). The data recorded by these waverider buoys were not used directly in the evaluation of the wave model results, but were used to check the results of WAVEC records.

The WAVEC sensor measures vertical acceleration (heave) as well as pitch and roll angles and the local Earth's magnetic field components. The elevation, north-south slope and east-west slope of the water surface are derived from these measurements. This calculation, as well as an initial error detection on signal transmission quality and orientation changes are performed by the microprocessor in a DIREC receiver at a shore station. From these data the DIREC calculates nine values of co- and quadrature spectral (C and Q) estimates denoted by:

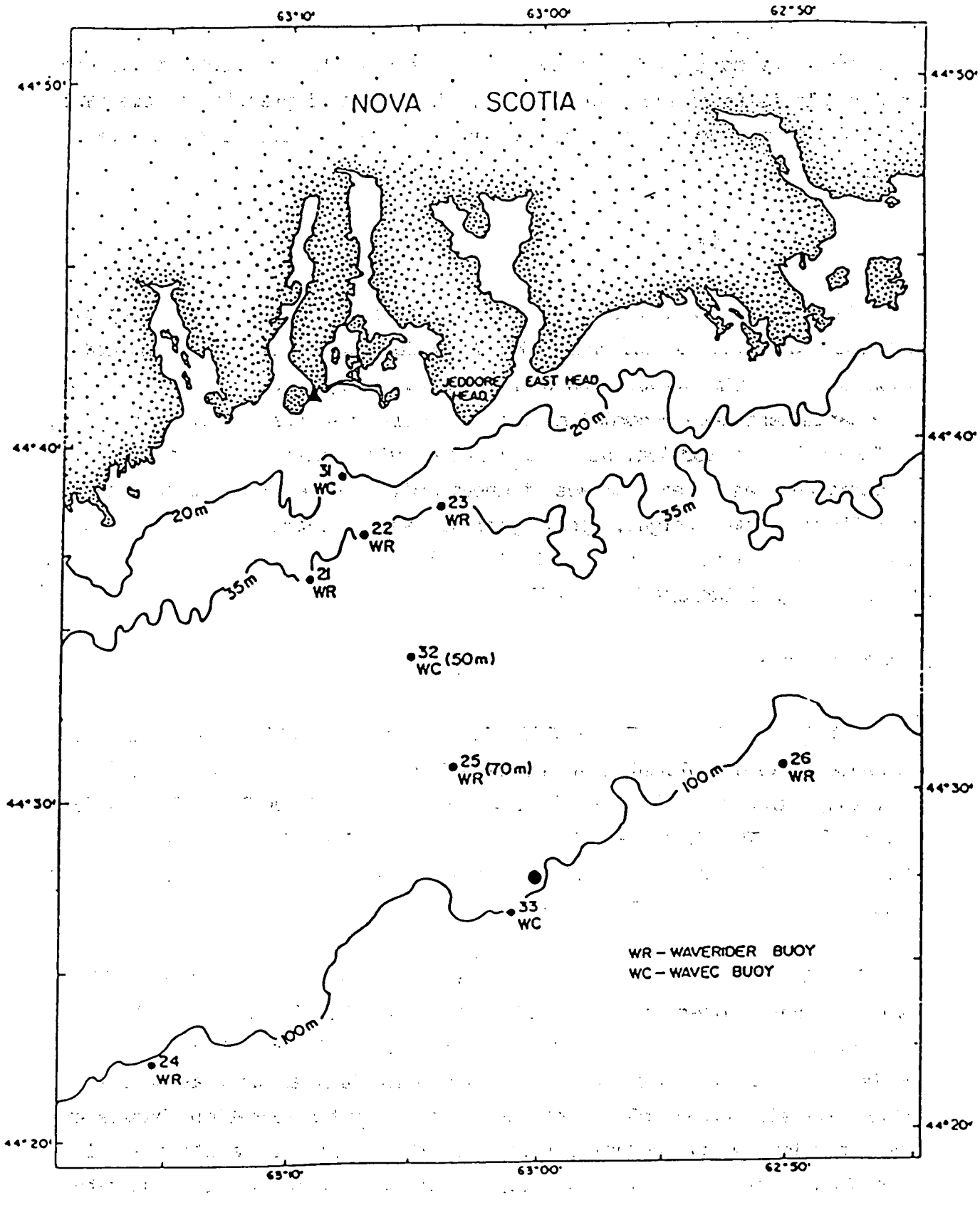

Figure 6. The BIO CASP-OC Wave array

CVV	CVN	QVN
CNN	CVW	QVW
CWW	CNW	QNW

where V = heave, N = slope north and W = slope west. Subsequent processing of the co-and quadrature spectral values to produce a two-dimensional energy spectra is described in subsection 4.4.4.

The nine spectral estimates are provided at 128 frequency bands extending from 0.00 Hz to 0.64 Hz in equal increments of 0.005 Hz. A block of data, consisting of 256 samples is collected every 200, and usually nine or 10 blocks are used to calculate the spectral values. The nine spectral values obtained in this way are provided at 1-h intervals over the periods indicated in Table 2.

Minimet buoy data. A minimet buoy providing meteorological data was deployed at the end of the Wave array at the position shown in Figure 6 The meteorological data collected included wind speed, wind direction, and sea temperature. Air temperature was not available because of instrument malfunction. Further, because of compass misalignment, the wind direction was in error by some 15 to 20 degrees, which was corrected in the post processing of the data. Wind measurements were taken at 3 m above sea level.

4.4 DATA-BASE PROCESSING

4.4.1 Quality Checks

All measured data were examined for out-of-range values by comparing suspicious values with corresponding values at nearly sites or by comparing two sources of observations from the same site. Values that were clearly out of range were deleted.

4.4.2 Wind Reduction

Wind was measured at various heights at the various sites as reported in Table 3. All observed winds, with the exception of the Minimet data, were reduced to a 19.5 m neutral wind, by using the procedure described by Cardone (1969 and 1978), see also MacLaren Plansearch Limited (1985).

4,4.3 Combining and Reformatting Observed Data

For each site, all available measured data were combined into a single time history which covers the two months CASP period. If both MANMAR and waverider data were available, priority was given to the latter. For example, at site 21a, MANMAR observations of wind speed and direction from the SEDCO 709 and JOHN SHAW were combined. To these observations were added waverider measurements of significant wave height and peak period (see Table 3). It should be noted that MANMAR observations do not include peak period. Therefore, if a waverider buoy was not deployed near a rig, peak period is missing, as was the case for sites 31a and 31b. The combined data were put into "Master Data File" format which was required by the evaluation software. A description of the Master Data File format is given in Appendix B.

4.4.4 Spectral Density Frequency Reduction

The ODGP model produces a two-dimensional energy spectrum in 15 unequal frequency bands and 24 equally spaced angles, and a one-dimensional energy spectrum in the same 15 frequency bands. The WAVECs, waverider, and NOAA buoys produced spectral values to a finer frequency resolution (i.e., 128, 90, and 48 frequency bands respectively). Thus, to

compare measured and model spectra on the same basis, it was necessary to reduce the observed data to 15 frequency bands with bandwidths and nominal frequencies that correspond closely to the ODGP values (Table 5).

In each case the reduction to 15 frequency bands was done so as to preserve the significant wave height as calculated from the original high-resolution data. The data in Table 6 describe the reduced frequency bands for the WAVEC and waverider buoys and show which of the original frequency bands were combined to produce each of the new 15 frequency bands. Of the 128 frequency bands provided by the WAVECs, only 75 bands have been used. Bands 1 through 5 and 81 through 128 have been discarded because for those frequencies, spectral values could not be distinguished from the background noise.

The NOAA buoy spectral data were reduced to 12 frequency bands (Table 7). In this case, only 12 bands could be defined because the first seven ODGP bands have a bandwidth of 0.006 Hz as compared with the constant NOAA buoy bandwidth of 0.01 Hz.

Although significant wave height (or equivalently the area under the spectral density curve) has been preserved in the reduction process, the higher degree of resolution of the original information has been lost. Two examples of the loss of resolution are given in Figure 7.

4.4.5 Two-Dimensional Spectral Estimates

The reduction of the co- and quadrature (C-Q) spectral estimates to produce two-dimensional power density estimates is accomplished using a method described by Long (1980). A computer program developed at BIO was modified and used for this purpose. Other wave parameters readily available from the co- and quadrature spectral estimates include one-dimensional energy spectra, significant wave height, mean period, peak period, mean direction, and peak direction.

TABLE 5

The 15 ODGP Frequency Bands

Band	Nominal Frequency (Hz)		Bandwidth (Hz)
1	7.285/180	= 0.0405	0.43/180
2	16/360	0.04444	1/180
3	18/360	0.05000	1/180
4	20/360	0.05556	1/180
5	22/360	0.06111	1/180
6	24/360	0.06667	1/180
7	26/360	0.07222	1/180
8	29/360	0.08056	1/ 90
9	33/360	0.09167	1/ 90
10	37/360	0.10278	1/ 90
11	42/360	0.11667	1/ 60
12	48/360	0.13333	1/ 60
13	57/360	0.15833	1/ 30
14	75/360	0.20833	1/ 15
15	111/360	0.30833	2/ 15

TABLE 6

Reduced WAVEC and Waverider Frequency Bands

New Band No.	Nominal Frequency (Hz)	Bandwidth (Hz)	Waverider Bands	WAVEC Bands
1	14.4/360 = .04	.9/180 = .005		6,7,8
2	16.2/360 = .045	.9/180 = .005		9
3	18/360 = .05	.9/180 = .005		10
4	19.89/360 = .05525	.99/180 = .0055	1	11
5	21.87/360 = .06075	.99/180 = .0055	2	12
6	23.94/360 = .0665	1.08/180 = .006	3	13
7	26.1/360 = .0725	1.08/180 = .006	4,5	14,15
8	29.178/360 = .08105	.999/90 = .0111	6,7	16,17
9	33.174/360 = .09215	.999/90 = .0111	8,9	18,19
10	37.17/360 = .10325	.999/90 = .0111	10,11	20,21
11	42.048/360 = .1168	.96/60 = .016	12-14	22-24
12	47.91/360 = .1331	.996/60 = .0166	15-18	25-28
13	56.898/360 = .15805	.999/30 = .0333	19-24	29-34
14	74.88/360 = .208	.999/15 = .0666	25-38	35-48
15	110.862/360 = .30795	1.9995/15 = .1333	39-90	49-80

TABLE 7

Reduced NOAA Buoy Frequency Bands

New Band No.	Nominal Frequency (Hz)	Bandwidth (Hz)	WAVEC Bands
1	13.5/360 = .0375	.01	1,2
2	17.1/360 = .0475	.01	3
3	20.88/360 = .058	.011	4
4	25.02/360 = .0695	.012	5
5	29.178/360 = .08105	.0111	6
6	33.174/360 = .09215	.0111	7
7	37.17/360 = .10325	.0111	8
8	42.048/360 = .1168	.016	9-10
9	47.91/360 = .1331	.0166	11-12
10	56.898/360 = .15805	.0333	13-15
11	74.88/360 = .208	.0666	16-22
12	110.862/360 = .30745	.1333	23-48

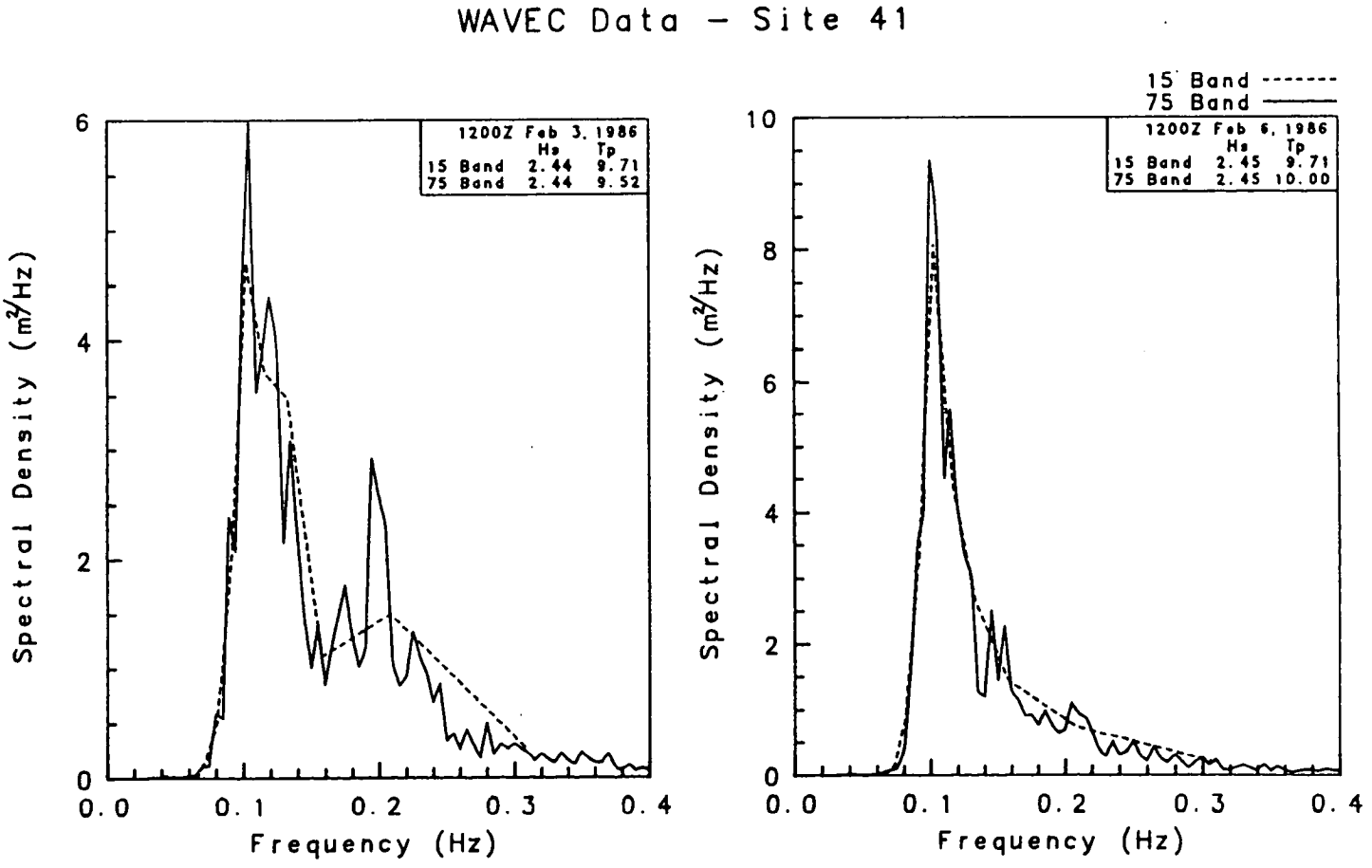

Figure 7. Comparison of 15- and 75- band spectra (WAVEC data, site 41).

4.5 WAVE MODEL RESULTS

4.5.1 Selection of Model Evaluation Sites

The ODGP model grid points at which model products are provided (see Figure 5) are further identified in Table 8. The selection of these particular grid points was based on several factors which include covering a large portion of the CASP study region and proximity to those measuring sites that produced a significant quantity of data.

The ODGP-CMC and ODGP-OPR model predictions at the selected grid points were compared to the observed wind-wave data at the corresponding sites in each region (see Table 3).

Only four METOC sites were selected because it is not the purpose to evaluate the METOC model per se, but only to provide additional comparison with the ODGP model products at a few selected deep-water sites.

4.5.2 Reformatting the Model Product

A time series of the ODGP model input wind and wave products for each site was put into the Master Data File Format as previously described. For the METOC predictions, only significant wave height is available for analysis time and for 12-, 24- and 36-h prognostic times. The CMC winds were not reduced to 19.5-m neutral winds because they already contain some boundry layer physics which may be upset by further reductions, whereas the operational winds used to run the ODGP-OPR are the 19.5-m neutral winds (see subsection 2.3).

These data are compiled and written on a nine-track tape for ESRF, and are used for models evaluation as described in Section 5.

TABLE 8

Model Grid Point Identification

Model	Region	Grid Point	Latitude (n)	Longitude (W)
ODGP-CMC/OPR	1 - U.S. east coast	236	38°45'	70°00'
	(Georges Bank)	277	41°15'	67°30'
	2 - Scotian Shelf	1013	43°45'	60°00'
		1014	43°45'	58°45'
	3 - Grand Banks	1127	46°53'	48°45'
ODGP-CMC	4 - shallow water	2	44°57'	62°50'
		7	44°51'	62°46'
		14	44°41'	62°51'
METOC	1 - U.S. east coast	277	41°15'	66°30'
	2 - Scotian Shelf	1013	43°45'	60°00'
		1014	44°00'	58°24'
	3 - Grand Banks	1127	46°30'	48°30'

5. EVALUATION OF MODEL PREDICTIONS

5.1 EVALUATION PROCEDURES

The following procedures are used to evaluate the model wave forecasts for the 15 January to 15 March study period.

1. Time series plots of forecasts vs. observed parameters. Time series of wind speed, wind direction, significant wave height, and peak wave period are plotted against corresponding observed values (when available) at each evaluation site, and for each forecast (lead) time. For the ODGP model, wind and wave parameters are plotted for lead times of 0, 12, 24, 36, and 48 h. For the METOC model, the only product is significant wave height and the lead times are 0, 12, 24, and 36 h. These plots provide excellent qualitative comparisons of the forecast and observed parameters. They are shown in Appendices C and D.

2. Statistical comparison of wind and wave forecasts vs. observations. A quantitative statistical analysis is carried out to provide an evaluation of the forecast surface winds and resulting model products. The statistical parameters considered in this study are:

Mean error (bias)	=	$\sum (x_1-x_2)/NPTS$
Mean absolute error	=	$\sum \lvert(x_1-x_2)\rvert/NPTS$
Root mean square error (RMSE)	=	$(\sum (x_1-x_2)^2/NPTS)^{1/2}$
Scatter index (SI)	=	(RMSE/AVE) x 100

where: x_1 = the model value (i.e., forecast)
x_2 = the observed value
AVE = the mean of observed values
NPTS = the number of data pairs.

For each model and for each forecast time, the above parameters are calculated for:

- each site individually - the entire CASP period
- each region - the entire CASP period
- regions 1, 2, and 3 combined - the entire CASP period
- regions 1, 2, and 3 combined - the four storm events combined.

The results of the above analysis are presented in Appendices C and D.

3. Linear regression and scatter diagrams. Scatter diagrams of the model wind speeds, predicted wave heights, and wave periods versus the corresponding observed data are produced as shown in Appendices C and D. In addition linear least-square regression is carried out and the regression lines are plotted on the scatter diagrams. The number of data points used in the scatterregression calculation is shown on each plot together with the correlation coefficient.

The linear regression equation used in this study is:

$$x_2 = a + bx_1$$

where: x_1 = predicted (model) values

x_2 = observed values

a = intercept with the vertical (x_2) axis and is a measure of the bias in model predictions

b = slope of the regression line (the closer to 1.0 the better are the model predictions).

The correlation coefficient (r), which is a measure of the degree of linear relationship between x_1 and x_2 is computed as follows:

$$r = SS_{xy}/(SS_x\ SS_y)^{1/2}$$

where: $$SS_x = \sum_{i=1}^{n} (x_i - \bar{x})^2$$

$$SS_y = \sum_{i=1}^{n} (y_i - \bar{y})^2$$

$$SS_{xy} = \sum_{i=1}^{n} (x_i - \bar{x})\ (y_i - \bar{y})$$

where: $x = x_1$ and $y = x_2$

4. One-dimensional spectral density plot comparison. The model spectra for analysis time only are plotted against the calculated spectra from the waverider buoy's measurements for a number of selected times during each storm event. Four times are singled out per storm; the first during the generation stage, two near the peak and one during the decay stage. The comparative spectral plots are shown in Appendix E.

5. Two-dimensional spectral density calculation and time series plots of wave directions. Directional wave measurements were available from the BIO's WAVEC buoys at three sites along the CASP-OC line along which the ODGP-CMC shallow water model was run. Two-dimensional contour plots, representing lines of constant power spectra as a function of frequency and direction can be obtained from BIO (Bash Toulany) and will be published by BIO in the near future. A full presentation and comparisons of the 2-D spectral plots is beyond the scope of this work, however, only the

calculated average and peak directions from ODGP-CMC and WAVEC records are presented in a form of time-series plots as shown in subsection 5.5.

NOTE: Peak direction is the direction of maximum wave energy, i.e., corresponding to maximum $S(f,\theta)$. Average wave direction is the vector average.

The results obtained from the evaluation of the ODGP-OPR, ODGP-CMC and METOC are presented in three Sections:

1. Deep-water model results for entire CASP period;
2. Shallow-water model results for entire CASP period; and
3. Storm study cases.

5.2 DEEP-WATER MODEL EVALUATION - THE ENTIRE CASP PERIOD

Time-series plots of wind and wave parameters, scatter diagrams and error statistics are presented in Appendix C. Summaries of the evaluation results are presented and discussed below.

1. Regions 1, 2, and 3 Combined. Examination of the bias figures in Table 9 for wind speed show that in general the operational wind model underpredicts wind speed whereas the CMC wind model overpredicts wind speed. The remaining wind speed error statistics (e.g. RMSE and SI) show no significant difference between the two wind models. The largest disparity occurs at analysis time. On the other hand, the wave height error statistics show a marked difference. The RMSE, SI, and absolute error for the ODGP-CMC model are in the order of twice as large as those for the ODGP-OPR model, and can be seen graphically in Figure 8. The overestimation of significant wave heights by ODGP-CMC model is mainly because of the large positive bias in CMC wind speed.

The regression statistics for wind speed and wave height show the same tendency as do the error statistics, (Table 10).

The error statistics for peak period for the two models are relatively close, with the OPR model again showing slightly better results. Both models have surprisingly low error statistics for peak period in view of the fact that the regression statistics show poor correlation and a regression line with a shallow slope.

The METOC analysis shows good skill on the whole in predicting significant wave height particularly at analysis time; but not as good as the ODGP-OPR model forecasts. This result is not unexpected for the analysis results as the METOC predictions at T_0 are essentially based on actual wave measurements.

2. Regions 1, 2 and 3 Individually. Table 11 summarizes the scatter index for regions 1, 2, and 3 individually for each prog time. the patterns detected in this particular statistic are supported by the remaining statistics for the three regions individually (see Appendix C). In addition, figures 9, 19 and 11 represent a summary of error statistics for wind speed and wave height in each region as a function of projection time. Figure 12 shows error statistics by region at analysis time (T = 0).

The following points are noted:

1) At analysis time, the ODGP-CMC and ODGP-OPR predictions (both winds and waves) are in close agreement at region 1, and differ significantly in regions 2 and 3 with the largest difference in region 3 (see Figure 12). The relative error is H_S is larger than that in wind speed, perhaps because of contributions from non-local wind field errors. For the ODGP-CMC model, the RMSE and SI deteriorate rapidly when moving from region 1 to region 3 and is graphically illustrated in Figures 9 to 12.

2) For region 1, as shown in Figure 9, the wind speed SI for both OPR and CMC models are in close agreement at analysis time and grow slowly with time, with slightly faster growth for the CMC. The wave height

TABLE 9

Error Statistics For Regions 1, 2, And 3 Combined

Prog. time (h)	Model	Wind Speed RMSE[1] (kts)	SI[2] (%)	Bias (kts)	Abs.Er[3] (kts)	Signigicant Wave Height RMSE (m)	SI (%)	Bias (m)	Abs.Er. (m)	Peak Period RMSE (s)	SI (%)	Bias (s)	Abs.Er. (s)
00	OPR	5.89	28	-1.26	4.54	0.85	30	0.23	0.65	1.94	22	-0.36	1.49
	CMC	7.59	36	0.91	5.74	1.88	65	1.02	1.33	2.05	24	0.49	2.05
	METOC					0.83	28	0.28	0.62				
12	OPR	7.22	35	-0.45	5.58	0.92	32	0.26	0.70	1.95	22	-0.39	1.49
	CMC	8.17	39	2.09	6.09	1.91	66	1.10	1.37	2.04	24	0.60	1.56
	METOC					1.20	41	0.34	0.88				
24	OPR	7.93	38	-0.45	6.16	0.98	34	0.24	0.74	1.95	22	-0.38	1.51
	CMC	8.55	41	2.54	6.40	1.96	69	1.19	1.43	2.19	25	0.72	1.65
	METOC					1.15	39	0.25	0.89				
36	OPR	8.39	40	-0.88	6.59	1.06	37	0.19	0.80	2.10	24	-0.39	1.62
	CMC	9.32	45	2.50	7.00	1.97	70	1.21	1.46	2.38	27	0.92	1.75
	METOC					1.23	42	0.21	0.95				
48	OPR	9.25	44	-1.06	7.23	1.07	37	0.14	0.84	2.14	25	-0.36	1.67
	CMC	9.71	47	2.88	7.47	1.97	70	1.18	1.47	2.47	28	0.95	1.84

[1] root mean square error
[2] Scatter index
[3] Absolute error
OPR = ODGP-OPR model
CMC = ODGP-CMC model

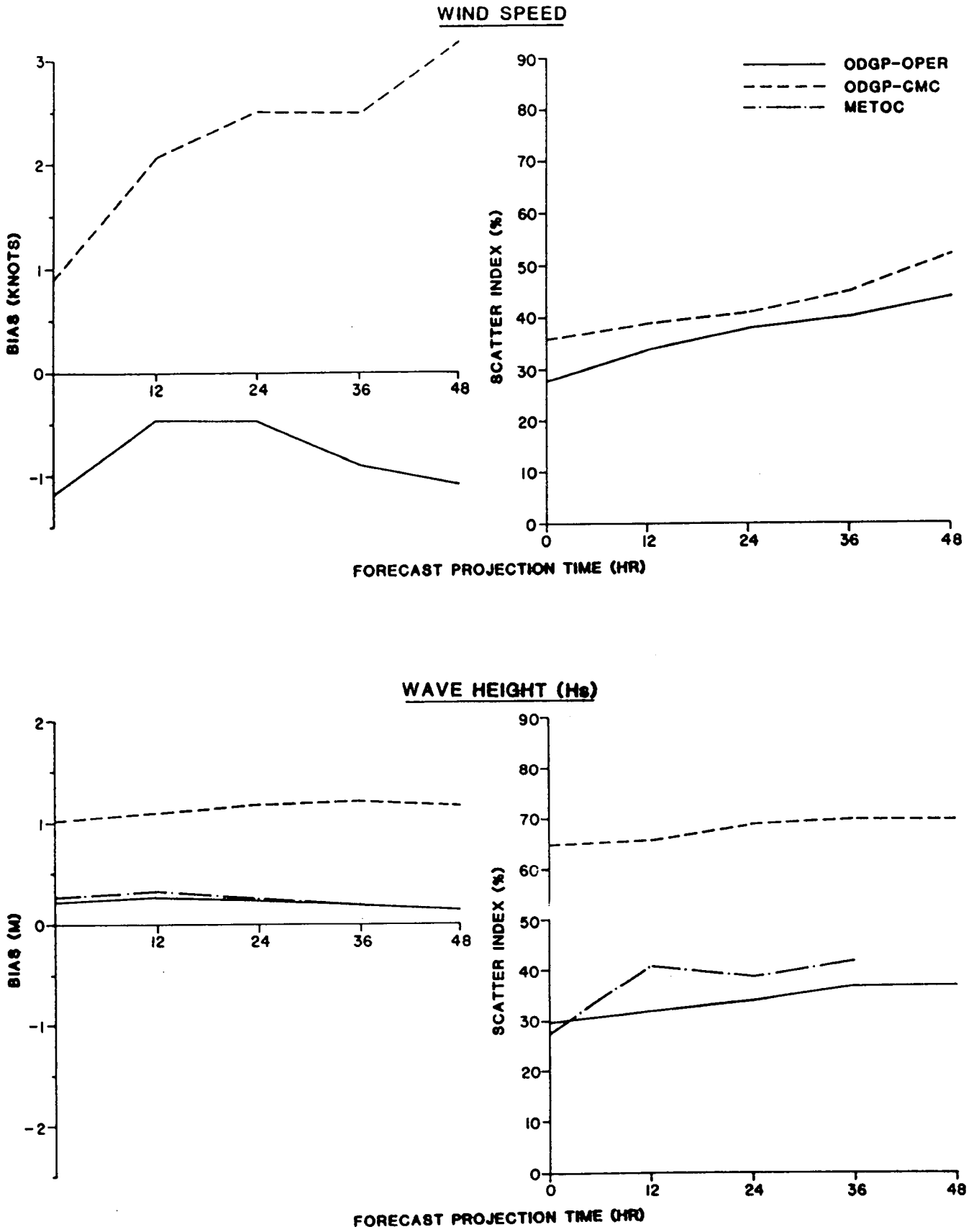

Figure 8. Error statistics for Regions 1, 2, and 3 combined.

TABLE 10

Regression Statistics For Regions 1, 2, And 3 Combined

Prog. Time (h)	Model	Wind Speed				Significant Wave Height				Wave Period			
		Slope[1]	Int.[2]	r[3]	N[4]	Slope	Int.	r	N	Slope	Int.	r	N
00	OPR	0.90	3.31	0.81	1312	0.78	0.44	0.81	1344	0.64	3.33	0.55	787
	CMC	0.66	6.44	0.71	1268	0.41	1.28	0.64	1299	0.54	3.69	0.57	762
	METOC					0.82	0.30	0.83	537				
12	OPR	0.77	5.10	0.69	1312	0.74	0.56	0.79	1344	0.64	3.56	0.55	787
	CMC	0.63	6.47	0.70	1270	0.42	1.22	0.65	1299	0.56	3.50	0.59	762
	METOC					0.63	0.88	0.61	543				
24	OPR	0.71	6.44	0.62	1312	0.70	0.71	0.76	1344	0.63	3.48	0.56	787
	CMC	0.61	6.49	0.67	1268	0.42	1.16	0.66	1295	0.53	3.74	0.57	760
	METOC					0.66	0.84	0.62	553				
36	OPR	0.66	7.75	0.58	1312	0.65	0.87	0.72	1344	0.55	4.17	0.49	787
	CMC	0.55	8.02	0.60	1260	0.41	1.16	0.66	1285	0.49	3.98	0.54	754
	METOC					0.60	1.05	0.56	553				
48	OPR	0.55	9.92	0.48	1312	0.65	0.91	0.69	1344	0.52	4.39	0.48	787
	CMC	0.51	8.46	0.56	1228	0.40	1.22	0.64	1275	0.46	4.29	0.51	748

[1] Slope of regression line.
[2] Intercept of regression line with vertical axis.
[3] Correlation coefficient.
[4] Number of data points.

SI between ODGP-OPR, ODGP-CMC, and METOC are similar except at analysis time where METOC wave errors are significantly lower. The METOC wave errors are also lower here than at other regions. The most likely explanation is the availability to METOC in real-time of significant wave height measurements from the NOAA buoy. The METOC analysis can therefore be readily forced into close agreement with the measured data. Wave height measurements are not referred to in the wave-model-based analysis.

3) For region 2, (see Figure 10), the trend of relative wind speed errors between ODGP-OPR and ODGP-CMC is different from that of region 1, with OPR in better agreement with observations than CMC at analysis time, but with little difference between the series at all forecast times. However, the wave height errors for ODGP-CMC are much greater than ODGP-OPR which suggest that non-local random and perhaps spatially coherent wind errors in the CMC winds primarily contribute to the observed wave error (see wind fields of the selected storm cases in Appendix F). The ODGP-OPR wave errors are slightly lower than the METOC wave height errors at analysis and all forecast times.

4) Region 3 shows yet a different kind of behaviour. In this case the SI and RMSE for both wind speed and wave height for the ODGP-OPR are significantly lower than the corresponding values for the ODGP-CMC (Figure 11). In particular, RMSE and SI for wave height differ by a factor greater than two. This difference is caused by combined local and non-local errors in the CMC wind field. Again the ODGP-OPR model predictions are comparable to those predicted by METOC at analysis time, but with higher skill in forecasting wave height (Figure 11).

3. Deep-Water Sites Individually. Table 12 summarizes the SI's corresponding to wind speed and wave height for each site individually for each prognostic time and for each model. It is interesting to notice the variability in the error statistics from one site to another even within same region (e.g., sites 21a, 21b, 31a, and 31b, where one ODGP grid point

TABLE 11

Scatter Index For Regions 1, 2, and 3

Prog. Time (h)	Model	Wind Speed			Sig.Wave Ht.			Peak Period		
		1	2	3	1	2	3	1	2	3
00	OPR	36[1]	28	24	31	26	31	22	22	-
	CMC	35	36	36	34	55	80	23	25	-
	METOC				18	28	28			
12	OPR	39	37	29	33	30	32	23	22	-
	CMC	40	38	40	35	57	82	24	23	-
	METOC				34	34	46			
24	OPR	39	40	33	35	32	35	23	22	-
	CMC	45	39	42	38	60	83	26	25	-
	METOC				33	36	42			
36	OPR	41	42	38	38	34	38	25	24	-
	CMC	48	44	45	42	62	83	27	28	-
	METOC				39	37	45			
48	OPR	46	46	40	41	37	35	25	24	-
	CMC	50	47	46	45	64	81	28	28	-

[1] Scatter index is expressed in percent.

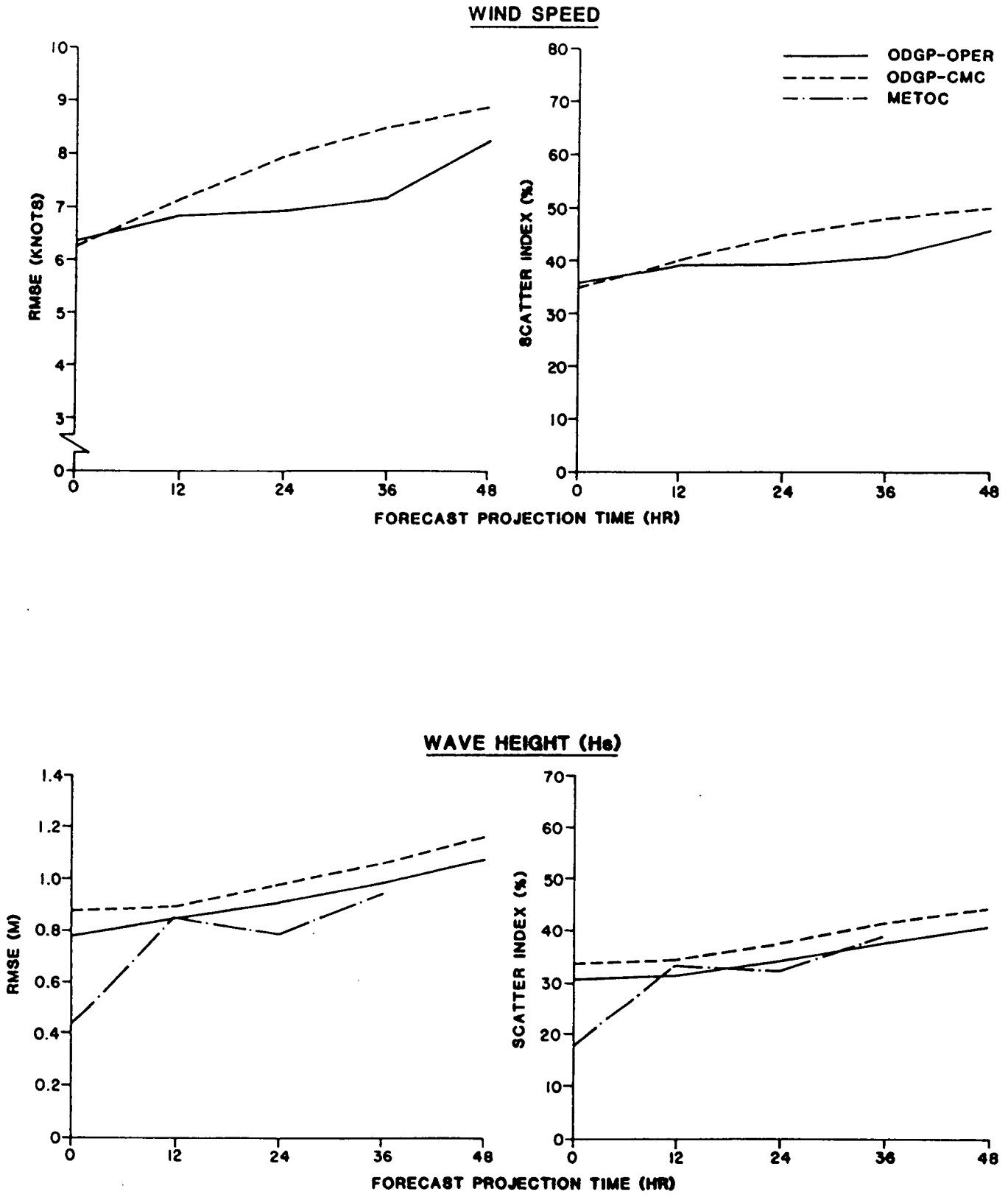

Figure 9. Error statistics for region 1, east coast of USA.

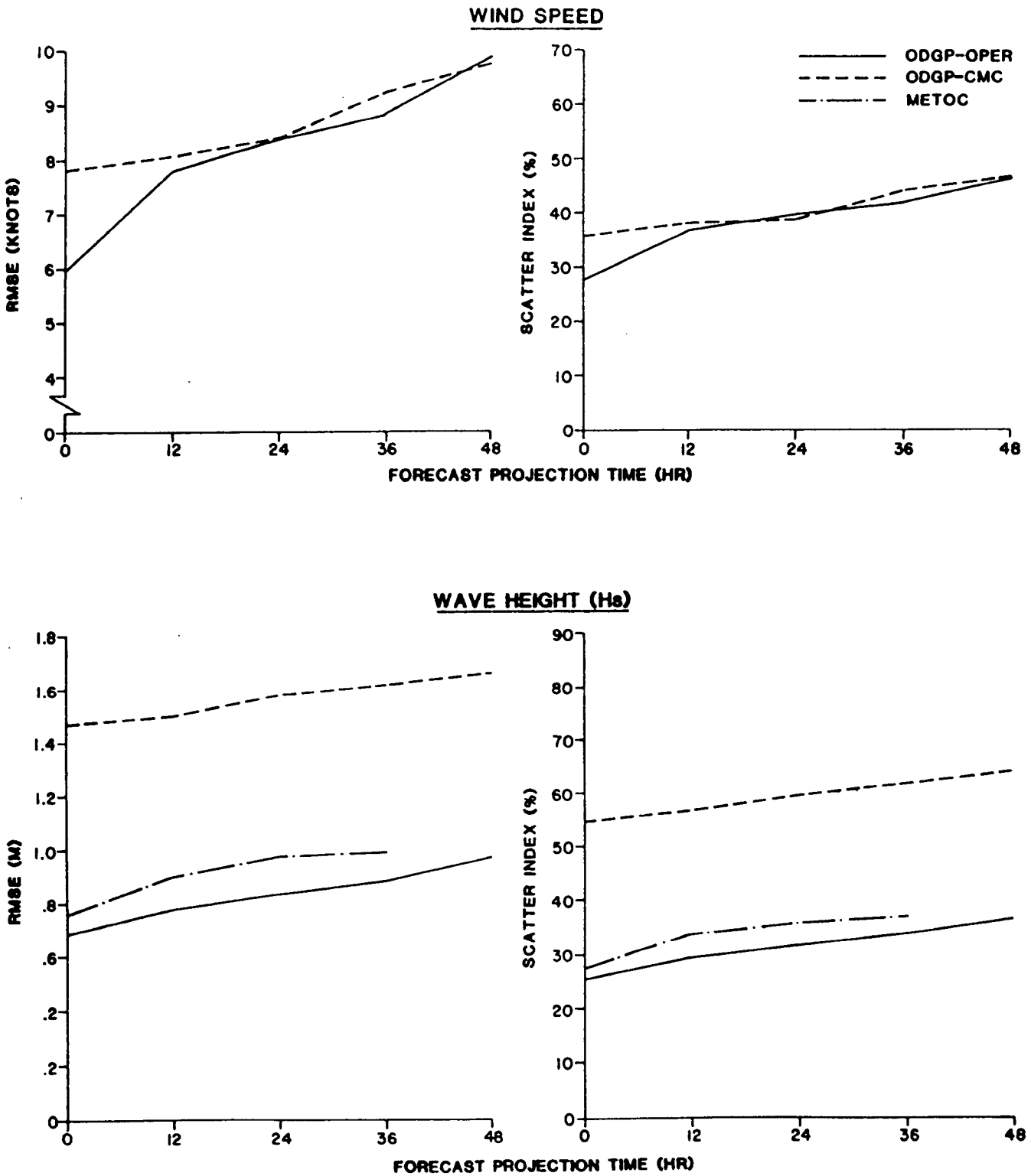

Figure 10. Error statistics for region 2, Scotian Shelf.

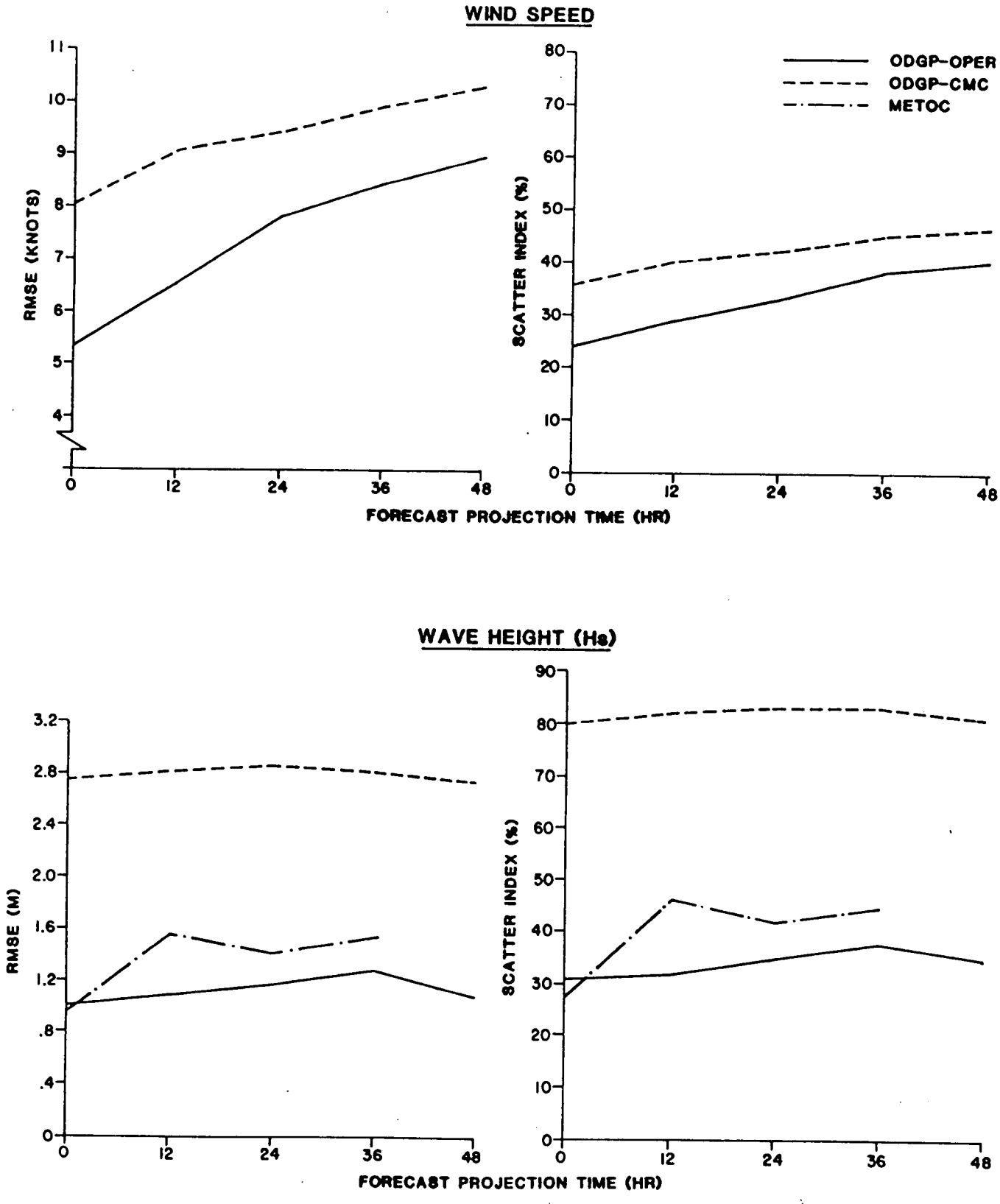

Figure 11. Error statistics for region 3, Grand Banks of Newfoundland.

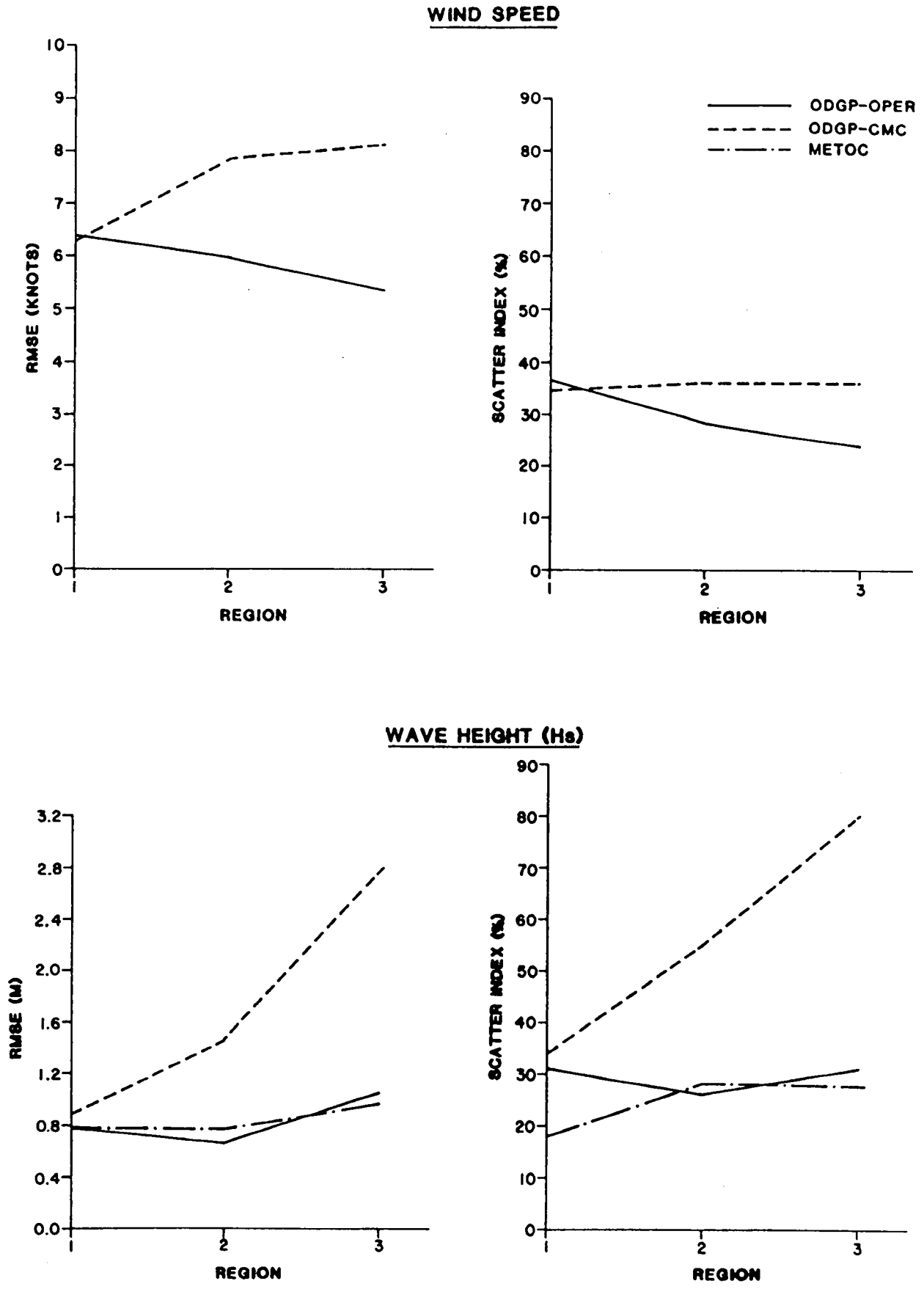

Figure 12. Summary of error statistics by region, analysis time (T=o).

TABLE 12

Scatter Index For Individual Sites

Prog. Time (h)	Mode	Wind Speed							Significant Wave Height						
		11	12	21a	21b	22	31a	31b	11	12	21a	21b	22	31a	31b
00	OPR	35[1]	37	27	27	31	25	23	31	31	26	23	31	26	35
	CMC	35	35	35	35	42	43	31	35	33	58	53	55	76	83
	METOC								-	18	28	26	35	27	29
12	OPR	39	38	37	35	40	31	28	34	30	30	26	36	27	36
	CMC	40	39	36	35	44	48	35	36	32	59	55	56	77	85
	METOC								-	35	33	31	41	46	45
24	OPR	38	43	39	39	42	37	34	35	35	31	28	40	27	38
	CMC	46	42	40	36	44	51	36	40	33	62	58	59	77	86
	METOC								-	33	37	35	37	46	43
36	OPR	41	40	42	40	43	37	38	38	39	32	30	42	32	42
	CMC	47	50	47	40	47	53	40	44	34	65	60	61	79	86
	METOC								-	39	39	36	36	43	46
48	OPR	46	45	48	45	47	40	40	41	43	36	34	42	30	38
	CMC	50	51	51	43	47	54	41	49	34	68	62	64	78	84
	METOC								-	-	-	-	-	-	-

[1] Scatter index (%)

represents each of the two sites). This difference may be due to local or mesoscale variation in wind field and error in wave measurements. The SI between sites in the same region varied from 10 to 30% (Table 12). These differences are evident in the time series plots of observed data.

5.3 SHALLOW-WATER MODEL EVALUATION - THE ENTIRE CASP PERIOD

Time series plots of wind and wave parameters, scatter diagrams, and error statistics are presented in Appendix D. Summaries of the evaluation results are presented and discussed. It should be recalled that only the ODGP-CMC model included the ultra-fine grid on which shallow-water growth and propagation algorithms were implemented. Errors in model-generated wave series at the shallow water sites may arise in errors in CMC input wind fields as reflected in ODGP-CMC deep-water wave errors, as well as in errors associated with shallow-water effects. It should be added that additional errors may be associated simply with the difficulty, even on the ultra-fine grid, of accounting for complex fetch restrictions associated with the complicated shoreline geometry during offshore or along-shore winds.

It would be extremely difficult to partition the wave height errors observed in the CASP shallow-water array to the various error sources, except perhaps through careful day-by-day comparison of deep water and shallow-water hindcast and measured wind and wave series, including comparisons of directional wave properties. Such analysis is generally beyond the scope of this study. However, it was obvious that during the first two weeks of the CASP, large-scale wave height errors in ODGP-CMC in deep water on the Scotian Shelf, in the form of large positive biases in model prediction, dominated the wave height errors observed along the CASP array. Also during this period, the WAVEC in 100-m water depth was not functional. Therefore, we have calculated and present in Table 13 summaries of wind speed and wave height scatter indices at the WAVEC sites (separately and combined) for the two periods 15 January to 15 March and 2

TABLE 13

Scatter Index For Shallow-Water Sites

Prog. time (h)	15 January to 15 March				Feb 2 - March 15					
	WIND		WAVE		WIND			WAVE		
Site	42	43	42	43	41	42	43	41	42	43
SI (%)	For individual sites									
00	56	56	53	74	56	56	56	32	35	40
12	72	72	55	74	72	73	73	36	39	47
24	81	81	59	78	81	84	84	49	53	62
36	82	82	64	82	82	84	84	62	63	72
48	91	91	70	86	91	93	93	74	77	90
SI (%)	For All Sites Combined									
00	56		55		56			35		
12	72		57		73			40		
24	81		63		84			54		
36	82		69		84			65		
48	91		76		93			79		

For site 41, WAVEC data were missing for the first two weeks (15 - 31 January).

TABLE 14
SUMMARY OF ERROR STATISTICS FOR REGION 4, SHALLOW WATER MODEL

PRODUCT	PARAMETER	15 January - 15 March Forecast Time					2 February - 15 March Forecast Time				
		00	12	24	36	48	00	12	24	36	48
Wind speed	Bias (knot)	4.48	6.66	6.83	6.18	6.56	4.75	6.94	7.15	6.36	6.75
	Mean Absolute Error (Knot)	5.88	7.62	8.20	8.06	8.44	5.81	7.60	8.36	8.12	8.49
	RMSE (knot)	7.45	9.51	10.74	10.76	12.00	7.46	9.6	10.99	10.97	12.20
	SI (%)	56	72	81	82	91	56	73	84	84	93
	Slope	0.50	0.44	0.33	0.28	0.19	0.53	0.46	0.34	0.28	0.20
	Correlation coeff.	0.70	0.67	0.53	0.43	0.32	0.72	0.70	0.55	0.44	0.33
	Intercept (knot)	4.43	4.90	6.54	7.86	9.42	3.8	3.90	6.19	7.65	9.16
	No. of Points	477	480	486	486	480	441	444	450	450	444
Sig. wave height	Bias (m)	0.30	0.37	0.41	0.41	0.49	0.00	0.10	0.15	0.14	0.25
	Mean Absolute Error (m)	0.57	0.61	0.68	0.74	0.82	0.37	0.42	0.49	0.58	0.70
	RMSE (m)	0.90	0.93	1.02	1.13	1.23	0.51	0.58	0.79	0.95	1.15
	SI (%)	55	57	63	69	76	35	40	54	65	79
	Slope	58	0.57	0.54	0.44	0.46	0.84	0.73	0.56	0.46	0.37
	Correlation coeff.	0.85	0.86	0.84	0.77	0.74	0.83	0.82	0.76	0.64	0.60
	Intercept (m)	0.52	0.48	0.53	0.63	0.65	0.22	0.33	0.57	0.73	0.82
	No. of Points	457	460	463	463	457	342	345	348	348	342
Peak period	Bias (s)	0.62	0.62	0.79	0.78	0.78	0.42	0.42	0.67	0.65	0.69
	Mean Absolute Error (s)	1.63	1.68	1.74	1.86	1.99	1.61	1.68	1.75	1.91	2.13
	RMSE (s)	2.33	2.39	2.41	2.56	2.72	2.4	2.47	2.51	2.69	2.92
	SI (%)	26	26	27	28	30	27	27	28	30	33
	Slope	0.52	0.50	0.51	0.47	0.43	0.46	0.44	0.44	0.39	0.34
	Correlation coeff.	0.63	0.62	0.61	0.59	0.56	0.55	0.54	0.52	0.52	0.47
	Intercept (s)	4.00	4.20	4.02	4.47	4.85	4.7	4.91	4.79	5.23	5.7
	No. of Points	457	460	463	463	457	342	345	348	348	342

February - 15 March. More detailed summaries of wind speed, significant wave height, and peak periods statistics at the shallow-water sites are given in Table 14 for the two periods.

The main characteristics of the summarized error statistics are noted here.

1. The wind speed scatter indices are significantly greater at analysis and all forecast times than for the region 2 deep-water results (see Figure 5.10). However, this increase arises principally in the large "apparent" positive bias in modelled winds relative to measured winds at the single Minimet station used for all shallow-water wind speed statistics. As noted in subsection 4.3.4, winds at the Minimet are measured at anemometer height of 3 m. Wind speeds were not adjusted to 20 m and, therefore, much of the "apparent" positive bias in the modelled winds is associated with differences in reference height. This bias also contaminates the scatter index as defined in this study.

2. For the entire CASP period, the wave height SI for all sites combined are identical at analysis time (at 55%) to the deep- water region 2 SI (see Table 11) and remain close to the deep- water errors up to 48 h. However, excluding the first two weeks, it provides a 20% decrease in shallow-water wave height SI at analysis time and 10-20% reductions at forecast time, relative to the errors for the full CASP period.

3. For the period 2 February to 15 March, during which error statistics at all water depths are available, a slight increase in scatter index is evident with decreasing depth at all forecast times. This effect is probably associated with the decrease in average wave energy levels (1.15 m at 25 m depth, versus 1.71 m at 100 m) with decreasing depth. As water depth and distance from shore decrease, the scatter in wave height specifications decreases also, but more slowly than the mean energy level, resulting in somewhat greater relative scatter.

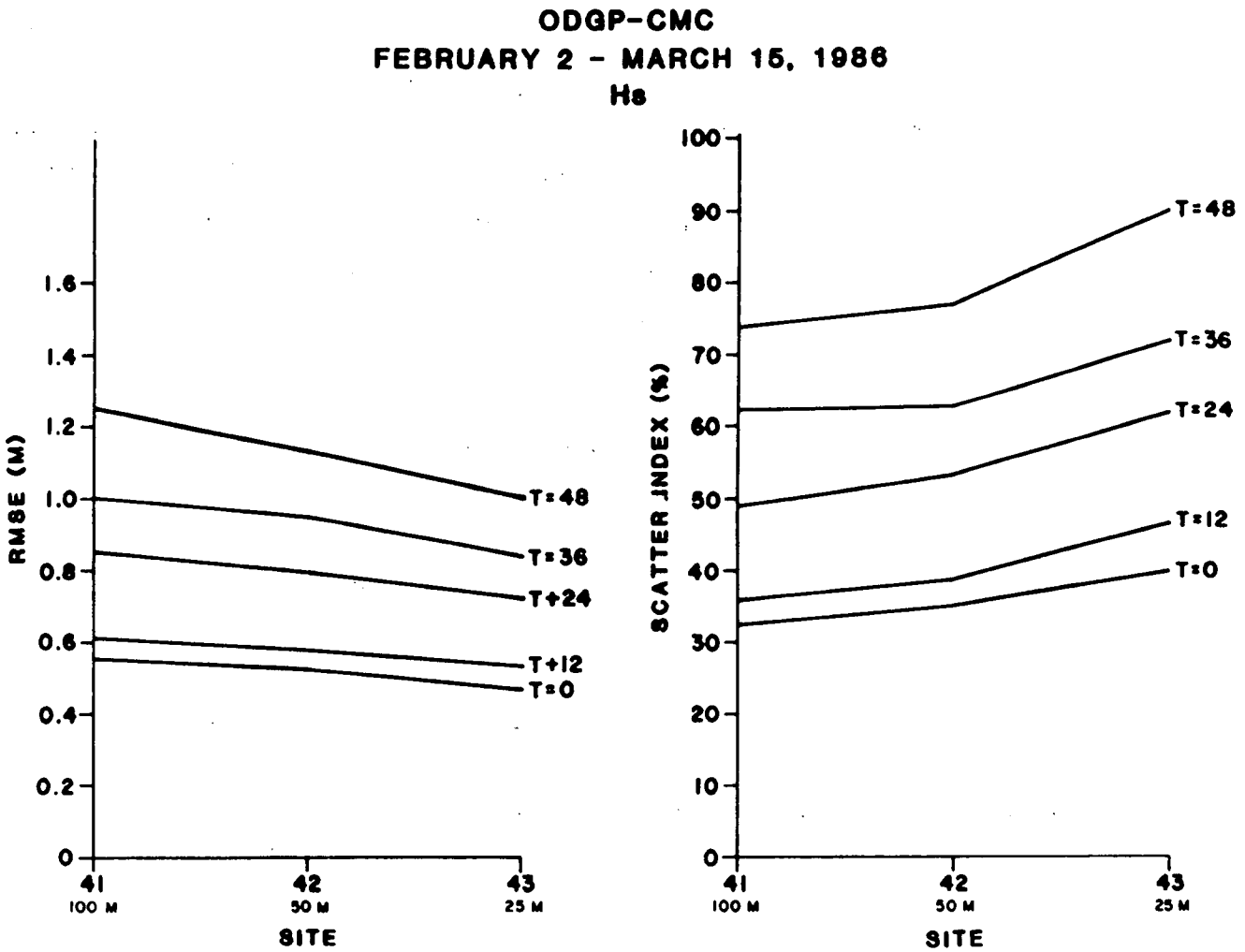

Figure 13. ODGP-CMC Shallow-water model errors in significant wave height prediction.

4. The shallow-water model predictions deteriorate rapdily with increasing forecast projection time (Figure 13).

5.4 STORM STUDY CASES

5.4.1 Selection of Storm Events

During the CASP study period, 16 intensive observation periods (IOPs) took place in which a representative population of storms were sampled. The durations of these IOPs are shown in Table 15. For the purpose of this study, four storms were selected for intensive evaluation of the alternate forecasts of sea-level pressure winds and sea states provided by the various operational numerical weather prediction products and sea-state analyses and forecasts. The storms were selected from among the CASP IOPs using the following guidelines:

(1) storms that occurred during or within several days following breaks in the CMC wind input were not selected.

(2) peak measured sea states in selected storms exceeded 5 m at either the Scotian Shelf or Grand bank sites.

(3) selected storms represented a wide range of different wave regimes.

(4) insofar as possible, the selection would not bias the performance of any particular model, i.e. selection was done regardless of model results.

The four storm events are listed below with the corresponding IOP number:

Storm 1 January 19 - 0000 GMT to January 23 - 0000 GMT (IOP 2);
Storm 2 January 26 - 1200 GMT to January 30 - 1200 GMT (IOP 3);
Storm 3 February 15 - 0000 GMT to February 19 - 0000 GMT (IOP 8);
Storm 4 March 10 - 0000 GMT to March 14 - 0000 GMT (IOP 15).

TABLE 15

A list of the casp intensive observation periods

IOP Number	Start Time		End Time	
	Date	Hour(GMT)	Date	Hour (GMT)
1.	15 January	1800	16 January	0300
2.	19 January	1200	22 January	0600
3.	27 January	1200	29 January	0000
4.	30 January	0600	31 January	1800
5.	2 February	0600	4 February	0000
6.	5 February	0600	6 February	1500
7.	12 February	0000	12 February	1200
8.	15 February	0600	17 February	0000
9.	22 February	0600	24 February	1200
10.	25 February	1200	27 February	0000
11.	28 February	0000	28 February	1800
12.	2 March	0600	3 March	1200
13.	5 March	1200	7 March	0000
14.	6 March	1800	8 March	0600
15.	10 March	1800	12 March	1800
16.	14 March	0000	15 March	1200

Storms are described below in terms of the storm track (storm tracks are shown in Figures 14 to 17), brief references to the storm effects at the measurement sites, and discussion of relative performance of weather model forecasts of storm track and central pressure. (See also Appendix F for wind field plots.)

5.4.2 Description of Storm Events

Storm 1 - 19 to 23 January 1986. This storm formed on 19 January in a trough of low pressure which extended from the Great Lakes to the Gulf of Mexico. The low centre (Figure 14) developed over the state of Kentucky around 0600 GMT on 19 January and moved eastward at about 15 knots. This storm continued its slow movement the next day as it turned northeastward moving through New England. By 1200 GMT of 20 January, the low had deepened to 988 mbar, but began to fill shortly afterwards. Winds peaked at 25 knots at site 21a on the 20 January. Seas peaked around 5 m at the same place and time. The centre of this low passed just north of Nova Scotia between 0600 and 1200 GMT on 21 January and turned eastward, increasing its speed to around 35 knots. Winds on the Scotian Shelf shifted from southwest to northwest as the cold front, trailing this low, moved through the area between 1800 GMT on 21 January and 0000 GMT on the 22 January. Winds decreased rapidly behind the cold front, and the low finally dissipated northeast of the Grand Bank after 0600 GMT on the same day. Winds and seas at the Grand Bank were light, because the low had weakened greatly by this time.

The ODGP-OPR did generally well on this storm in predicting both the storm track and the central pressure. The 24-h forecast of central pressure valid 20 January 1200 GMT was 6 mbar too high, and the 48-h forecast valid 21 January 1200 GMT was 8 mbar too low. Both the LFM and CMC models predicted the storm track well, but both did not fair as well as the ODGP-OPR in predicting the central pressure. The CMC 48-h forecast valid 20 January 1200 GMT was 18 mbar high. The LFM 48-h forecast valid 21 January 1200 GMT was 9 mbar high.

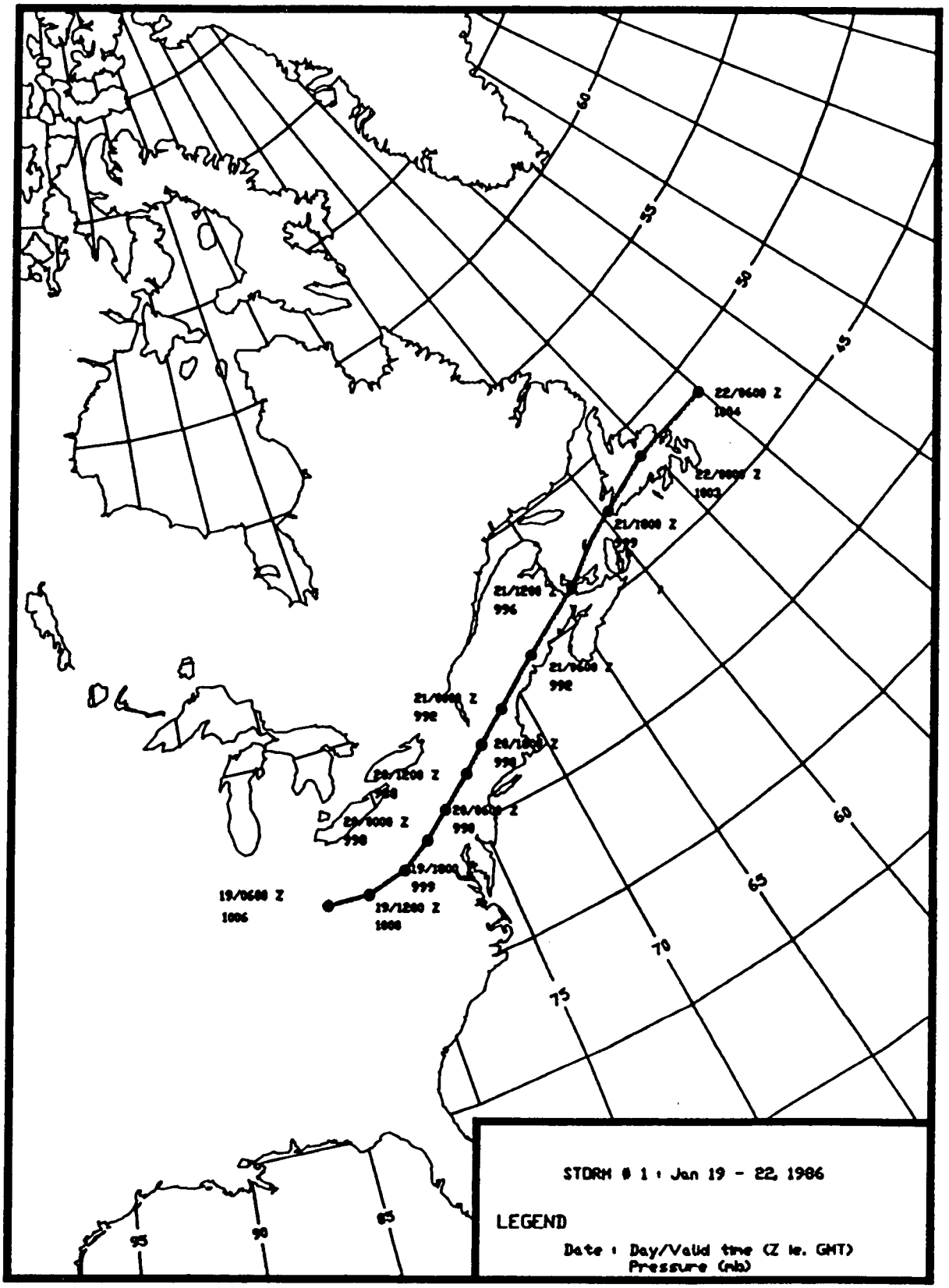

Figure 14. Low pressure centre track for Storm #1.

The CMC 48-h valid 22 January 0000 GMT did not forecast the filling of the low toward the end of the storm, and was 7 mbar too low.

Storm 2 - 26 to 30 January 1986. This double-centre system first developed on a stationary front that was located along the entire east coast of the United States on 26 January (Figure 15). Two strong high-pressure systems were located on either side of this frontal system. One was a 1052-mbar high located just east of the Grand Bank on 27 January. The other was a 1049 mbar high located over the northern plains states on 26 January. That high would weaken greatly as it moved south whereas the high over the Atlantic would remain strong through the end of the month.

The first low developed on the stationary front over the North Carolina coast at 0000 GMT on 26 January, 1986. This low moved up the east coast and into New England on 27 January, deepening rapidly from 998 mbar at 0000 GMT Ton 26 January to 982 mbar at 1200 GMT of the same day. A strong pressure gradient developed between this low and the high just east of the Grand Banks. Strong southeast winds began over the Scotian Shelf on 26 January and ended on 28 January.

The secondary low developed on a cold front, which was trailing the primary low, near buoy 44004 at 0000 GMT on 28 January. This storm moved northeastward, passing just west of Nova Scotia at 1200 GMT on 28 January. This low deepened explosively as it turned northward later the same day deepening from 988 mbar at 0000 GMT 28 January to 964ar at 0000 GMT 29 January. This low continued its rapid deepening as it moved northward through 1200 GMT on 29 January when its central pressure fell to 952 mbar. The highest winds at site 21a occurred during the morning of 28 January, peaking around 40 knots. Seas peaked at site 21a between 5.5 m and 6 m on the afternoon of 29 January and diminished rapidly on 30 January.

There were two separate periods of southeasterly gales on the Grand Banks (site 31b). The first occurred during the day (29 January) when maximum wind speeds near 33 knots (at site 31b) were recorded. At the same

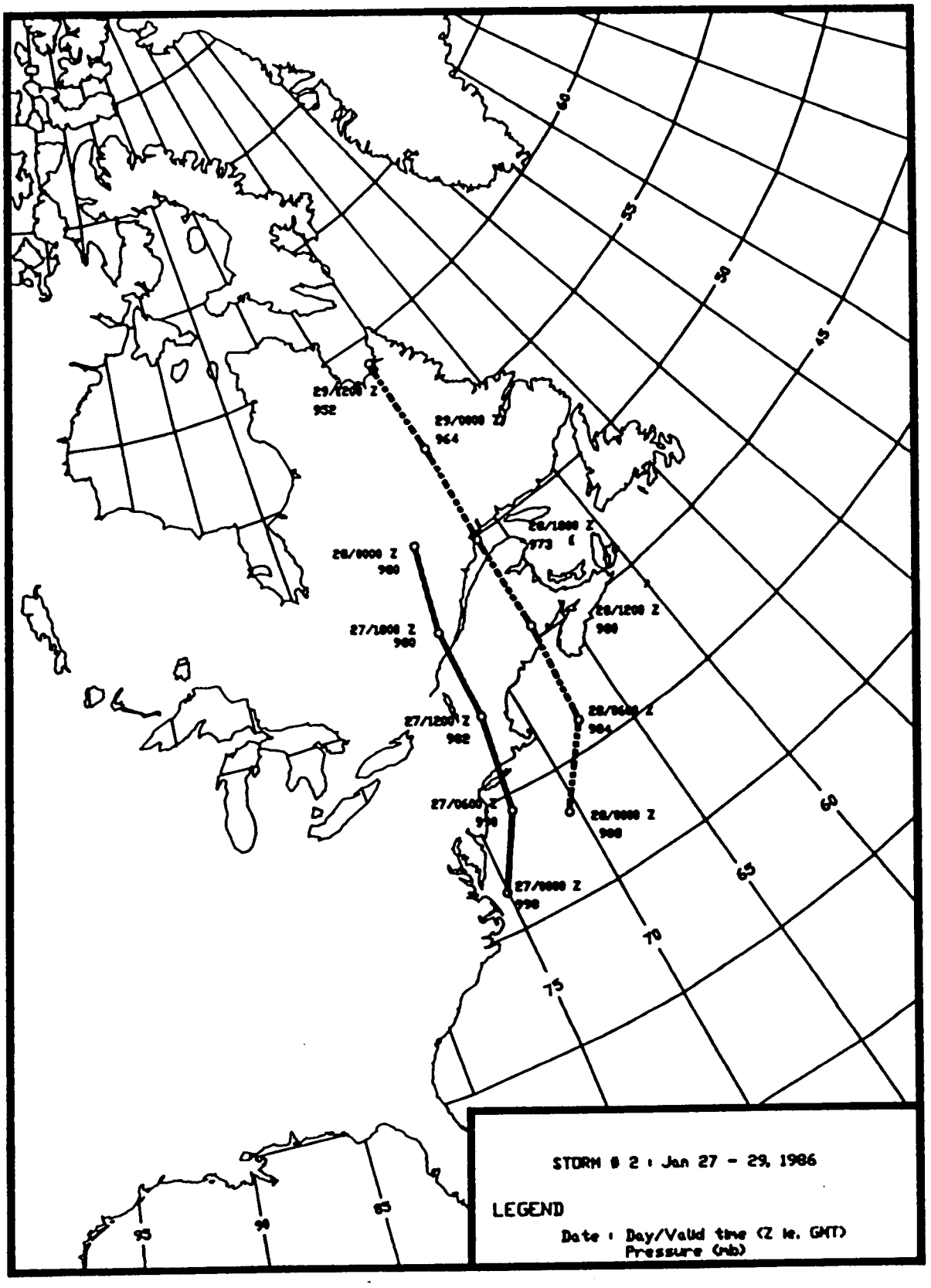

Figure 15. Low pressure centre track for Storm #2.

site, a peak wind also near 33 knots was recorded during the day on 31 January. Seas increased rapidly on 29 January, peaking around 4 m later the same day. Seas slowly diminished for the next few days.

All models predicted the track of the first low fairly well. However, the central pressure of the low was not well forecast. The LFM and CMC models consistently under deepened the first low at all forecast times except for LFM 24-h forecast valid 1200 GMT on 27 January, which was 2 mbar low. The ODGP-OPR outperformed the LFM and CMC models most of the time, one exception being the above case in which the 3 mbar was added to the LFM's 2-mbar error.

The formation of the second low was not picked up by any model. When it was finally forecast, all the models consistently moved the low too far north. The LFM and ODGP-OPR model predictions of the central pressure on this second low were more accurate than for the first low. The CMC model forecasts, except for the 48-h forecasts, were not as good as for the first low.

Storm 3 - 15 to 19 February 1986. This storm developed on a cold front that was moving through the Mississippi valley on 14 February, 1986. After moving off the New Jersey coast between 0600 and 1200 GMT on 15 February, this low moved east-northeastward, passing over the Scotian Shelf at 0000 GMT on 16 February (Figure 16). The low deepened explosively and assumed "bomb" characteristics on 15 February as it deepened from 1005 mbar at 1200 GMT that day to 976 mbar at 1200 GMT on 16 February. The low deepened by another 16 mbar in the next 12 h. After moving over the Scotian Shelf, the low moved northeastward at 20 knots, passing over the eastern tip of Newfoundland at 1800 GMT on 16 February. This low then turned to the north-northeast, decreased in forward speed, and began to weaken later on 17 February. At site 21a, on the Scotian Shelf, winds became very light as the low moved over the site, then increased rapidly to near 40 knots by the end of the day. Seas peaked around 4 m at the same time. On the Grand

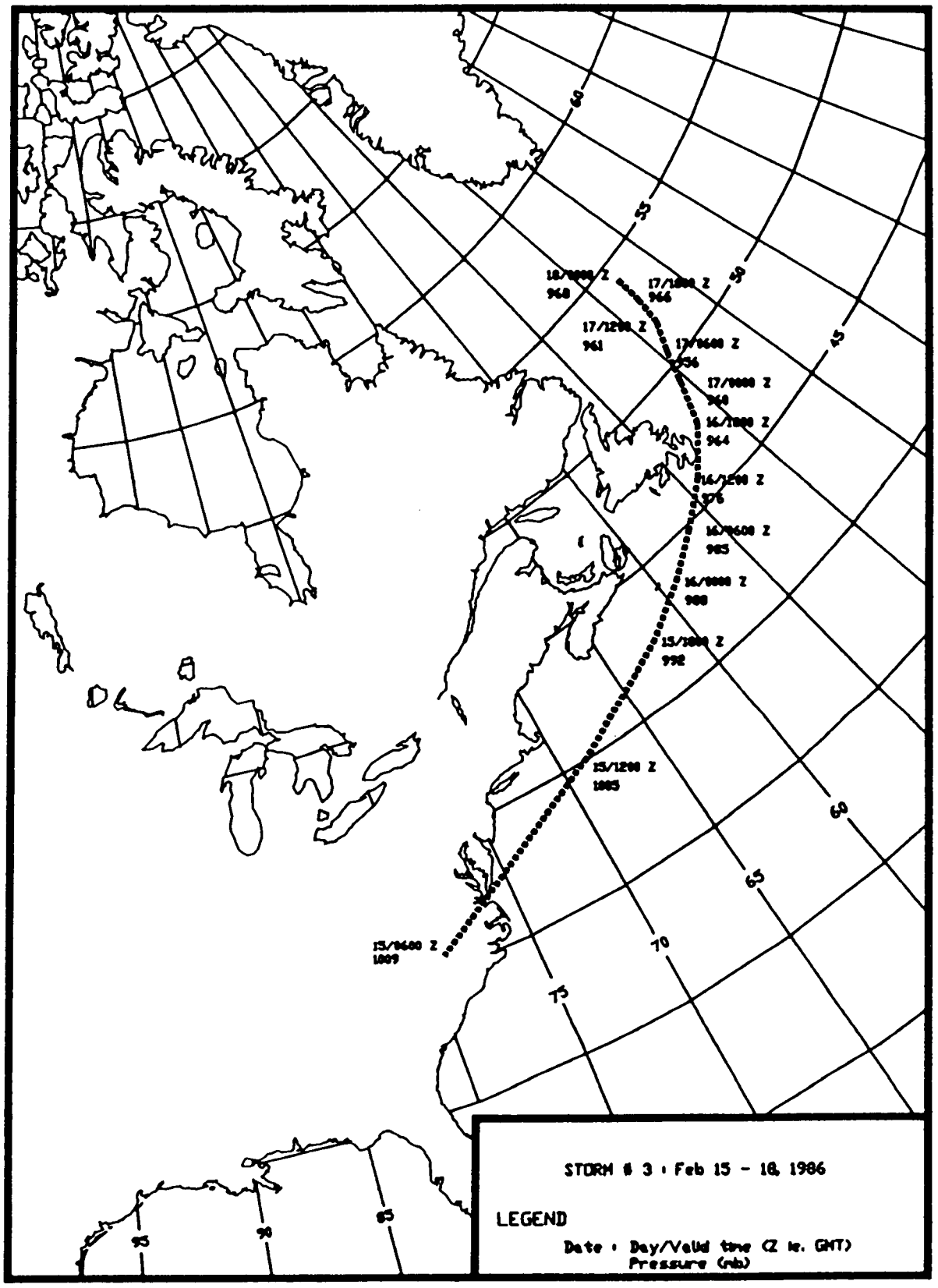

Figure 16. Low pressure centre track for Storm #3.

Banks, at site 31b, winds increased rapidly on 16 February and peaked around 45 knots later on the 17 February. Seas peaked (at site 31b) around 7.5 m during the evening of 17 February and decreased rapidly afterwards.

All forecast models fairly accurately predicted the track of the low, and there are no major errors to report. Both the NGM and CMC models made large errors in predictions of the central pressure of the low. Once again neither model predicted the rapid deepening of the low. For the 12-h forecast valid at 0000 GMT on 17 February, the NGM was 14 mbar high and the CMC was 16 mb high. For the 48-hr forecast, valid at 0000 GMT 17 February, the NGM was 26 mbar high and the CMC was 23 mbar high. The ODGP-OPR forecasts improved the forecasts of the central pressure of the low compared to the NGM and CMC models. The largest errors in the ODGP-OPR occurred for the forecasts valid at 0000 GMT 18 February, for which the ODGP-OPR was 8 mbar high at the 12-h and 16 mbar high at the 48-h forecast.

Storm 4 - 10 to 14 March 1986. As shown in Figure 17, this low developed over the Northern Rockies in the United States on 8 March and moved eastward into the Great Lakes region on 11 March. A warm front, extending southeast from the low, moved through the Scotian Shelf at 1200 GMT on 11 March, with southeast winds shifting to the southwest. This storm moved through northern New England as a 988-mbar low on 11 March and moved eastward over Newfoundland at 0000 GMT on 12 March. The warm front extending from the low moved through the Grand Banks between 0000 and 0600 GMT on 12 March. The cold front extending from this low moved through the Scotian Shelf at the same time. Winds peaked near 30 knots at site 21a, and seas peaked near 4.5 m on 12 March. The low moved just north of the Grand Banks at 1200 GMT on 12 March, and the cold front, trailing this low, moved through at the same time. The low then turned towards the northeast at 40 knots later on 12 March and deepened to a 969 mbar low at 0600 GMT on 13 March. Winds on the Grand Banks (at site 31b) peaked around 40 knots on 12 March and did not diminish significantly until later on 14 March. Seas increased rapidly and peaked at site 31b around 6.5 m later on 12 March, after which they steadily decreased through 15 March.

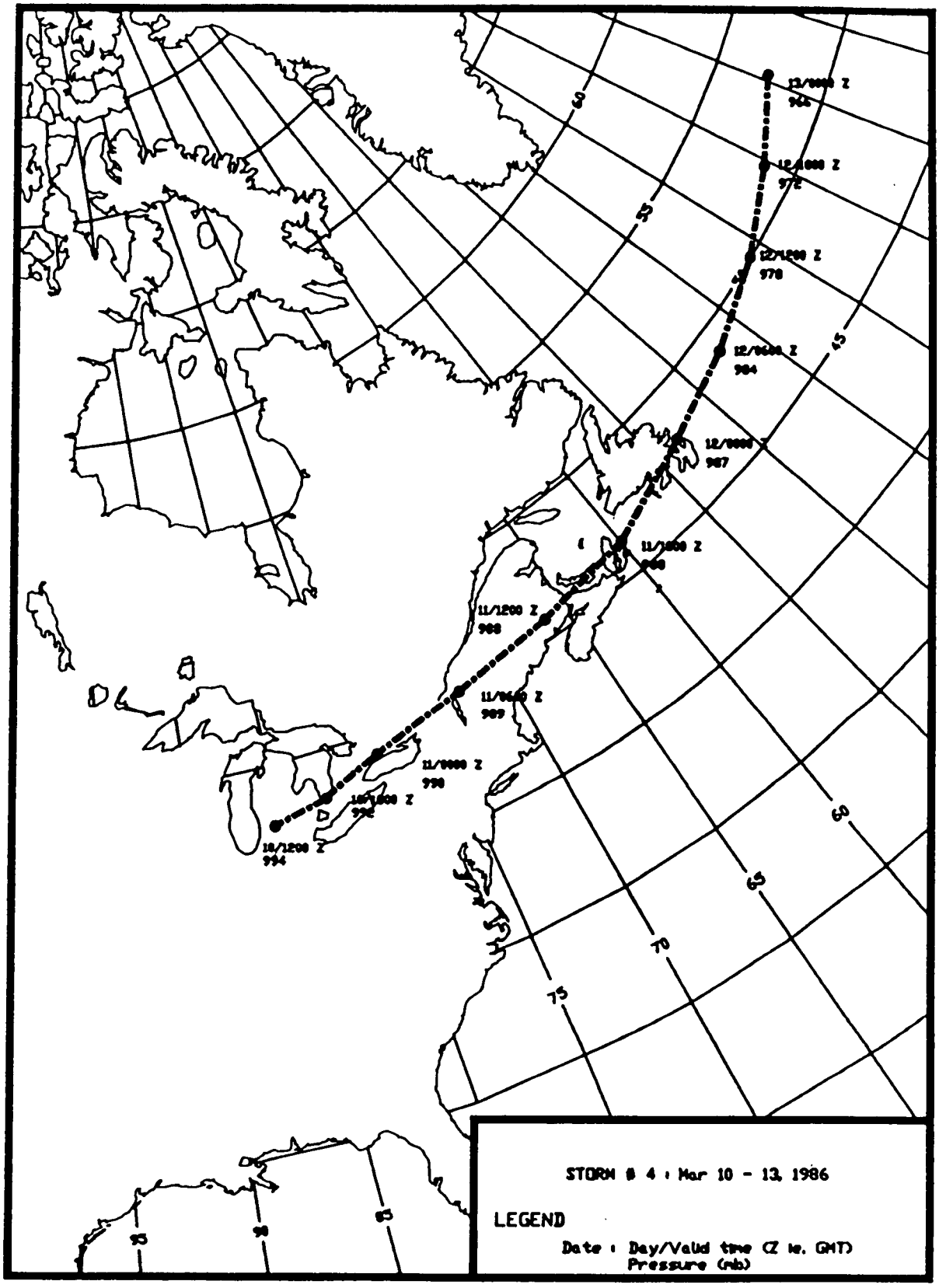

Figure 17. Low pressure centre track for Storm #4.

There were significant errors in all three models in forecasts of the storm track. In particular the models did not specify the rapid eastward movement. The CMC model was slightly better than the other models, in this regard. In predicting central pressure, the CMC model consistently outperformed both the NGM and ODGP-OPR, especially for the 48-h forecasts. The NGM did well the first two days of the storm, but when the low began deepening later on, the NGM did not keep up with the deepening rate. The ODGP-OPR model had large errors with forecasts valid 0000 GMT on 12 March. Those forecasts (12-, 24-, 48-h forecasts) over deepened the low significantly. The 12-h forecast was 7 mbar too low, and the 48-h forecast was 9 mbar low. Other forecasts by the ODGP-OPR were generally unbiased.

5.4.3 Comparison of Weather Model Prediction

In an attempt to study errors in the NWP models (i.e. LFM/NGM, ODGP-OPR and CMC), this Section presents a systematic intercomparison of alternate forecasts of central pressure and position of the five separate low pressure systems which comprise the four storm periods selected for intensive evaluation. This analysis is performed to provide an indication of differences between forecast pressure fields, which may be related to differences between forecast surface wind fields and, therefore, to differences between deep-water forecasts produced from OPR and CMC winds.

The comparison is presented in terms of the mean and standard deviation between forecast and analysis central pressure, latitiude and longitude of lows, stratified by forecast projection time (12, 24, and 48 h), and model (LFM/NGM, OPR, CMC). The analysis data are taken from the reanalysed six-hourly surface pressure charts produced in real time as part of the OPR system. These analyses reflect rig, buoy, and ship reports available up to 3 h after the cut-off time for the NOAA or AES surface analyses transmitted on facsimile, and, therefore, should be the most accurate source of verification data. Forecast data were read directly from the forecast surface pressure panels on the graphical display of the

LFM/NGM and CMC transmitted on facsimile. The NOAA LFM model was used for the first two storm periods, and the NOAA NGM model was used for the last two storm periods.

Comparisons of forecast and analysis pressure and position were made for all matches possible during the storm periods defined as follows:

Low 1	1200 GMT 19 January	- 0000 GMT 22 January
Low 2	0000 GMT 27 January	- 0000 GMT 28 January
Low 3	0000 GMT 28 January	- 1200 GMT 29 January
Low 4	1200 GMT 15 February	- 0000 GMT 18 February
Low 5	1200 GMT 10 March	- 1200 GMT 12 March

Verification statistics are presented for individual lows in Table 16. The number of comparisons available for each model differ slightly because some CMC facsimile transmissions were missed, and comparisons were possible for the ODGP-OPR forecast only after the low had entered the domain of analysis (basically east of 80°W).

Table 16 presents a summary of the verification statistics over all storms, stratified by forecast projection time and model. The central pressure mean errors (forecast minus analysis) are consistently positive for all models and increase with increasing forecast range. However, up to 24 h the mean pressure errors for the OPR forecasts are only around 1 mbar, which indicates that the man-machine mix procedures are effective in improving the forecasts provided by the LFM/NGM models. The scatter in the OPR forecasts is also slightly improved relative to that of the underlying numerical forecasts. OPR mean pressure errors at 48 h are about one-half of those of the LFM/NGM. CMC pressure errors are close to those of the LFM/NGM model, which is somewhat surprising, considering that CMC surface wind forecasts tend to be positively biased. However, in the case of the CMC model, the sign of the central pressure error may not be a good indicator of the relative accuracy of the forecast pressure gradients about the low centre.

Table 16

Verification of central pressure and position

LFM/NGM, OPR and CMC forecasts in selected CASP storms[1]

		LFM/NGM[2]			OPR[3]			CMC[4]		
Parameter	Tau (h)	Mean[1]	SD	No.[5]	Mean[1]	SD	No.	Mean[1]	SD	No.
Pressure (mb)	12	5.0	3.9	25	1.0	4.1	23	5.2	3.6	24
	24	6.2	6.6	25	1.1	5.4	23	6.0	6.4	22
	48	8.9	8.4	25	3.7	7.4	23	6.7	7.2	23
Latitude (deg. N)	12	0.1	1.8	25	0.1	1.5	23	.4	1.8	24
	24	0.0	2.2	25	0.7	1.8	23	1.5	2.6	22
	48	0.1	2.2	25	0.3	2.6	23	1.6	2.7	23
Longitude (deg. W)	12	1.8	1.7	25	1.9	3.4	23	2.5	3.8	24
	24	1.9	1.9	25	2.1	3.6	23	1.8	3.3	22
	48	1.8	3.1	25	2.0	4.1	23	1.8	3.8	23

[1]Mean errors: forecast minus observed.

[2]NOAA Limited-Area Fine Mesh (LFM) Model to 7 February, 1986; Nested Grid Model (NGM) after 7 February, 1986.

[3]OPR: MacLaren Plansearch/Oceanweather operation forecast system.

[4]CMC: AES Canadian Meteorological Centre Spectral atmospheric numerical forecast model.

[5]No. is number of comparisons - They are different due to missing of some facsimile transmissions.

The forecast mean errors of storm latitude for the LFM/NGM and OPR models are generally small and negligible. There is indicated in the statistics a tendency for northward displacement in CMC forecasts relative to actual tracks with mean displacements of about 1.6 at 48 h. However, as shown in Table 5.8, this error is contributed to mainly by Low 3, which moved almost due north, suggesting simply positive CMC errors in translation velocity in this case.

The forecast mean errors of storm longitude are positive for all models and forecast projections (a positive error means a forecast position is west of the verification position). This statistic is believed to reflect a tendency for the models to move low systems eastward slower than observed.

5.4.4 Verification of Storm Predictions

The time series behaviour of wind and wave parameters are of course included in the continuous series presented in Appendices C and D for the entire CASP period. Scatter diagrams and error statistics for the storm cases only are given in Appendix F. Appendix E contains comparisons of selected measured and model hindcast one-dimensional spectra in each region in each storm. At deep-water sites, both ODGP-OPR and ODGP-CMC analysis-hour spectra are compared to "measured" spectra, whereas at the CASP shallow sites, only ODGP-CMC analysis-hour spectra may be compared. Summaries of the statistical evaluation results for the combined storm cases are given in Tables 17 and 18 and Figures 18 to 22. The principal features for these evaluation results are discussed by region.

Regions 1, 2, and 3 combined. The basis error characteristics found for the entire CASP period are exhibited as well for the storm cases (see Figures 8 and 18). The ODGP-CMC wind speeds are positively biased at all forecast project times, which produces a strong positive bias in wave height. It should be added that this bias is much more evident in the

TABLE 17

Summary of Error Statistics for all deep-water sites
(Regions 1, 2, and 3 combined) for storm cases

Forecast	Wind Speed				Significant Wave Height				Peak Period	
	BIAS (knot)	RMSE[1] (knot)	SI[2] (%)	r[3]	BIAS (m)	RMSE (m)	SI (%)	r	RMSE (s)	SI (%)
00-h										
ODGP-OPR	-1.18	6.1	29	0.81	0.10	0.89	29	0.83	1.86	20
ODGP-CMC	3.46	8.2	38	0.78	1.74	2.56	82	0.67	1.83	20
METOC	-	-	-	-	0.34	0.90	29	0.84	-	-
12-h										
ODGP-OPR	-0.30	7.3	35	0.72	0.12	0.96	31	0.81	1.9	20
ODGP-CMC	5.04	9.2	44	0.77	1.80	2.59	83	0.67	1.9	20
METOC	-	-	-	-	0.30	1.30	42	0.60	-	-
24-h										
ODGP-OPR	0.18	7.3	34	0.73	0.13	1.05	34	0.78	2.1	23
ODGP-CMC	5.99	10.5	49	0.70	1.91	2.69	86	0.65	1.9	21
METOC	-	-	-	-	0.40	1.36	44	0.61	-	-
36-h										
ODGP-OPR	-0.23	8.0	38	0.66	0.12	1.12	36	0.74	2.2	23
ODGP-CMC	6.15	11.2	53	0.65	1.97	2.73	88	0.64	2.0	22
METOC	-	-	-	-	0.33	1.37	45	0.57	-	-
48-h										
ODGP-OPR	-0.27	8.8	41	0.58	0.07	1.10	35	0.74	2.2	24
ODGP-CMC	6.39	11.9	56	0.59	1.97	2.73	88	0.61	2.1	22

[1] Root Mean Square Error.
[2] Scatter Index.
[3] Correlatin Coefficient.

TABLE 18

Summary of Scatter Indices for storm cases for each region

Forecast	Wind Speed				Significant Wave Height			
	Region 1	Region 2	Region 3	1, 2 & 3 Combined	Region 1	Region 2	Region 3	1, 2 & 3 Combined
00-h								
ODGP-OPR	41	29	24	29	36	23	29	29
ODGP-CMC	38	36	41	38	34	73	103	82
METOC	-	-	-	-	12	29	30	29
12-h								
ODGP-OPR	46	36	28	35	40	26	30	31
ODGP-CMC	48	40	46	44	35	73	105	83
METOC	-	-	-	-	32	31	44	42
24-h								
ODGP-OPR	40	35	31	34	43	29	33	34
ODGP-CMC	58	43	53	49	40	75	109	87
METOC	-	-	-	-	27	33	53	44
36-h								
ODGP-OPR	45	39	33	38	45	31	35	36
ODGP-CMC	64	47	55	53	45	76	109	88
METOC	-	-	-	-	49	32	53	45
48-h								
ODGP-OPR	49	44	34	41	44	33	32	35
ODGP-CMC	69	51	57	56	47	76	109	88

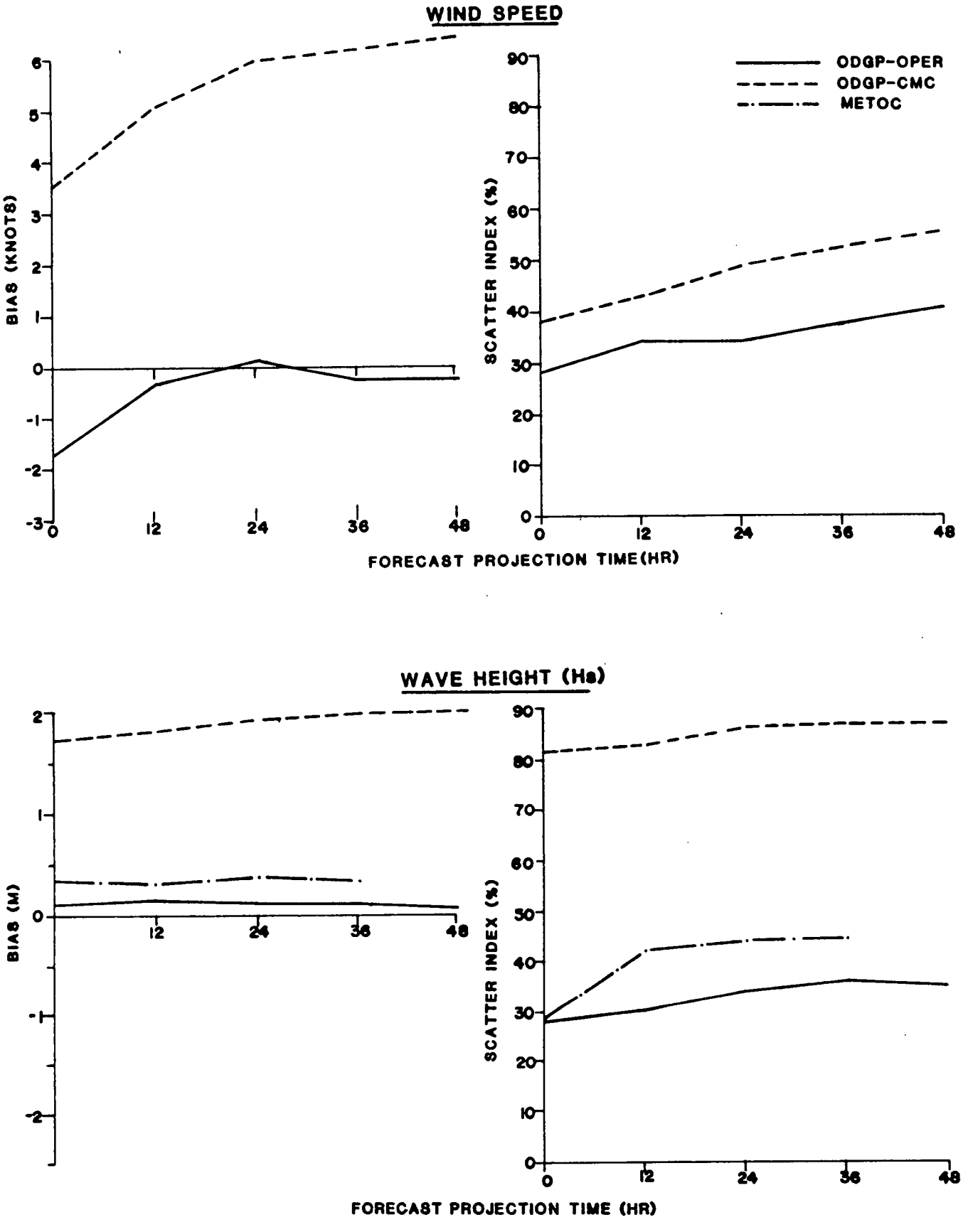

Figure 18. Error statistics of regions 1, 2, and 3 combined for storm cases.

first two storm cases than the last two cases. ODGP-OPR wind speeds exhibit negligible bias at forecast hours, which contributes to the low bias seen in ODGP-OPR wave height analyses and forecasts.

The scatter in wind speed and wave height predictions in the storm cases is virtually the same as for the entire CASP period. In comparison with METOC prediction of H_s, the ODGP-OPR shows noticeable skill for all forecasts (i.e. 12- to 36-h progs).

Regions 1, 2, and 3 individually. The summary of wind and wave errors at analysis time stratified by region (Figure 19 and Table 18) show virtually the same magnitude and trends as the comparable statistics for the entire period (Figure 12). The only significant difference is an apparent improvement in region 1 METOC errors in storms. Again this particular statistic mainly reflects the ability of METOC analyses to assimilate high-quality observations at analysis time in region 1, the same observations in fact used as the verification data base in this region. The increase in wave SI in the ODGP-CMC predictions from regions 1 to 3 is even greater in storms than overall.

The growth of wind and wave error with time in storm cases in individual regions is discussed for each region.

For region 1, as shown in Figure 20 the growth of wind RMSE and SI with forecast projection time is faster in storms than overall for ODGP-CMC, whereas the errors for ODGP-OPR in storms grow at about the same rate as for the whole CASP period, but are at all forecast hours slightly greater in storms than overall. The trend in wave SI is the same in storms as overall for all three series, except that up to 36 h, ODGP-CMC errors are slightly lower than ODGP-OPR. As shown in Figure 19, ODGP-OPR wave SI is greater in region 1 than in the Canadian east coast. It may be associated with the fact that the ODGP fine grid extends only over regions 2 and 3.

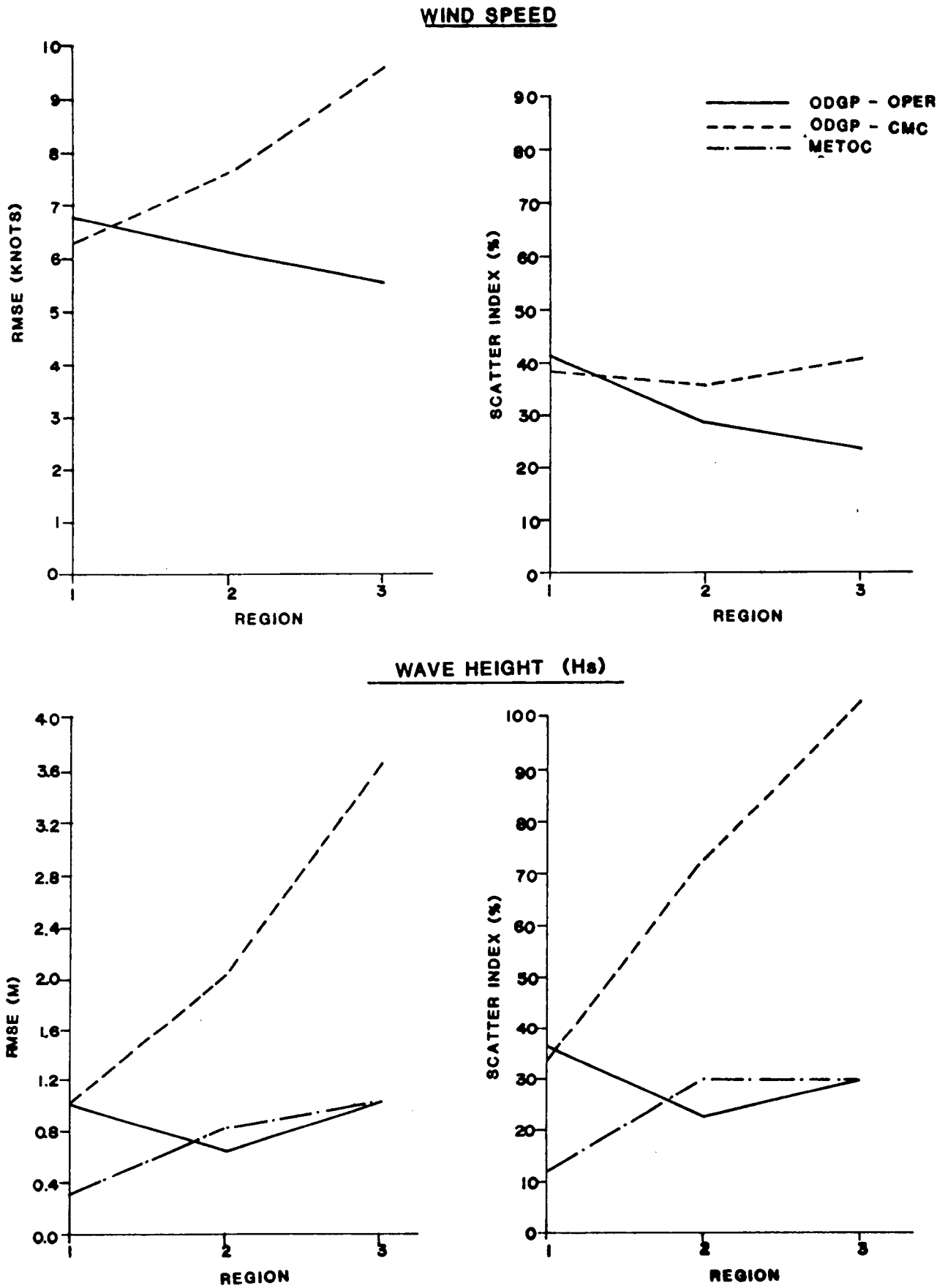

Figure 19. Summary of error statistics by regions for analysis time (T=0) storm cases.

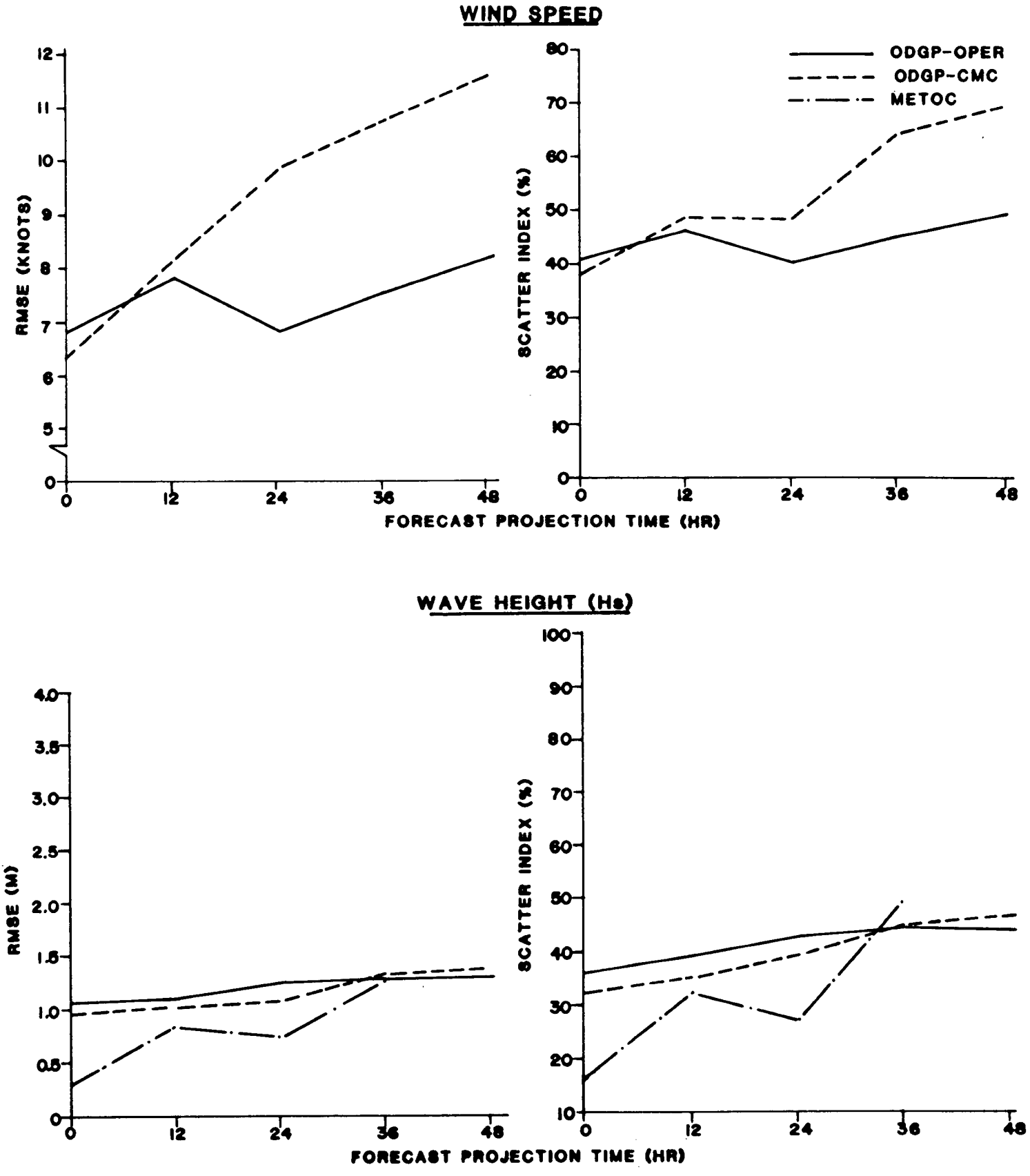

Figure 20. Error statistics for region 1 (U.S. east coast) storm cases.

For region 2, as shown in Figure 21, there is little difference between the wind speed errors for the entire CASP period and for storms only, except that the ODGP-OPR wind SI is actually lower in storms than it is overall, whereas the ODGP-CMC is virtually the same in storms as it is overall. The slight improvement in ODGP-OPR wind in storms seems to be reflected in a slight reduction in ODGP-OPR wave SI in storms relative to overall, at all forecast hours. The METOC wave SI is also slightly improved in storms, though the SI remain 5-10% greater than the ODGP-OPR. On the other hand, the ODGP-CMC wave errors are significantly greater in storms at all forecast hours than overall, though again this result derives mainly from the spectacular errors in the CMC winds and waves in the first two of the four storms studies. ODGP-OPR is slightly better than METOC particularly at T_0 and forecast up to 24 h.

For region 3, (see Figure 22) the ODGP-OPR wind and wave errors in storms are basically the same in magnitude and trend as overall (see Figure 11). The ODGP-CMC wind errors are degraded, however, by 2-3 m/s (RMS) and 5-10% in scatter index, which contributes apparently to significantly larger wave errors for ODGP-CMC in storms on the Grand Banks than overall. METOC wave errors are also relatively more degraded in storms on the Grand Banks than overall and than seen in other regions.

The error statistics provided in Table 9 (i.e. average for entire CASP period) and Table 17 (i.e. average for the 4 storm cases) show that the ODGP-OPR provided a negative bias for the wind speed (i.e. underestimated the winds) yet the predicted H_S was slightly overpredicted (i.e. positive bias). This may indicate that the ODGP model is tuned to low wind speeds, so CMC errors (which have larger positive bias) are magnified.

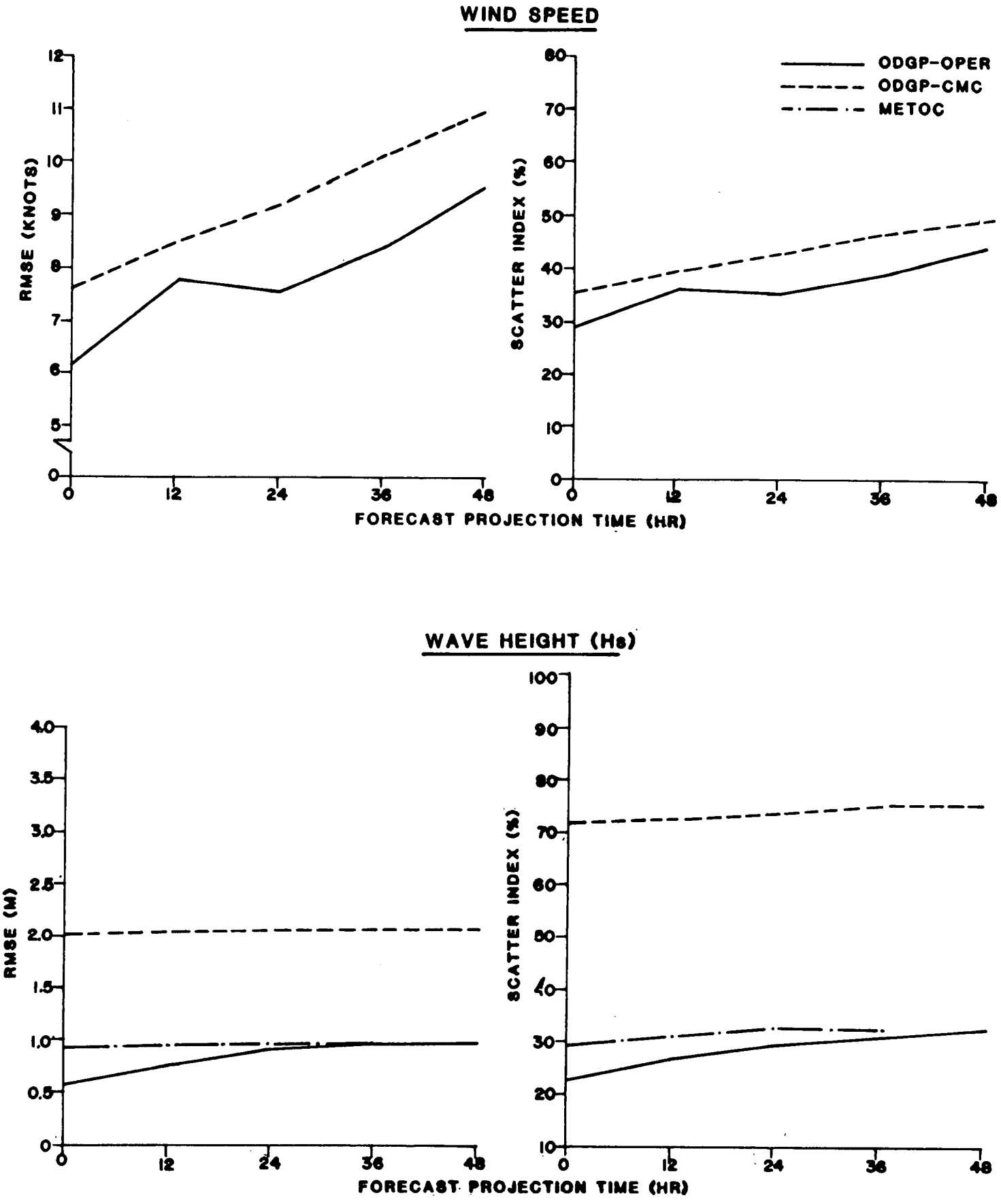

Figure 21. Error statistics for region 2 (Scotian Shelf) storm cases.

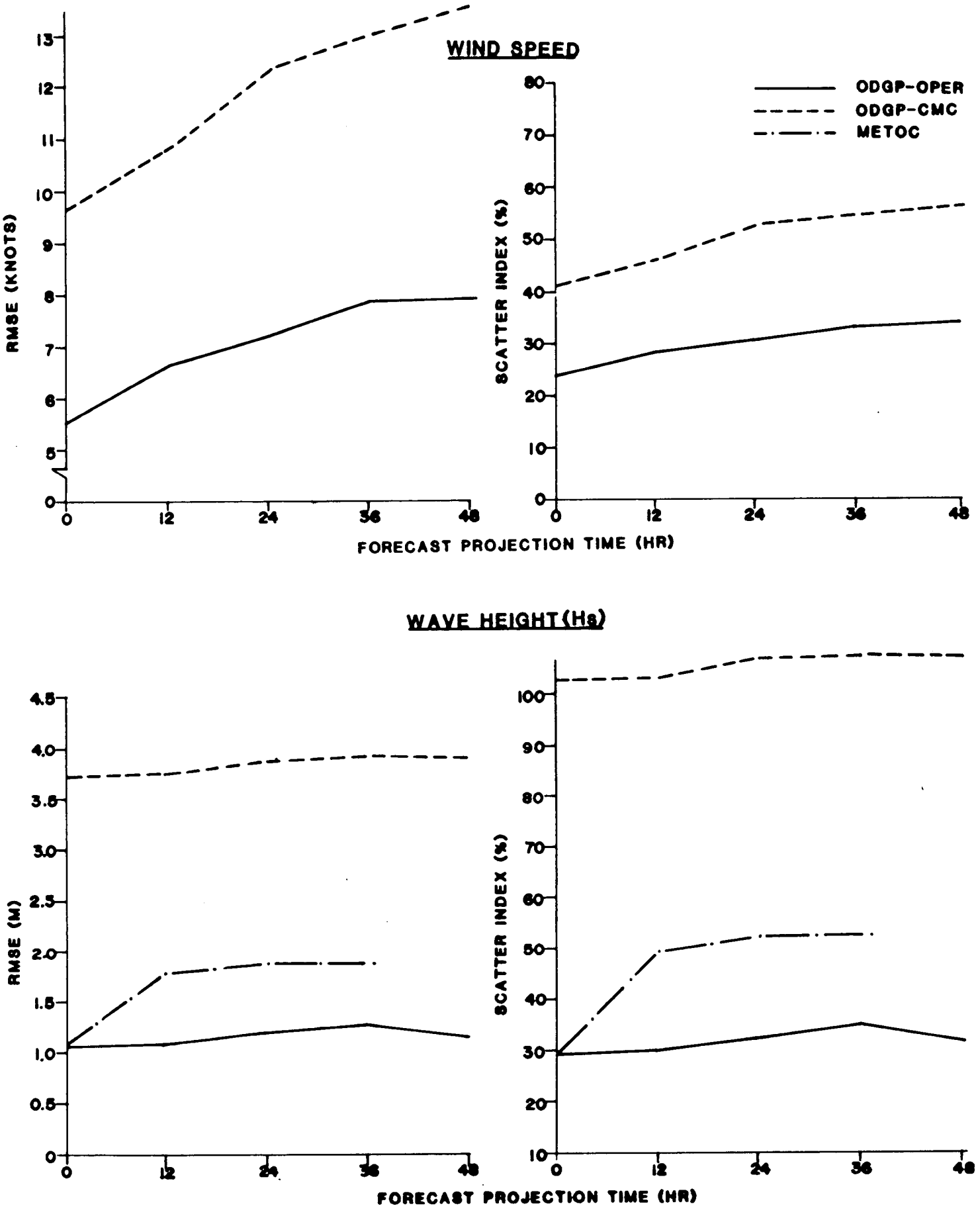

Figure 22. Error statistics for region 3 (Grand Banks) storm cases.

5.5 VERIFICATION OF MEAN AND PEAK WAVE DIRECTIONS

Directional wave measurements were only available from BIO's WAVEC records in the CASP-OC area. Therefore, only model predictions of wave direction from the ODGP-CMC shallow-water model were compared against the measured values. It should be mentioned that, an additional directional (WAVEC) waverider buoy was deployed at Petro-Canada's wellsite (Terra Nova I-97) on the Grand Banks of Newfoundland. However, the recorded data for this buoy were not available for the inclusion in this report.

Time series plots of predicted and observed mean and peak wave directions are presented in Figure 23, 24 and 25 for the CASP-OC sites 41, 42 and 43, respectively. The shown mean directions are the mean vector values which are calculated from the model or WAVEC 2-D spectral energy values. The peak wave direction is the direction at the peak energy. All directions are given in degrees measured clockwise from true North (i.e. same as wind direction convention). Wind directions are given for analysis time (T=0) only.

As shown in Figures 23 - 25, a good agreement between the predicted and observed directions was obtained.

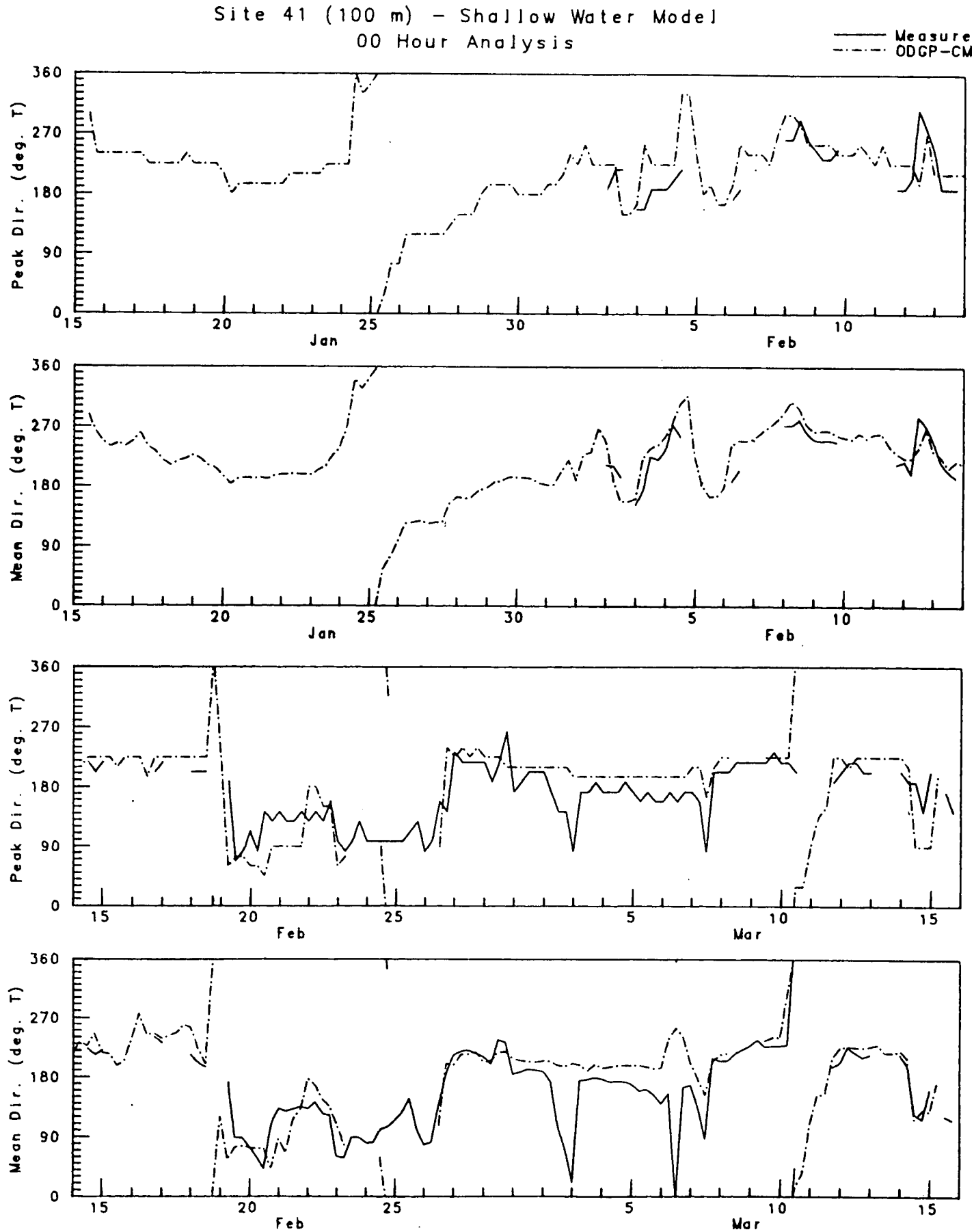

Figure 23. Time series plots of measured vs. model predicted wave directions at Site 41 (100 m).

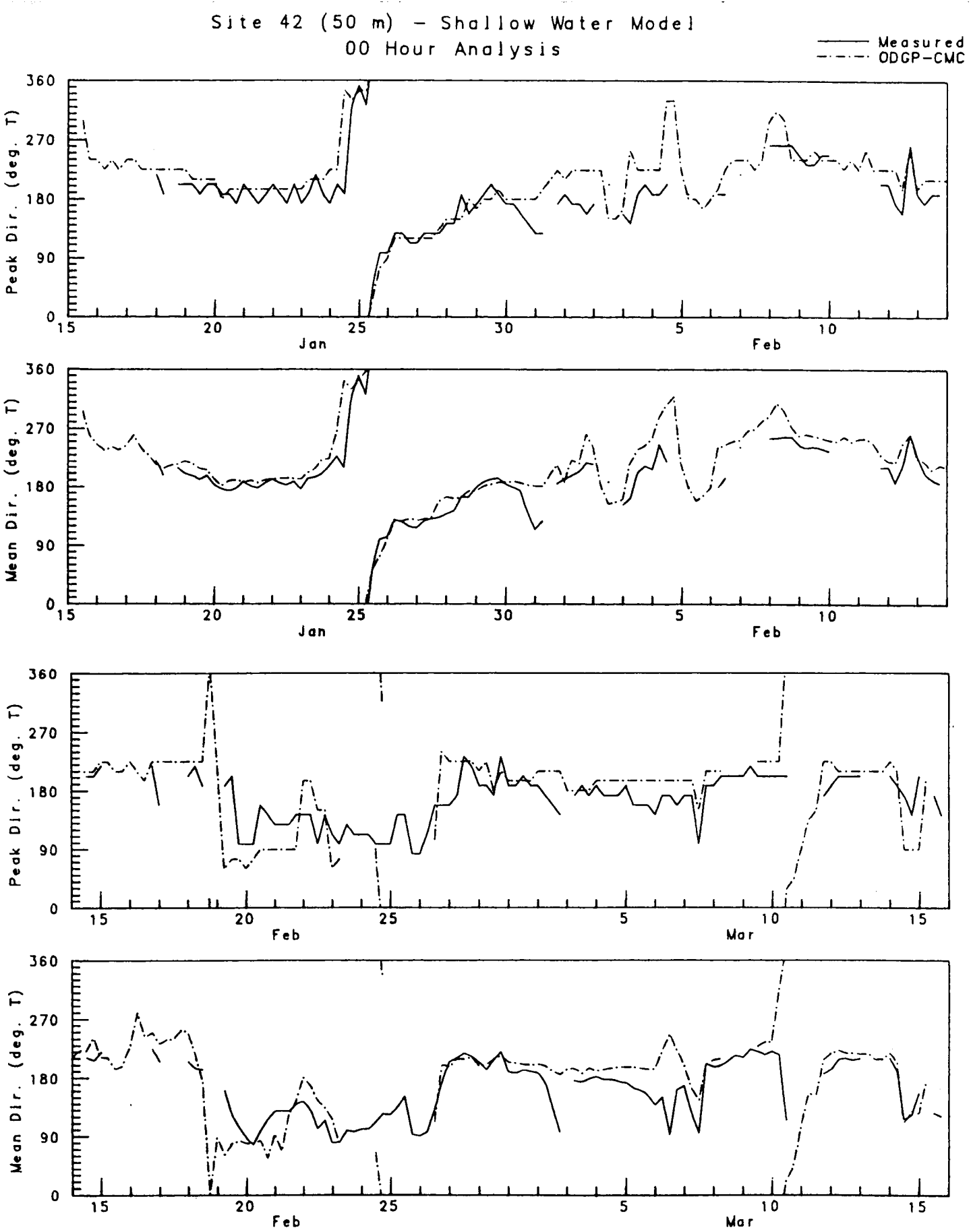

Figure 24. Time series plots of measured vs. ODGP-CMC predicted wave directions at Site 42 (50 m).

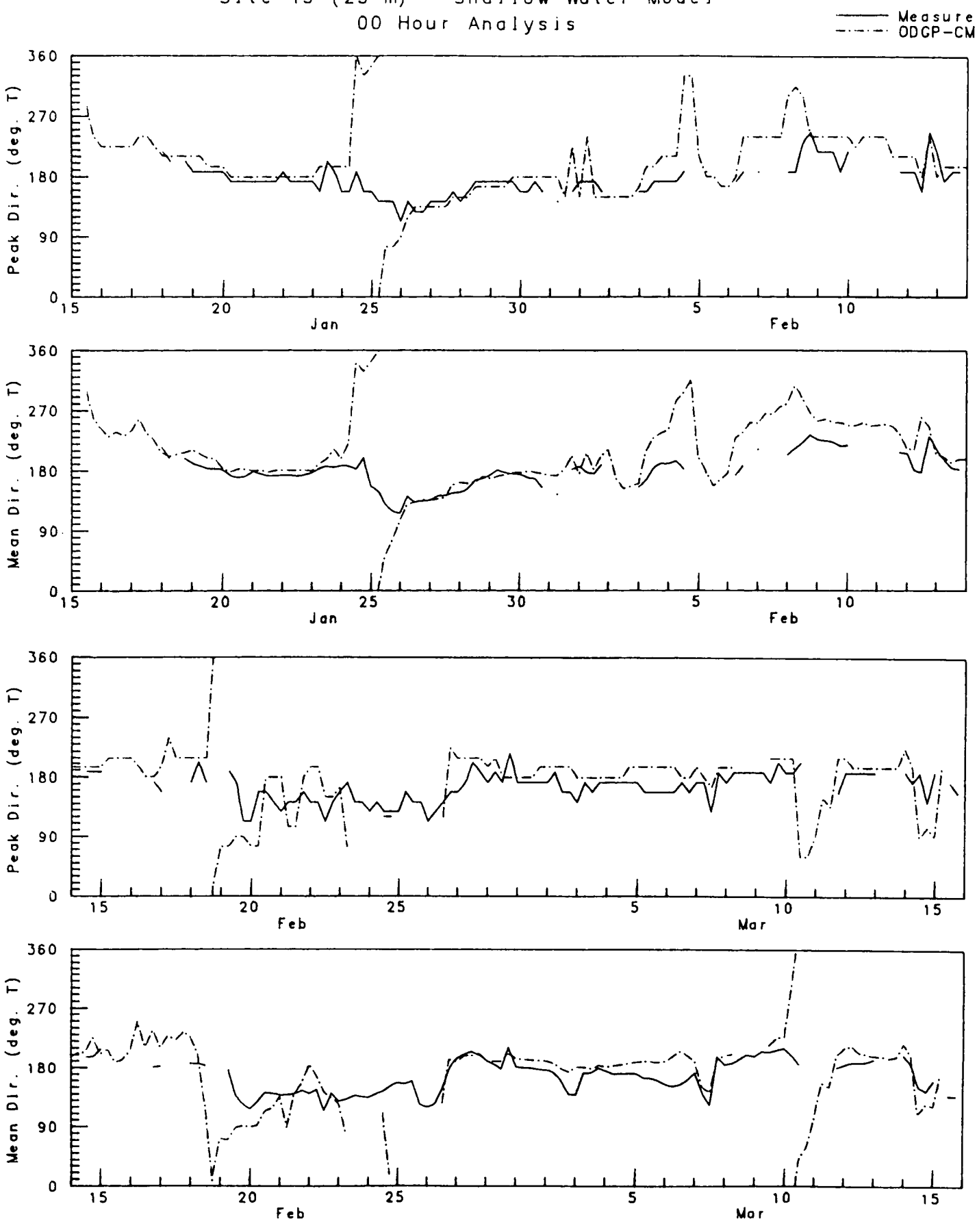

Figure 25. Time series plots of measured vs. ODGP-CMC predicted wave directions at Site 43 (25 m).

6. SUMMARY AND CONCLUSIONS

6.1 SUMMARY

This report describes the work carried out to set-up and test a regional ocean wave model to provide real-time wave forecasts during the two month duration of the CASP field experiment, 15 January - 15 March, 1986. The ODGP spectral ocean wave model was selected for this test. A modified version of the model (called ODGP-CMC) which includes shallow-water equations describing wave propagation in the CASP-OC area was considered. The model was driven by winds obtained from the CMC operational spectral weather prediction model. The CMC winds used for this test were extracted at 0.998 sigma-level, which is approximately 16m above the ocean surface in a standard atmosphere. These winds were suitably interpolated to the model's grid points and used without any modification to drive the ODGP-CMC wave model.

In addition, the results from the operational version of the ODGP (ODGP-OPR which was routinely running in real-time at Oceanweather/MacLaren Plansearch) were obtained and compared to the ODGP-CMC model results. The ODGP-OPR version is identical to the ODGP-CMC deep-water model but driven by winds obtained from the NOAA LFM/NGM numerical weather prediction model's surface pressure and man-machine analysis which incorporates Cardone's Marine Planetary Boundary Layer equations. The sea ice margin was considered in both models by updating their boundaries from ice charts received from the AES ice central in Ottawa (ice concentration of 3/10 or greater was considered as solid boundary).

The implementation of the ODGP-CMC model followed closely the timeliness used for the ODGP-OPR model. Basically; the model was executed twice daily in a hindcast/forecast cycle for 00 and 12 GMT (i.e. tau 0) initial states. In each run the model provided wave predictions at 6-h intervals extending from T+0 to T+48 hour forecast.

A large amount of field measurements were collected during the CASP field experiment. In addition, the METOC wave charts were obtained. The METOC wave height predictions were then compared with ODGP model results at a number of observation sites.

The results from the two models were evaluated against wind/wave data measured at seven deep water sites on the east coast of the U.S.A. and George's Bank, Scotian Shelf and slope, and the Grand Banks. In addition, the shallow water model (ODGP-CMC) was evaluated at three sites along the CASP-OC wave array where directional wave measurements were available.

This study provided a comprehensive evaluation and statistical measures of the accuracy of the operational wave model (ODGP) when driven by two different wind fields (CMC and OPR). The side-by-side evaluation of the ODGP-CMC and ODGP-OPR provides insights into the cause of the main difference between the two models, i.e. input wind fields. Certainly, the CMC provided winds with a large positive bias, which grew with forecast projection times. This, in turn, contributed to the large errors in wave height predictions.

In this test, the ODGP operational wave model predicted sea state accurately with a mean scatter index of 30% at T+0 to 37% at T+48 h with RMSE in the range of 0.85 to 1.07 m, respectively.

When driven by CMC winds, the same model predicted wave height with scatter index of 60 to 70% and RMSE of 1.88 to 1.97m at T+0 and T+48h, respectively. Wave peak periods were predicted with better accuracy by both models (22 to 28% scatter index).

The mean errors in wind speed from the two models at the evaluation sites were not as large as those of the wave heights. This may be due to contributions from non-local random and perhaps spatially coherent wind errors in the CMC winds. A detailed evaluation of the model's wind fields was presented for the selected four storm study cases. This analysis has

shown clearly the spatial differences in the two winds fields, particularly in the vicinity of the low pressure centres. It also showed the improvement in wind field prediction due to the man-machine mix procedure.

The 1-D shallow-water wave model was tested only with CMC winds along the CASP-OC wave array. The accuracy of this model is a function of deep-water input spectra at the end of the 1-D array, treatment of local winds (particularly offshore winds) and the treatment of shallow-water wave propagation. for the entire CASP period, the errors in the shallow-water wave height predictions were close to the deep water errors. When excluding the periods when the input deep-water spectra were incorrect (i.e. the first two weeks of CASP period), the model predicted the wave height with RMSE of 0.5m and scatter index of 35%. The predicted mean and peak wave directions were in close agreement with those obtained from measured WAVEC data.

METOC predictions showed a comparable skill to the ODGP-OPR at analysis time (T+0) whereas the ODGP-OPR provided a better skill in forecast mode.

6.2 CONCLUSIONS

From the scatter diagrams of model predictions versus observations and the resulted correlation coefficients, it is evident that the objective winds from the CMC model at T_0 resulted in a significantly worse intital T_0 wave height field than that obtained from the use of the OPR man-machine winds. This indicates that a better initial CMC wind field at T_0 will definitely improve the ODGP-CMC wave predictions not only at T_0, but also at 12, 24, 36 and 48 h forecasts (as the average errors in wind speed from OPR and CMC models become closer at 36 and 48 h forecasts).

It should be emphasized that all CMC winds used in the CASP runs were obtained directly from the V9 spectral model output (including the T_0 winds). As suggested by Mr. A.O. Mycyk (COGLA, personal communications),

the NWP spectral model Sigma 1 analysis wind (at T_0) is often not very correspondent to the objective MSL analysis for same time. This is a function of the transformation the model performs to reduce MSL to Sigma 1 (or Sigma 0.998) level. Because of this, the winds taken from the CMC objective MSL analysis at T_0 (which was not available in real-time during the CASP test) would be much closer to true winds. These concerns must be addressed in the future utilization of the CMC spectral operational model winds for driving an ocean wave model in Canadian waters.

This study has demonstrated that a spectral wave model can be used successfully in an operational setting to provide guidance for wave forecasts off the east coast of Canada. The assessment of the effect of this guidance on improving the sea state forecasting during the CASP field experiment was the responsibility of the AES forecasters, and was difficult to quantify. However, it was demonstrated that the ODGP model guidance has been very effective in providing accurate site specific wave forecasts to offshore operators since its implementation at MacLaren Plansearch in 1984.

The following conclusions can be drawn from this study:

1. The feasibility of driving a discrete spectral ocean wave model from surface winds derived from a CMC NWP model has been demonstrated in real-time during the CASP. About equal computer resources were required to generate deep-water analyses and forecasts on a 2-D nested grid system as were required for the shallow-water wave predictions on a 1-D array of grid points laid out along the CASP-OC array. Under nominal operational conditions, wave forecasts were delivered twice daily to the CASP desk by analysis hour (0000 GMT, 1200 GMT) plus 7 hours.

2. Difficulties in the operational implementation of the forecast system arose mainly in accessing wind files from the CMC computer system rather than in communication and transmission of wind

files from the CMC computer to the computer used to run the wave model. This can be overcome when the model is set-up and run automatically on the CMC computer facilities once the NWP model is executed and the wind fields are available.

3. In general, errors in wave analyses and forecasts produced from CMC winds (ODGP-CMC) are greater than analyses and forecasts provided by the same wave model (ODGP-OPR) driven by winds derived in man-machine mix procedures from NOAA LFM/NGM NWP model output. The source of the errors in ODGP-CMC wave analyses and forecasts are due to large bias and scatter in CMC wind fields.

4. Shallow-water wave analyses and forecasts in the CASP array derived from ODGP-CMC model were quite skillful when errors in the deep-water input 2-D spectra at the deep end of the CASP array were small. It is difficult within the CASP array to separate errors associated with shallow-water transformations of deep-water input energy from effects of sheltering and fetch restrictions associated with irregular shoreline geometry.

6.3 RECOMMENDATIONS

This study has demonstrated the importance of accurate wind specifications for driving an operational ocean wave model suitable for providing accurate sea state forecasting in the Canadian waters. Furthermore, the study has shown the need to adjust the CMC winds for application to a spectral ocean wave model.

At the time the CASP test took place, CMC was unable to provide winds from the objective analysis which is believed to be superior than the T_0 prognostic winds used in the present study. However, this is now possible, therefore, it is recommended to evaluate these winds and if proven to be suitable, they should be used operationally in the future.

It is also recommended that the sources of errors in the CMC winds, analysis and forecast, are to be studied in detail. This includes errors arising in the CMC boundary layer treatment, surface pressure field forecast behaviour (i.e. cyclogenesis, etc.), and dependence of errors on storm track. As a minimum effort, at least the CASP storm events should be rehindcast using the corrected CMC winds as input to the wave model.

In this study no attempt was made to assess the value of the shallow water parametrization and the effect of model guidance on the improvement of marine forecasts off the east coast of Canada (i.e. to see what the forecast would have been without it?) This was beyond the scope of this study and should be studied in the future.

The 1-D shallow water wave model which was tested within the CASP-OC area provided encouraging results for the periods when the input deep-water spectra were correct. However, further research work and more detailed verification studies are required, before a suitable model is used operationally, e.g. run a two-dimensional shallow-water model. The main limitation to implement such a model for real-time operation is the required large computer resources. Perhaps, this can be overcome by running the model on a super computer like the CRAY or CYBER 205 after proper vectorization of the source code.

Finally, it is recommended to maintain at least one deep-water and one shallow-water directional wave measurement stations for long term operation, with real-time processing of the data, and run forecast systems in an operational or quasi-operational mode for a longer period of time to provide reasonable data sets for proper model evaluation.

7. REFERENCES

Bouws, E., J.J. Ephraums, J.A. Ewing, P.E. Francis, H. Gunther, P.A. Janssen, G.J. Komen, W. Rosenthal and W.J. De Voogt. 1985. A shallow water intercomparison of three numerical wave prediction models (SWIM). Quarterly Journal of the Royal Meteorological Society, 111: 1087-1112.

Cardone, V.J. 1969. Specification of the wind distribution in the marine boundary layer for wave forecasting. Geophysical Science Laboratory, New York University. Report TR-69-1. Available from NTIS AD#702-490, New York, N.Y.

Cardone, V.J., W.J. Pierson, and E.G. Ward. 1976. Hindcasting the directional spectrum of hurricane generated waves. Journal of Petroleum Technology 28: 385-394.

Cardone, V.J. 1978. Specification and prediction of the vector wind on the U.S. continental shelf for application to an oil slick tragectory forecast program. Final Report for NOAA, U.S. Department of Commerce, Silver Spring, Maryland.

Cardone, V.J. and D. Szabo. 1985. Impact of uncertainty in specfication of offshore wind on accuracy of wind hindcasts and forecasts. Proceedings of International Workshop on Offshore Winds and Icing. Halifax, N.S., Oct. 7-11, 1985.

Coté, L.J., J.O. Davis, W. Marks, R.J. McGough, E. Mehr, W.J. Pierson, F.J. Ropek, G. stephenson, and R.C. Vetter. 1984. The directional spectrum of a wind generated sea as determined from data obtained by the Stereo Wave Observation Project (SOWP). Meteorological Paper, New York University, New York, N.Y. 2(6): 88 p.

Creswick, W.S. 1983. The CMC operational spectral forecast model. CMC information 22-38, May 1983.

Daley, R., C. Girard, J. Henderson and I. Simmonds 1976. Short term forecasting with a Multi-Level Spectral perimitive Equation Model, Part I - model formulation. Atmosphere, 14 (2): 98-133.

Delage, Y. 1985. Surface turbulent flux formulation in stable conditions for atmospheric circulation models. American Meteorological Monthly Weather Review, 113 (1): 89-98.

Eid, B.M., V.J. Cardone, and J.A. Greenwood. 1985. Evaluation of two operational spectral ocean wave models: SOWM and ODGP. Paper presented at the 19th Annual Congress of the CMOS, Montreal, Quebec. June 12-14.

Forrestall, G.Z., E.G. Ward, V.J. Cardone, and L.E. Borgmann. 1978. Kinematics of surface gravity waves in tropical storm Delia. Journal of Physical Oceanography, 8: 888-909.

Forrestall, G.Z., E.G. Ward, and V.J. Cardone. 1980. Directional wave spectra and wave kinematics in hurricanes Carmen and Eloise. Proceedings 17th International Coastal Engineering Conference ASCE, Sydney, Australia, March 23-28, 1980.

Grant, W.D., and O.S. Madsen. 1982. Movable bed roughness in unsteady oscillatory flow. Journal of Geophysical Research 87 (C1): 469-481.

Greenwood, J.A., and V.J. Cardone. 1977. Development of a global ocean wave propagation algorithm. Final report to U.S. Navy Fleet Numerical Weather Central, Monterey, California, Contract N-00228-76-C-3081.

Long, R.B. 1980. The statistical evaluation of directional spectrum estimates derived from pitch/roll buoy data. Journal of Physical Oceanography, 10: 944-952.

MacLaren Plansearch Limited. 1985. Evaluation of the spectral ocean wave model (SOWM) for supporting real-time wave forecasting in the Canadian east coast offshore. Report submitted to the Atmospheric Environment Service, Department of the Environment,

Mitsuyasu, H., et.al. 1985. Observations of the directional spectrum of ocean waves using a cloverleaf buoy. Journal of Physical Oceanography 5: 750-760.

Morgan, H.R. 1971. The analysis and forecast of sea and swell conditions in deep water. Atmospheric Environment Service, Technical Memo. 763.

Pierson, W.J., and L. Moskowitz. 1964. A proposed spectral form for fully developed wind seas based in the similarity theory of S.A. Kitaigorodskii. Journal of Geophysical Research 69: 5181-5190.

Pierson, W.J., L.J. Tick, and L. Baer. 1966. Computer based procedures for preparing global wave forecasts and wind field analyses capable of using wave data obtained by a space craft. Sixth Naval Hydrodynamics Symposium, ACR-136, Office of Naval Research, Department of the Navy, Washington, D.C., 499-532.

Reece, A.M., and V.J. Cardone. 1982. Test of wave hindcast model results against measurements during four different meteorological systems. Fourteenth Annual Offshore Technology Conference, Houston, TX, May 1982. OTC #4323.

Resio, D.T. 1981. The estimation of wind-wave generation in a discrete spectral model. Journal of Physical Oceanography, 10: 510-525.

Seymour, R.J. 1977. Estimating wave generation on restricted fetches. ASCE Journal of Waterways, WW 2: 251-264.

SWAMP (Sea Wave Modelling Project). 1985. Ocean wave modelling. Plenum Press, New York, N.Y. 256 P.

Whalen, J.E., and M.K. Ochi. 1978. Variability of wave spectral shapes associated with hurricanes. Offshore Technology Conference 10: OTC 3228.

APPENDICES

APPENDIX A

ODGP GROWTH ALGORITHM

A.1 ODGP GROWTH ALGORITHM (CMPE24)

A.1.1 Mathematical Method: General

The account below is taken with minor modifications from Cardone et al. (1974).

Resonance Mechanism

The basis of the resonance mechanism parameterizations employed in the spectral growth models of Inoue (1967), Pierson, Tick and Baer (1966), Barnett (1968), Ewing (1971) and others is the form for the atmospheric turbulent pressure spectrum proposed by Priestley (1965), who made field measurements of pressure fluctuations over mowed grass. This spectrum can be written

$$\Pi(\omega,\theta) = \frac{4\phi(\omega)}{2\pi^2} \left\{ \frac{\gamma}{\gamma^2 + (k\cos\theta - \kappa)^2} \right\} \left\{ \frac{\delta}{\delta^2 + k^2\sin^2\theta} \right\} \tag{A.1}$$

where k is defined by $\omega^2 = gk$, $\omega = 2\pi f$, Θ is the angle from the wind direction and κ is ω/U_c, where U_c is a convection velocity. According to Priestley, γ and δ were determined as

$$\delta = .52\kappa^{.95} \tag{A.2}$$

$$\gamma = .33\kappa^{1.28} \tag{A.3}$$

Since κ is not a mere numeric, but has the dimensions of a wave number, (A.2) and (A.3) are dimensionally impossible. The correlations actually found by Priestley are:

$$\beta\gamma = 0.41(\beta\kappa)^{1.28},$$

$$\beta\delta = (\beta\gamma)^{0.74}/0.84,$$

where $\beta = 1$ meter; whence we deduce

$$\beta\delta = 0.5170\ (\beta\kappa)^{0.9472}.$$

The adopted computational forms, however, agree neither with (A.2) and (A.3) as given by Inoue nor with Preistley; they are

$$\beta\gamma = 0.33(\beta\kappa)^{1.25},\ \delta = 0.52\kappa$$

For $\kappa < .02\ m^{-1}$, γ and δ are best approximated by evaluating (A.2) and (A.3) at $\kappa = .02\ m^{-1}$. In the adopted computational form,

$$\beta\gamma = 0.33(.02)^{1.28} \simeq 2.207 \times 10^{-3};$$

thus γ is discontinuous at $\beta\kappa = .02$. The value of δ was <u>not</u> stabilized for small κ.

$\phi\ (\omega)$ was expressed as $\phi(\omega) = \Phi\psi(\omega)$ with $\psi(\omega) \simeq 1.23/\omega^2$ and Φ a scalling factor. In terms of the pressure spectrum, the linear growth rate can be written

$$A(\omega,\theta), = \omega^5 g^{-3} \rho_w^{-1} \Pi(\omega,\theta) \qquad (A.4)$$

where ρ_w is water density and g is the gravitational acceleration.

Inoue (1967), following Snyder and Cox (1966), adopted a scalling factor proportional to the fourth power of the wind speed

$$\phi = A^{*}.u^{4}, \qquad (A.5)$$

fit A* with linear wave growth rates measured by Snyder and Cox (1966) in the field, and was thereby able to integrate (A.4) over ±90° to the wind direction to obtain the linear growth term; but Cardone et al, (1974) found it advisable to compute linear growth for each direction separately. A reasonable compromise between the measurements of Priestley and of Snyder and Cox was obtained by reducing Inoue's A term constant by a factor of 3. A numerical coefficient in CMPE24 has been verified by Cardone to incorporate all mathematical and physical constants and all empirical factors (including the coefficients of γ and δ), in the aforesaid equations.

Instability Mechanism

The Miles-Phillips instability growth parameterization (i.e. B term in equation (1)) remains unchanged from the PTB formulation, and can be written as a function of wave direction as

$$B/\omega = \left\{5.0\ e^{-7000[ARG-.031]^2} + 2612\ ARG^2 e^{-.0004(ARG)^{-2}}\right\} \div 3600.$$

where ARG is $u_* \cos\theta/C$, and C is wave phase speed. (A.6)

Kitaigorodskii Range

An important aspect of all (as far as we know) existing spectral hindcast models is the parameterization of dissipative wave breaking effects by the adoption of some limiting or fully developed state to limit component growth for effectively long fetch or duration. The so-called equilibrium range

$$S_\infty(f) = \frac{\alpha g^2}{(2\pi)^4 f^5}$$

where $\alpha = 8.1 \times 10^{-3}$, g is gravity, and f is frequency has been widely adopted to describe this limit for frequencies higher than the fully developed peak frequency. The constant α, as given above, has been verified repeatedly in the literature, especially for open ocean wave measurements.

A recent study of the behavior of the high frequency gravity and gravity-capillary regions of the wave spectrum (Pierson and Stacy 1972) has verified, however, the existence of a range of frequencies in the fully developed part of the spectrum that obeys the form originally proposed by Kitaigorodskii (1962) and expressed in terms of frequency as

$$S_k(f) = \left\{ \frac{\alpha g^2}{(2\pi)^4 u_{*_{min}} f_2} \right\} \frac{u_*}{f^4} \qquad (A.7)$$

where u_* is friction velocity, $u_{*_{min}}$ is a critical friction velocity, and f_2 is the upper limit to which this form applies. The lower frequency to which this form applies is given by Pierson and Stacy as

$$f_{min} = \frac{u_{*min}}{u_*} f_2 \quad . \tag{A.8}$$

It follows that in the Kitaigorodskii range, the spectral density exceeds the equilibrium value by the factor

$$\frac{S_k(f)}{S_\infty(f)} = \frac{f}{f_{min}} \quad .$$

There are few measurements to precisely fix the values of u_{*min} and f_2 in (A.7). For u_* in cm/sec and f in hz, the available data suggests $u_{*min} = 12 \pm 3$ and $f_2 = 3 \pm 5$ to give nominally

$$f_{min} = 36/u_* \tag{A.9}$$

Hence, for even moderately strong wind speeds (u_* 1m/sec), f_{min} lies well outside the range of interest for wave hindcasting. At high wind speeds, however, this range apparently moves into the region of the spectrum that contributes significantly to the total variance. For incorporation of this range into the hindcast model in Phase I of NYU's ODGP modelling study executed in 1972 a value of 22.5 was chosen for $u_{*min} \cdot f_2$; this value has since been revised downward to 18.0.

Recent work by Kitaigorodskii (1983), Leykin and Rozenberg (1984), and Donelan and Pierson (1983) tends to discredit the existence of an ω^{-4} range in the form given by Pierson and Stacy and used in CMPE24

This ω^{-4} range and the computational assumption that the integrated band is always in equilibrium with the local wind combine to inflate the total variance produced by CMPE24 and at short fetches.

Directionnl Growth Revision

The modification to previous growth models that grew each directional component explicitly required the introduction of a quasi-intuitive dissipation mechanism to preserve the concept of the SWOP angular spreading form in the fully developed directional distribution. The procedure adopted in CMPE24 is perhaps best revealed in the following step-by-step description of what happens at a grid point to the 24 numbers representing the 15° bandwidth variance elements for a particular frequency:

1. For each directional band within 90° of the wind direction (θ_ω), at the local grid point, compute the fully developed variance, $S_\infty(\theta_i)$ by applying the SWOP spreading function to the appropriate one-dimensional fully-developed spectral form S_∞.

2. Cycle through the directional bands that satisfy $\theta_\omega - 90° < \theta_i < \theta_w + 90°$ at the grid point for the given frequency. If $S(\theta_i) > S_\infty(\theta_i)$, flag this direction and remember $S(\theta_i) - S_\infty(\theta_i)$. If $S(\theta_i) \leq S_\infty(\theta_i)$, compute $A(\theta_i)$ and $B(\theta_i)$, that is, the linear and exponential growth rates appropriate to the given direction and grid point wind speed, and solve

$$\frac{d}{dt} T(\theta_i) = A(\theta_i) + B(\theta_i) T(\theta_i), \qquad \text{(A.10)}$$

where

$$T(\theta_i) = S(\theta_i)\left\{1 - [S(\theta_i)]^2 [S_\infty(\theta_i)]^{-2}\right\}^{-\frac{1}{2}},$$

for a time step of DELTHR hours. Oceanweather's practice, in all wave models involving both growth and propagation (i.e. all models other than pure duration tests) is to grow for half a time step, then propagate for a full time step, then grow for the remaining half time step.

3. Again, cycle through the directional bands within 90° of the wind and compute the one-dimensional variance.

$$\sum S = \sum_{\theta_w - 90^\circ}^{\theta_w + 90^\circ} S(\theta_i) \qquad \text{(A.11)}$$

If $\Sigma S < \Sigma S_\infty$, go to Step 4. If $\Sigma S > \Sigma S_\infty$, that is, this time step has produced an overdeveloped one-dimensional variance, then eliminate the one-dimensional overdeveloped S_∞-S by reducing each overdeveloped directional component flagged in (2) at a rate proportional to the degree of overdevelopment.

4. Cycle through those directional bands that are within (θ_w + 180°) ± 90° and apply the dissipation function.

It should be added that Steps 1 through 3 are not applied if the one-dimensional spectrum is initially overdeveloped, so as not to affect the swell propagation capabilities of the model; the energy implicitly dissipated in the angular redistribution effected by this new procedure is presumed to go into wave breaking.

A.1.2 Mathematical Method: Specific

The computational procedures of CMPE24 are outlined as follows:

1. Initialize highest frequency band to zero in 24 directions. This band is exempt from standard growth and propagation: on return from CMPE24, the spectrum in the highest band is either zero (KWAX = 14) or a fully developed spectrum (KWAX =15).

2. If the wind speed at the grid point is less than 5 knots, return to calling program.

3. Compute the friction velocity u_* by solving

$$kU_{19.5} = u_* \log_e (Z/Z_0),$$

where $k = 0.4$, $Z = 65$ft., $Z_0 = c_1 u_*^{-1} + c_2 u_*^2 - c_0$, $c_1 = .00073627$ $\text{ft}^{-2}\text{sec}^{-1}$, $c_2 = .0013045$ $\text{ft}^{-1}\text{sec}^2$, $c_0 = .0014534$ ft.

4. Compute the wind speed at height 6.1 meters.

5. Compute sundry trigonometric functions of the angle between a band and the wind direction, entering into the SWOP spreading function.

6. Compute for KWAX (14 or 15) bands, the 1-dimensional fully developed spectrum (Pierson-Moskowitz, with the ω^{-4} regime of equation (A.7) grafted on), and the coefficients BBX and BCX used in the spreading function.

7. Compute the frequency spectrum before growth, SIGMA (I), by summing the current spectrum over 12 downwind bands.

8. Loop over frequency; if current frequency spectrum is overgrown, or P-M frequency spectrum is negligible, do nothing; else:

9. Loop over 12 downwind bands. Compute EMAXX, the saturated spectrum in the frequency-direction band. In the 15th frequency band, the new spectrum has been set to EMAXX.

10. If the frequency-direction (f-d) band is overgrown, prepare for cutback; if f-d band exceeds 95% of saturation, grow at once to saturation; else:

11. Compute the exponential growth coefficient; compute the linear growth coefficient; integrate equation (A.10).

12. Cutback the overdeveloped bands (equation (A.11) and its subsequent checks). Note that this code is reached only when the frequency spectrum is underdeveloped before growing and overdeveloped after.

13. Compute downwind energy, exclusive of integrated band: 14 frequencies, 12 directions.

14. Dissipate upwind energy: 14 frequencies, 11 directions; i.e. the band containing the upwind direction and 5 bands on either side. A deep water dissipation mechanism is included in the PTB method, to model attenuation of swell moving against the wind sea. With

$$S_w = \sum_i S_w(f_i)$$

$$\frac{S_D(f_i,\theta_j)}{S_o(f_i,\theta_j)} = \left(e^{-D\sqrt{S_w} f_i^4} \right)^N \qquad \text{(A.12)}$$

where $S_o(f_i,\theta_j)$ is a component travelling against the wind, $S_D(f_i,\theta_j)$ is the component after dissipation over one time step, and $N = 4$ if θ_j is opposite to the wind, $N = 3.5$ if θ_j is $\pm 15°$ to the wind, $N = 3$ if θ_j is $\pm 30°$ to the wind, and so on, and D controls the degree of attenuation for a specified time step.

The fourth-power frequency dependence rests on an alleged analogy with eddy viscosity. Equation (A.12) is similar to equation (51) in Pierson (1982) which was used in SOWM.

ADDITIONAL REFERENCES

Barnett, T.P. 1968. On the generation, dissipation and prediction of ocean wind waves. Journal of Geophysical Research, 73: 513-529.

Cardone, V.J., C.B. Greenwood, J.A. Greenwood, W.J. Pierson, R.A. Salfi and R.A. Stacey. 1974. Development of wave hindcasting methods applicable to hurricanes. Final Report, Ocean Data Gathering Program-Analysis Phase. Submitted to Shell Development Company.

Donelan, M., and M.J. Pierson. 1983. The sampling variability of estimates of spectra of wind-generated gravity waves. Journal of Geophysical Research, 88 (C7): 4381-4392.

Hasselmann, K., T.P. Barnett, E. Bouws, H. Carlson, D.E. Cartwright, K. Enke, J.. Ewing, H. Gienapp, D.E. Hasselmann, P. Kruseman, A. Meerburg, P. Muller, D.J. Olbers, K. Richter, W. Sell, and H. Walden. 1973. Measurements of wind-wave growth and swell decay during the Joint North Sea Wave Project (JONSWAP). Deutsche Hydrographische Zeitschrift, Supplement A8, 12.

Inoue, T. 1967. On the growth of the spectrum of a wind generated sea according to a modified Miles-Phillips mechanism and its application to wave forecasting. Geophysical Sciences Laboratory, New York University, N.Y. TR-67-5,

Kitaigorodskii, S.A. 1962. Applications of the theory of similarity to the analysis of wind generated wave motions as a stochastic process. Akad. Nauk. SSSR. Bull. Sci. Geophysical Series No. 1: 73-80.

Kitaigorodskii, S.A. 1983. On the theory of the equilibrium range in the spectrum of wind generated gravity waves. Journal of Physical Oceanography 13 (5): 816-827.

Leykin, I.A., and A.D. Rozenberg (1984). Sea-tower measurements of wind-wave spectra in the Caspian Sea. Journal of Physical Oceanography 14 (1): 168-176.

Miles, J.W. 1957. On the generation of surface waves by shear flows. Journal of Fluid Mechanics 3: 185-204.

Phillips, O.M. 1958. The equilibrium range in the spectrum of wind generated waves. Journal of Fluid Mechanics 4: 426-434.

Pierson, W.J. 1982. The spectral ocean wave model (SOWM) a Northern Hemisphere computer model for specifying and forecasting ocean wave spectra. Prepared for the David Taylor Naval Ship Research and Development Command under Contract N00167-80-M-4781.

Snyder, R., and C.S. Cox. 1966. A field study of the wind generation of ocean waves. Journal of Marine Research 14: 141-177.

APPENDIX B

MASTER DATA FILE FORMAT

DATABASE STRUCTURE

Tape Data Field

1. SITE S_1, (2 fields):
   - first field
     - 1 = East Coast of U.S.A.; Region (1)
     - 2 = Scotian Shelf; Region (2)
     - 3 = Grand Banks; Region (3)
     - 4 = CASP-OC; Region (4)
   - second field = site number (e.g. 1, 2, 3,...)

2. LOCATION (9 fields): Latitude (4 fields) and Longitude (5 fields) of a given location (i.e. measuring site or model grid point).

3. DATE (8 fields): YYMMDDHH (HH in GMT) (e.g. 86011500)

4. DATA SOURCE, S_2, (2 fields):
   - first field:
     - 1 = measured data
     - 2 = ODGP-CMC
     - 3 = ODGP-OPR
     - 4 = METOC
   - second field:

     For obs.:
     - 0 = site a
     - 1 = site b
     - 2 = site c

     For model:
     - 0 = deep water
     - 1 = shallow water
     - 2 = wave direction information (i.e. average and peak period)

5. RECORDS

a) Waves (measured or predicted)

/$H_sH_sH_s$/$P_pP_pP_p$/ (6 fields)

where $H_sH_sH_s$ = significant wave height (H_s) in metres and tenth of metres (e.g. 3.7m = 037)

$P_pP_pP_p$ = Wave "Peak" period in seconds and tenth of seconds (e.g. 10.5s = 105; 8.7 = 087)

b) Winds (measured or model)

/ffddd/ffddd/ZZZ/

where ff = wind speed in knots (2 fields)
ddd = wind direction in degree (true) (3 fields: 0-360)
ZZZ = anemometer height above MWL in metres and tenth of meters, i.e. in decimetre (e.g. 20.5 = 205)

Note: The first set of wind speed and direction refers to the effective neutral winds at 19.5m and the second set is the measured winds at a given anemometer height (ZZZ).

c) Additional Information Field

Any additional data is recorded following the above data fields. This includes the following:

For observation file, the water and air temperature is entered (8 field) as follows:

/$S_nT_wT_wT_w$/$S_nT_aT_aT_a$/

where S_n = Sign of temp. (zero or blank for temp. above zero and 1 for temp. below zero)

$T_wT_wT_w$ = Sea surface temperature in degrees and tenth of degrees Celsius

$T_aT_aT_a$ = Air temperature in degrees and tenth Celsius (e.g. 15.4 = 154, 0.8 = 008)

For Forecast Mode, this additional field will include the 12, 24 and 48 hour forecasts (h_s P_p f and d) in the following format:

/tt/$H_sH_sH_s$/$P_pP_pP_p$/ffddd/tt/$H_sH_sH_s$/$P_pP_pP_p$/ffddd/...etc.

where tt = lead time (i.e. 12, 24, 36 or 48)

For wave direction, this additional field is used as follows:

/000/$\Theta_p\Theta_p\Theta_p$/

where Θ = mean wave direction (°T)
Θ_p = peak wave direction (°T)

Card Image of a Record in the Master Data File Format

	Location				Date Time					Waves		Wind[1]		Wind[2]			Additional Information if Necessary
S_1	N dg	Lat m.	W dg	Long m.	Yr	Mo	Dy	Hr	S_2	H_s	P_p	SPD	DIR	SPD	DIR	Z	
xx	xx	xx	xxx	xx	xx	xx	xx	xx	xx	xxx	xxx	xx	xxx	xx	xxx	xxx	
Field No.	1	2	3		4	5	6	7	8	9	10	11	12	13	14	15	16

Field Number	Column No.	Element
01	01-02	Site Code Number (1, 2 or 3) and rig location number
02	03-06	Latitude (N;degrees and minutes)
03	07-11	Longitude (W;degrees and minutes)
04	12-13	Year (e.g. 83, 84, etc.)
05	14-15	Month
06	16-17	Day
07	18-19	Hour - GMT (e.g. 00, 06, 12, etc.)
08	20-21	Data Source code (e.g. 10, 20, 30 or 40)
09	22-24	Significant Wave Height (H_S, in decimeter)
10	25-27	Wave Peak Period (P_p, in seconds)
11	28-29	Wind speed at standard (model) height
12	30-32	Wind direction at standard (model) height
13	33-34	Wind speed measured at anemometer height
14	35-37	Wind direction measured at anemometer height
15	38-40	Anemometer height above sea level (decimeter)
16	41-80	Additional data (may vary depending on source type, available data, etc.)

NOTE:

1) $Wind_1$ means wind data measured, analyzed or computed at a unified height above the sea level (which is used in SOWM/ODGP computations)

   $Wind_2$ is the actual winds "measured" at the anemometer level (Z)

2) All missing data should be replaced by -9 or -99 or -999, etc. depending on the number of data fields.

3) All data are in INTEGER form as described previously.

4) Wind direction is given in degrees measured clockwise from True North (°T).

5) Wave directions (Peak or Mean) in degrees measured clockwise from True North (°T), same as winds.

APPENDIX C

DEEP-WATER MODEL RESULTS

- TIME SERIES PLOTS
- SCATTER DIAGRAMS & REGRESSION ANALYSIS

Measured Data vs. Model Predictions

January 15, 1986 to February 14, 1986
NOAA Buoy 44004 – Site 11
00 Hour Analysis

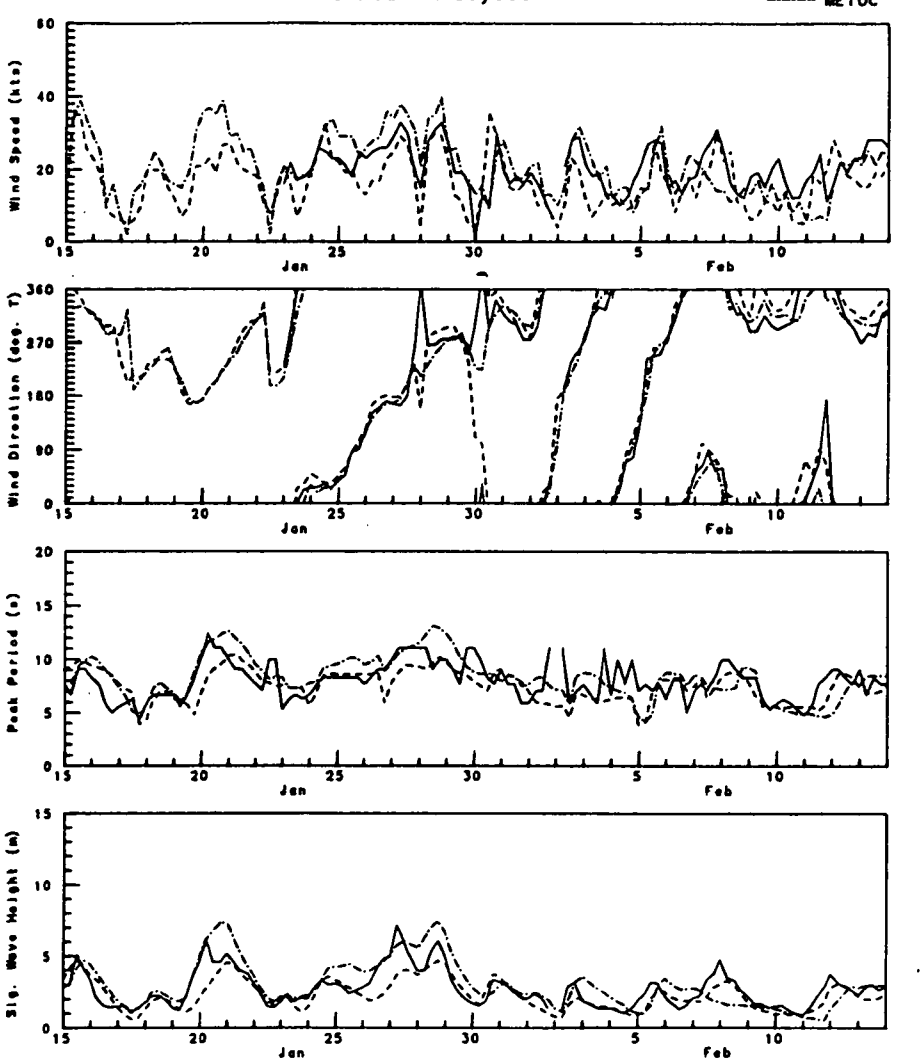

Measured Data vs. Model Predictions

February 14, 1986 to March 16, 1986
NOAA Buoy 44004 – Site 11
00 Hour Analysis

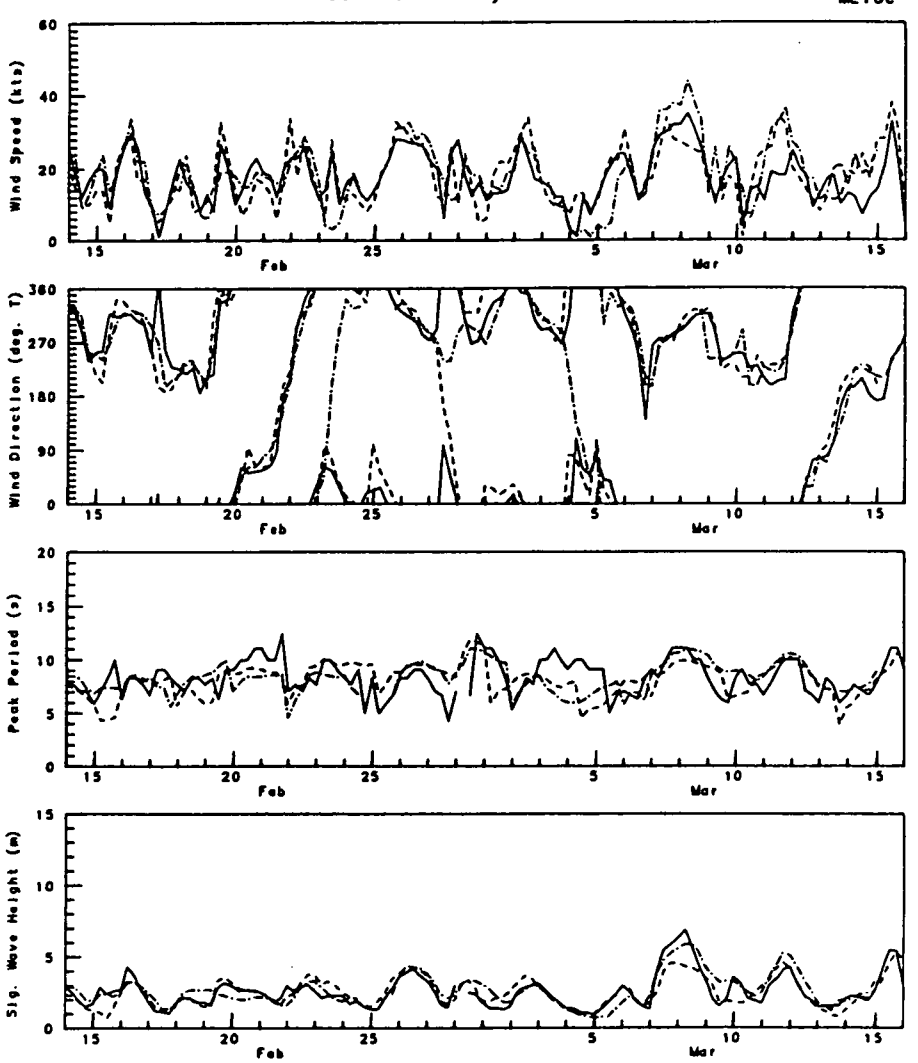

Measured Data vs. Model Predictions

January 15, 1986 to February 14, 1986
NOAA Buoy 44004 - Site 11
12 Hour Forecast

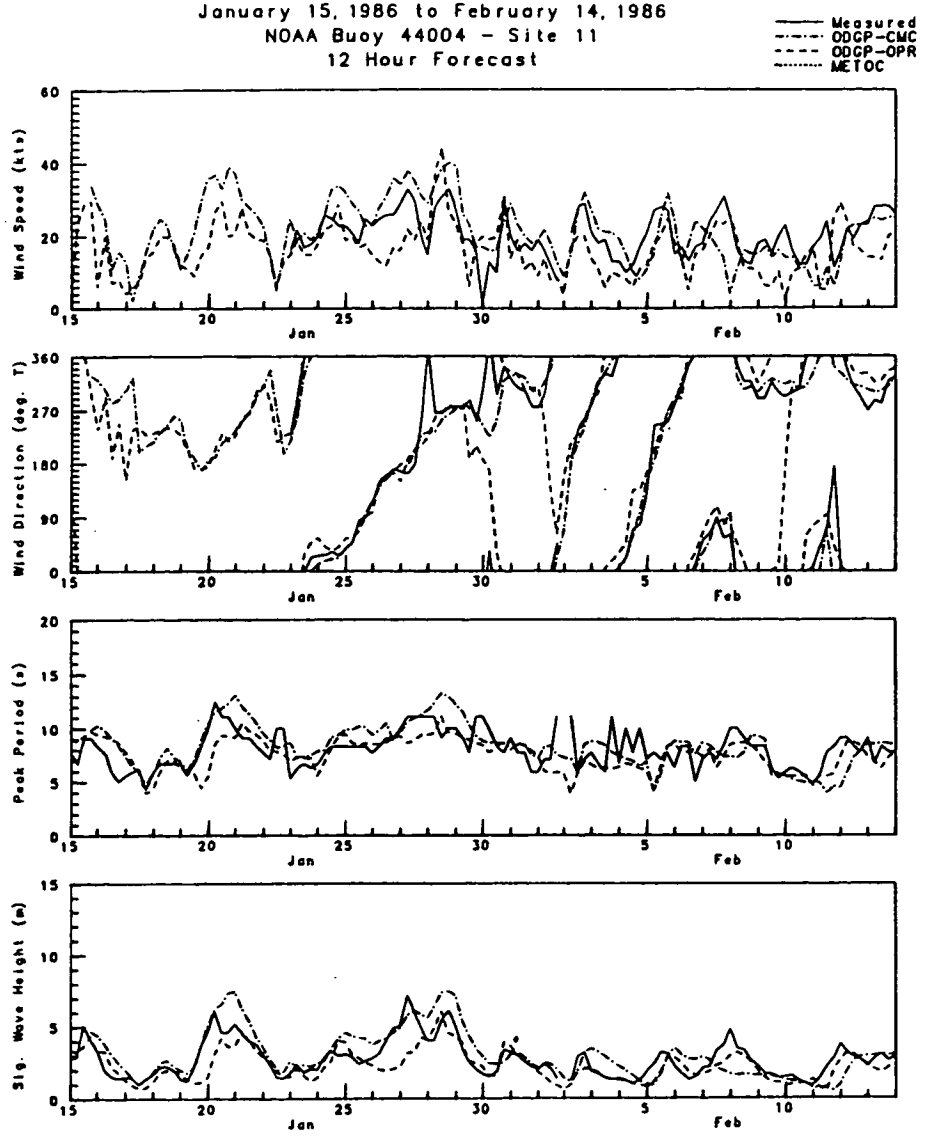

Measured Data vs. Model Predictions

February 14, 1986 to March 16, 1986
NOAA Buoy 44004 - Site 11
12 Hour Forecast

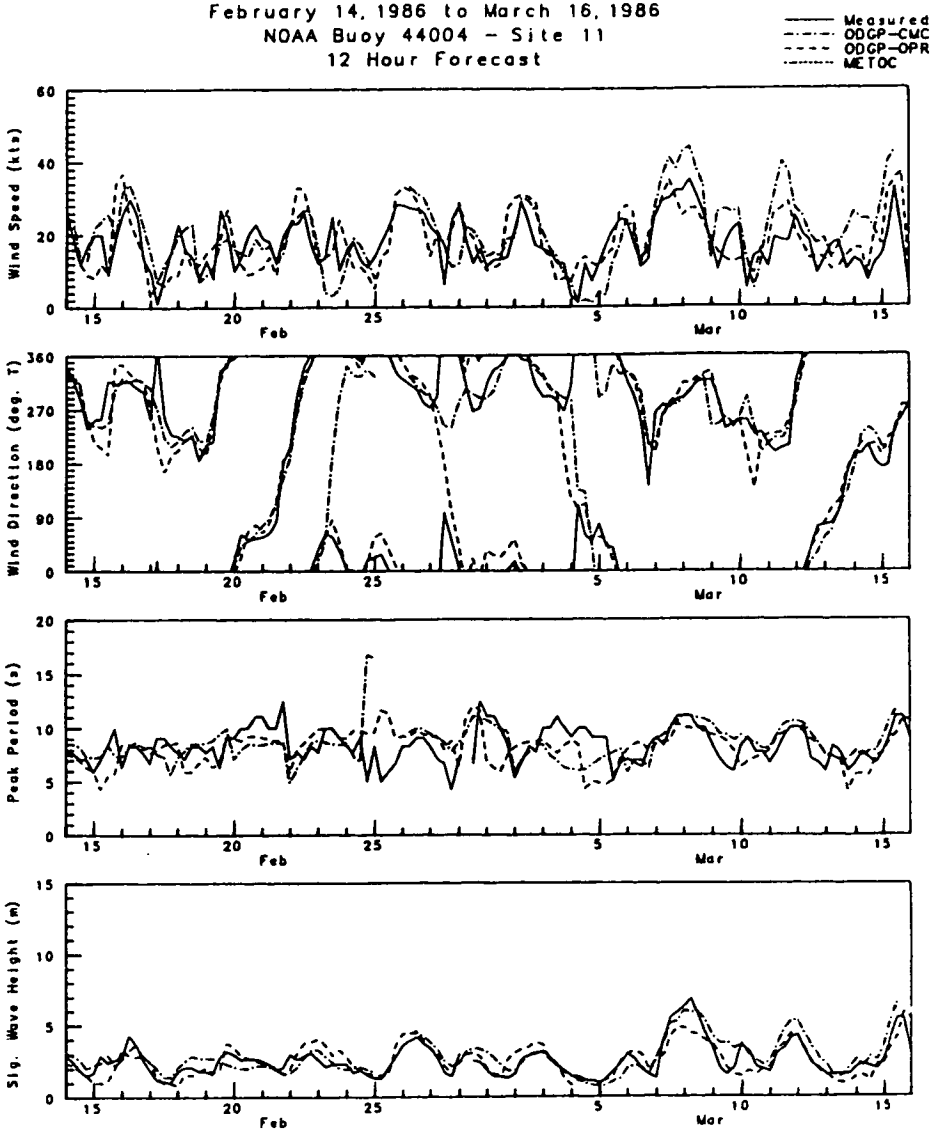

Measured Data vs. Model Predictions

January 15, 1986 to February 14, 1986
NOAA Buoy 44004 – Site 11
24 Hour Forecast

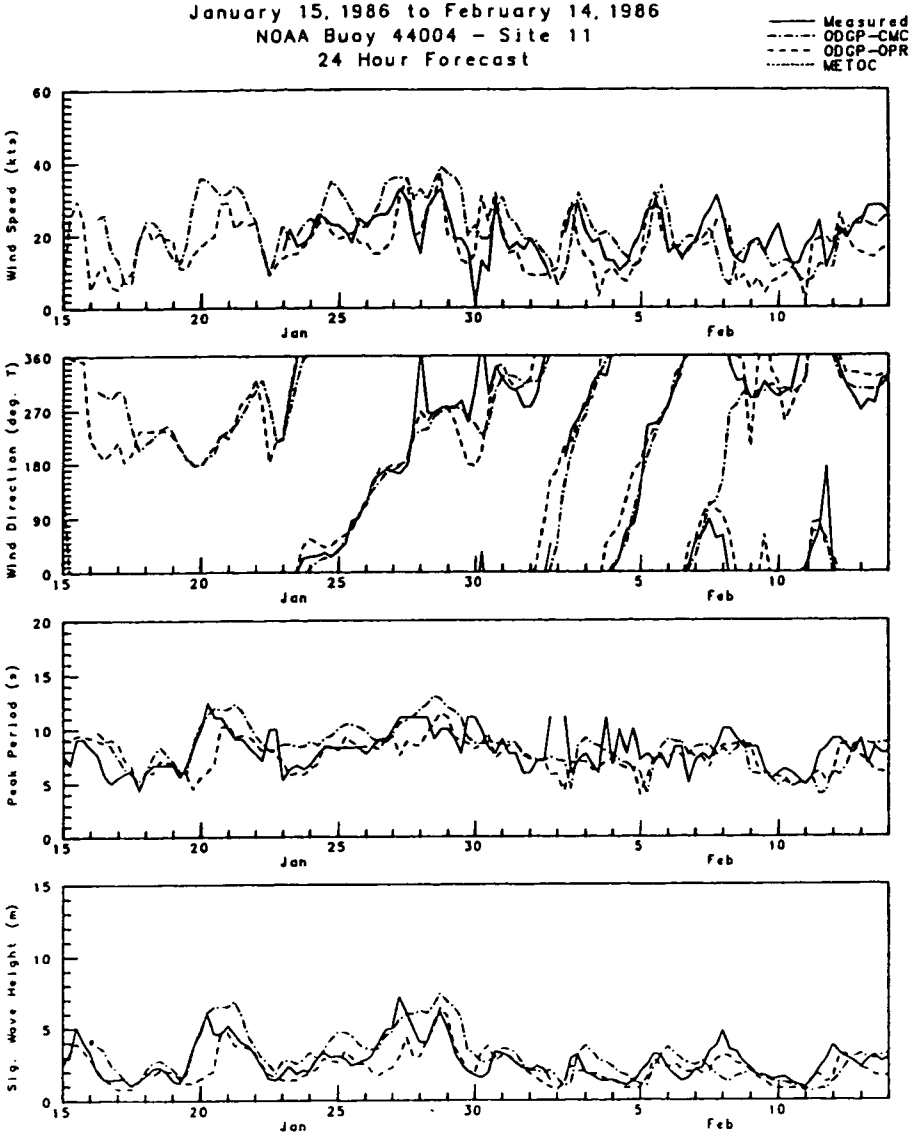

Measured Data vs. Model Predictions

February 14, 1986 to March 16, 1986
NOAA Buoy 44004 – Site 11
24 Hour Forecast

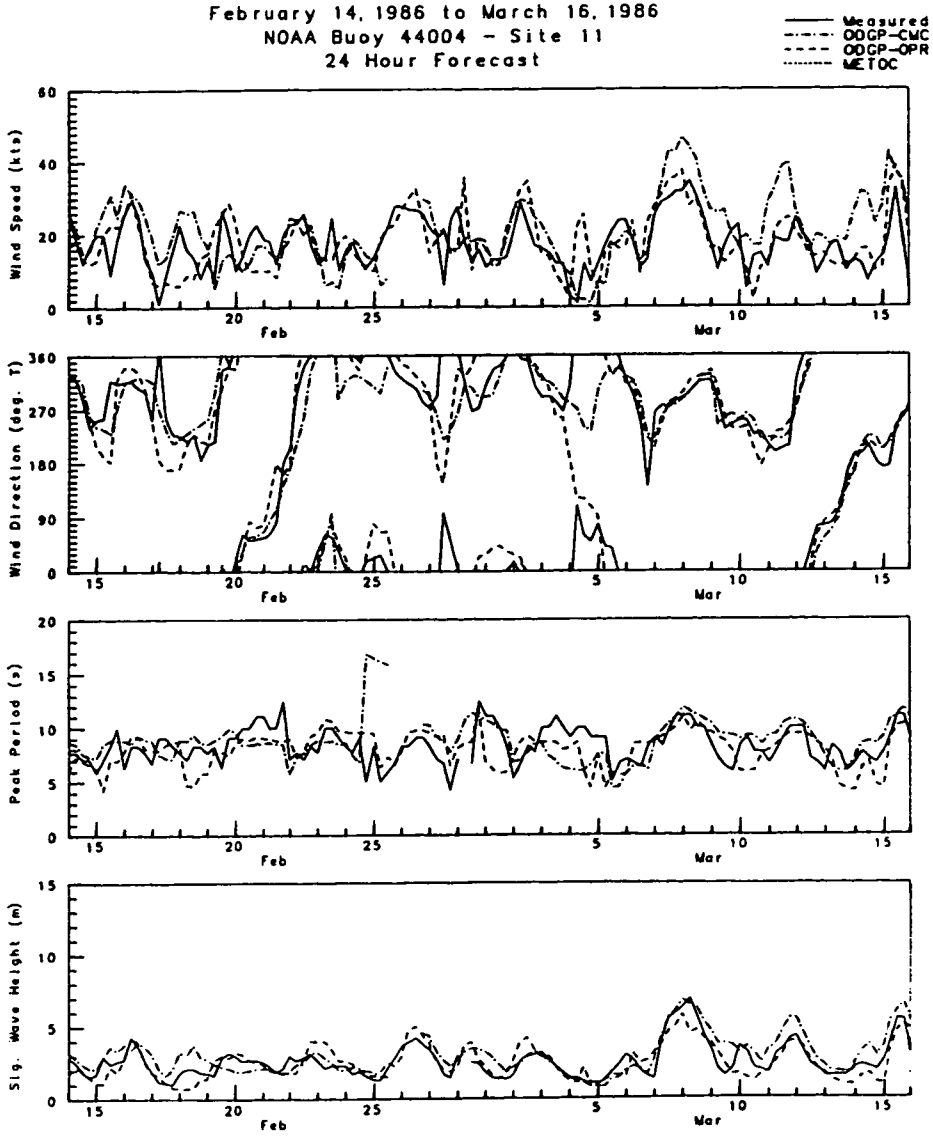

Measured Data vs. Model Predictions

January 15, 1986 to February 14, 1986
NOAA Buoy 44004 – Site 11
36 Hour Forecast

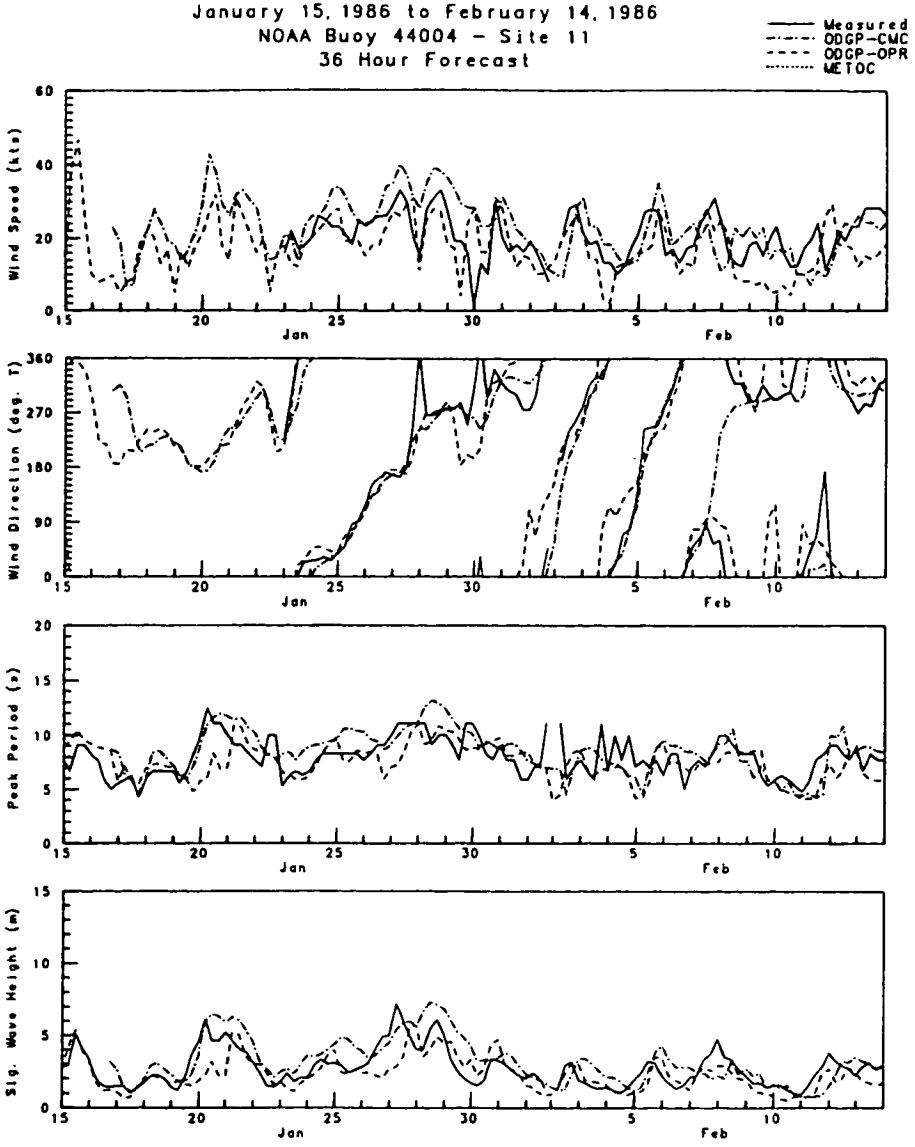

Measured Data vs. Model Predictions

February 14, 1986 to March 16, 1986
NOAA Buoy 44004 – Site 11
36 Hour Forecast

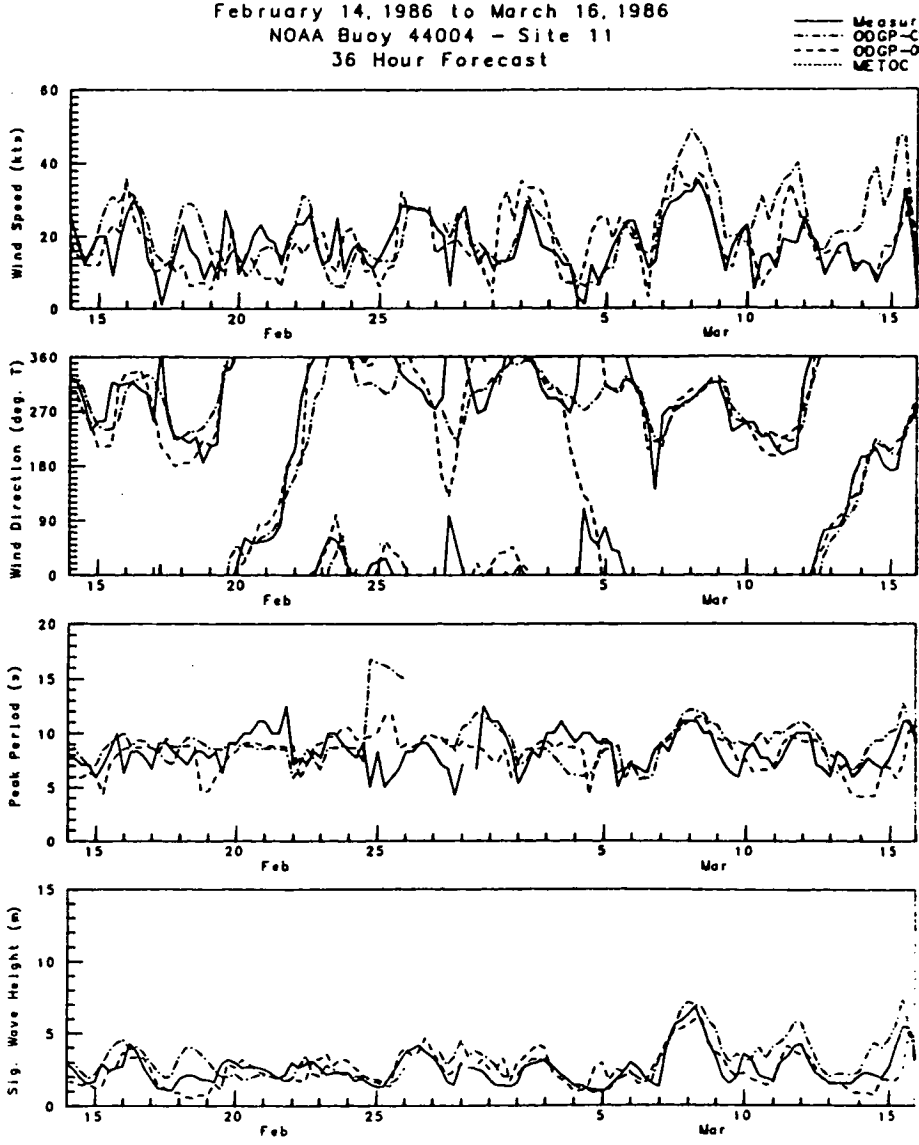

Measured Data vs. Model Predictions

January 15, 1986 to February 14, 1986
NOAA Buoy 44004 - Site 11
48 Hour Forecast

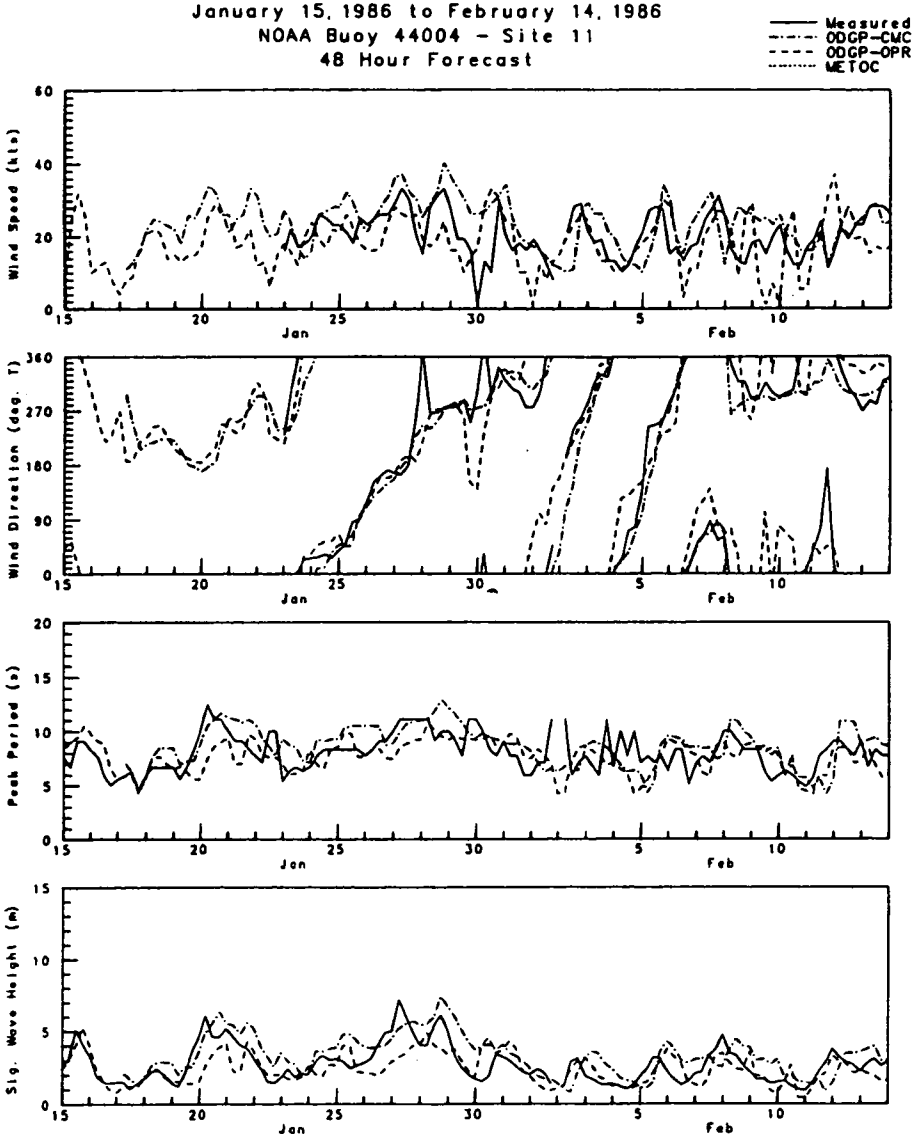

Measured Data vs. Model Predictions

February 14, 1986 to March 16, 1986
NOAA Buoy 44004 - Site 11
48 Hour Forecast

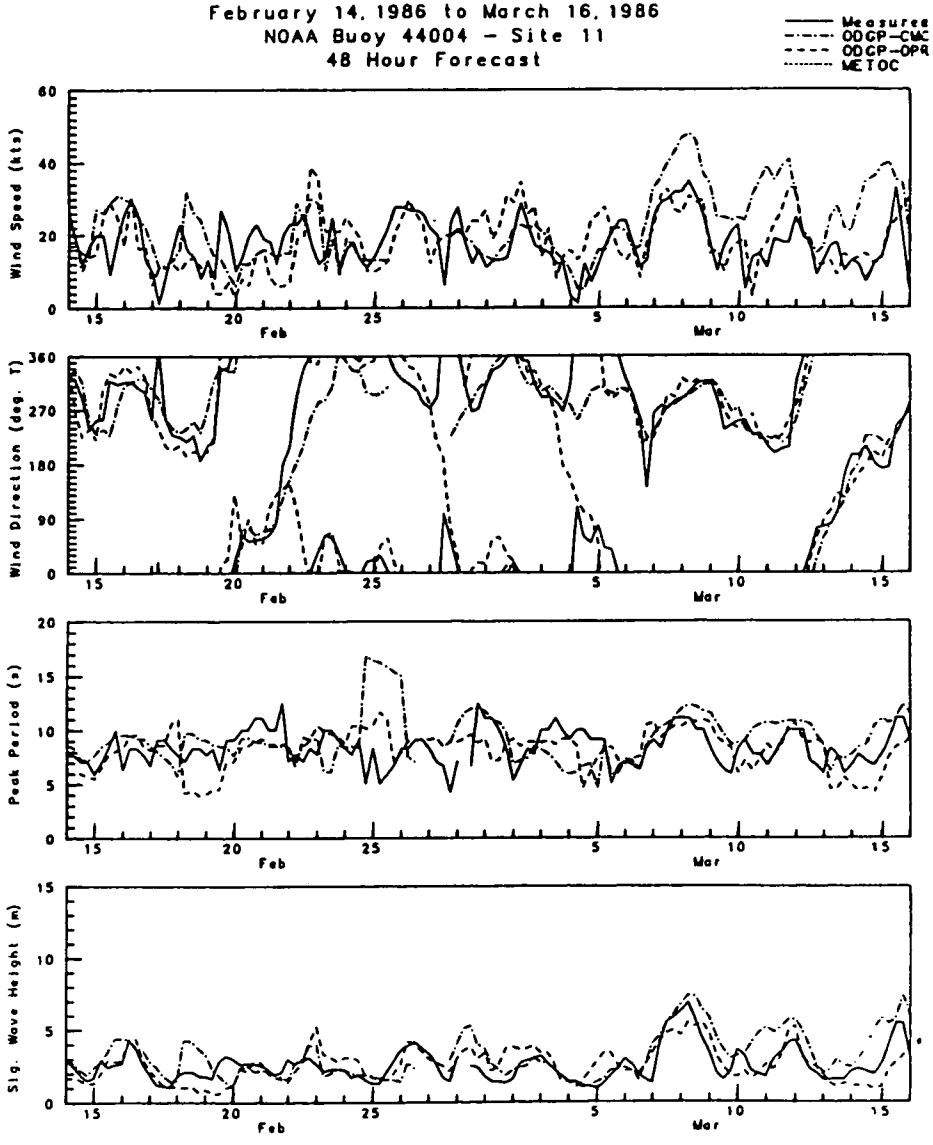

Measured Data vs. Model Predictions

January 15, 1986 to February 14, 1986
NOAA Buoy 44011 - Site 12
00 Hour Analysis

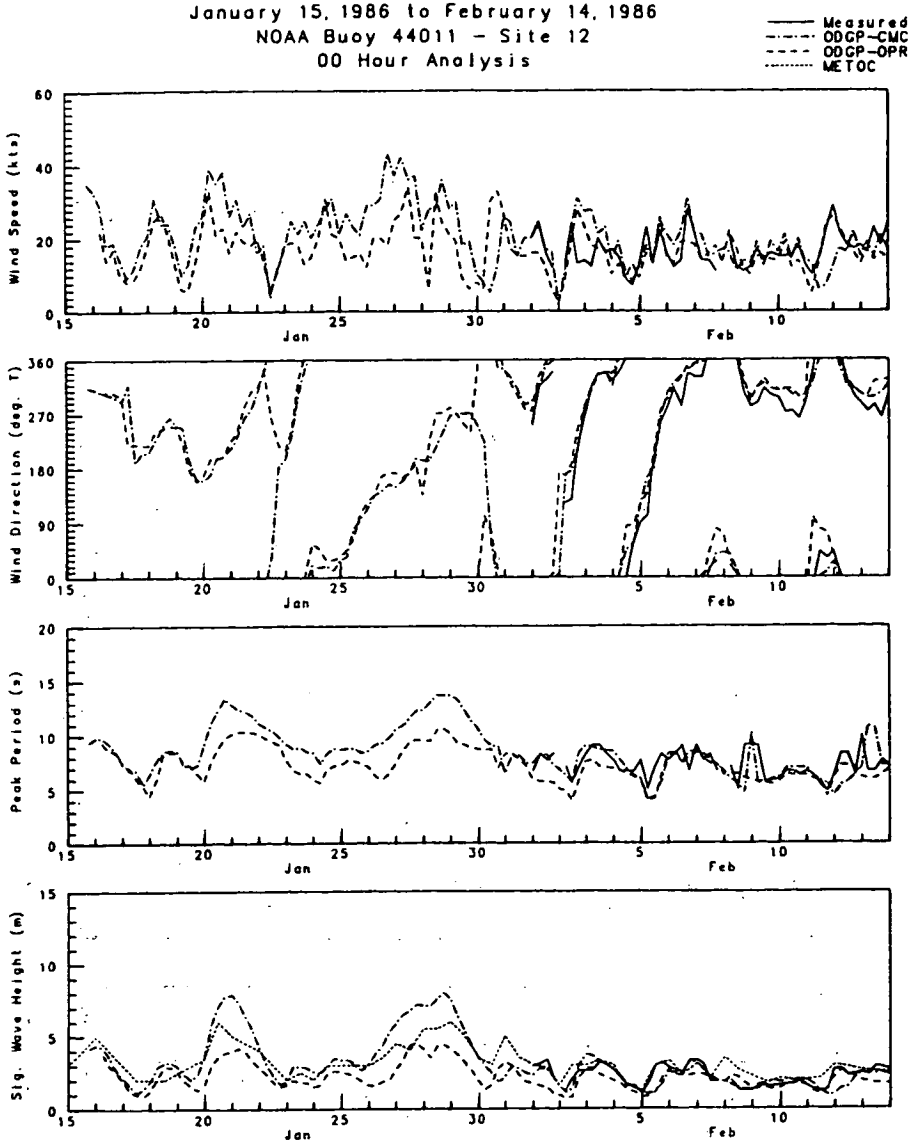

Measured Data vs. Model Predictions

February 14, 1986 to March 16, 1986
NOAA Buoy 44011 - Site 12
00 Hour Analysis

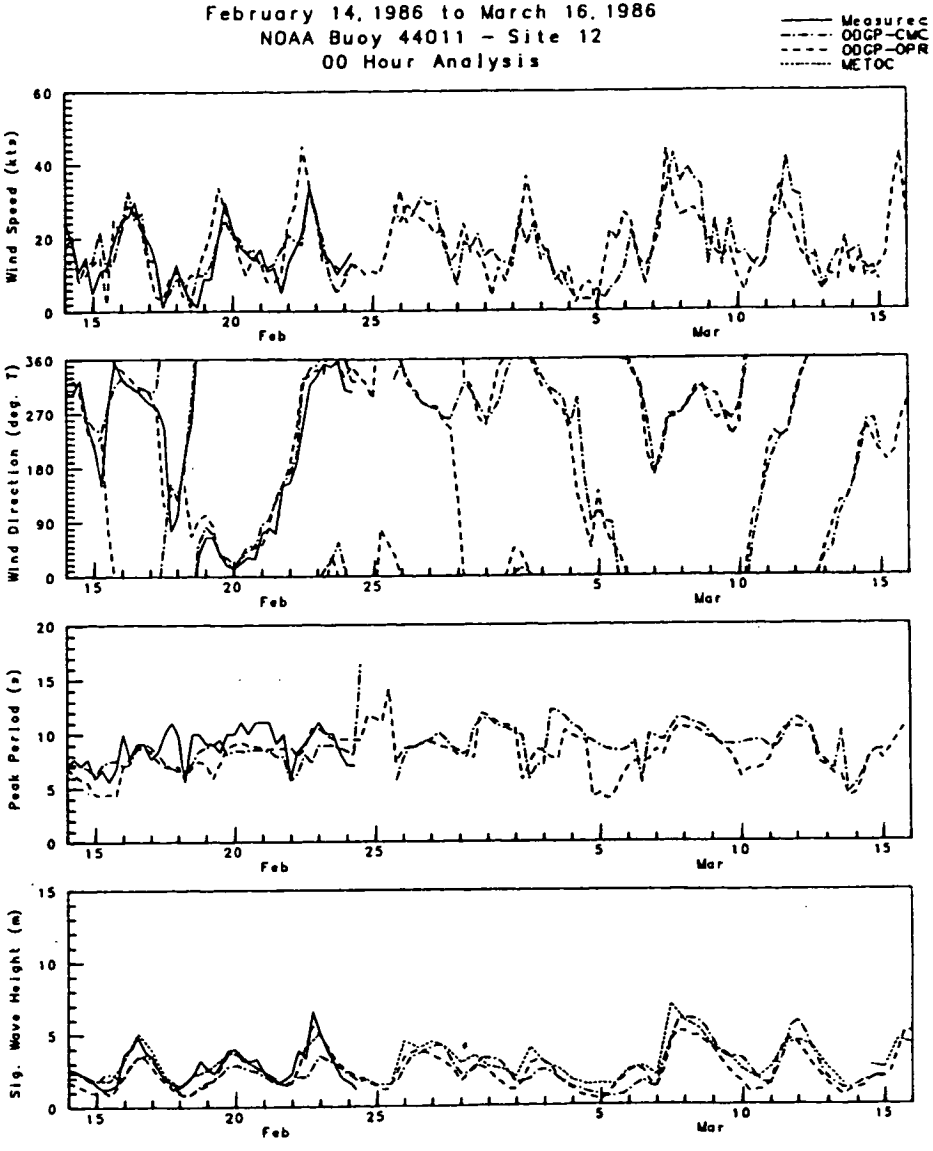

Measured Data vs. Model Predictions

January 15, 1986 to February 14, 1986
NOAA Buoy 44011 – Site 12
12 Hour Forecast

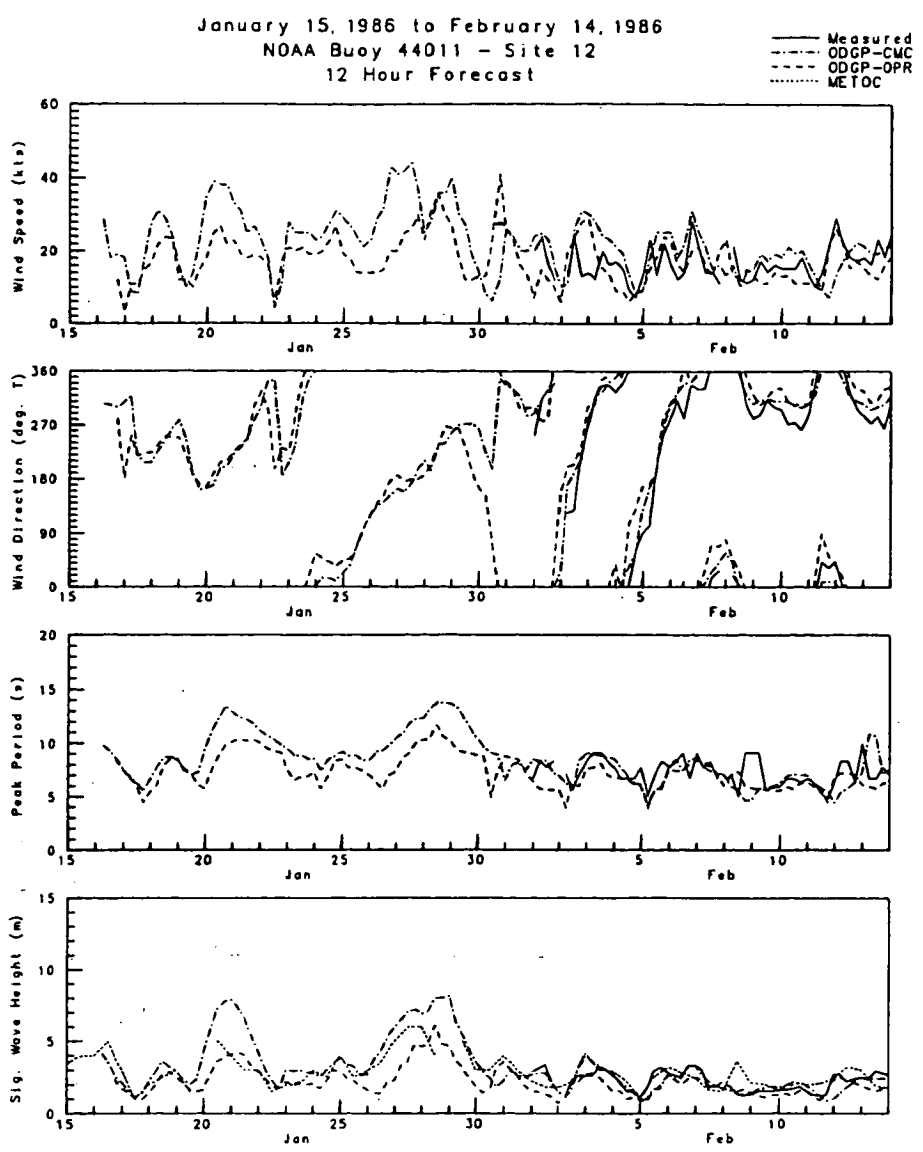

Measured Data vs. Model Predictions

February 14, 1986 to March 16, 1986
NOAA Buoy – Site 12
12 Hour Forecast

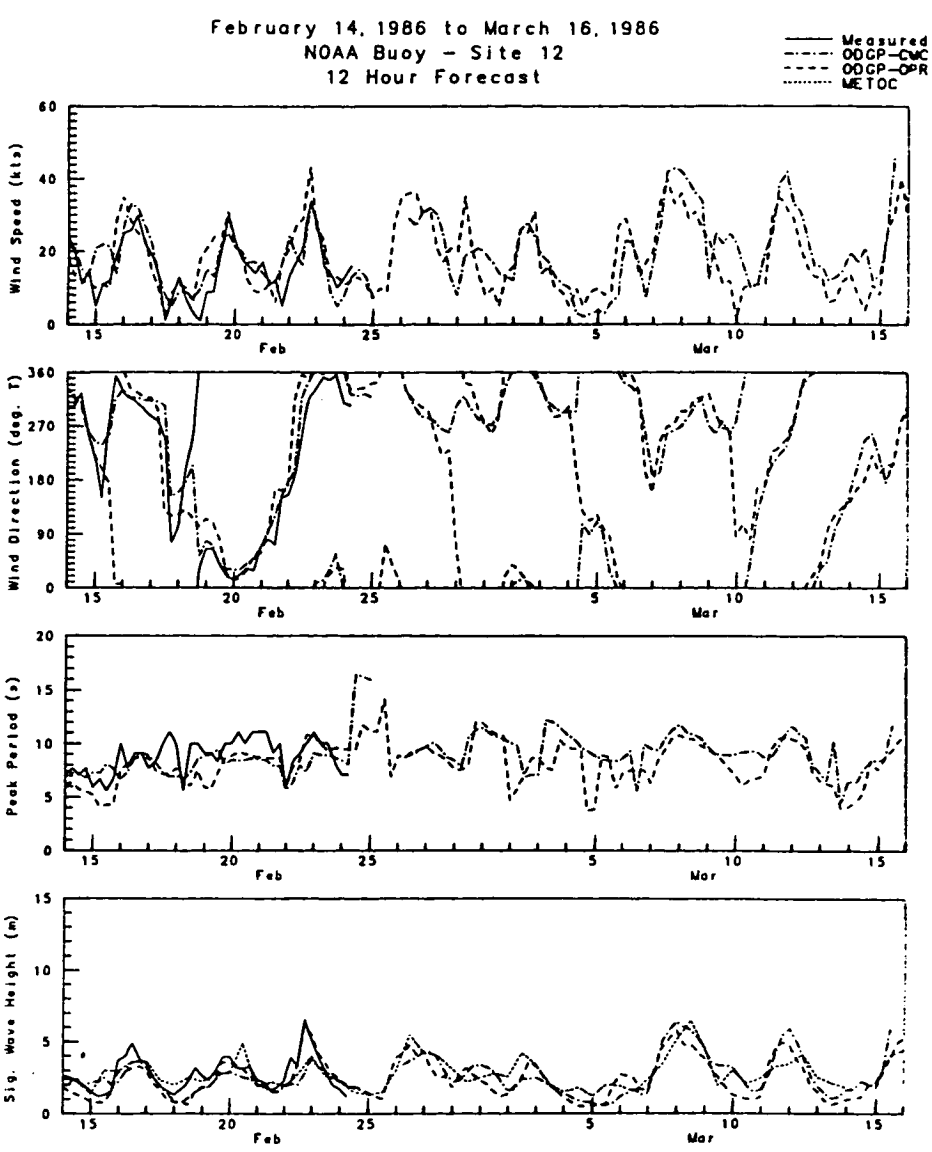

Measured Data vs. Model Predictions

January 15, 1986 to February 14, 1986
NOAA Buoy 44011 - Site 12
24 Hour Forecast

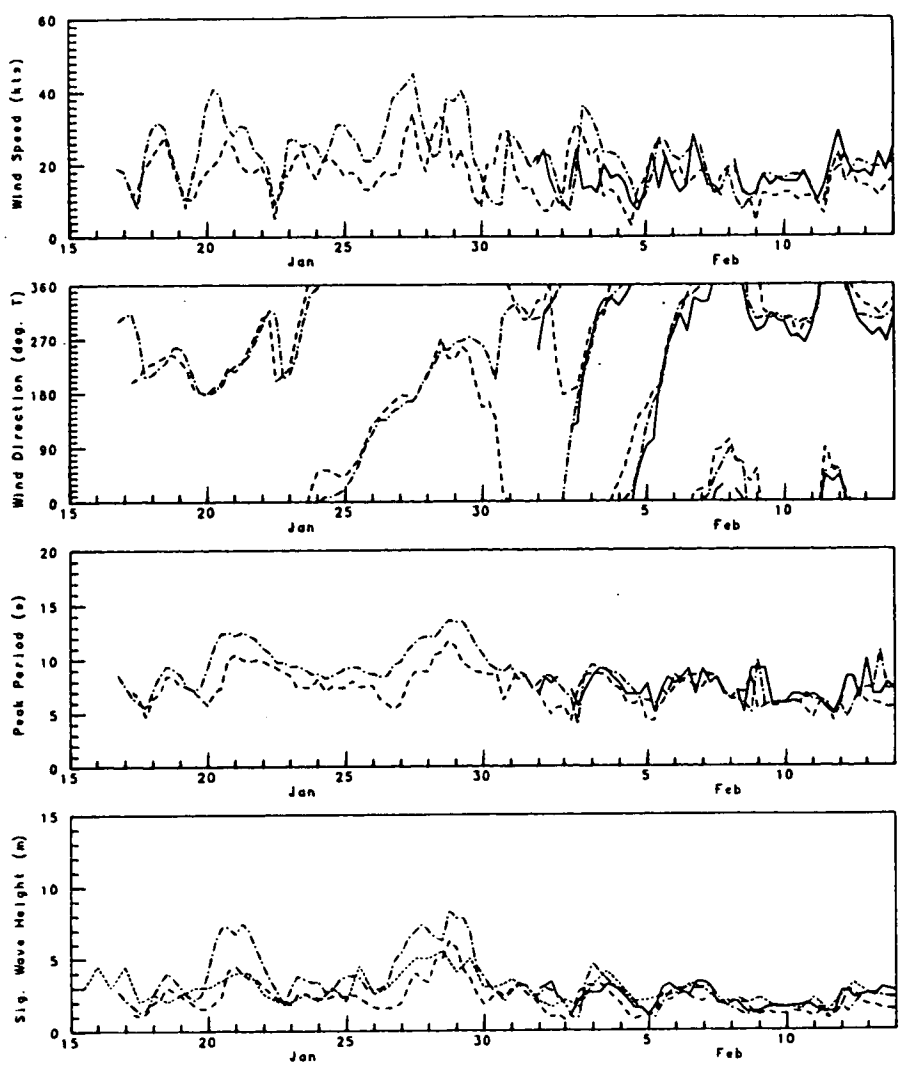

Measured Data vs. Model Predictions

February 14, 1986 to March 16, 1986
NOAA Buoy 44011 - Site 12
24 Hour Forecast

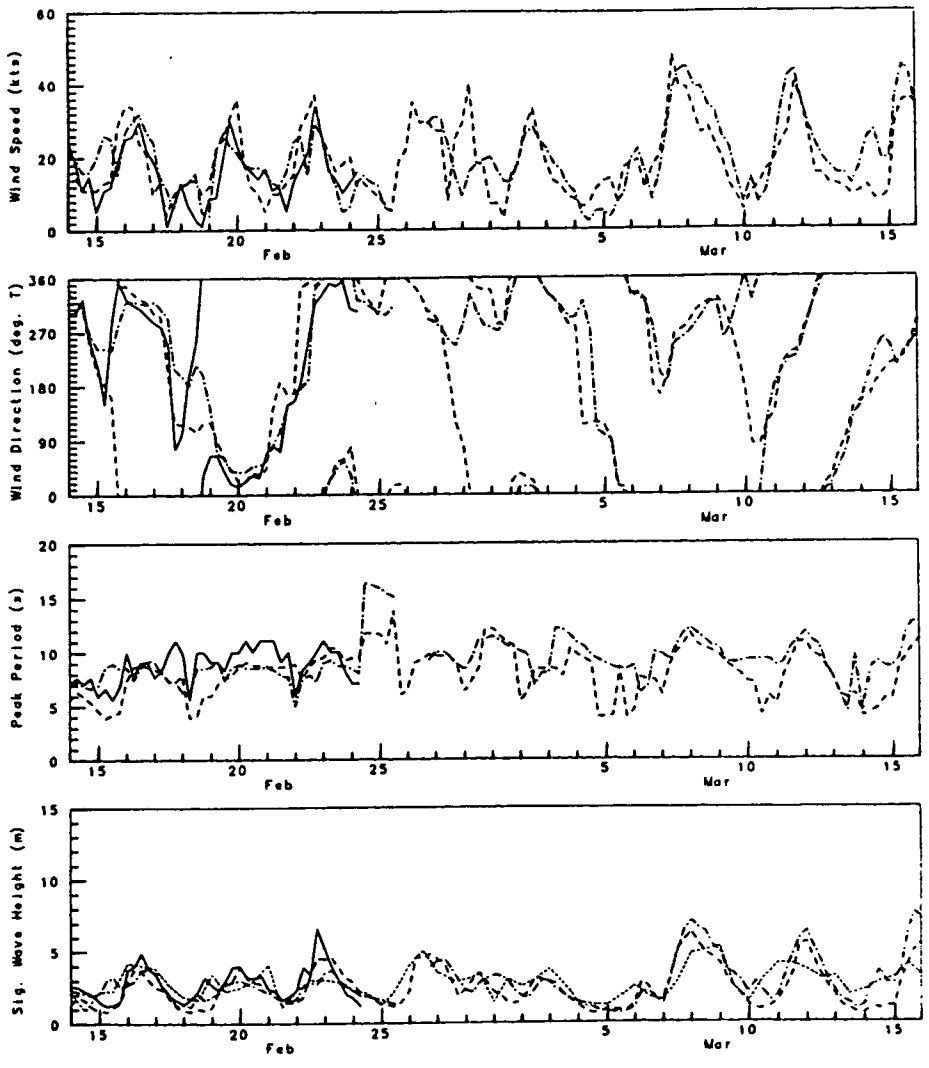

Measured Data vs. Model Predictions

January 15, 1986 to February 14, 1986
NOAA Buoy 44011 - Site 12
36 Hour Forecast

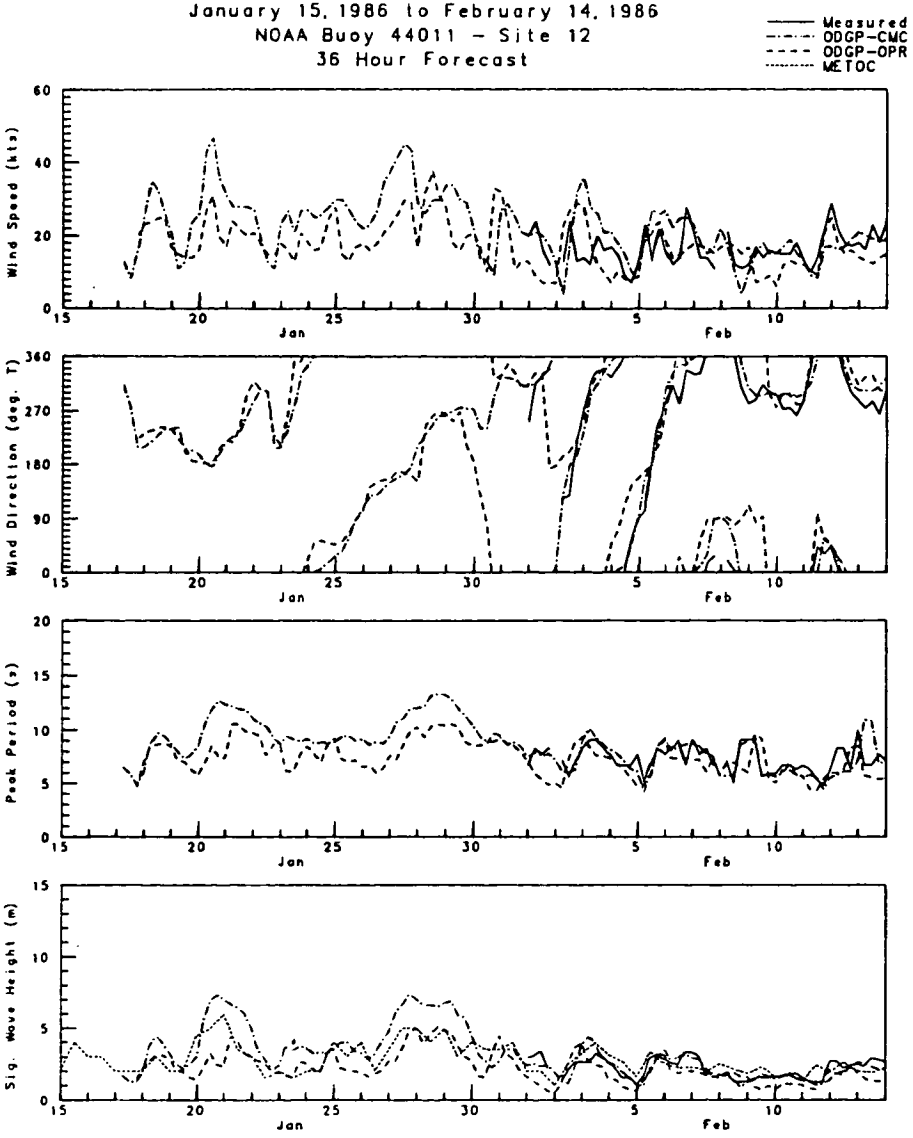

Measured Data vs. Model Predictions

February 14, 1986 to March 16, 1986
NOAA Buoy 44011 - Site 12
36 Hour Forecast

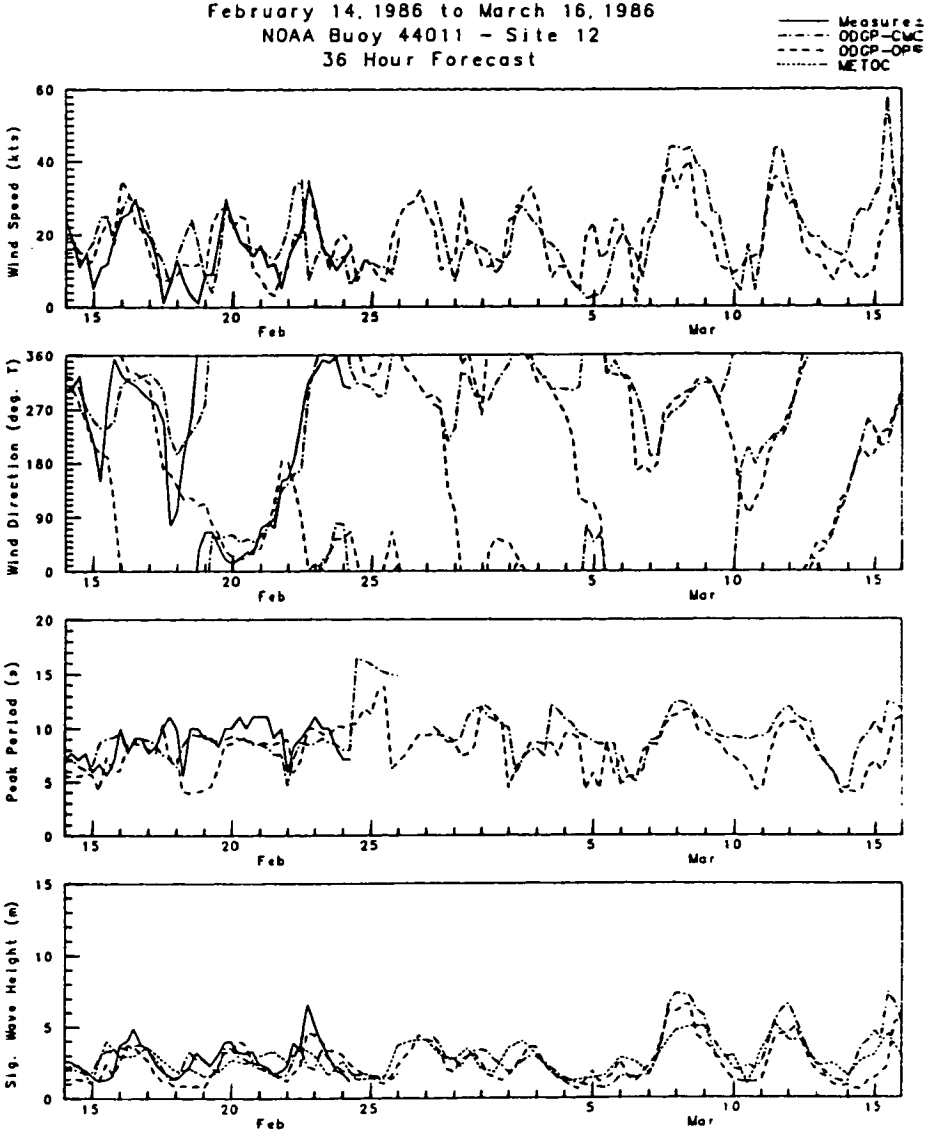

Measured Data vs. Model Predictions

January 15, 1986 to February 14, 1986
NOAA Buoy 44011 – Site 12
48 Hour Forecast

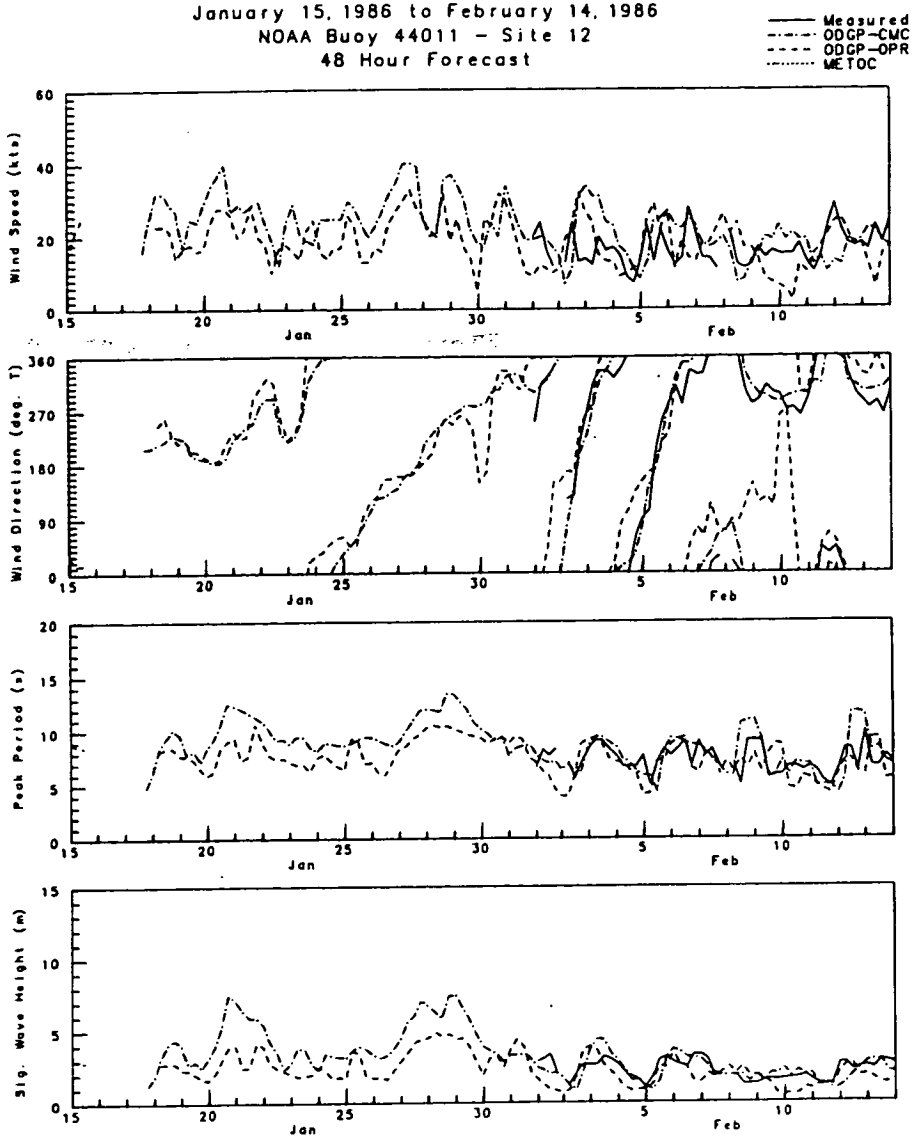

Measured Data vs. Model Predictions

February 14, 1986 to March 16, 1986
NOAA Buoy – Site 12
48 Hour Forecast

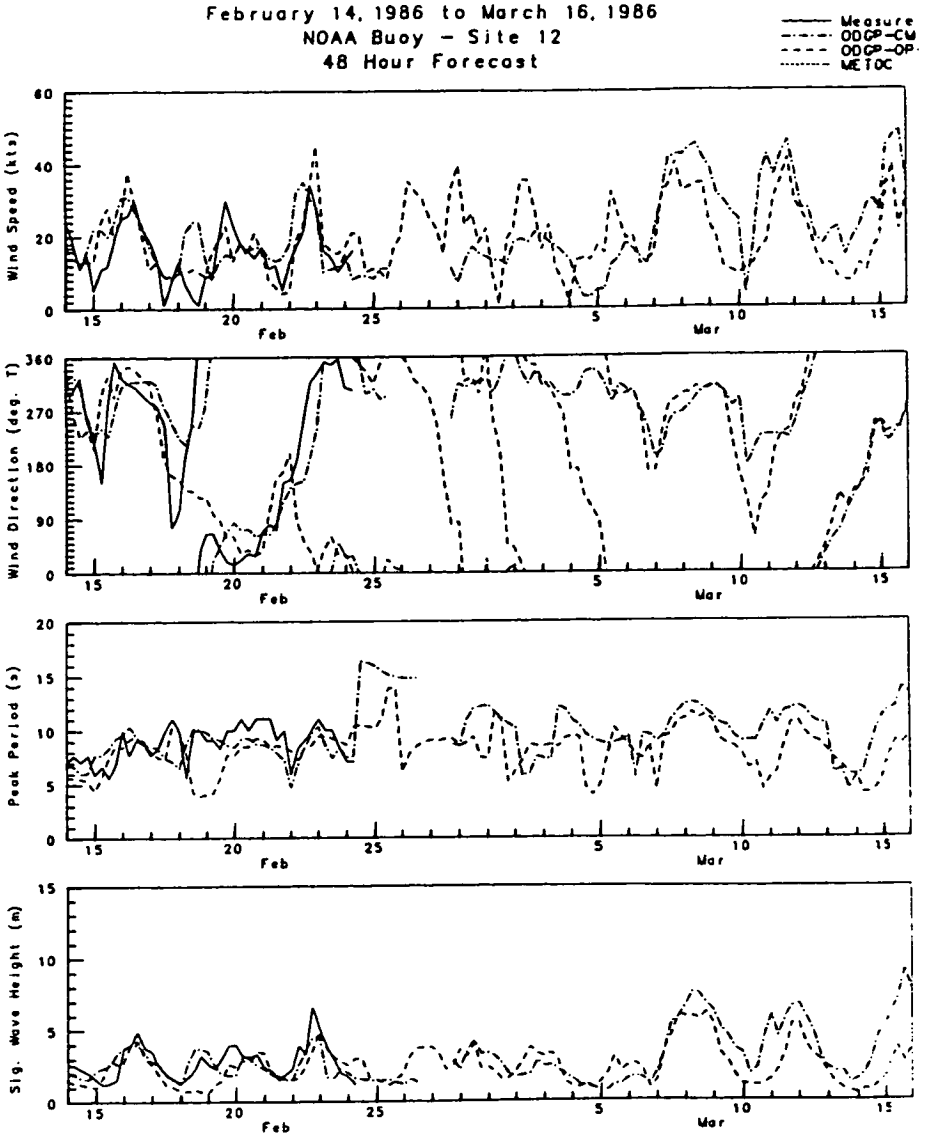

Measured Data vs. Model Predictions

January 15, 1986 to February 14, 1986
Scotian Shelf - Site 21a
00 Hour Analysis

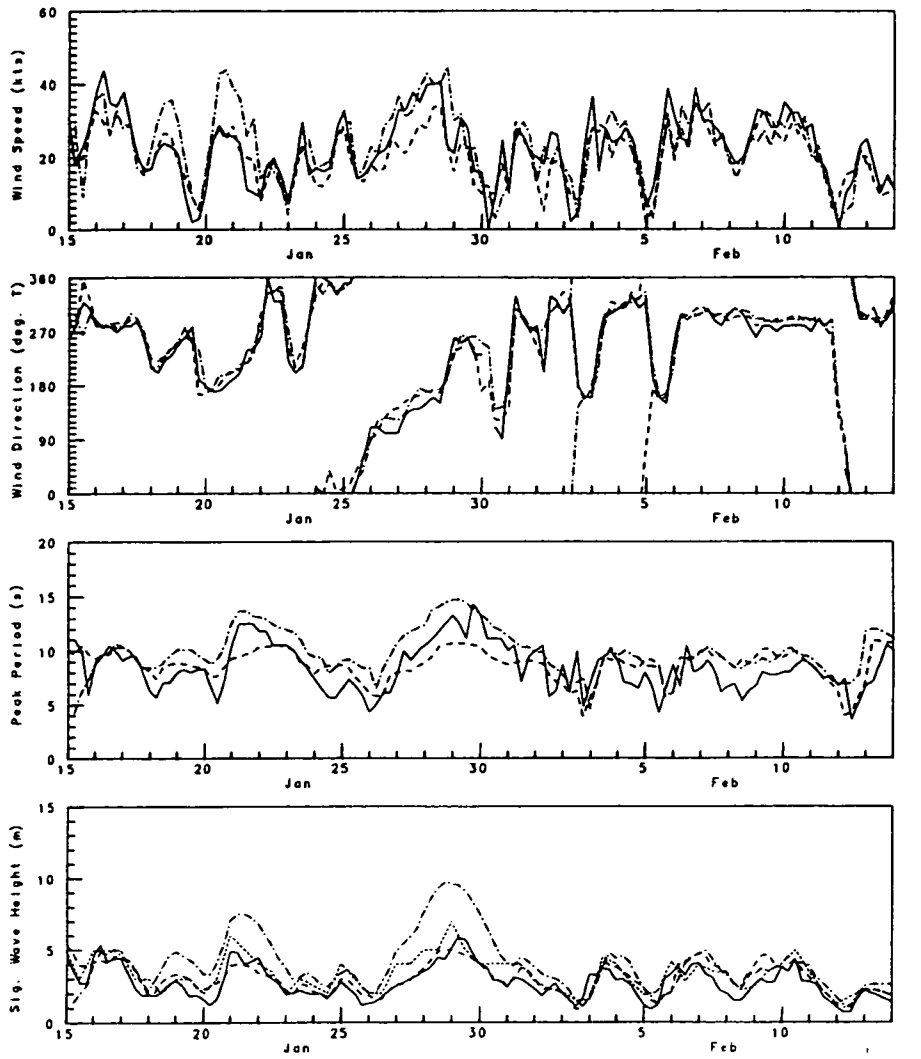

Measured Data vs. Model Predictions

February 14, 1986 to March 16, 1986
Scotian Shelf - Site 21a
00 Hour Analysis

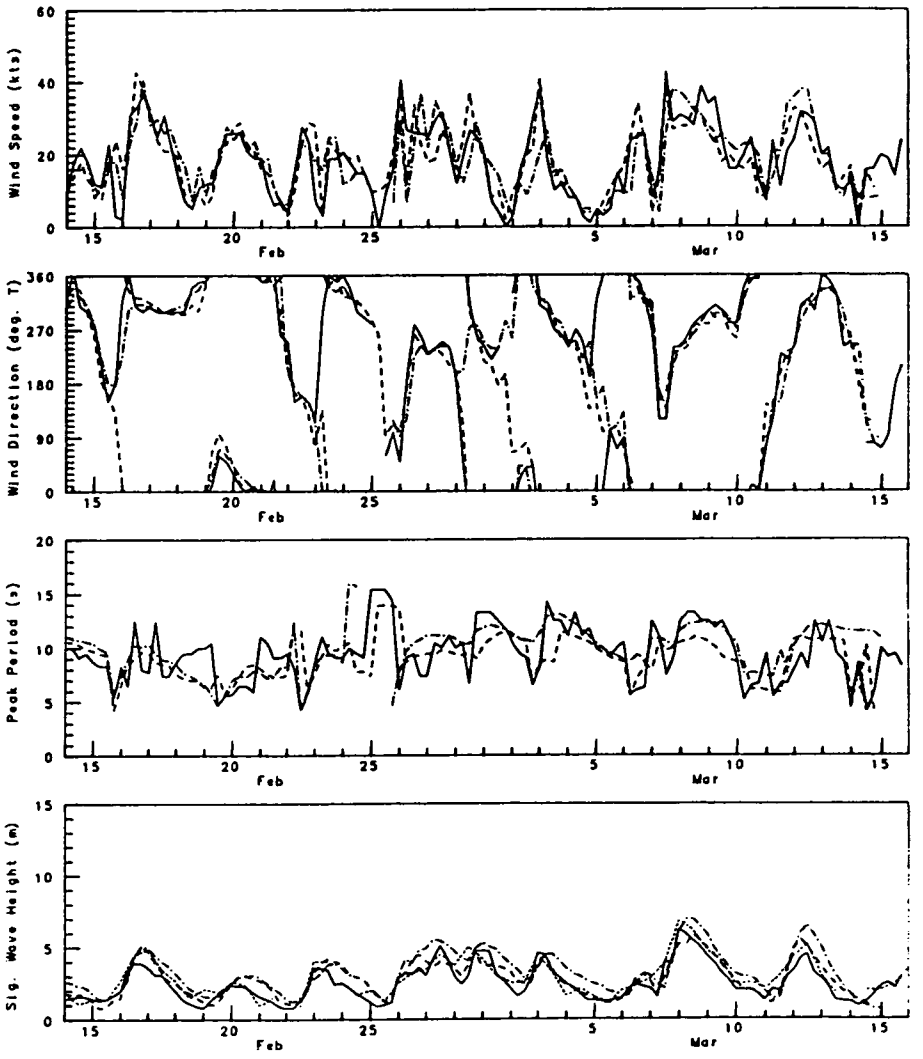

Measured Data vs. Model Predictions

January 15, 1986 to February 14, 1986
Scotian Shelf - Site 21a
12 Hour Forecast

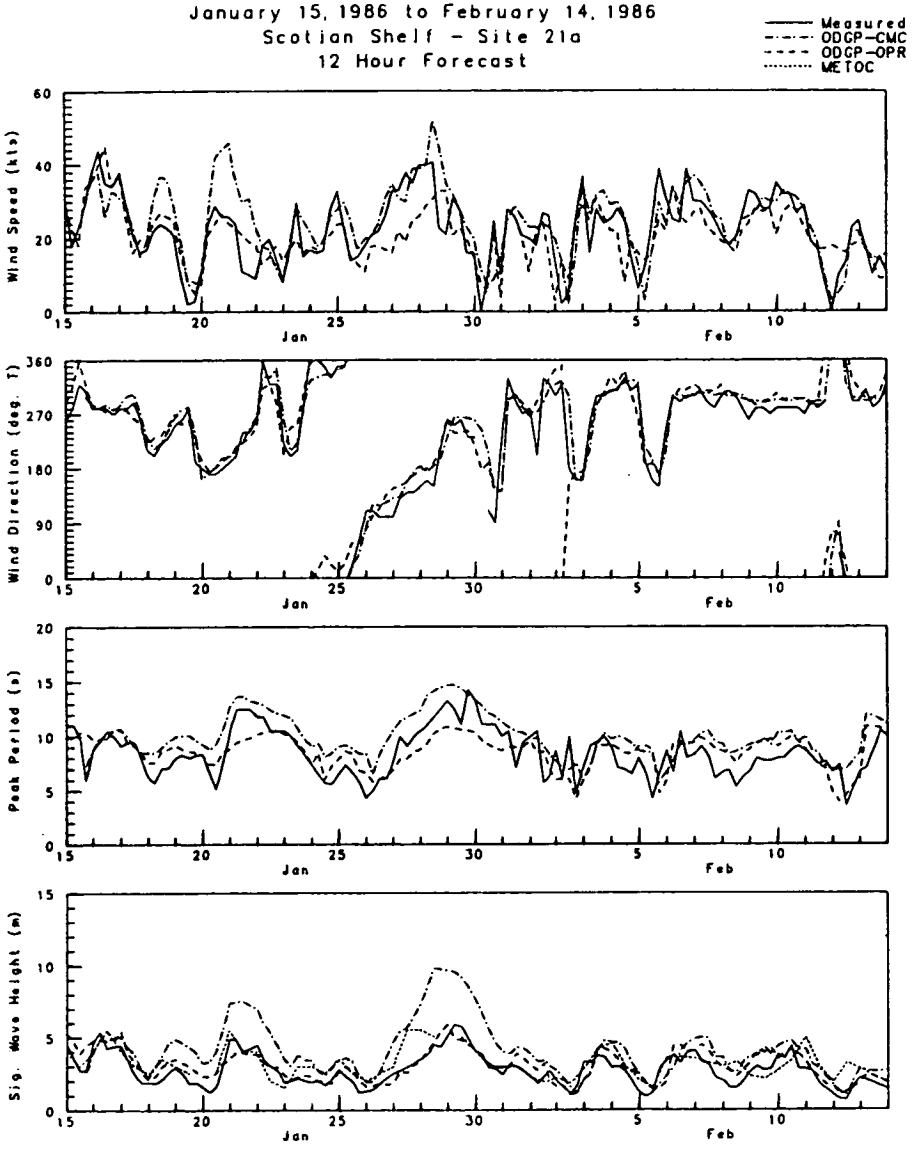

Measured Data vs. Model Predictions

February 14, 1986 to March 16, 1986
Scotian Shelf - Site 21a
12 Hour Forecast

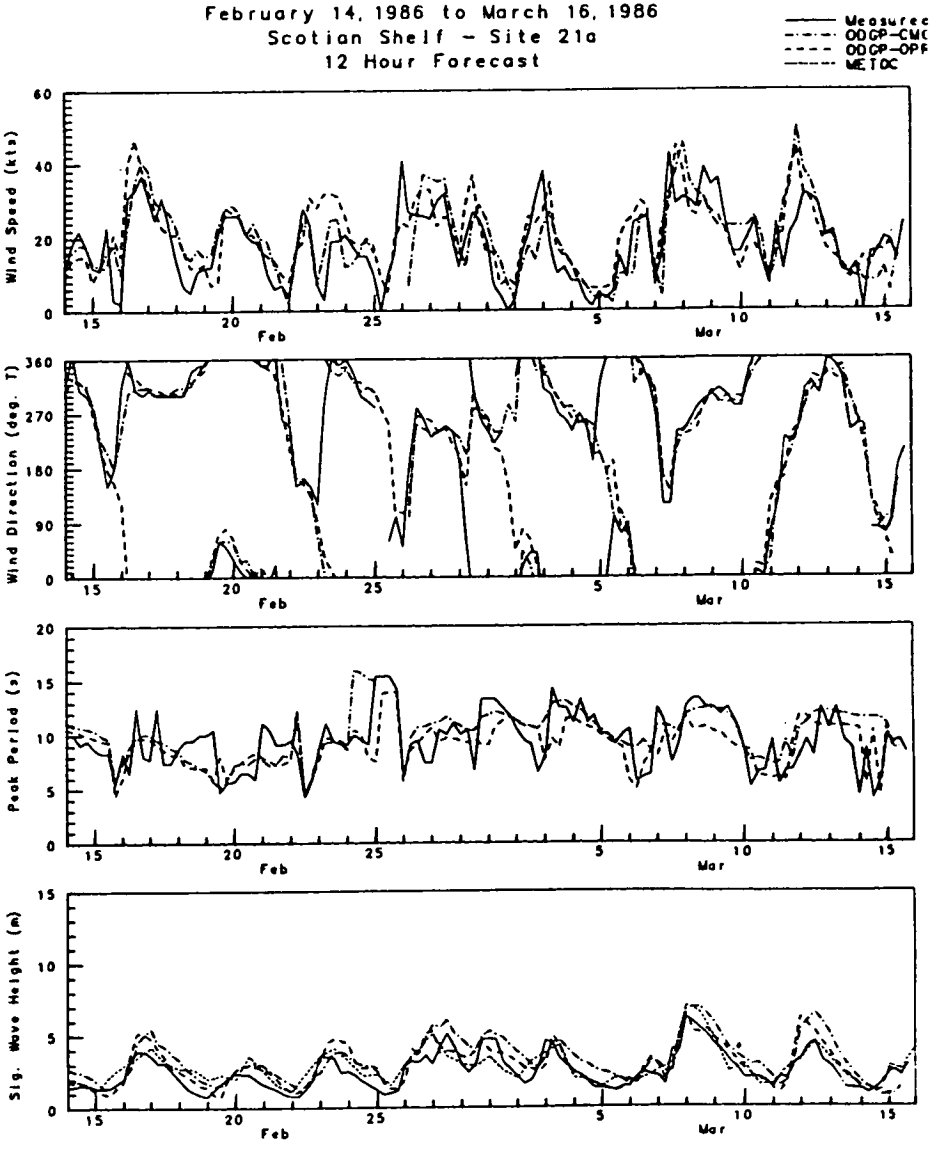

Measured Data vs. Model Predictions

January 15, 1986 to February 14, 1986
Scotian Shelf - Site 21a
24 Hour Forecast

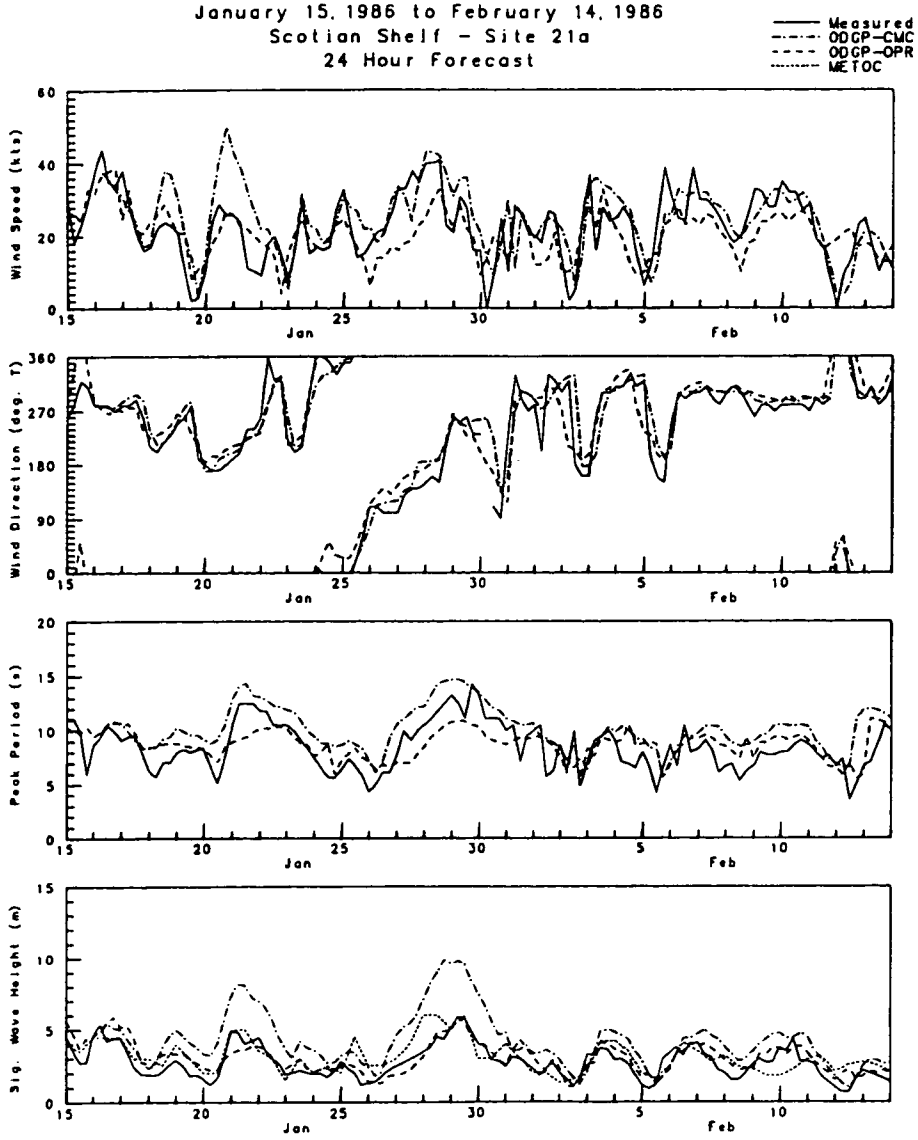

Measured Data vs. Model Predictions

February 14, 1986 to March 16, 1986
Scotian Shelf - Site 21a
24 Hour Forecast

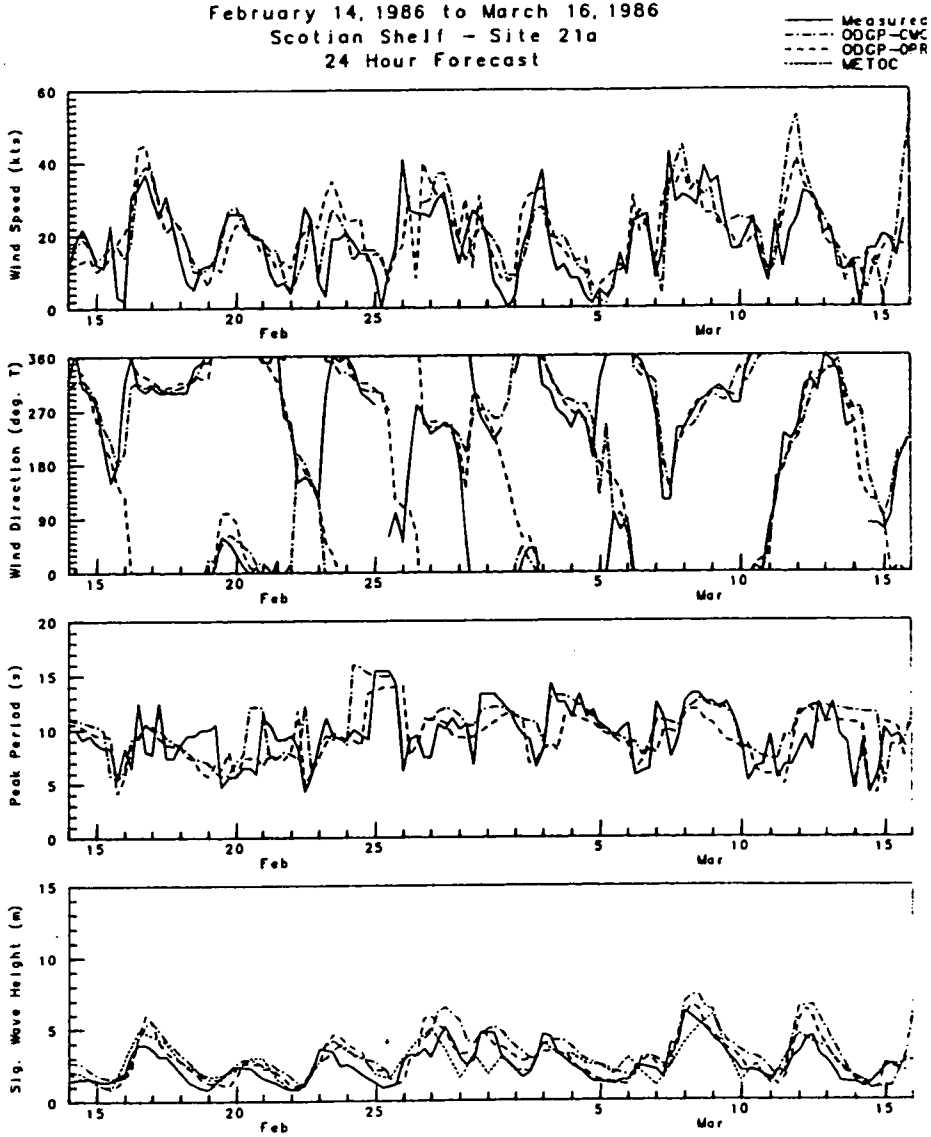

Measured Data vs. Model Predictions

January 15, 1986 to February 14, 1986
Scotian Shelf - Site 21a
36 Hour Forecast

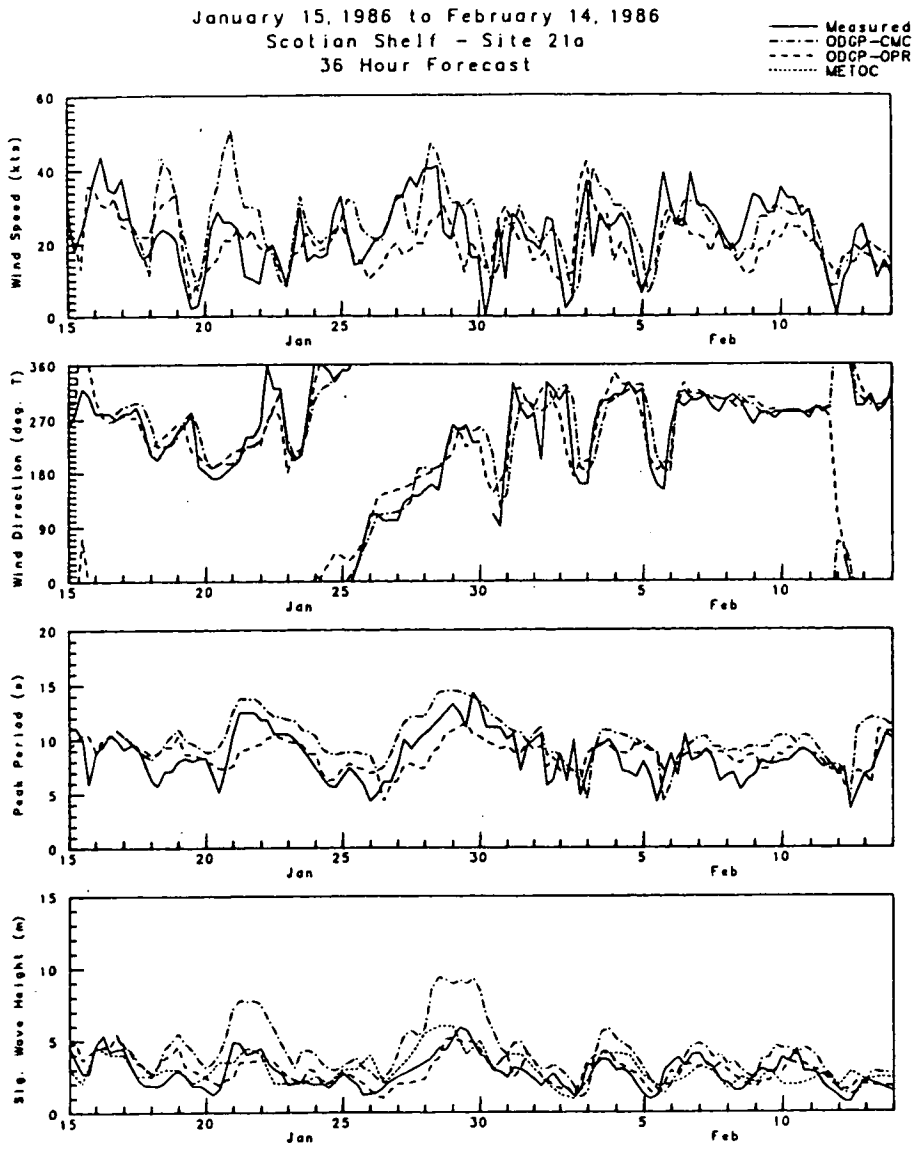

Measured Data vs. Model Predictions

February 14, 1986 to March 16, 1986
Scotian Shelf - Site 21a
36 Hour Forecast

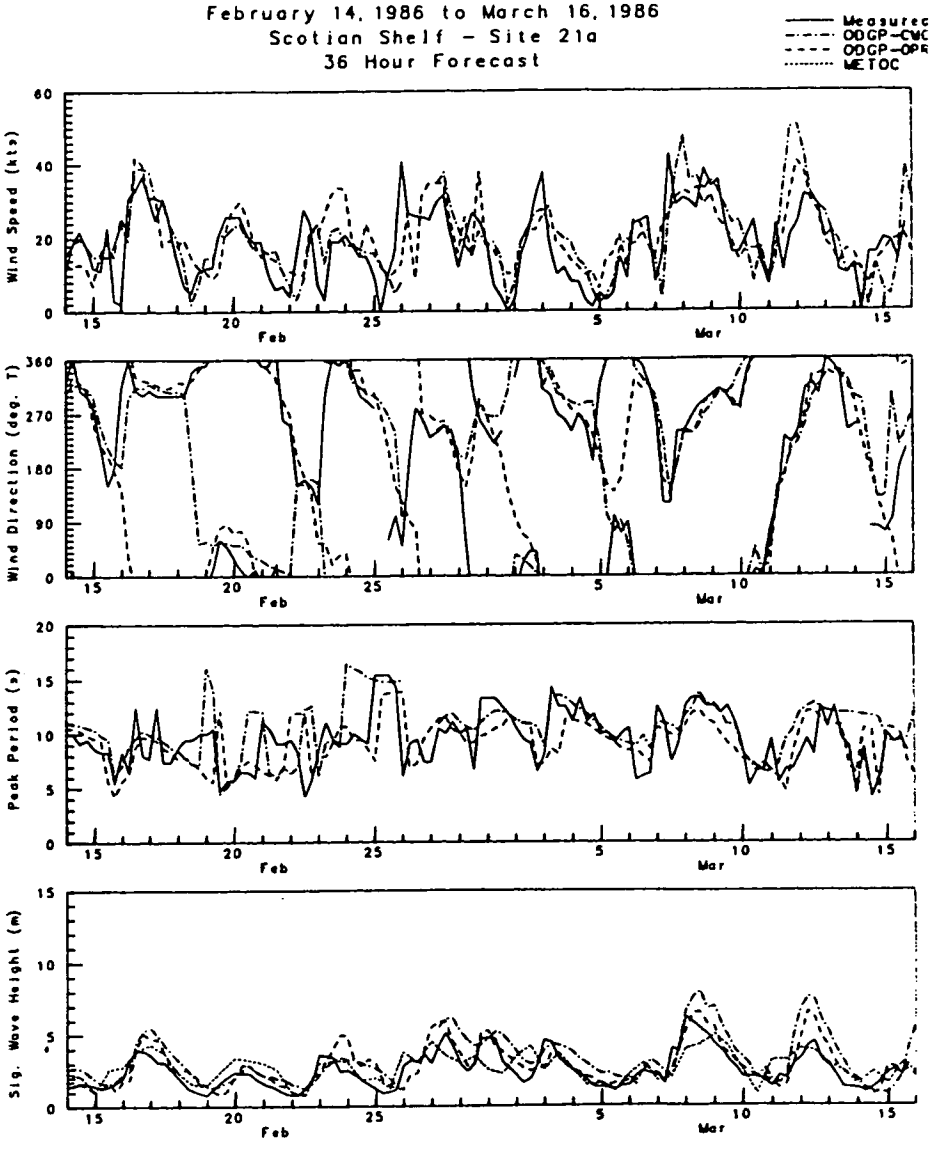

Measured Data vs. Model Predictions

January 15, 1986 to February 14, 1986
Scotian Shelf - Site 21a
48 Hour Forecast

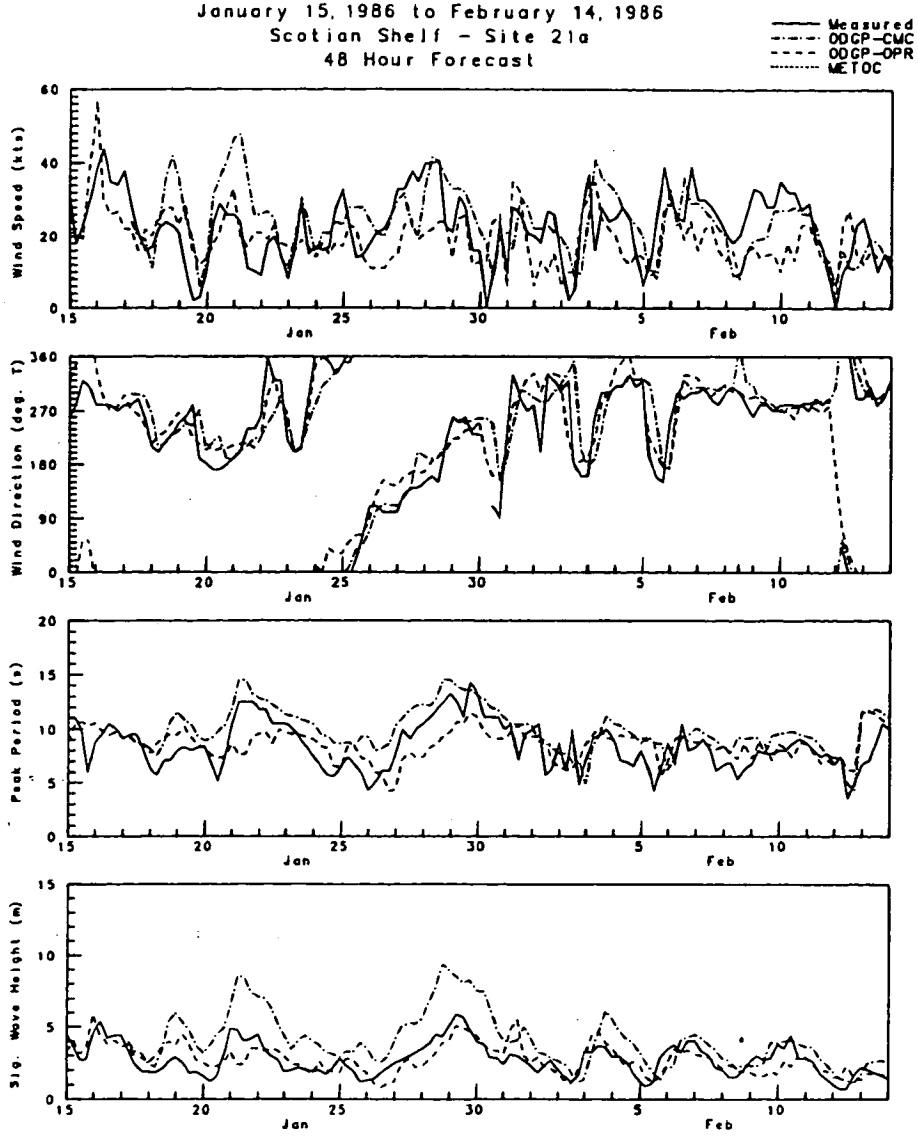

Measured Data vs. Model Predictions

February 14, 1986 to March 16, 1986
Scotian Shelf - Site 21a
48 Hour Forecast

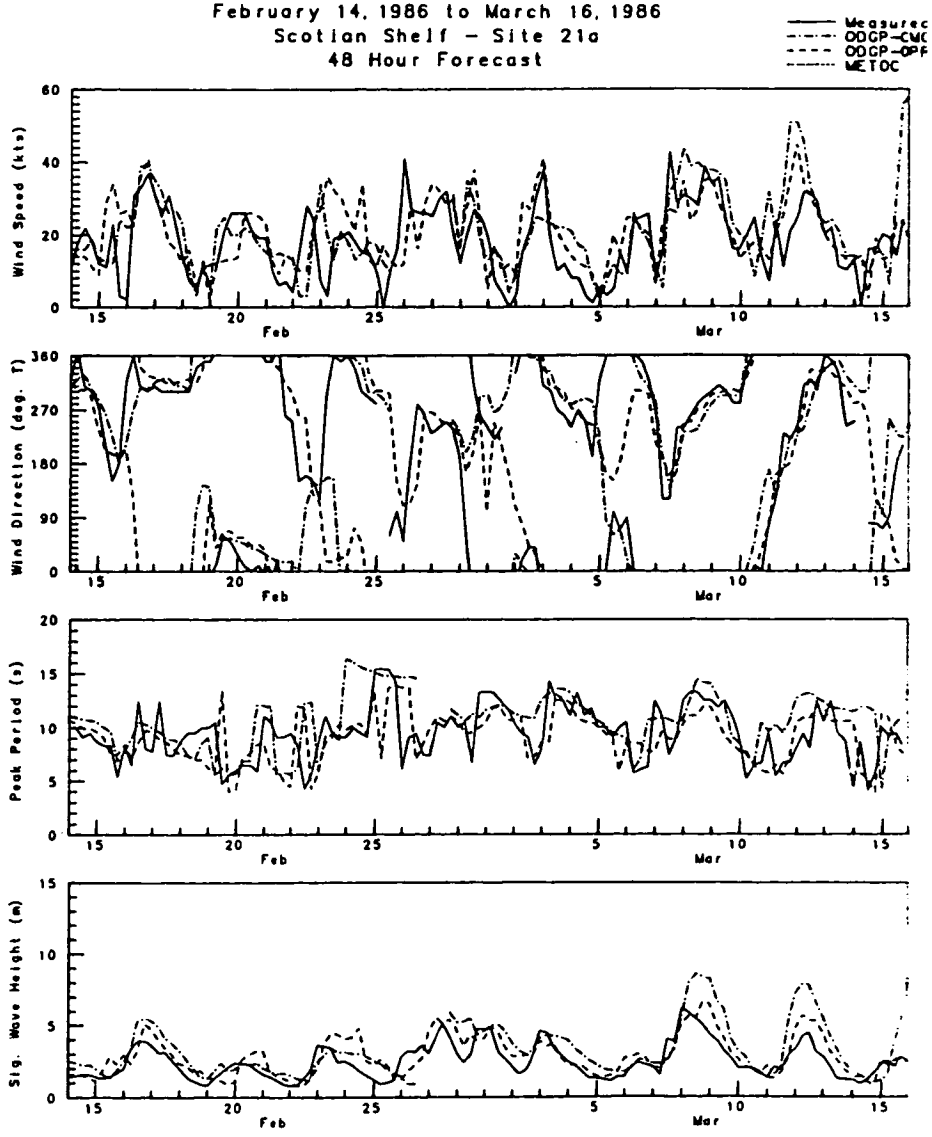

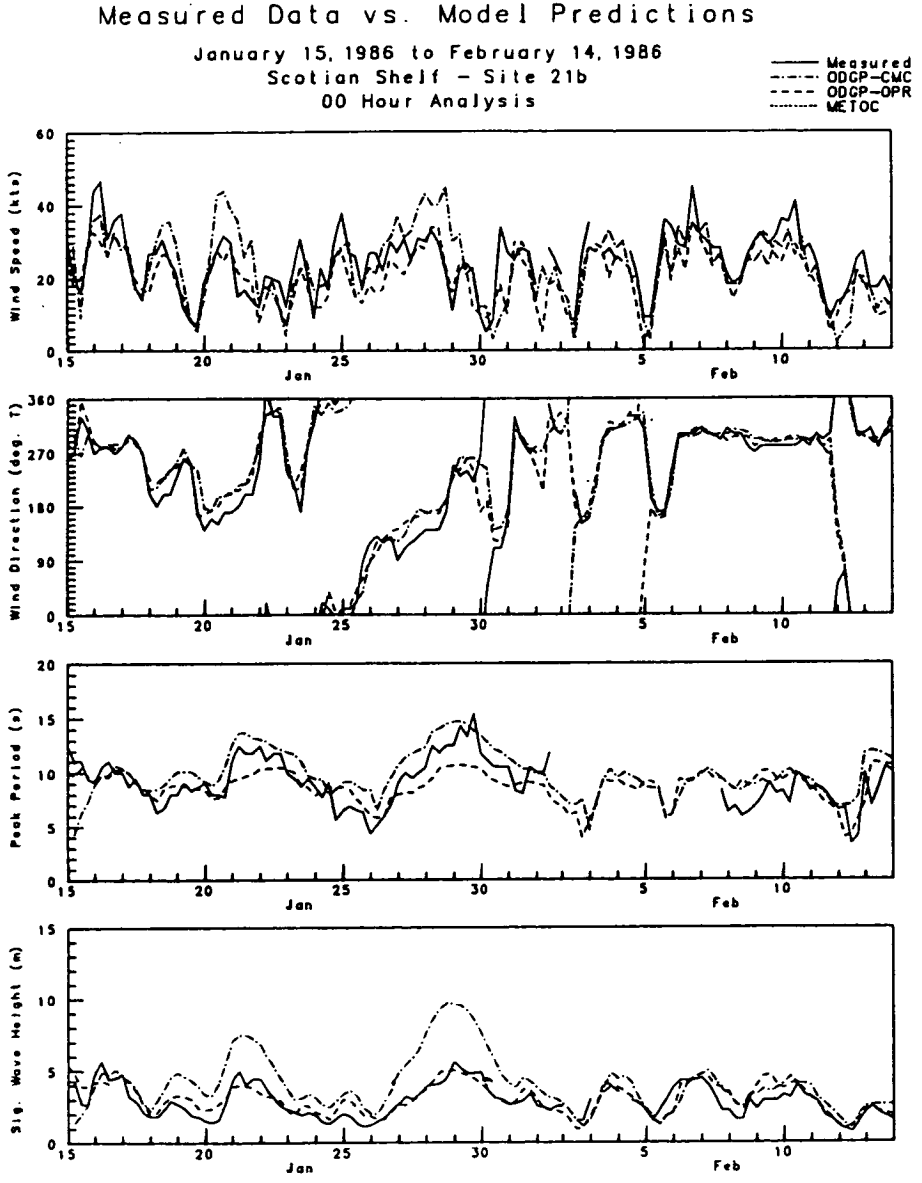
Measured Data vs. Model Predictions
January 15, 1986 to February 14, 1986
Scotian Shelf - Site 21b
00 Hour Analysis
Measured
ODGP-CMC
ODGP-OPR
METOC
Wind Speed (kts)
Wind Direction (deg. T)
Peak Period (s)
Sig. Wave Height (m)
Jan
Feb

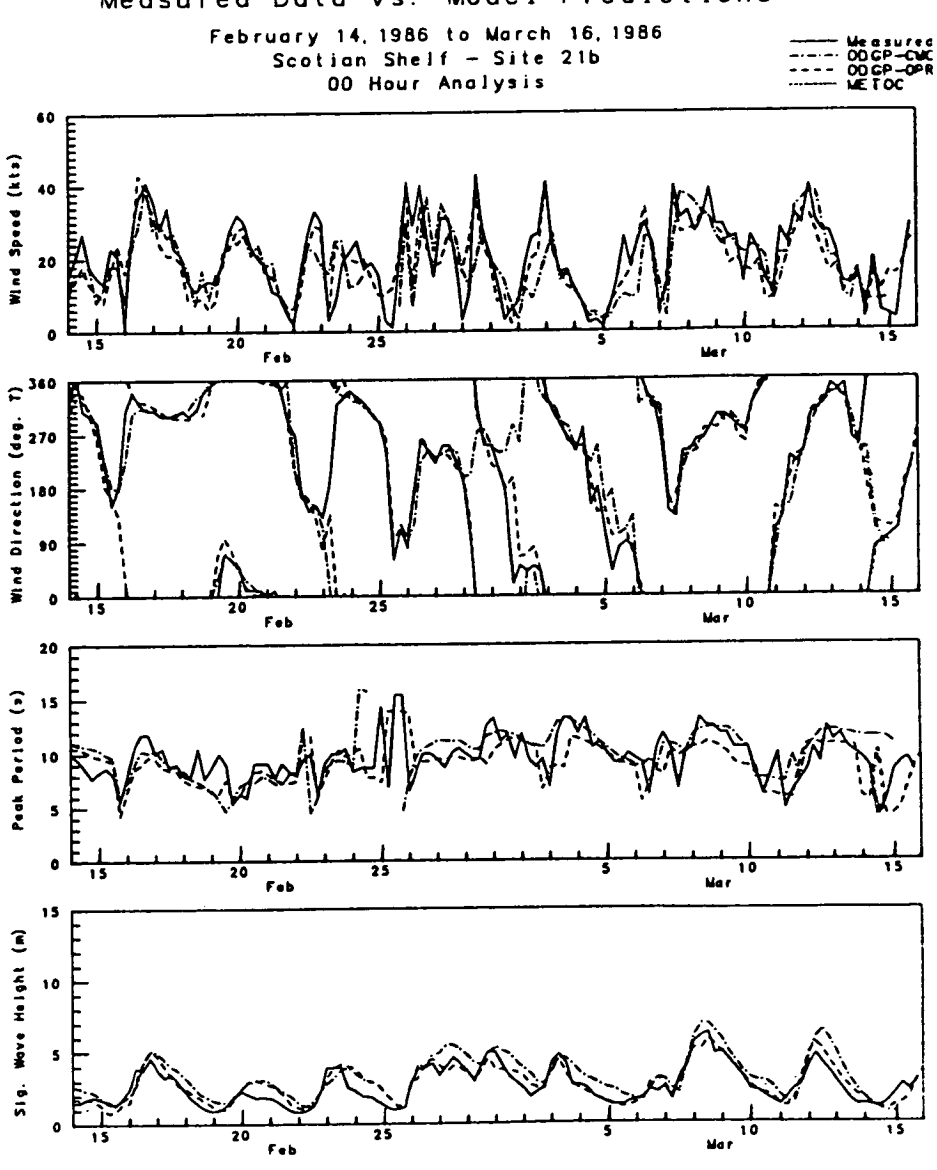
Measured Data vs. Model Predictions
February 14, 1986 to March 16, 1986
Scotian Shelf - Site 21b
00 Hour Analysis
Measured
ODGP-CMC
ODGP-OPR
METOC
Wind Speed (kts)
Wind Direction (deg. T)
Peak Period (s)
Sig. Wave Height (m)
Feb
Mar

Measured Data vs. Model Predictions

January 15, 1986 to February 14, 1986
Scotian Shelf – Site 21b
12 Hour Forecast

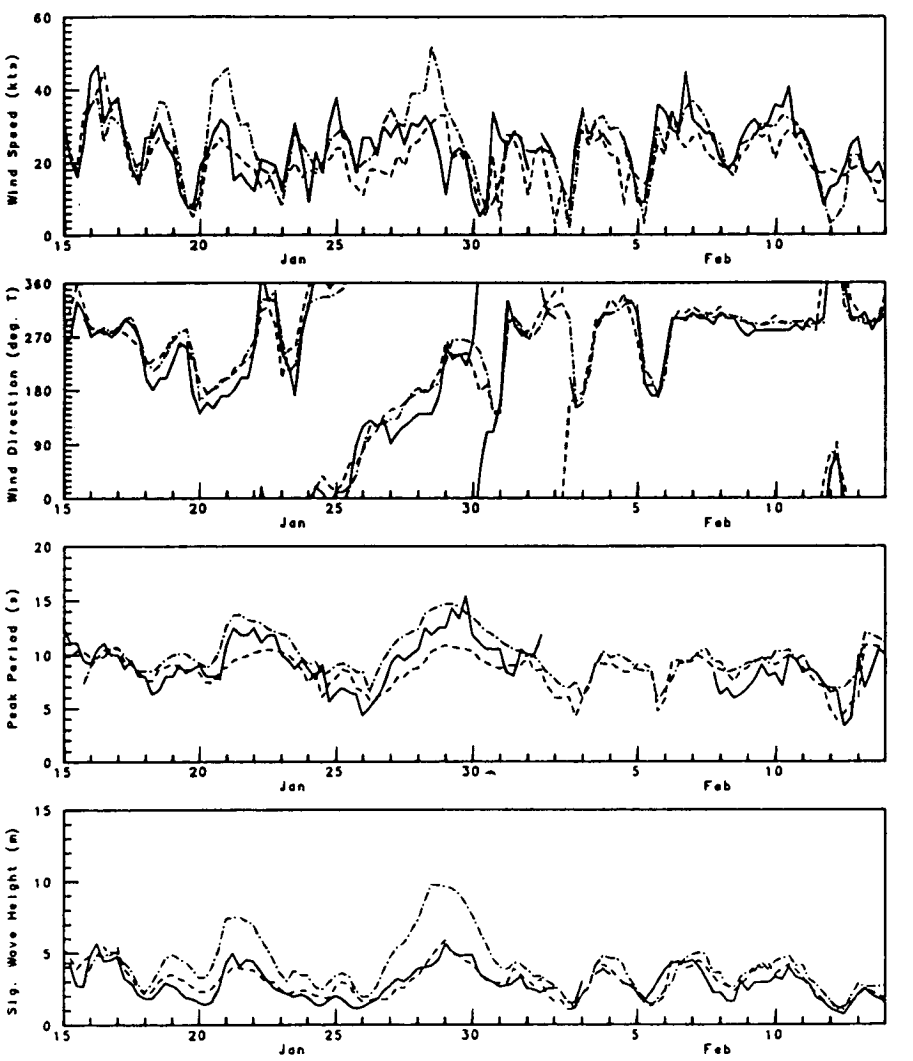

Measured Data vs. Model Predictions

February 14, 1986 to March 16, 1986
Scotian Shelf – Site 21b
12 Hour Forecast

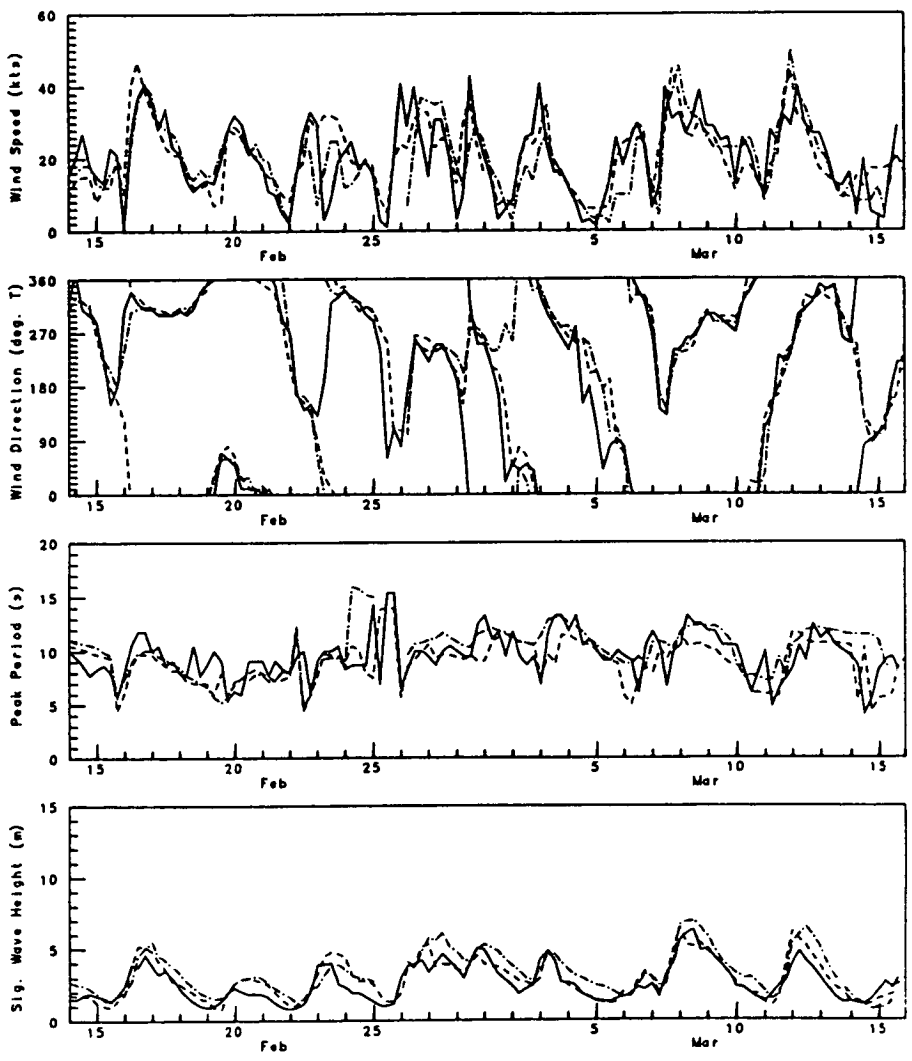

Measured Data vs. Model Predictions

January 15, 1986 to February 14, 1986
Scotian Shelf – Site 21b
24 Hour Forecast

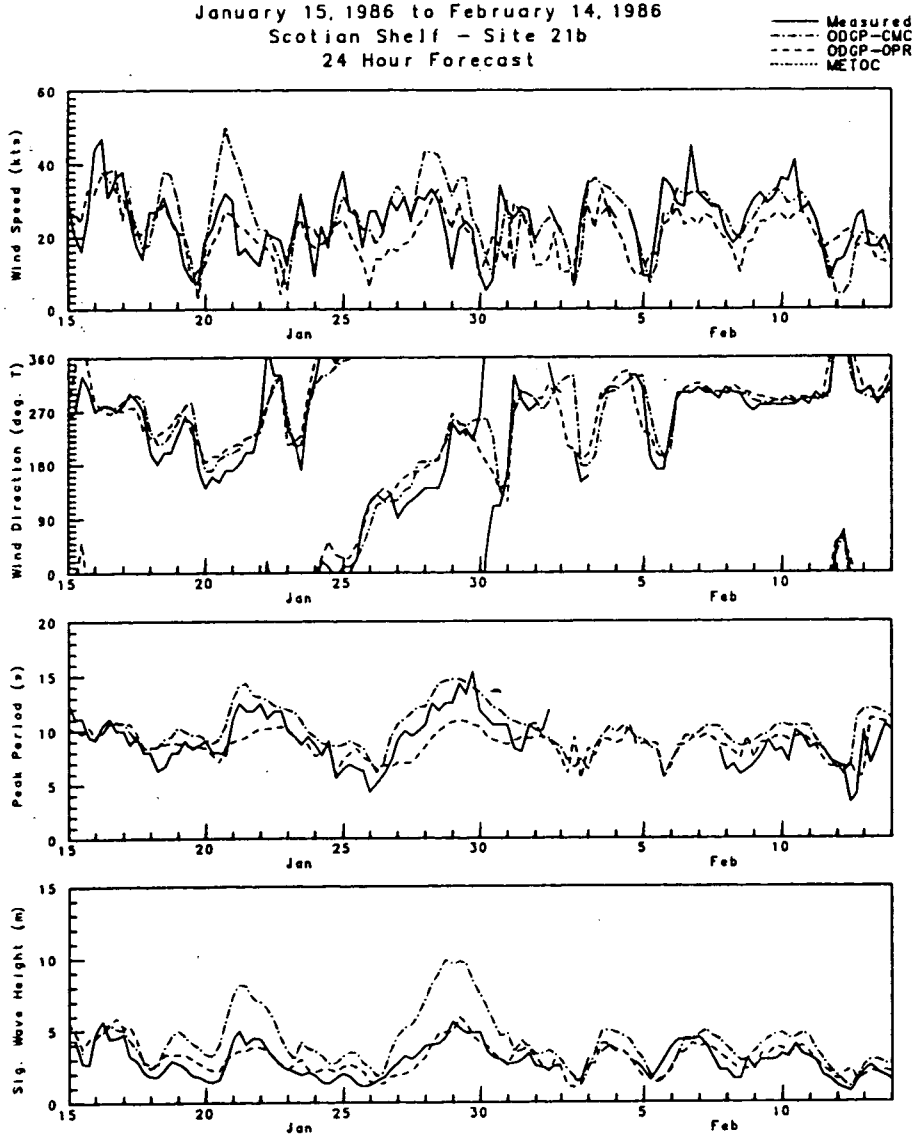

Measured Data vs. Model Predictions

February 14, 1986 to March 16, 1986
Scotian Shelf – Site 21b
24 Hour Forecast

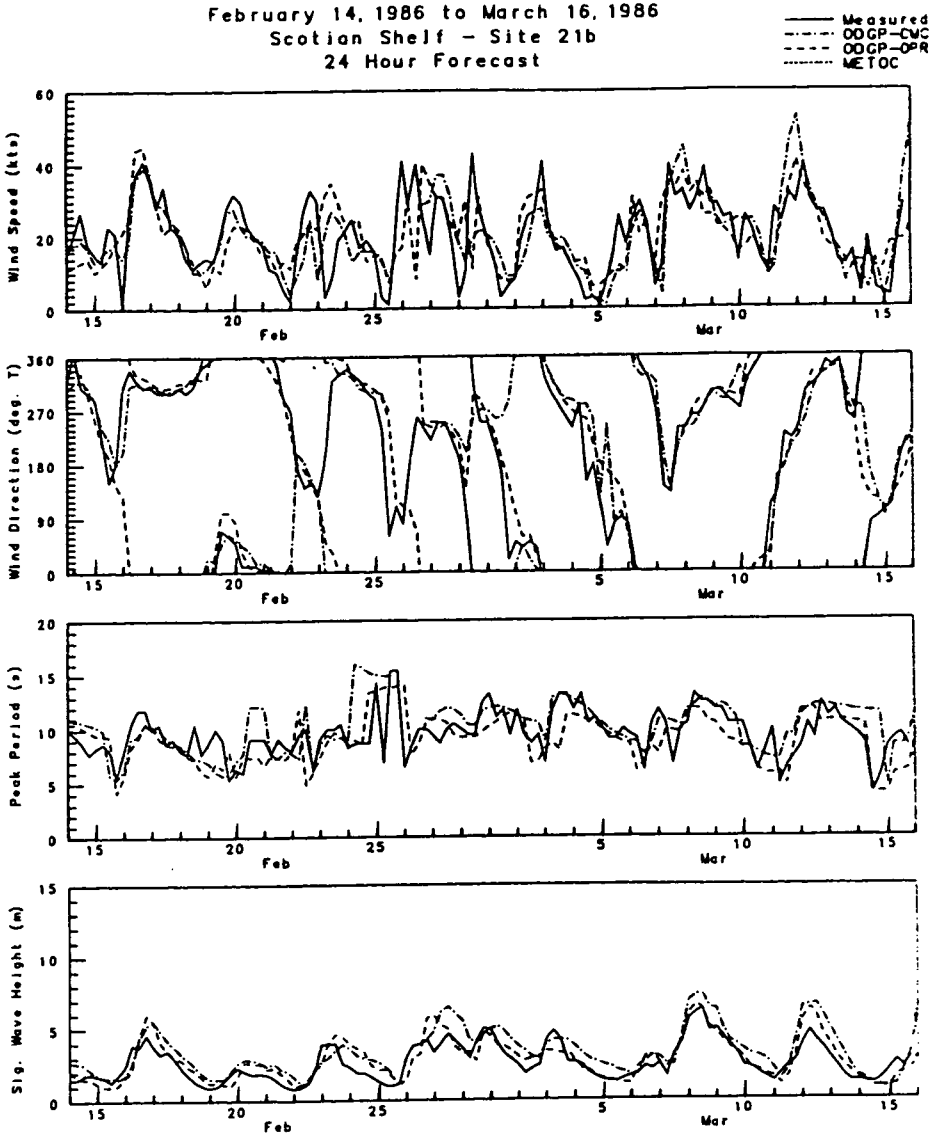

Measured Data vs. Model Predictions

January 15, 1986 to February 14, 1986
Scotian Shelf - Site 21b
36 Hour Forecast

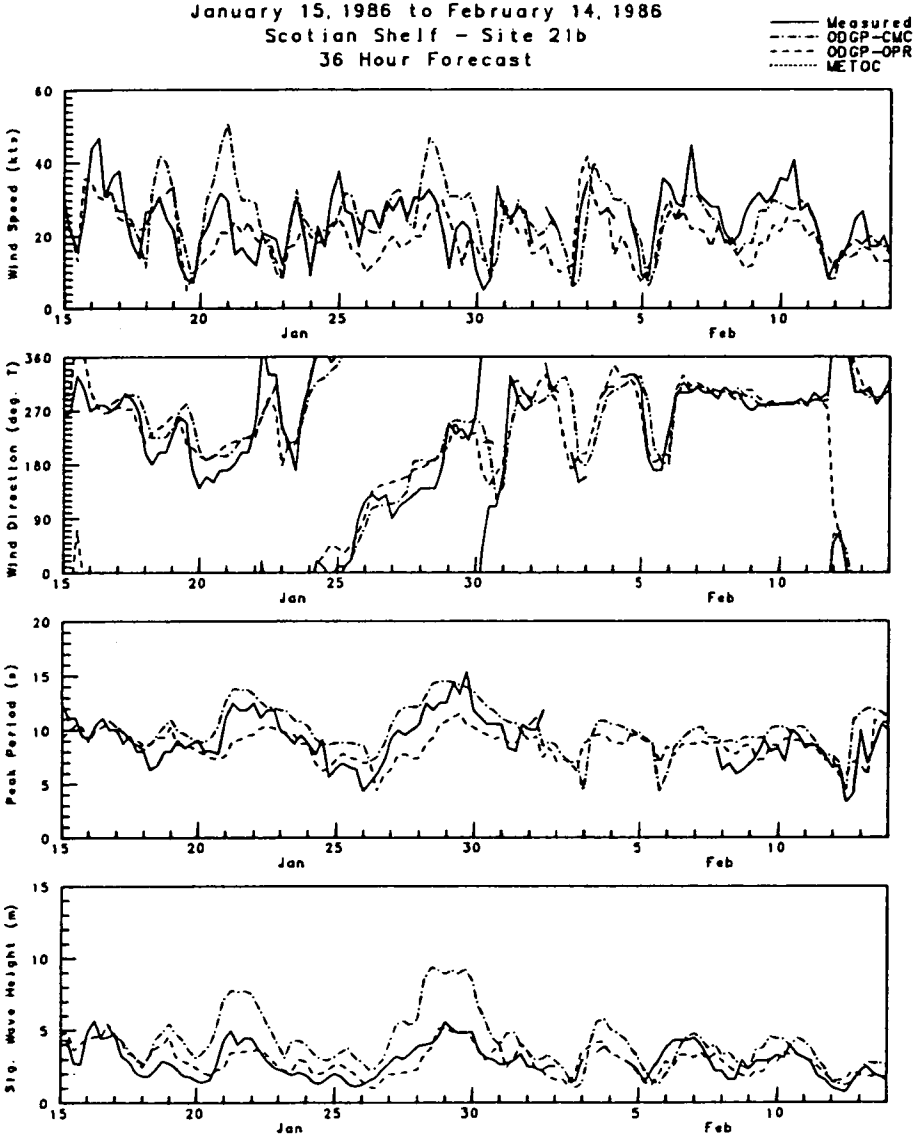

Measured Data vs. Model Predictions

February 14, 1986 to March 16, 1986
Scotian Shelf - Site 21b
36 Hour Forecast

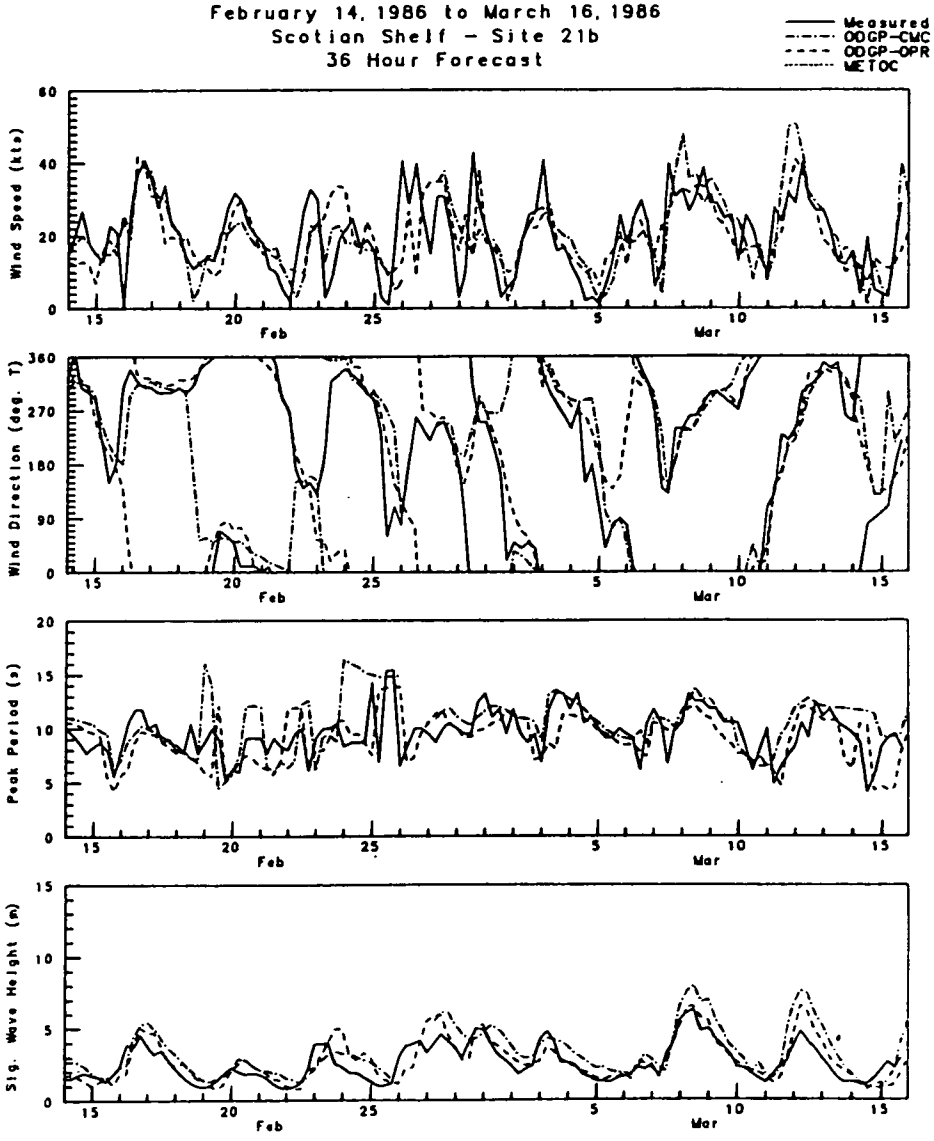

Measured Data vs. Model Predictions

January 15, 1986 to February 14, 1986
Scotian Shelf - Site 21b
48 Hour Forecast

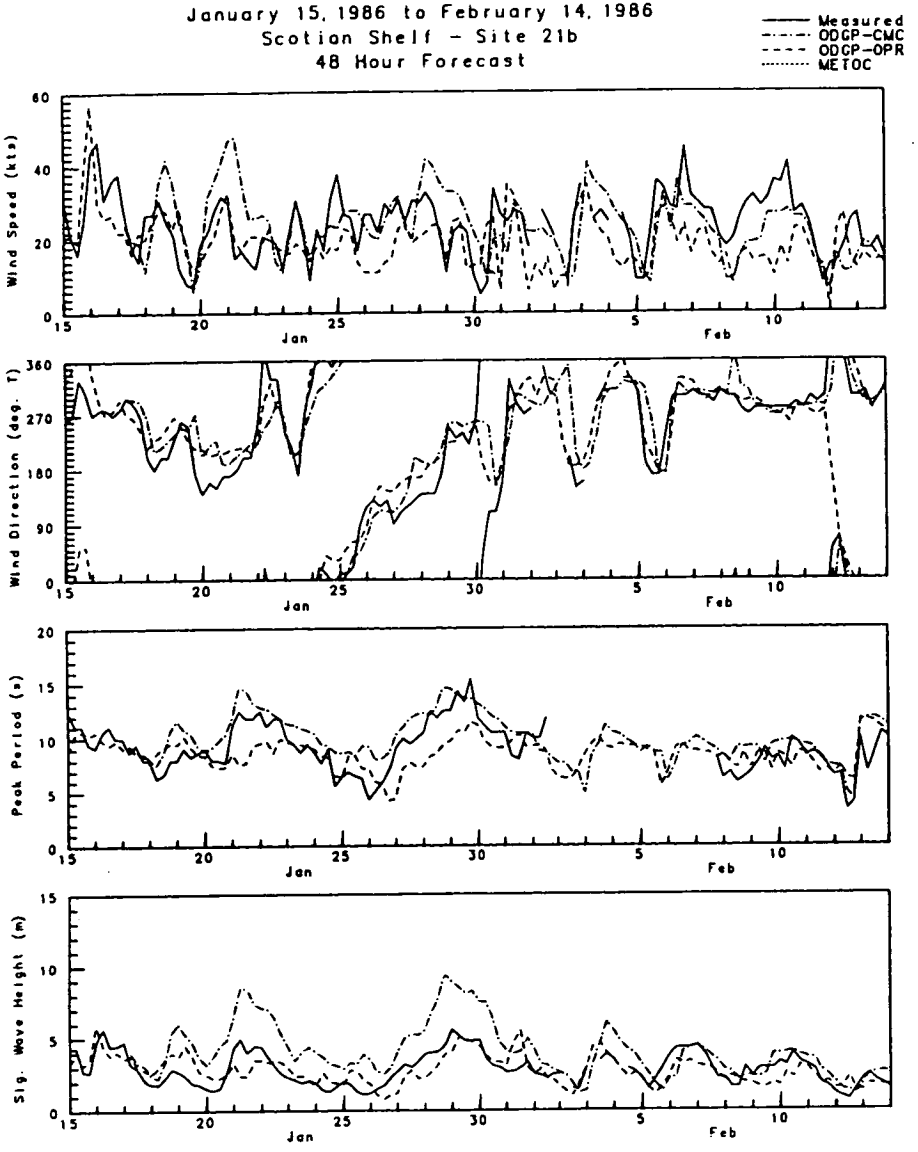

Measured Data vs. Model Predictions

February 14, 1986 to March 16, 1986
Scotian Shelf - Site 21b
48 Hour Forecast

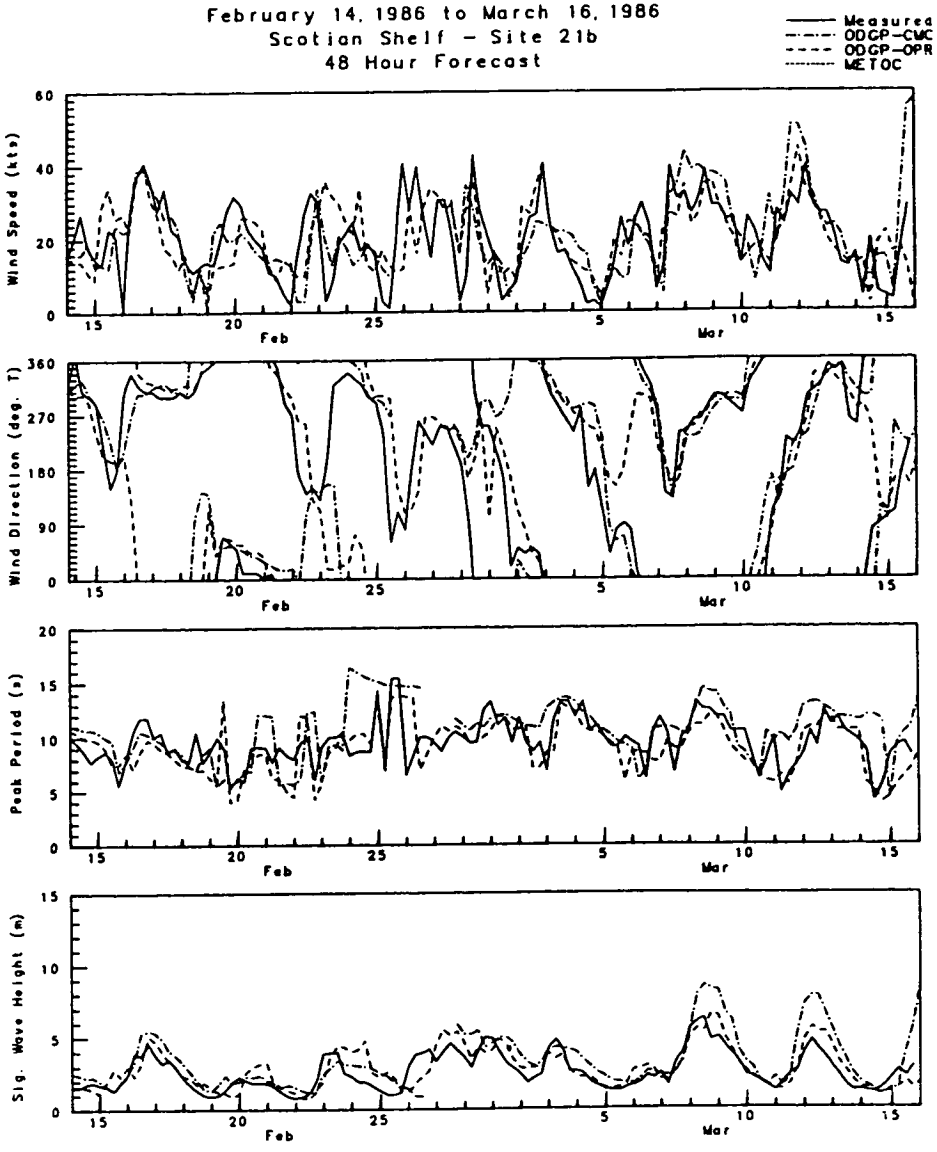

Measured Data vs. Model Predictions

January 15, 1986 to February 14, 1986
Scotian Shelf - Site 22
00 Hour Analysis

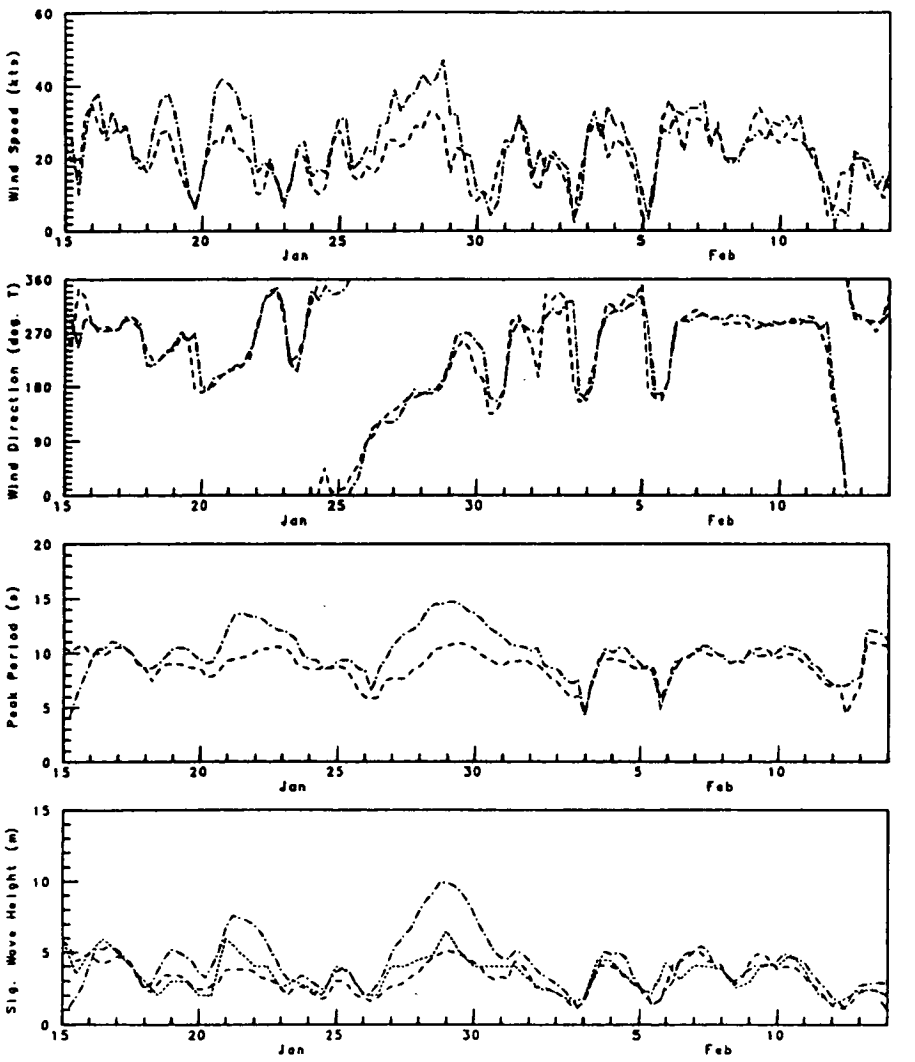

Measured Data vs. Model Predictions

February 14, 1986 to March 16, 1986
Scotian Shelf - Site 22
00 Hour Analysis

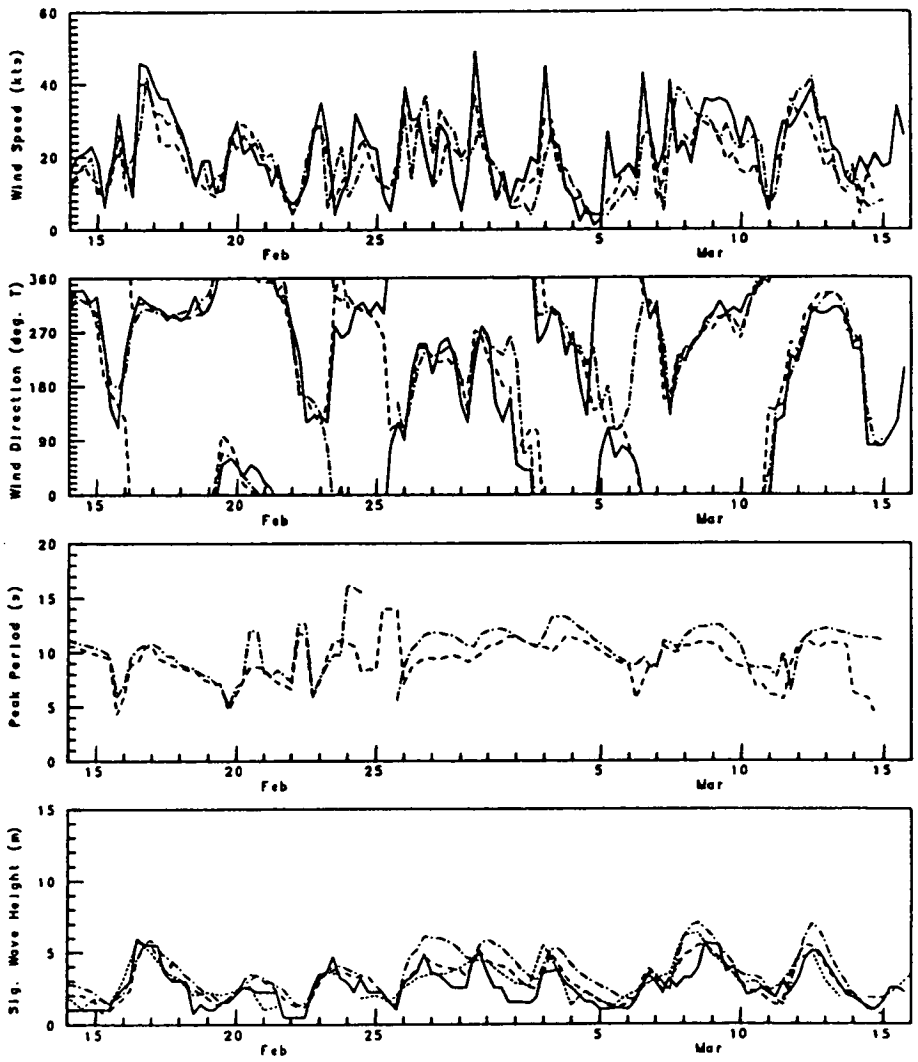

Measured Data vs. Model Predictions

January 15, 1986 to February 14, 1986
Scotian Shelf - Site 22
12 Hour Forecast

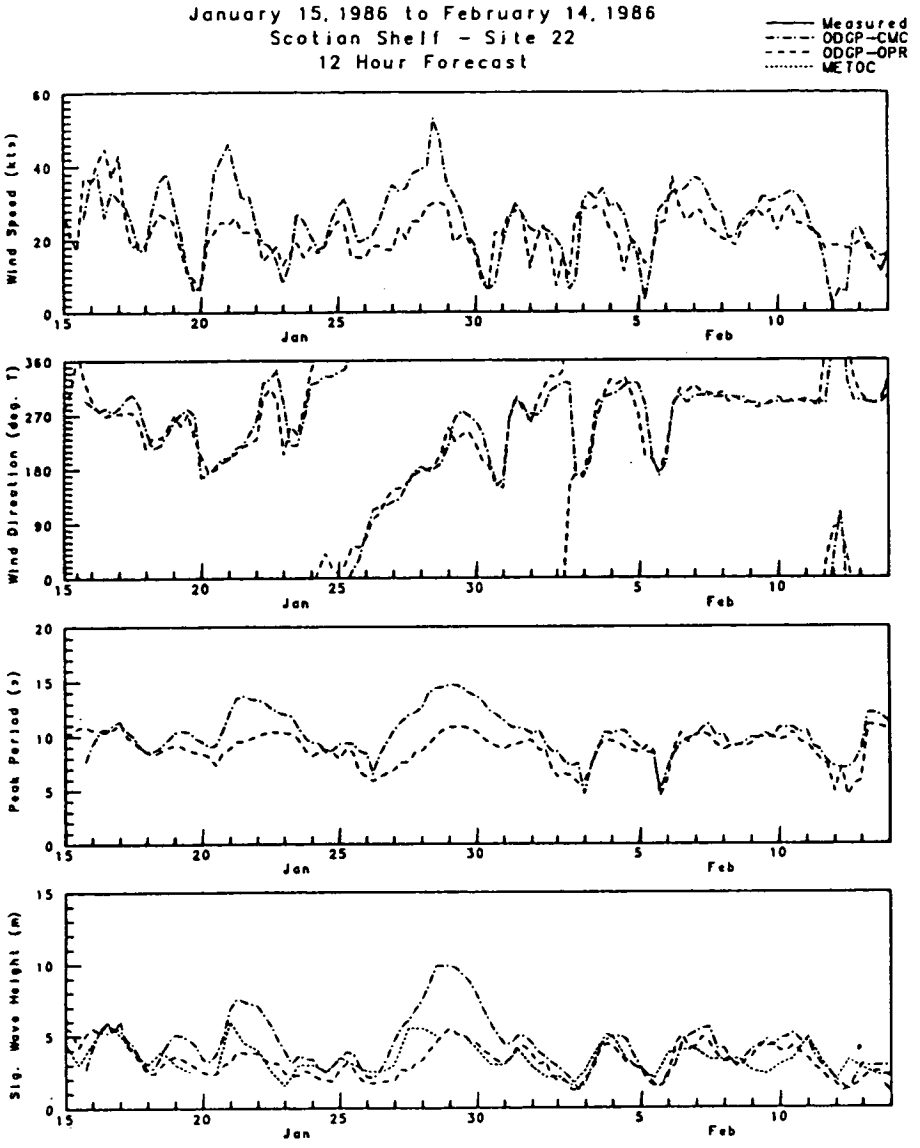

Measured Data vs. Model Predictions

February 14, 1986 to March 16, 1986
Scotian Shelf - Site 22
12 Hour Forecast

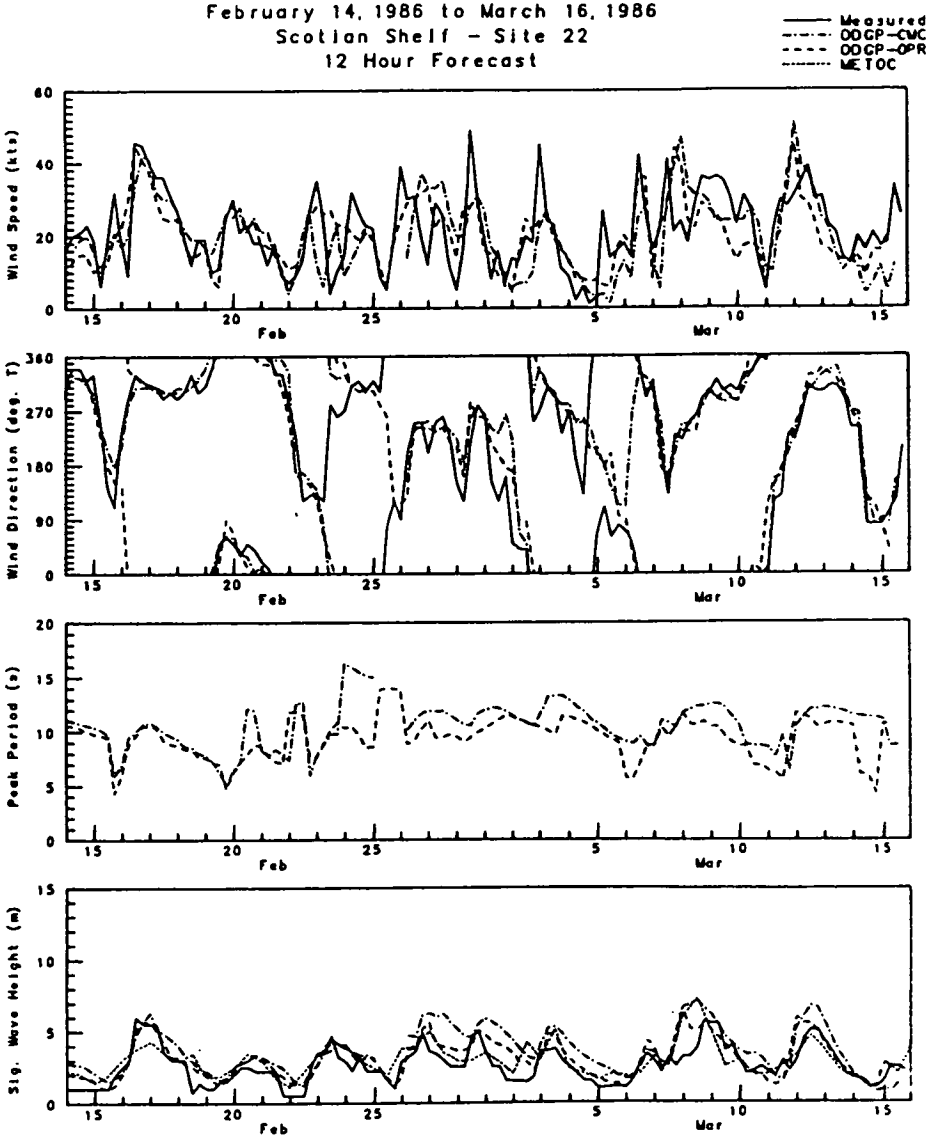

Measured Data vs. Model Predictions

January 15, 1986 to February 14, 1986
Scotian Shelf - Site 22
24 Hour Forecast

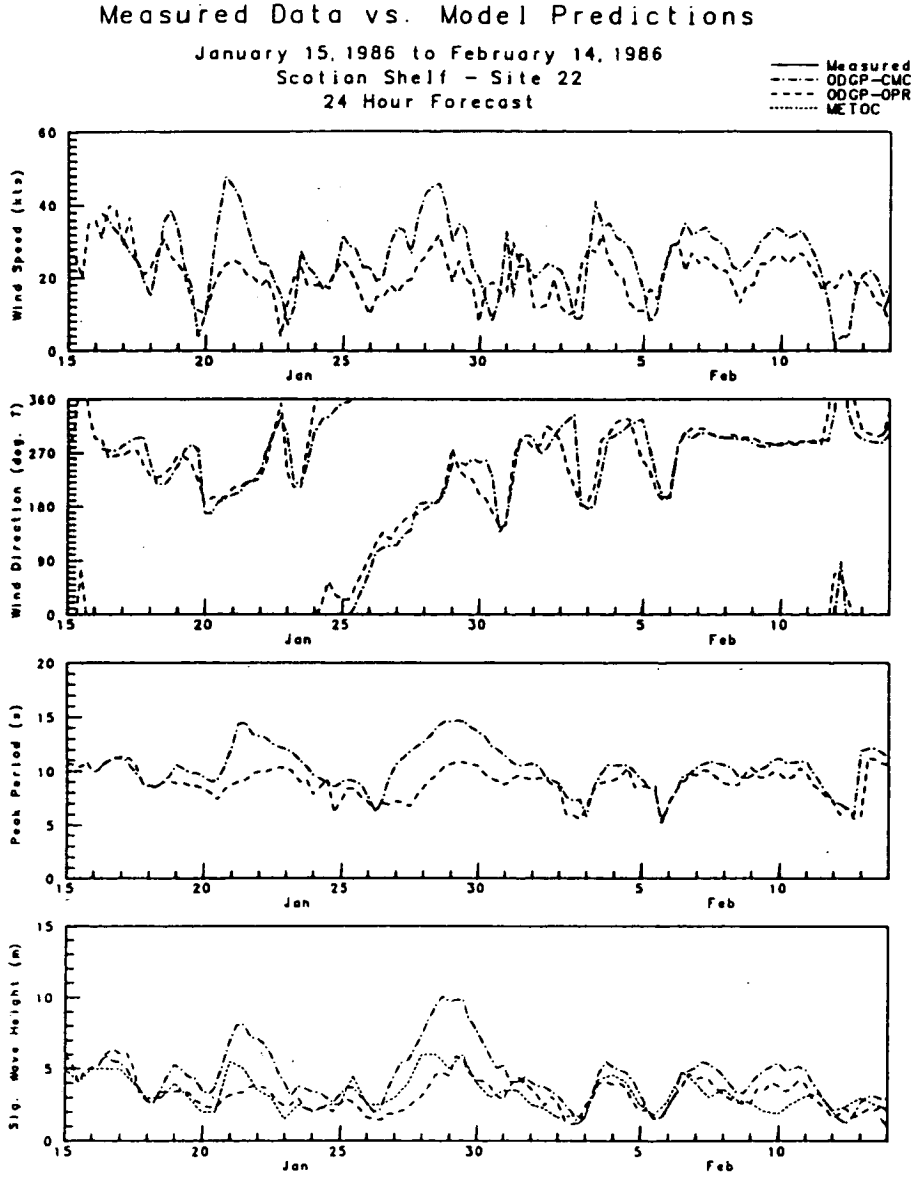

Measured Data vs. Model Predictions

February 14, 1986 to March 16, 1986
Scotian Shelf - Site 22
24 Hour Forecast

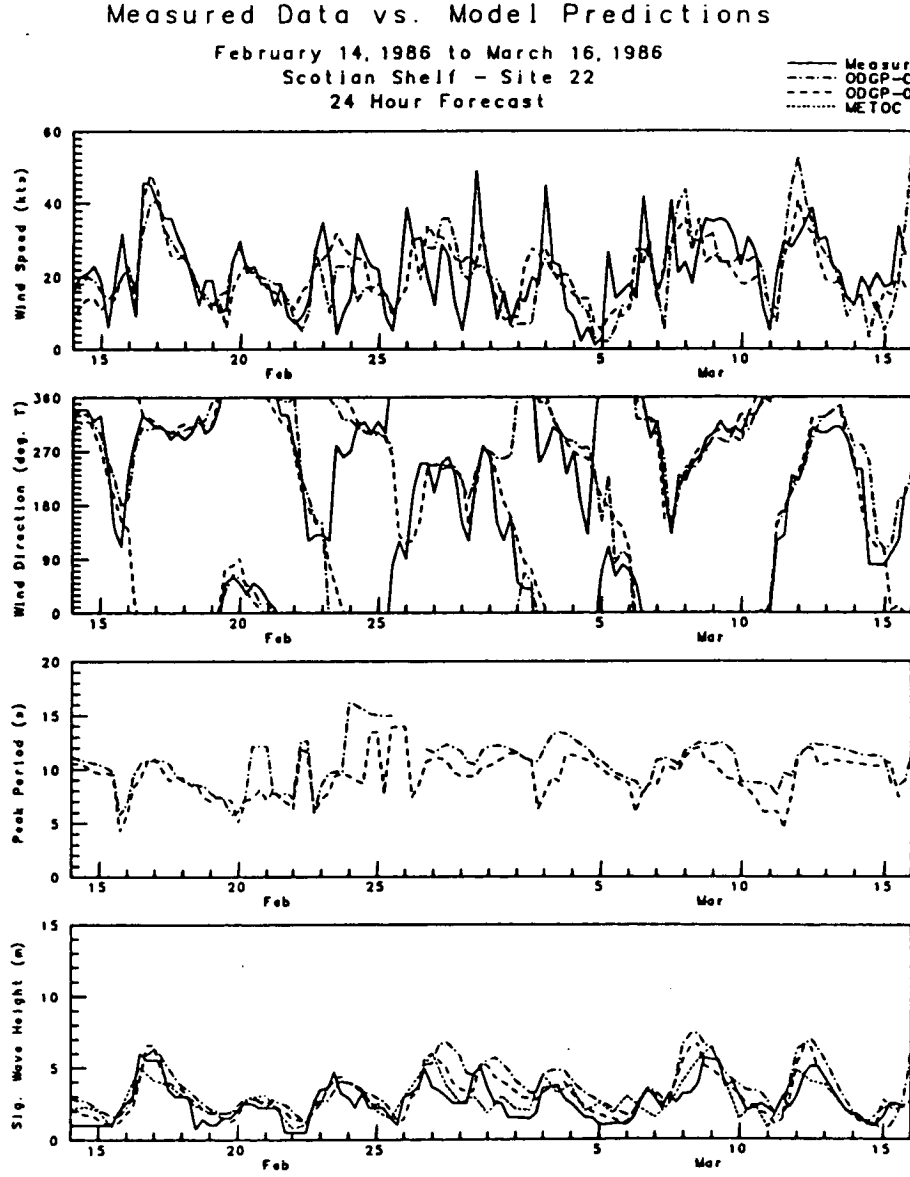

Measured Data vs. Model Predictions

January 15, 1986 to February 14, 1986
Scotian Shelf - Site 22
36 Hour Forecast

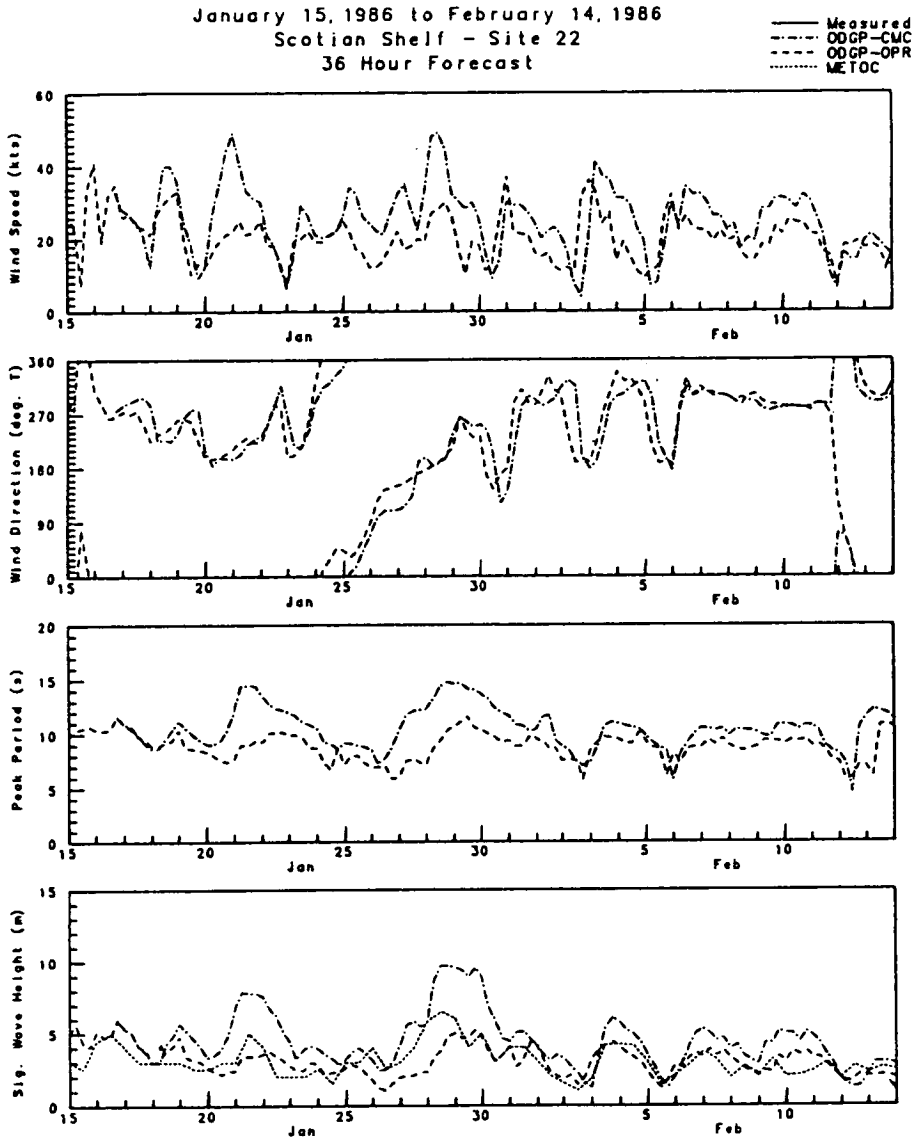

Measured Data vs. Model Predictions

February 14, 1986 to March 16, 1986
Scotian Shelf - Site 22
36 Hour Forecast

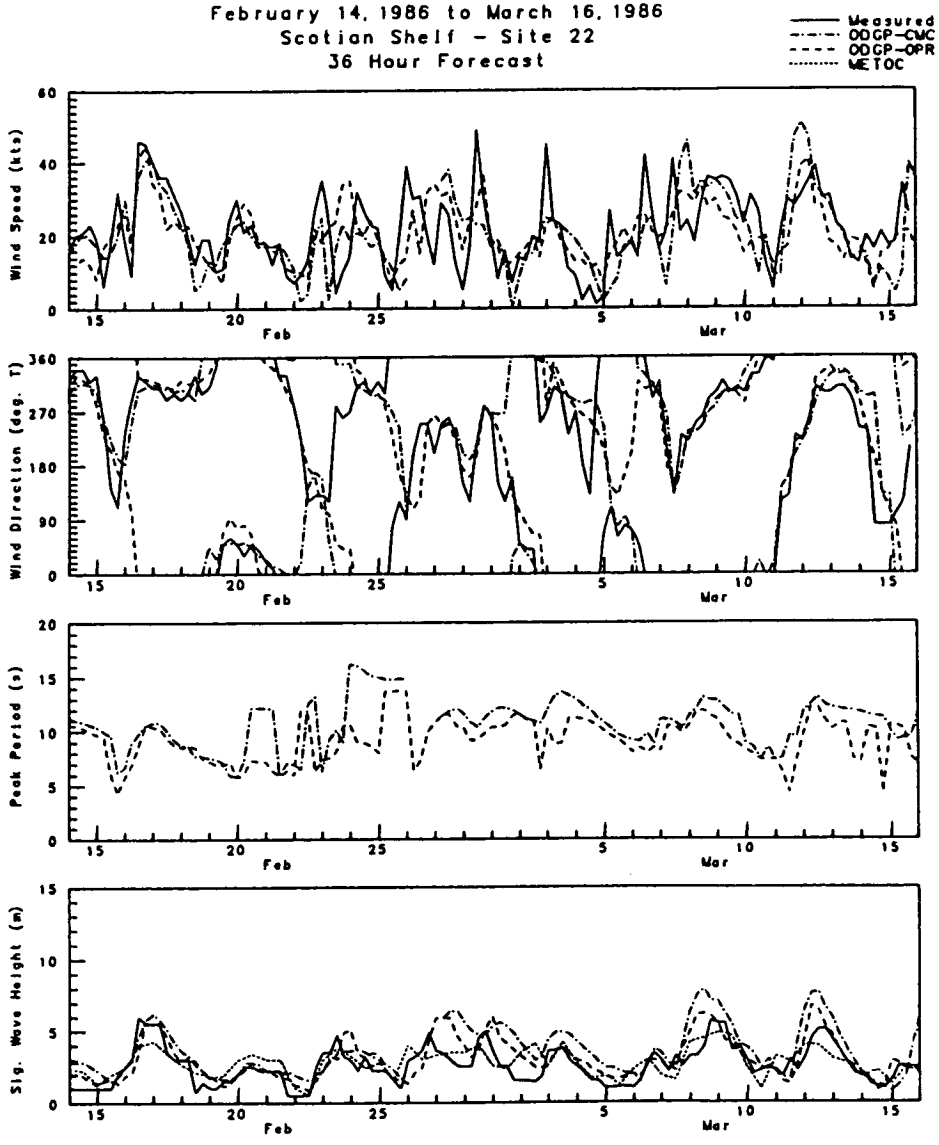

Measured Data vs. Model Predictions

January 15, 1986 to February 14, 1986
Scotian Shelf - Site 22
48 Hour Forecast

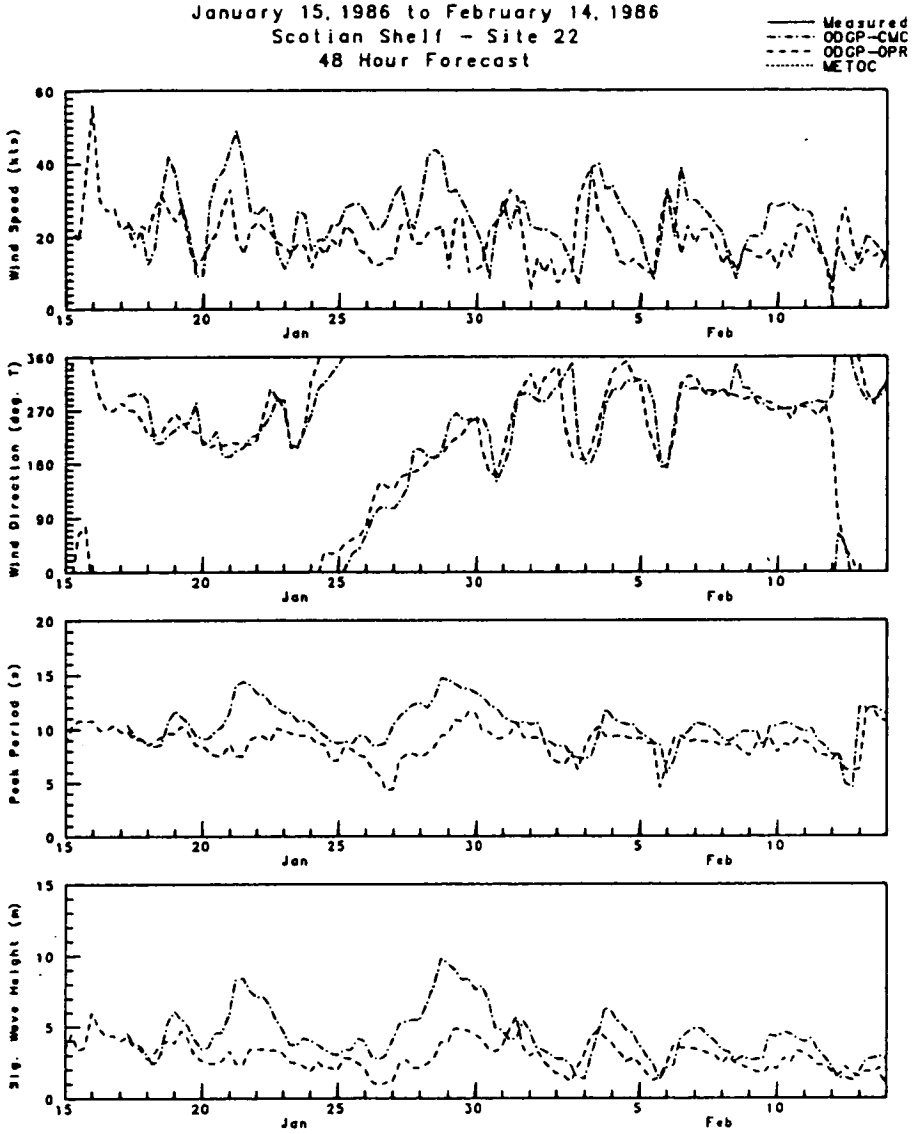

Measured Data vs. Model Predictions

February 14, 1986 to March 16, 1986
Scotian Shelf - Site 22
48 Hour Forecast

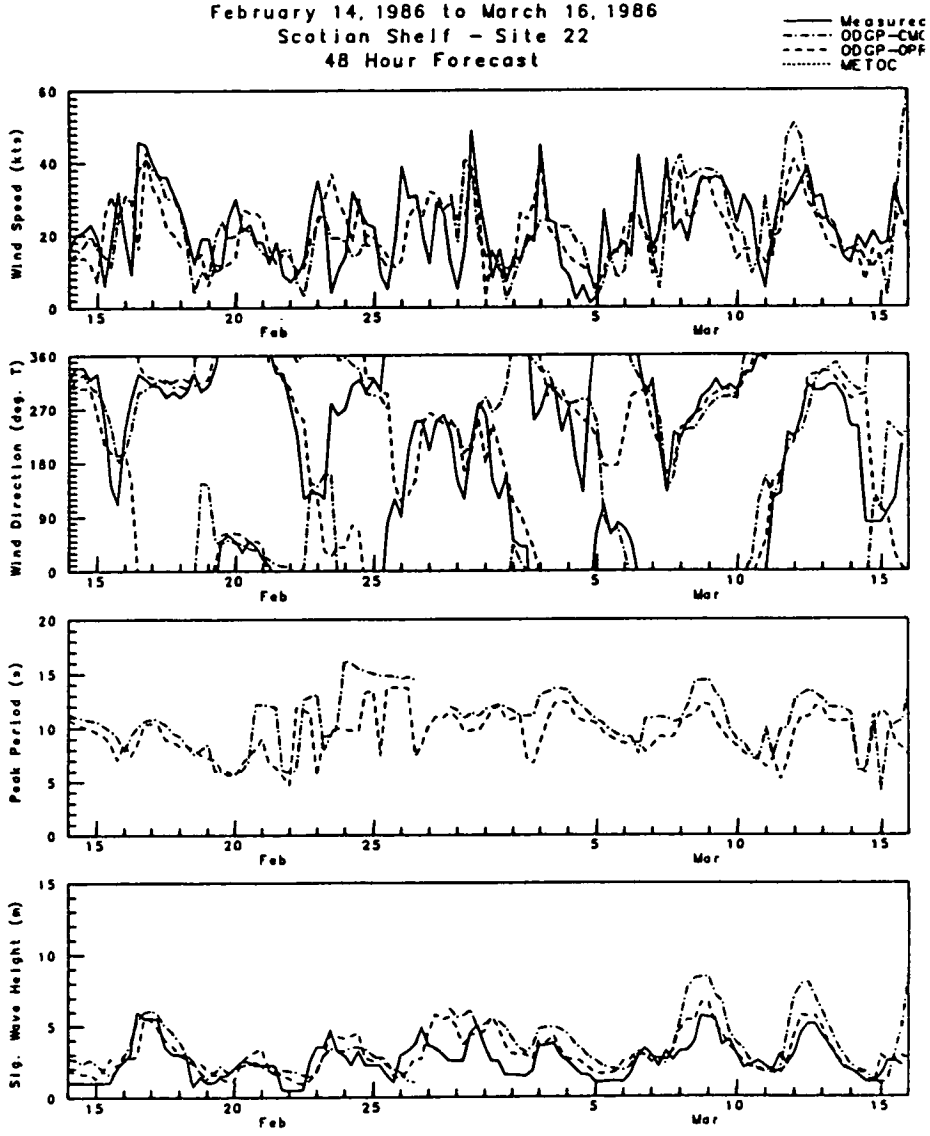

Measured Data vs. Model Predictions

January 15, 1986 to February 14, 1986
Grand Banks – Site 31a
00 Hour Analysis

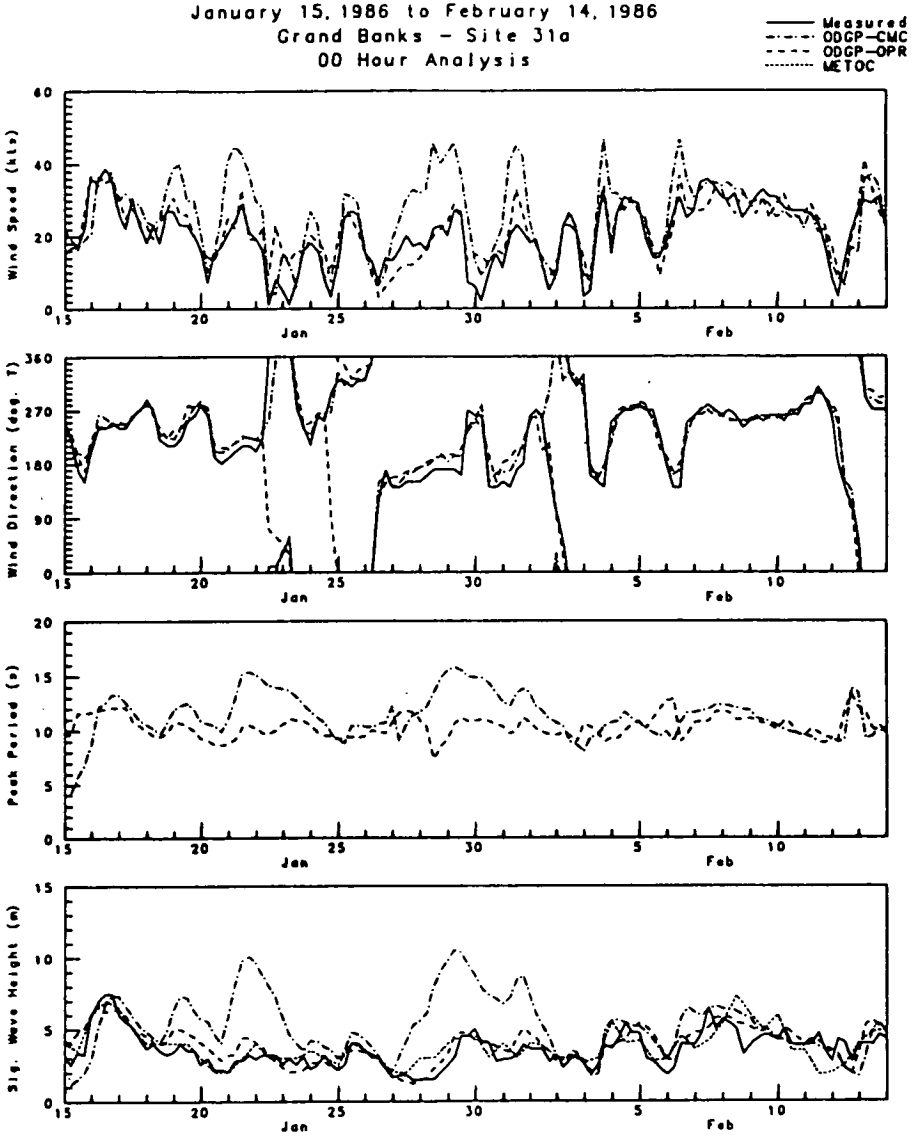

Measured Data vs. Model Predictions

February 14, 1986 to March 16, 1986
Grand Banks – Site 31a
00 Hour Analysis

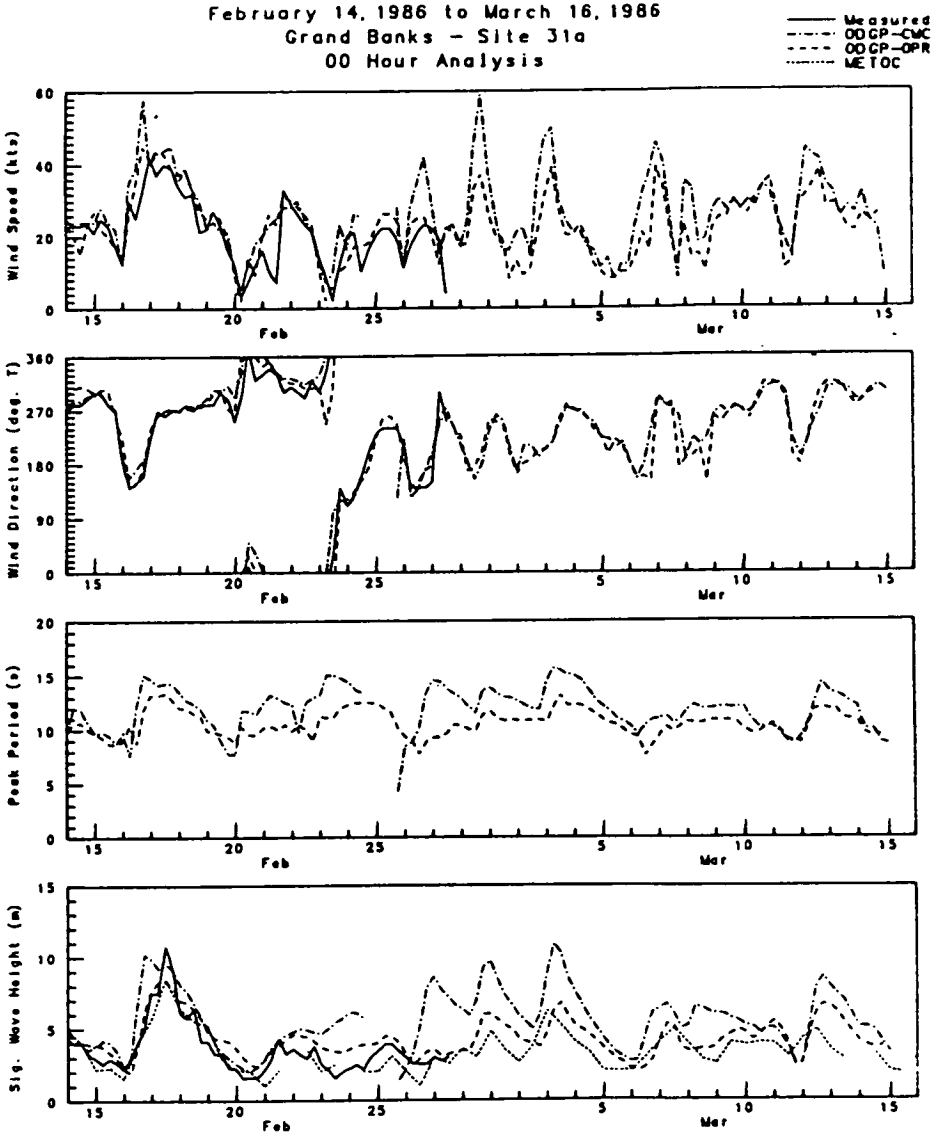

Measured Data vs. Model Predictions

January 15, 1986 to February 14, 1986
Grand Banks – Site 31a
12 Hour Forecast

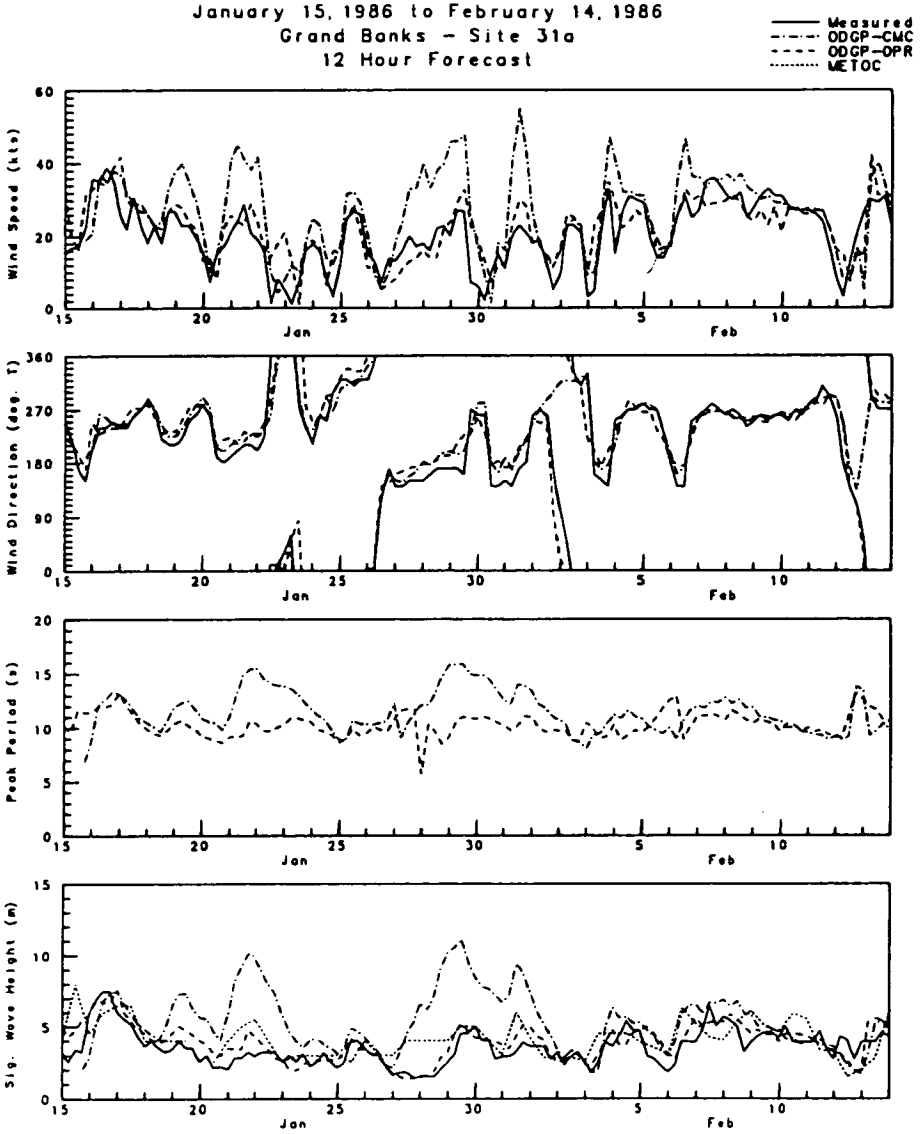

Measured Data vs. Model Predictions

February 14, 1986 to March 16, 1986
Grand Banks – Site 31a
12 Hour Forecast

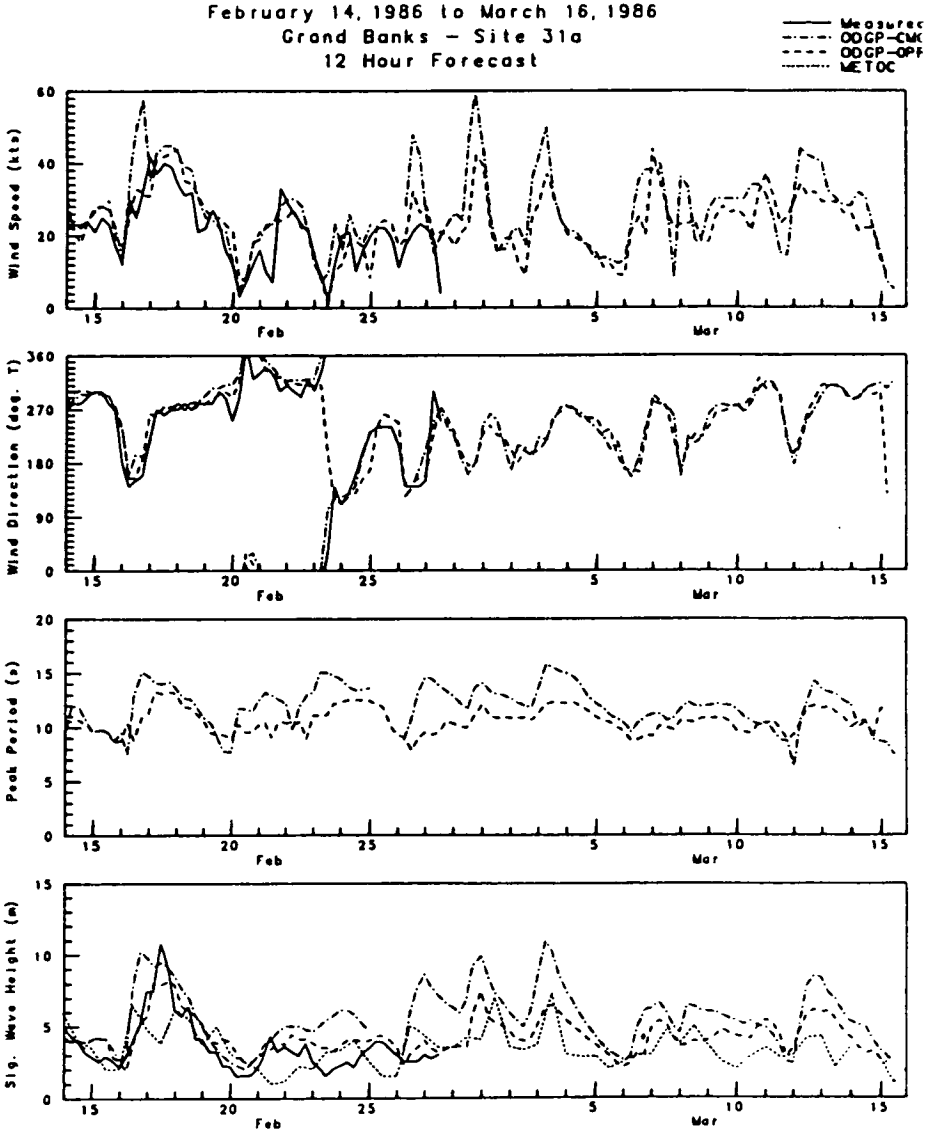

Measured Data vs. Model Predictions

January 15, 1986 to February 14, 1986
Grand Banks - Site 31a
24 Hour Forecast

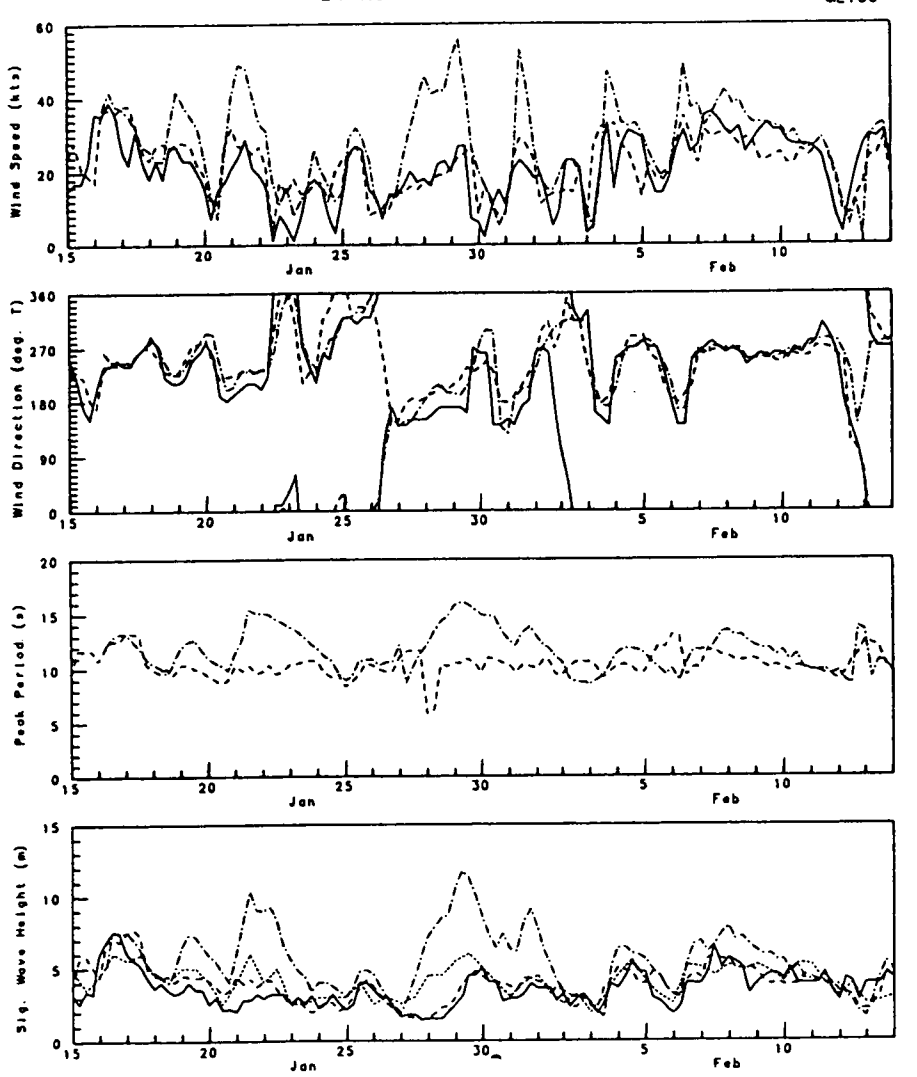

Measured Data vs. Model Predictions

February 14, 1986 to March 16, 1986
Grand Banks - Site 31a
24 Hour Forecast

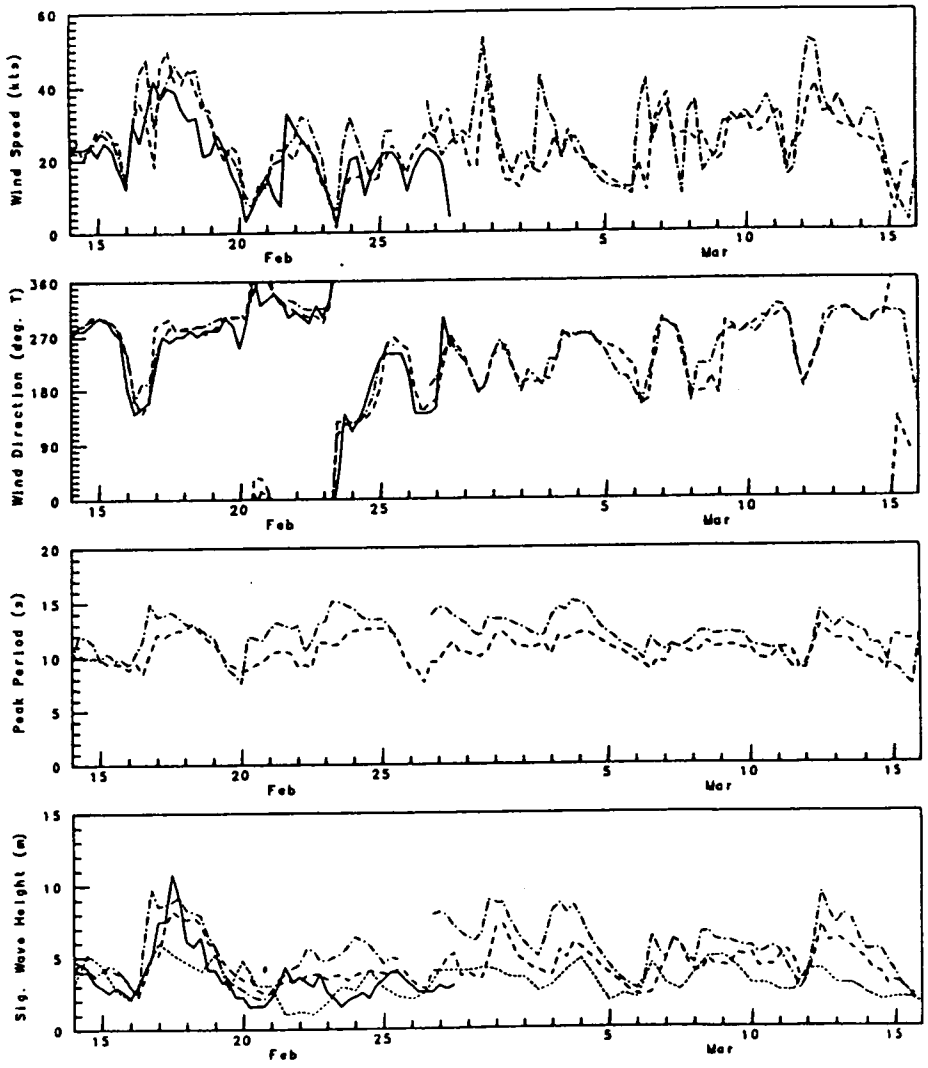

Measured Data vs. Model Predictions

January 15, 1986 to February 14, 1986
Grand Banks – Site 31a
36 Hour Forecast

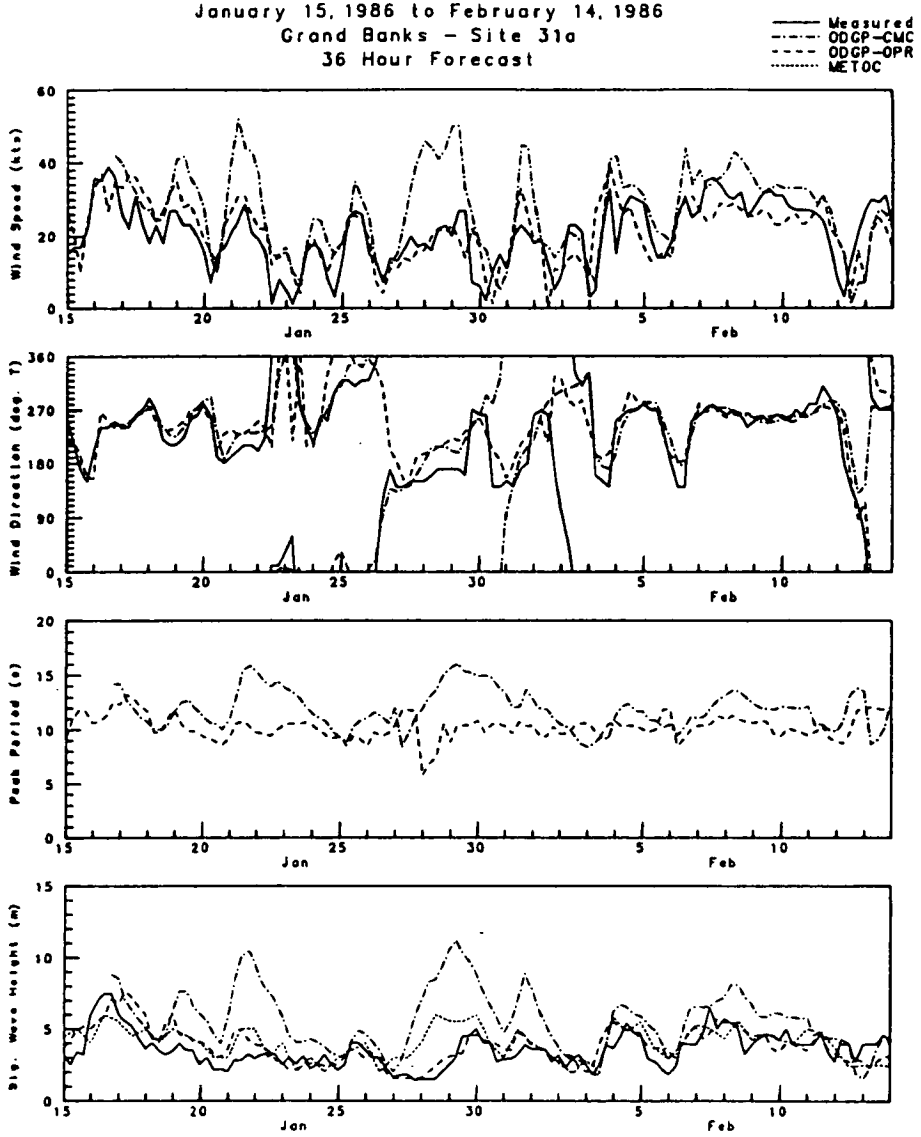

Measured Data vs. Model Predictions

February 14, 1986 to March 16, 1986
Grand Banks – Site 31a
36 Hour Forecast

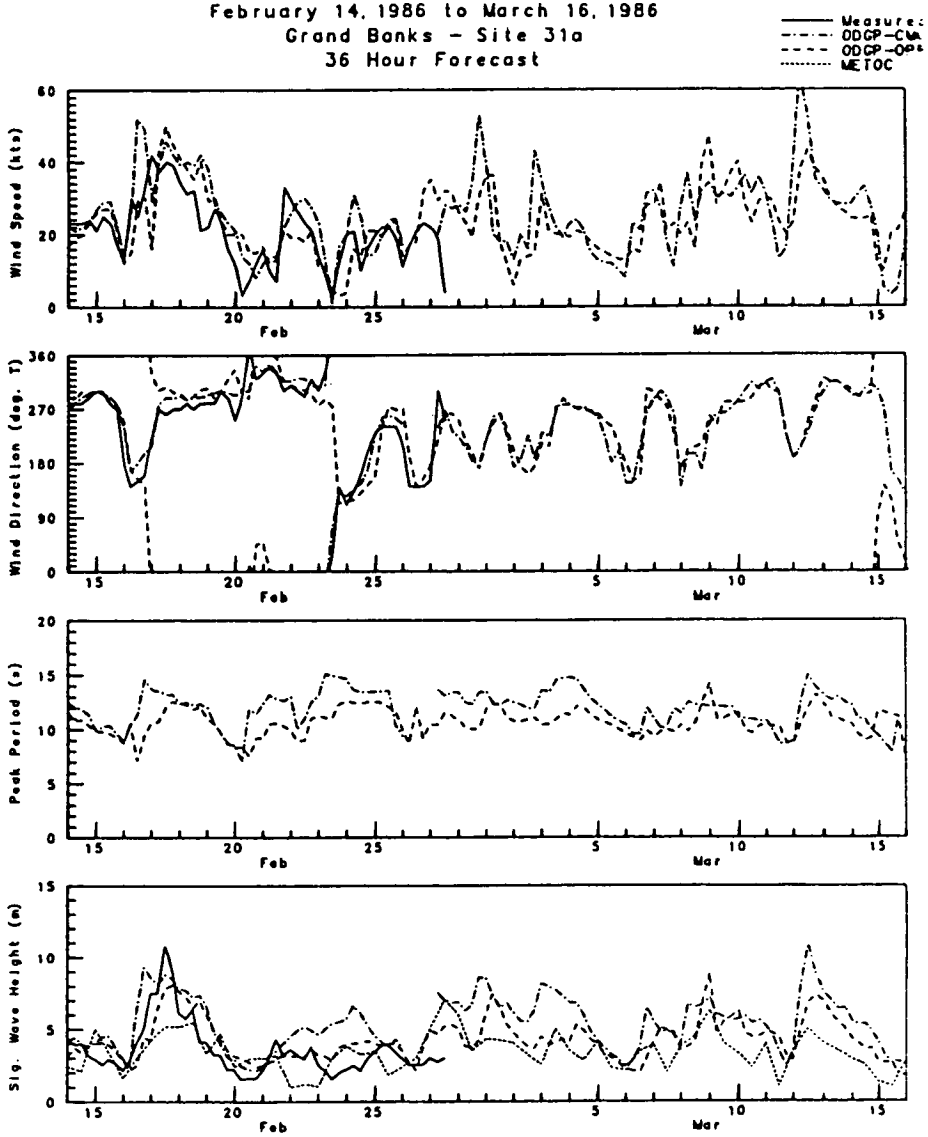

Measured Data vs. Model Predictions

January 15, 1986 to February 14, 1986
Grand Banks – Site 31a
48 Hour Forecast

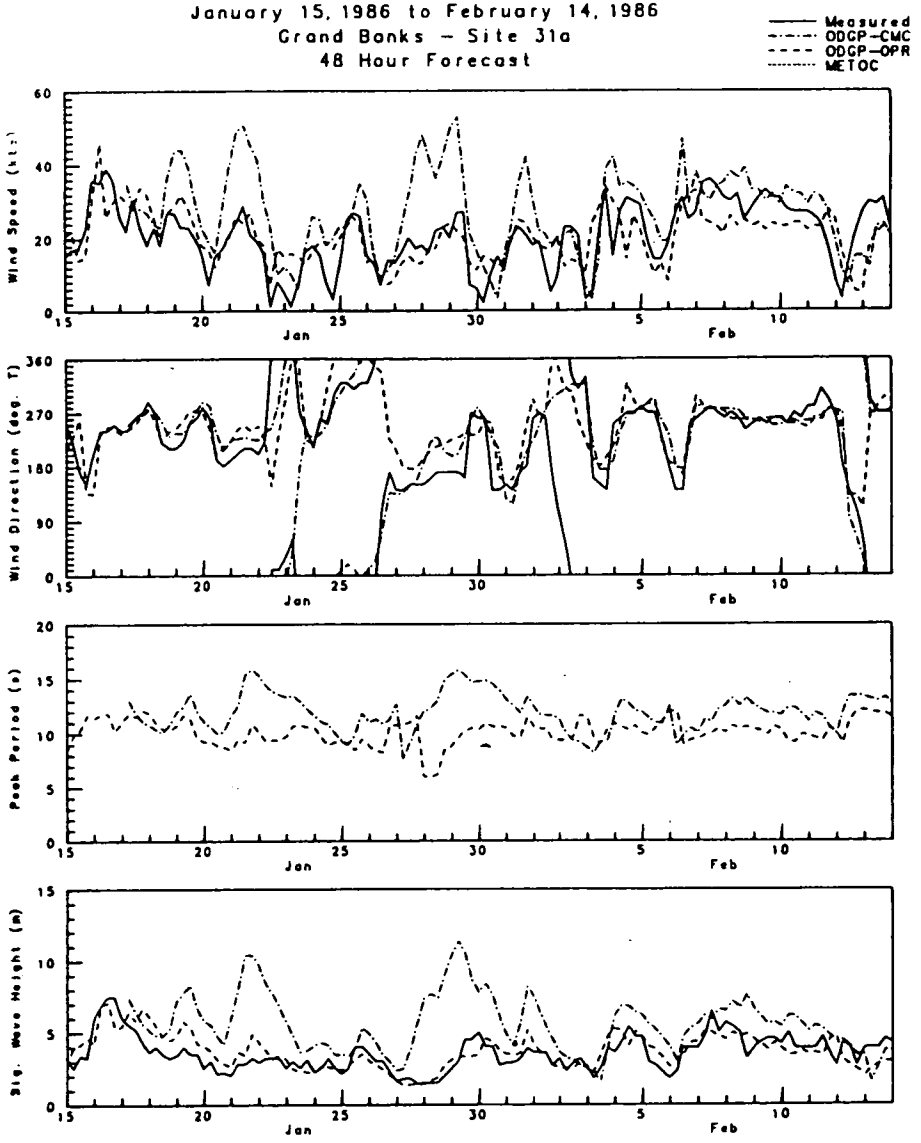

Measured Data vs. Model Predictions

February 14, 1986 to March 16, 1986
Grand Banks – Site 31a
48 Hour Forecast

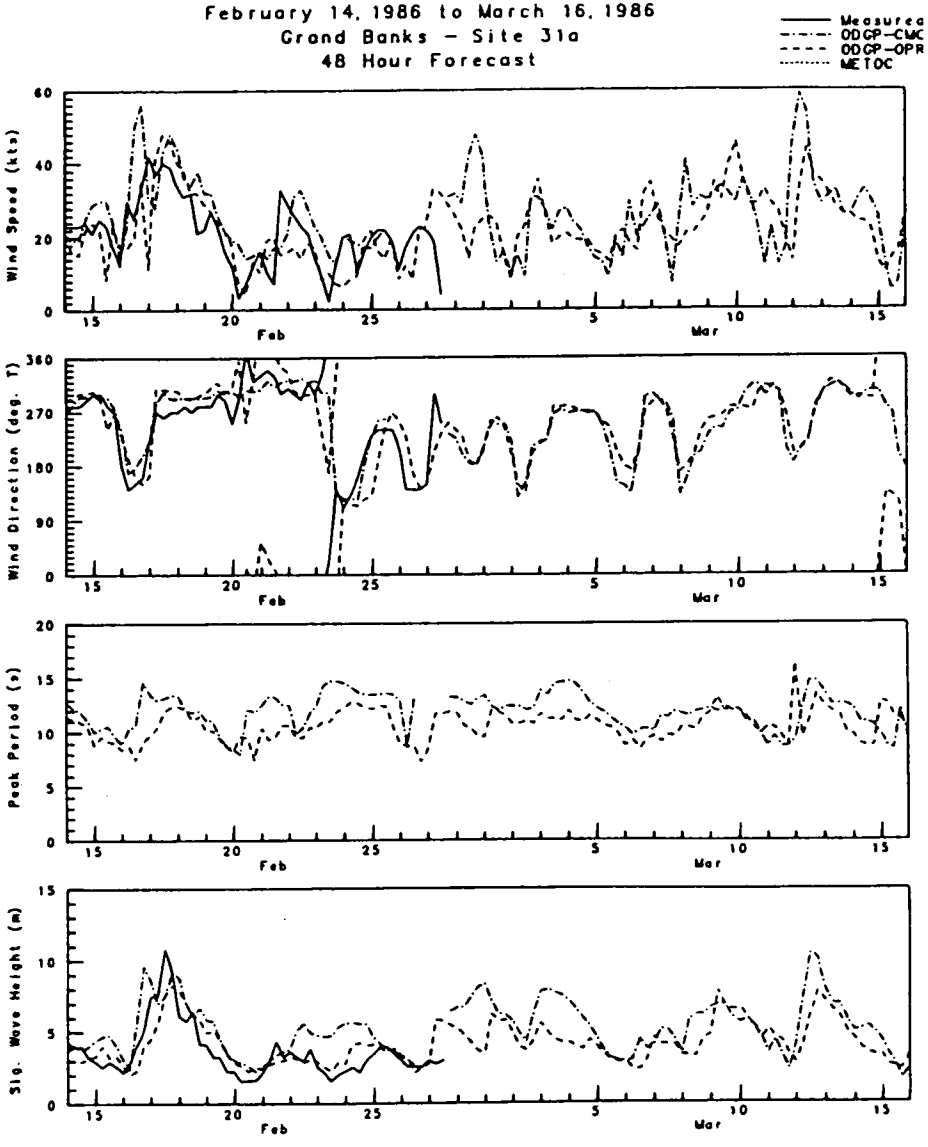

Measured Data vs. Model Predictions

January 15, 1986 to February 14, 1986
Grand Banks – Site 31b
00 Hour Analysis

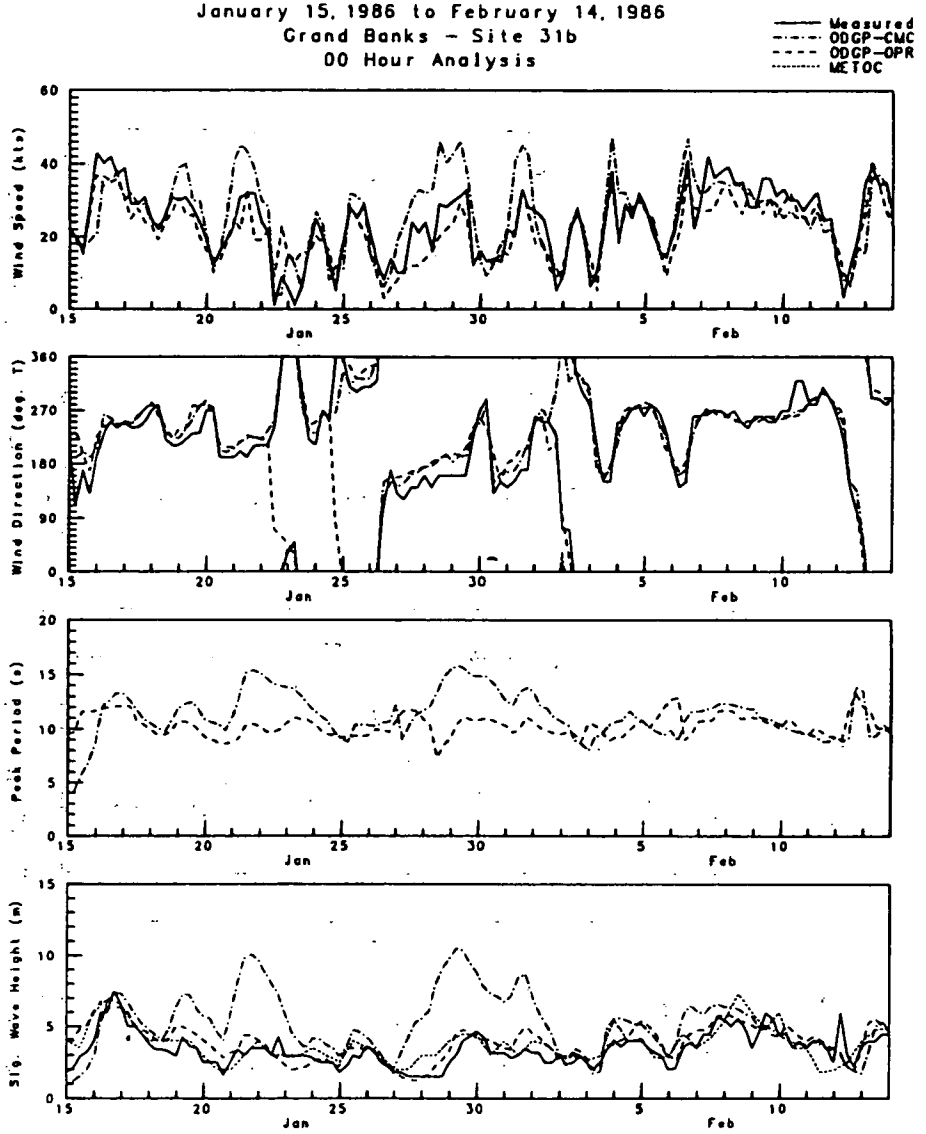

Measured Data vs. Model Predictions

February 14, 1986 to March 16, 1986
Grand Banks – Site 31b
00 Hour Analysis

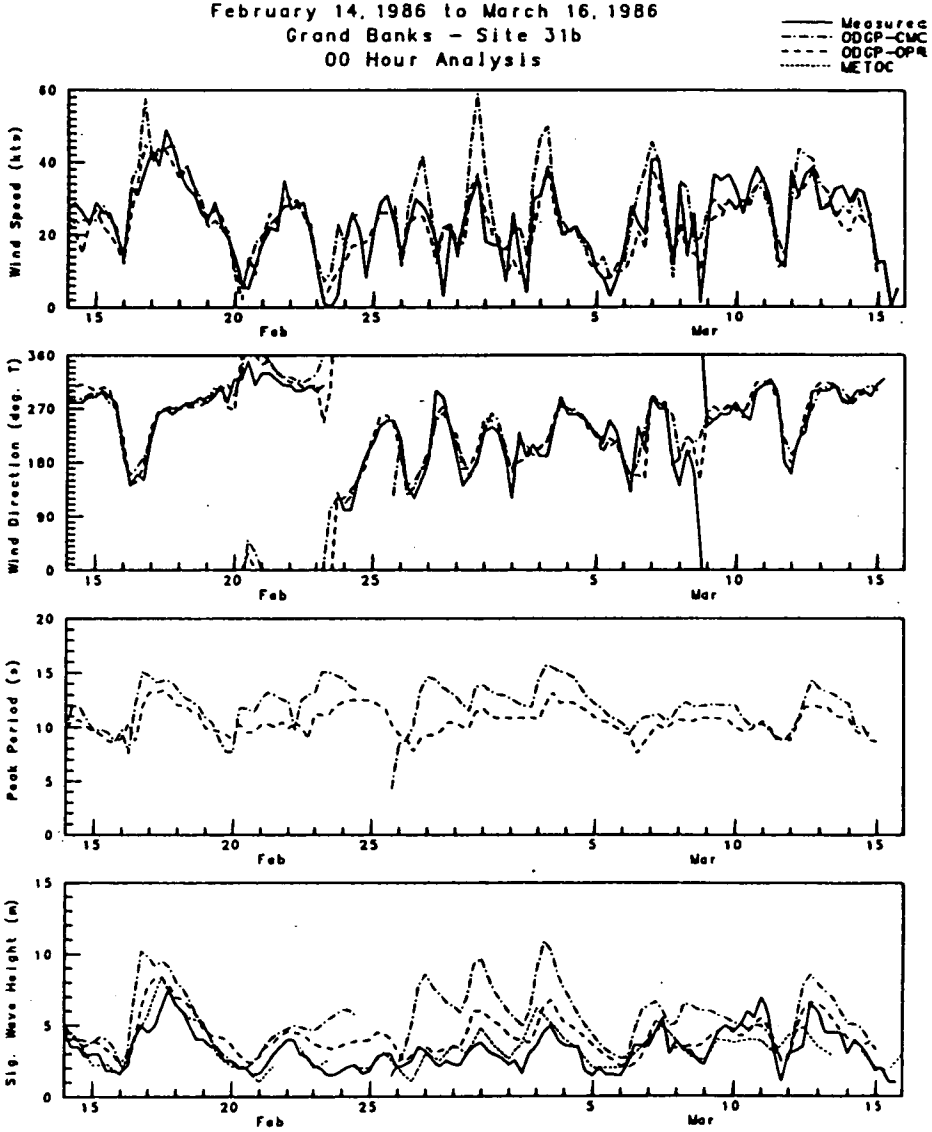

Measured Data vs. Model Predictions

January 15, 1986 to February 14, 1986
Grand Banks – Site 31b
12 Hour Forecast

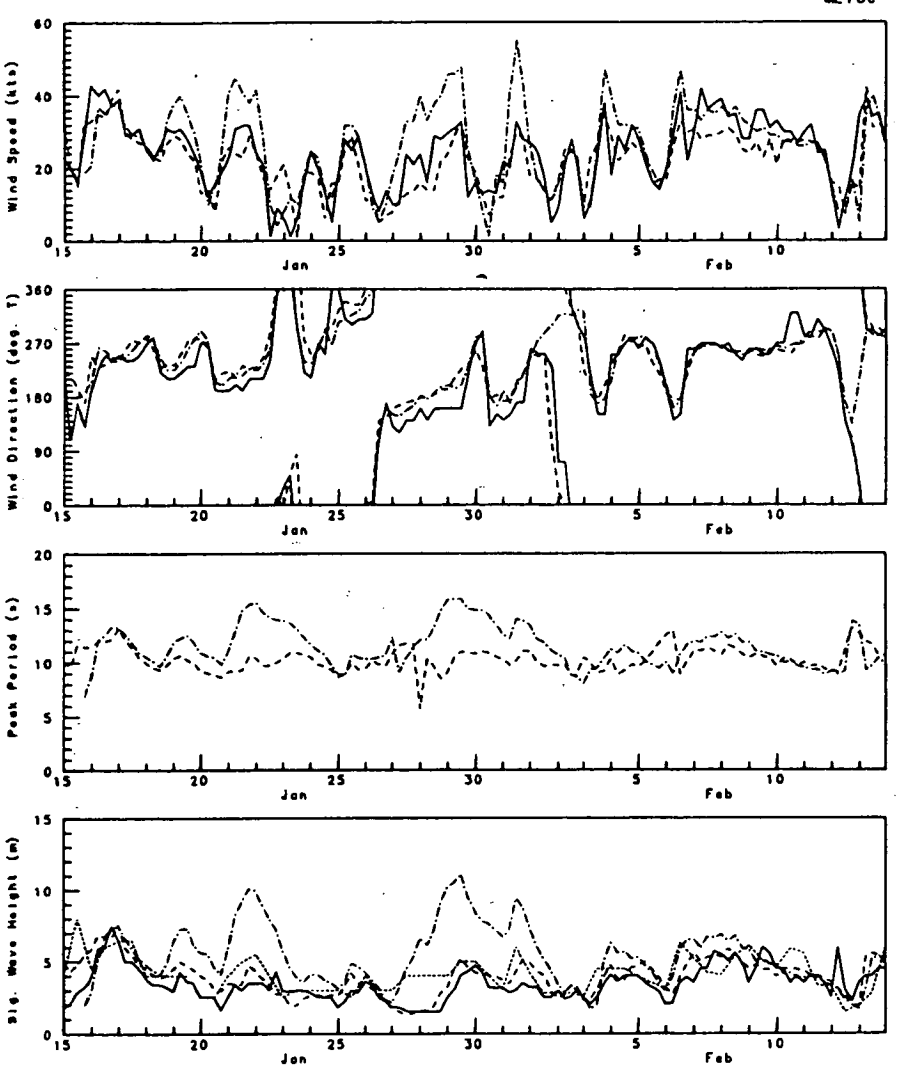

Measured Data vs. Model Predictions

February 14, 1986 to March 16, 1986
Grand Banks – Site 31b
12 Hour Forecast

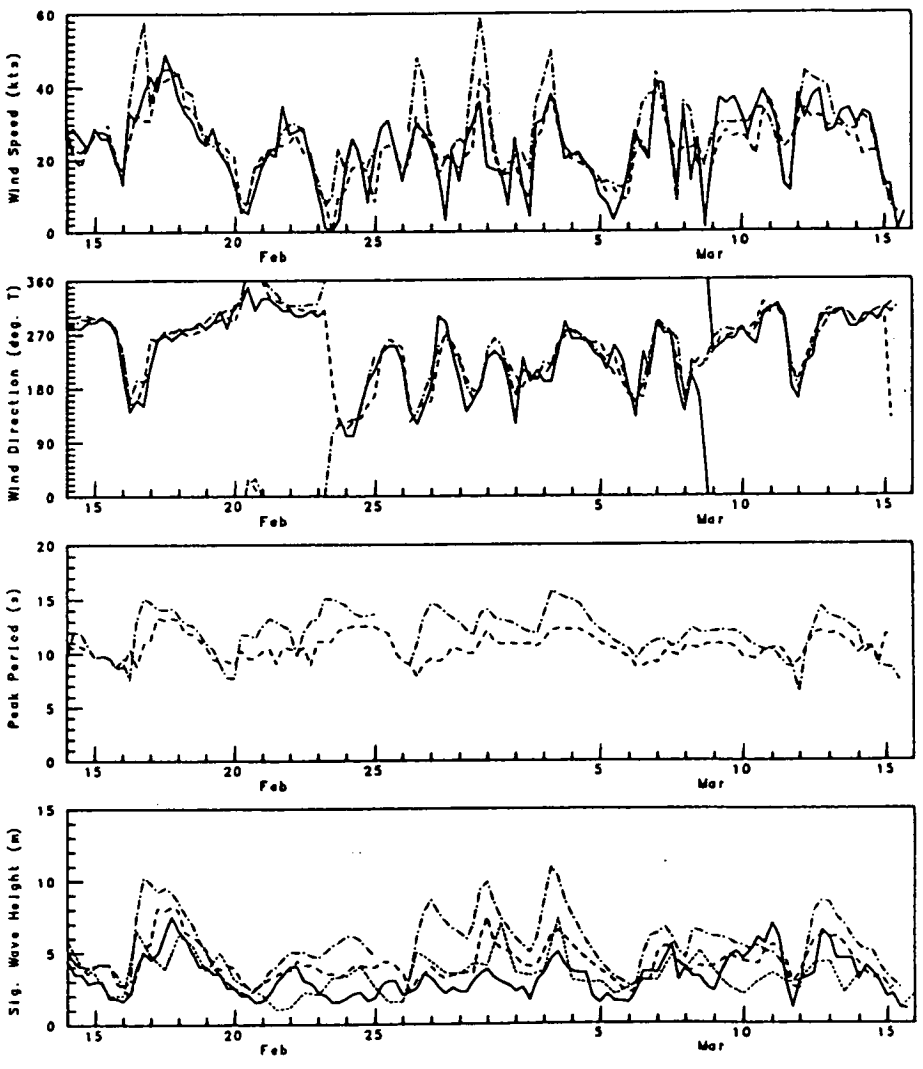

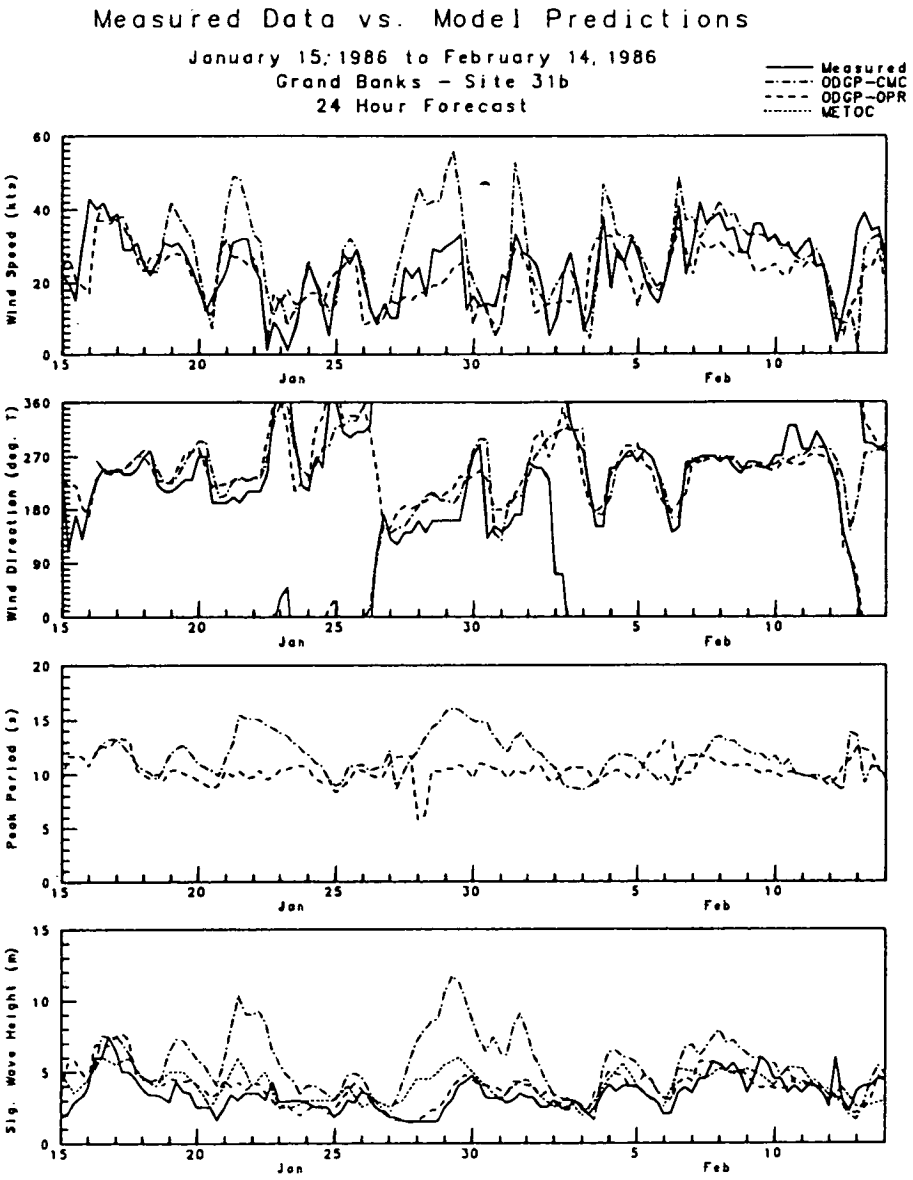
Measured Data vs. Model Predictions
January 15, 1986 to February 14, 1986
Grand Banks - Site 31b
24 Hour Forecast
Measured
ODGP-CMC
ODGP-OPR
METOC
Wind Speed (kts)
Wind Direction (deg. T)
Peak Period (s)
Sig. Wave Height (m)
Jan
Feb

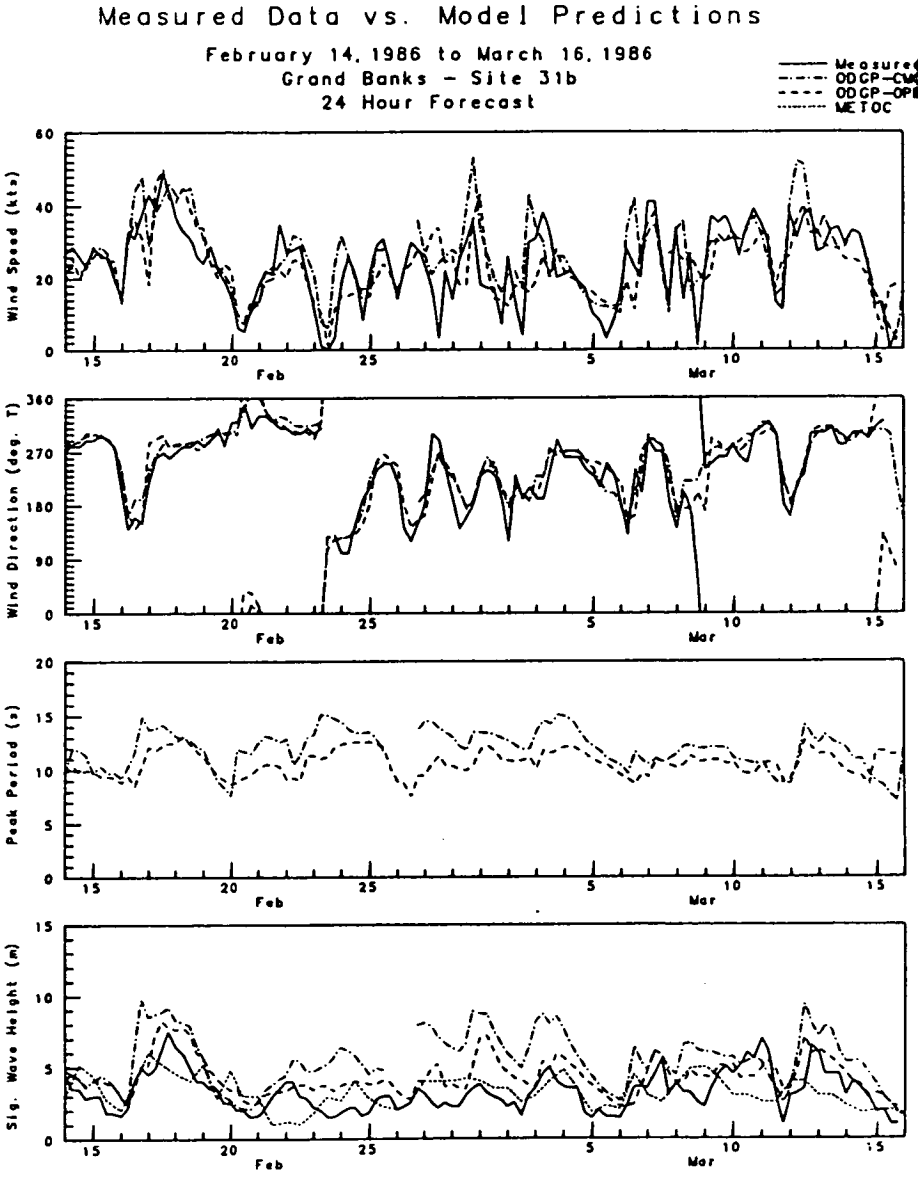
Measured Data vs. Model Predictions
February 14, 1986 to March 16, 1986
Grand Banks - Site 31b
24 Hour Forecast
Wind Speed (kts)
Wind Direction (deg. T)
Peak Period (s)
Sig. Wave Height (m)
Feb
Mar

Measured Data vs. Model Predictions

January 15, 1986 to February 14, 1986
Grand Banks – Site 31b
36 Hour Forecast

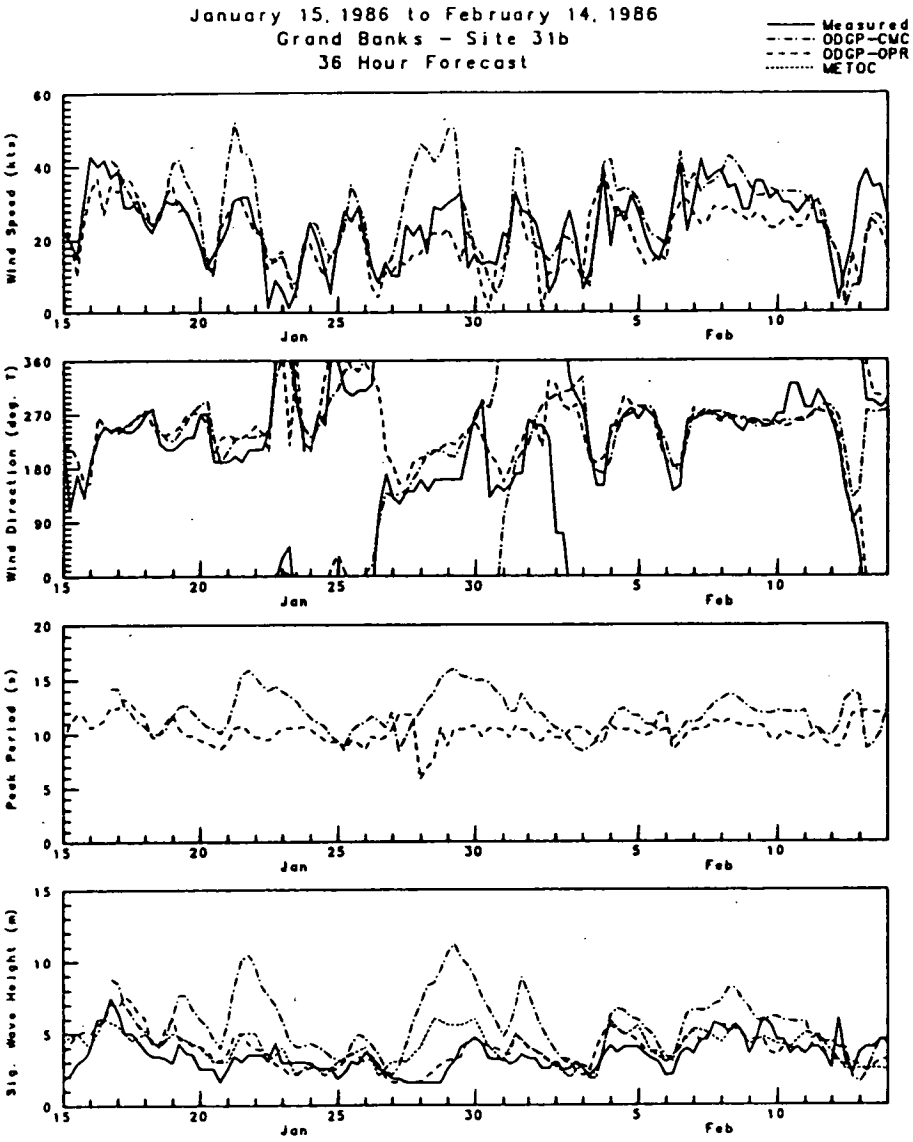

Measured Data vs. Model Predictions

February 14, 1986 to March 16, 1986
Grand Banks – Site 31b
36 Hour Forecast

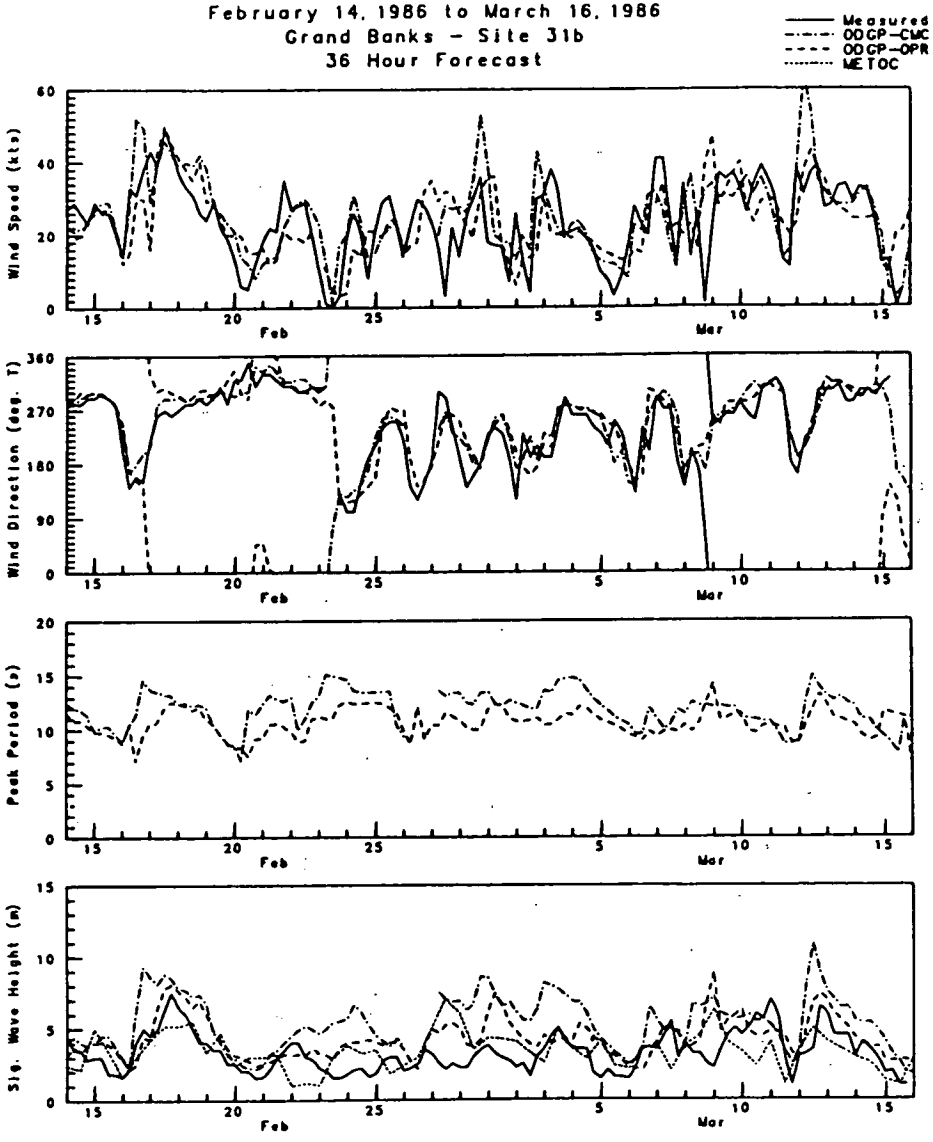

Measured Data vs. Model Predictions

January 15, 1986 to February 14, 1986
Grand Banks – Site 31b
48 Hour Forecast

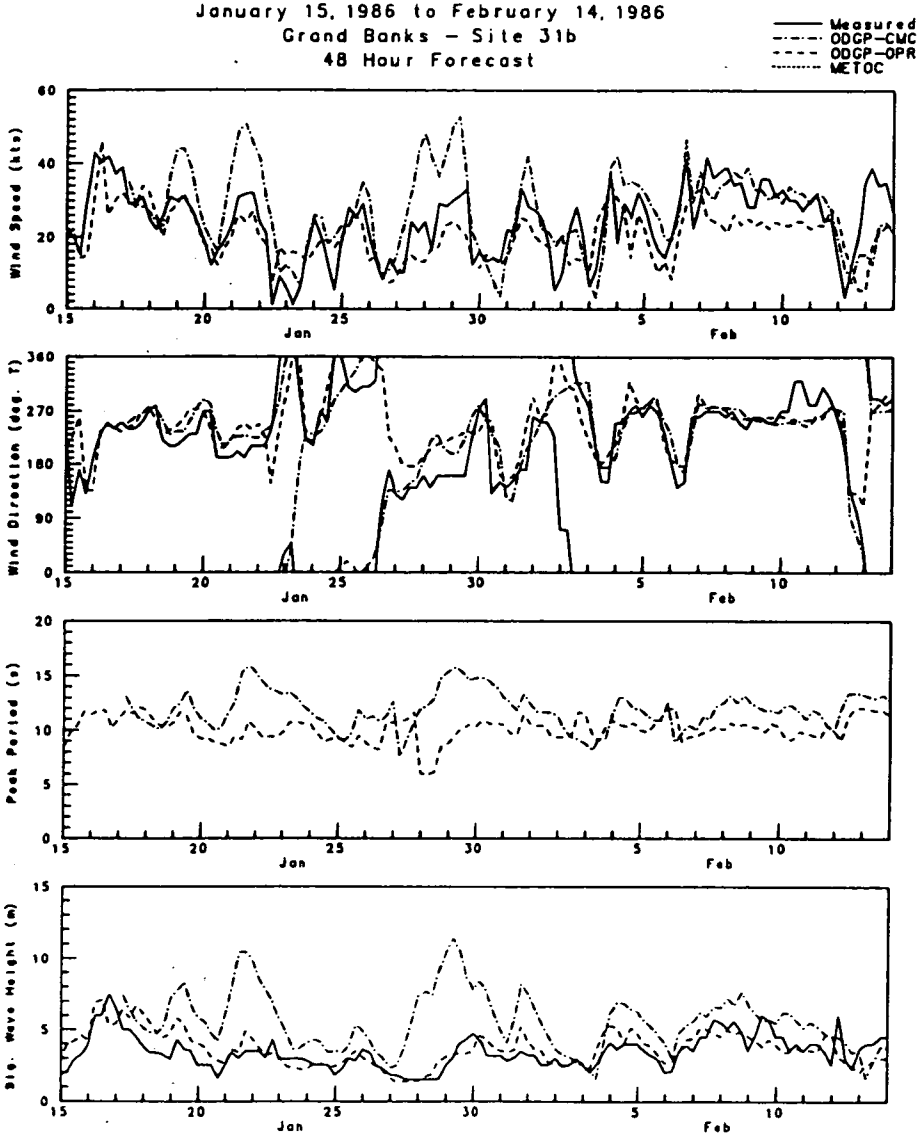

Measured Data vs. Model Predictions

February 14, 1986 to March 16, 1986
Grand Banks – Site 31b
48 Hour Forecast

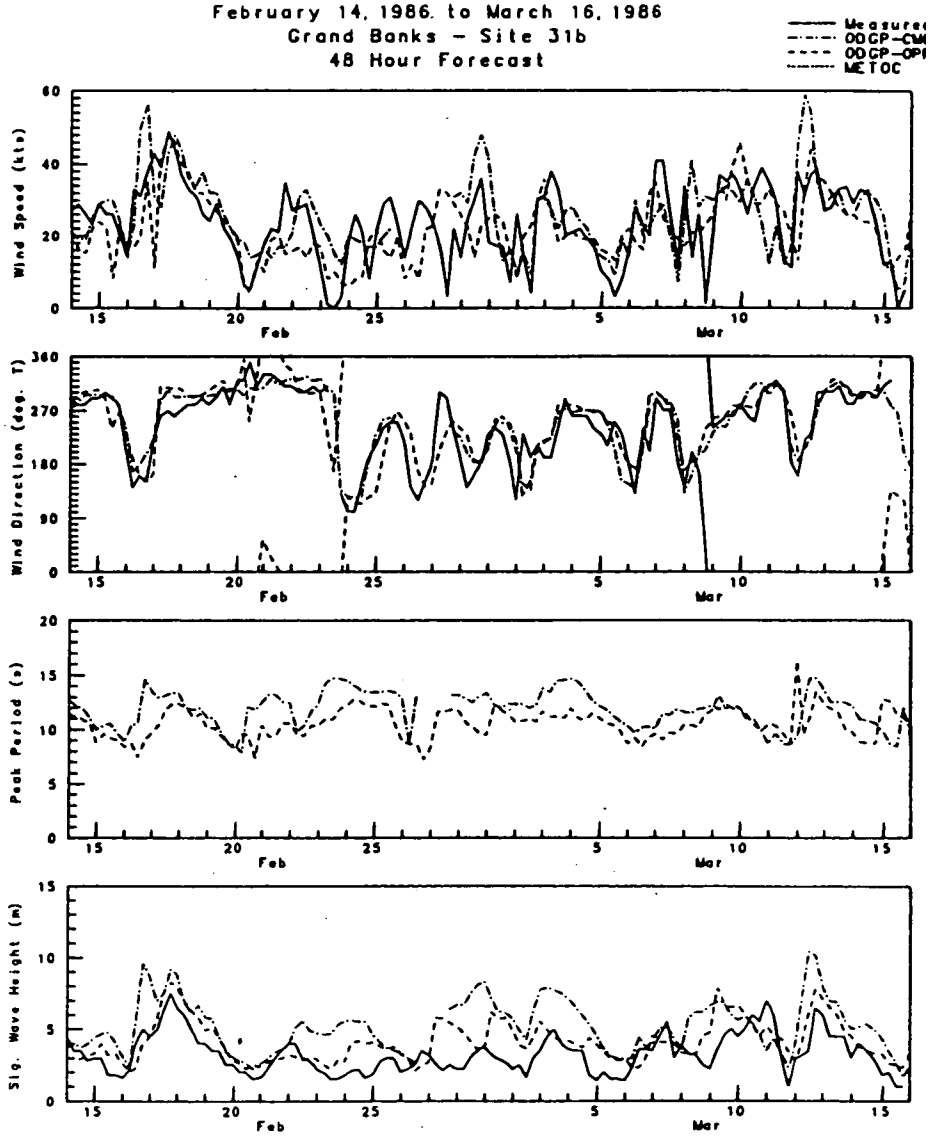

Measured Data vs. Model Predictions
January 15, 1986 to March 16, 1986
ODGP-CMC All Sites
00 Hour Analysis
Number of Points: 1268
Correlation Coeffecient: 0.713

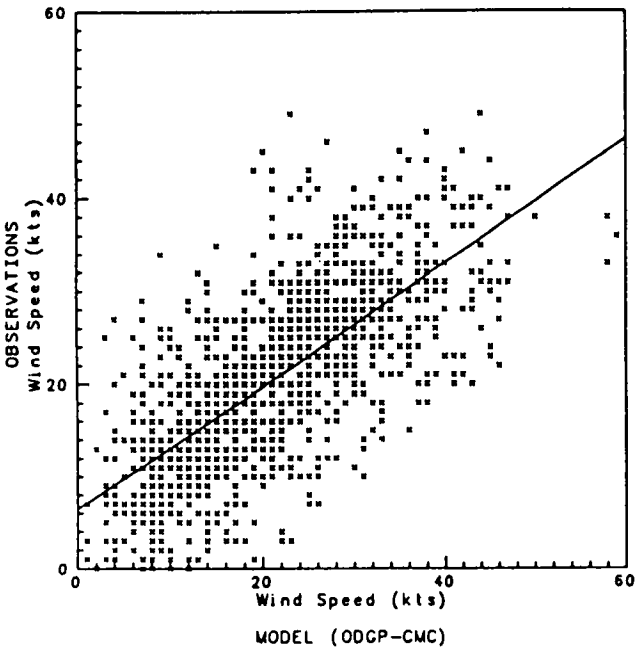

Measured Data vs. Model Predictions
January 15, 1986 to March 16, 1986
ODGP-OPR All Sites
00 Hour Analysis
Number of Points: 1312
Correlation Coeffecient: 0.805

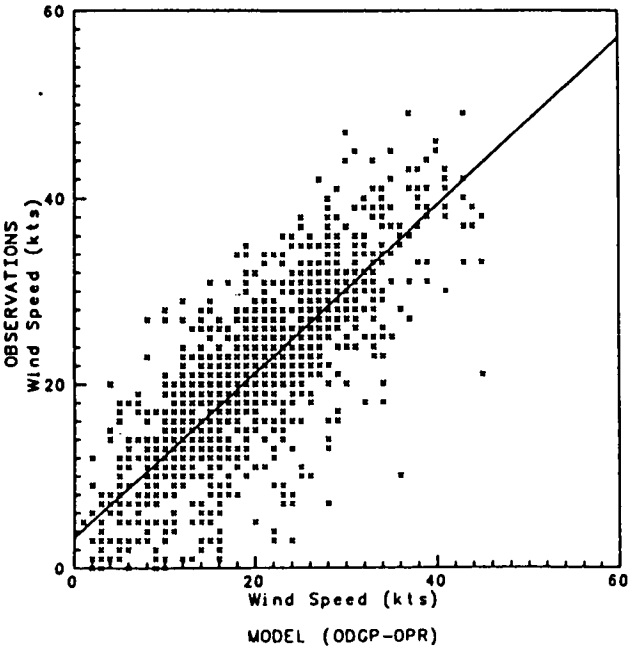

Measured Data vs. Model Predictions
January 15, 1986 to March 16, 1986
ODGP-CMC All Sites
00 Hour Analysis
Number of Points: 1299
Correlation Coeffecient: 0.641

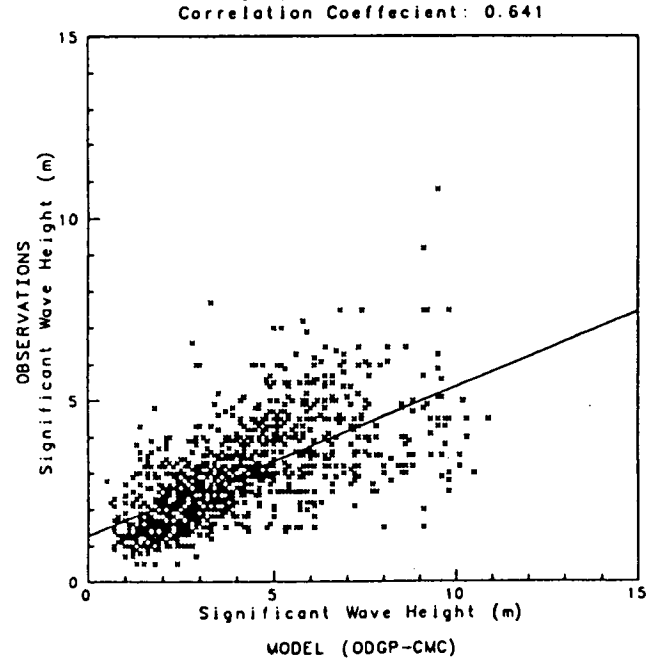

Measured Data vs. Model Predictions
January 15, 1986 to March 16, 1986
ODGP-OPR All Sites
00 Hour Analysis
Number of Points: 1344
Correlation Coeffecient: 0.813

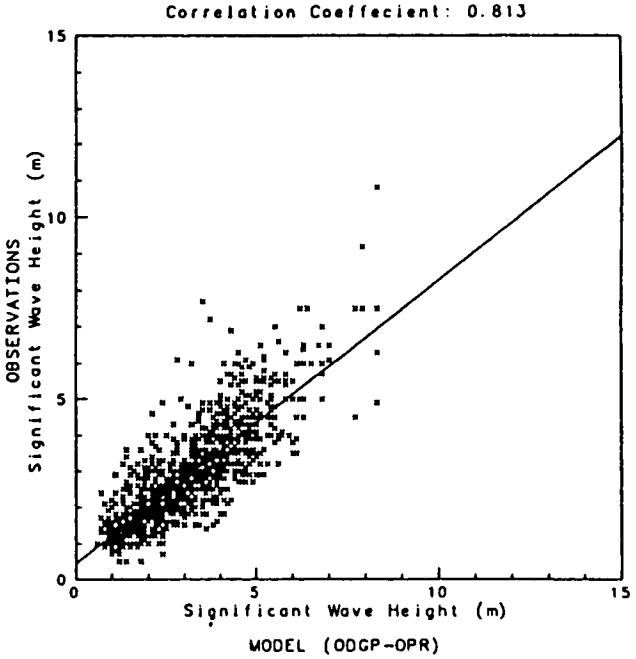

Measured Data vs. Model Predictions
January 15, 1986 to March 16, 1986
ODGP-CMC All Sites
12 Hour Forecast
Number of Points: 1270
Correlation Coeffecient: 0.699

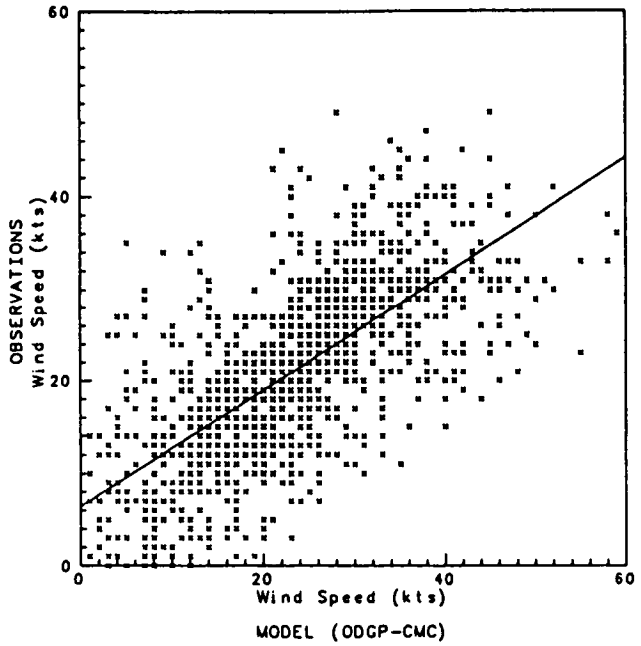

Measured Data vs. Model Predictions
January 15, 1986 to March 16, 1986
ODGP-OPR All Sites
12 Hour Forecast
Number of Points: 1312
Correlation Coeffecient: 0.689

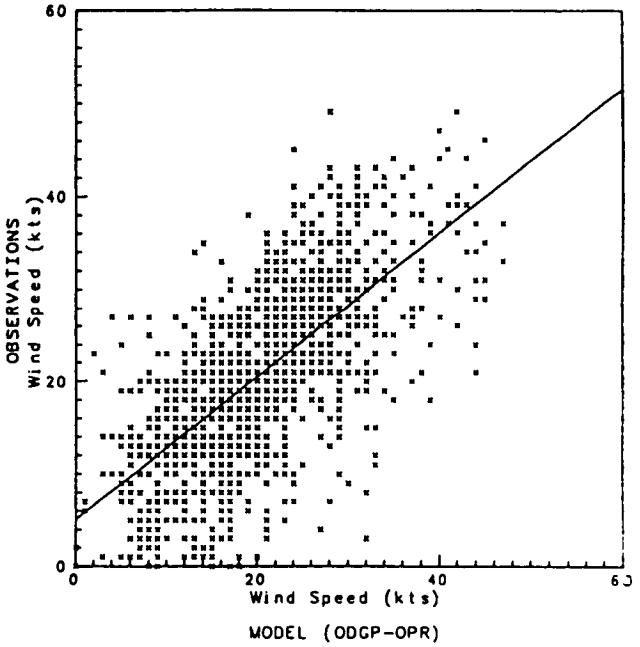

Measured Data vs. Model Predictions
January 15, 1986 to March 16, 1986
ODGP-CMC All Sites
12 Hour Forecast
Number of Points: 1299
Correlation Coeffecient: 0.650

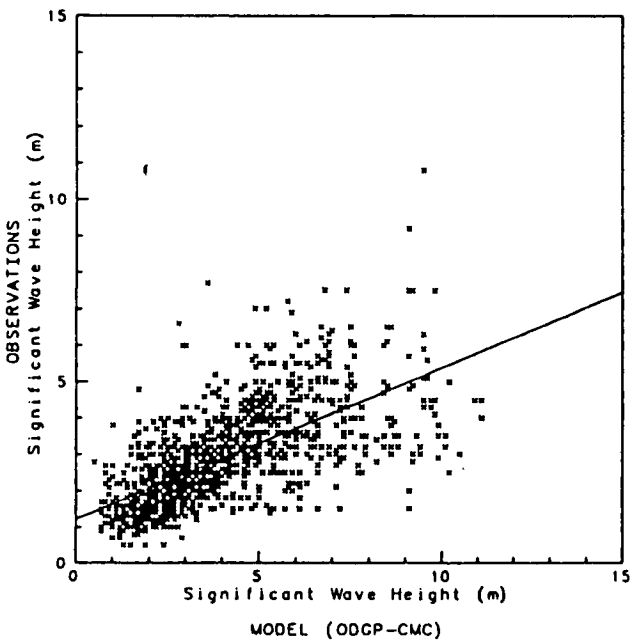

Measured Data vs. Model Predictions
January 15, 1986 to March 16, 1986
ODGP-OPR All Sites
12 Hour Forecast
Number of Points: 1344
Correlation Coeffecient: 0.792

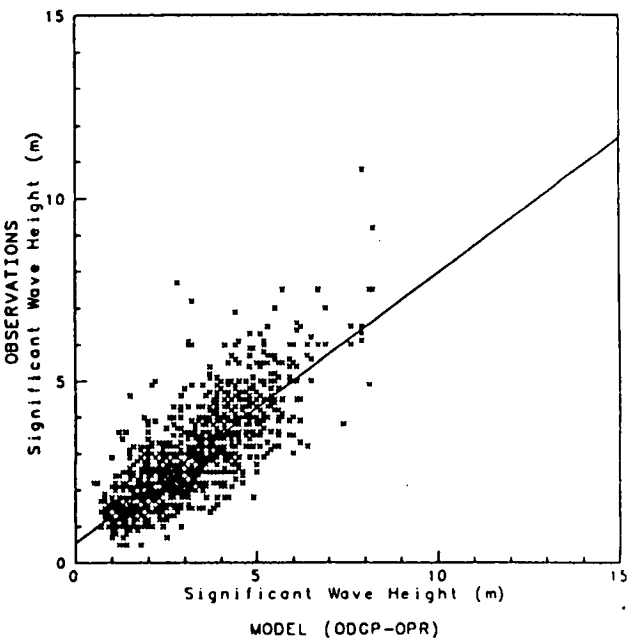

Measured Data vs. Model Predictions
January 15, 1986 to March 16, 1986
ODGP-CMC All Sites
24 Hour Forecast
Number of Points: 1268
Correlation Coeffecient: 0.674

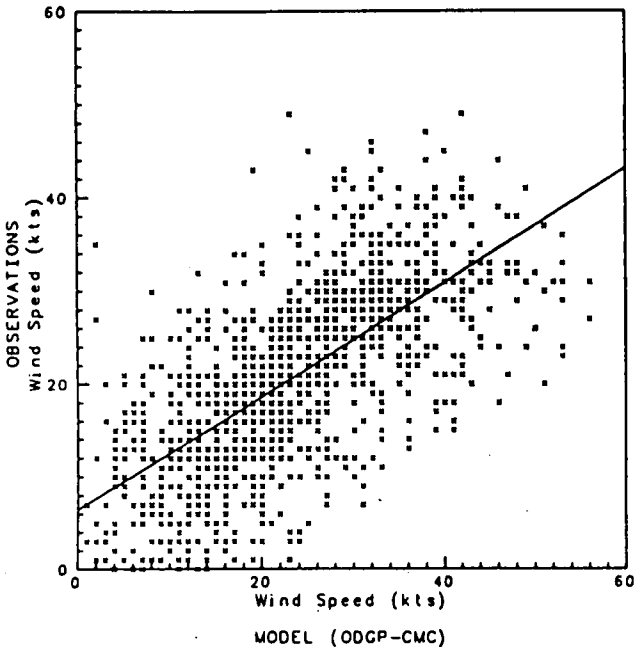

Measured Data vs. Model Predictions
January 15, 1986 to March 16, 1986
ODGP-OPR All Sites
24 Hour Forecast
Number of Points: 1312
Correlation Coeffecient: 0.618

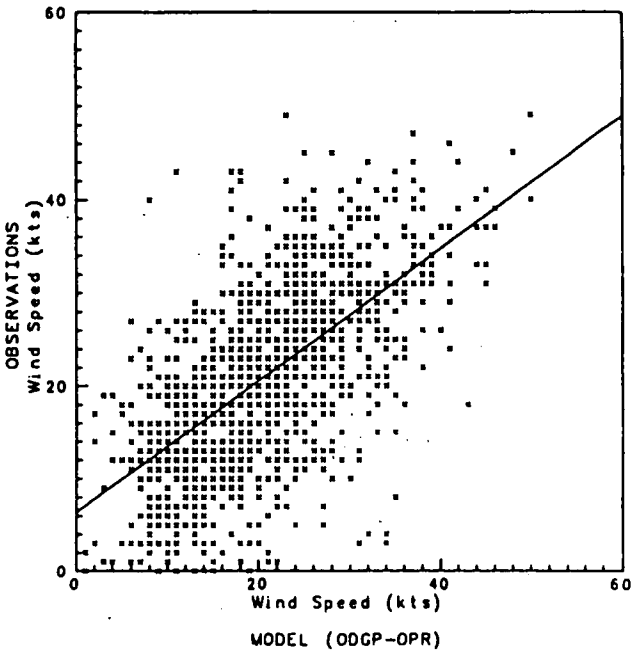

Measured Data vs. Model Predictions
January 15, 1986 to March 16, 1986
ODGP-CMC All Sites
24 Hour Forecast
Number of Points: 1295
Correlation Coeffecient: 0.659

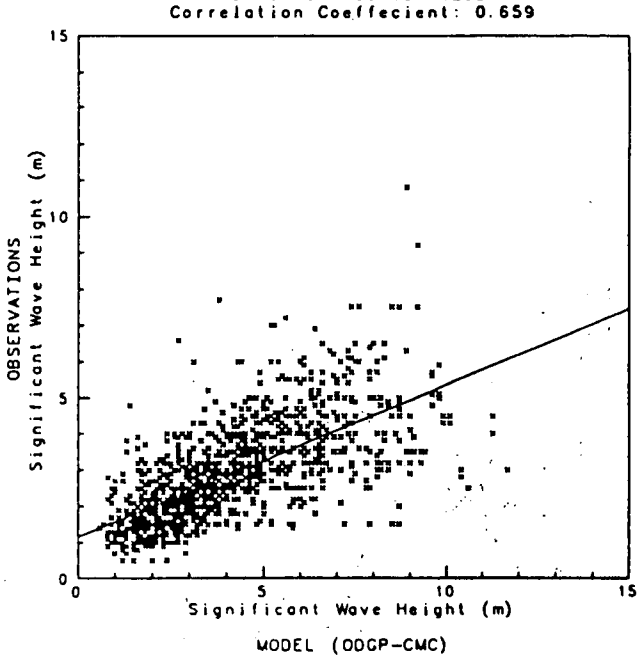

Measured Data vs. Model Predictions
January 15, 1986 to March 16, 1986
ODGP-OPR All Sites
24 Hour Forecast
Number of Points: 1344
Correlation Coeffecient: 0.764

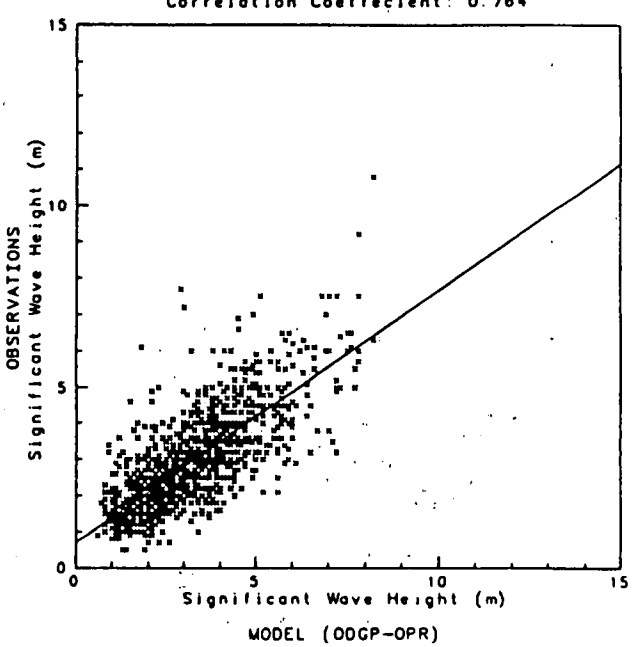

Measured Data vs. Model Predictions
January 15, 1986 to March 16, 1986
ODGP-CMC All Sites
36 Hour Forecast
Number of Points: 1260
Correlation Coeffecient: 0.604

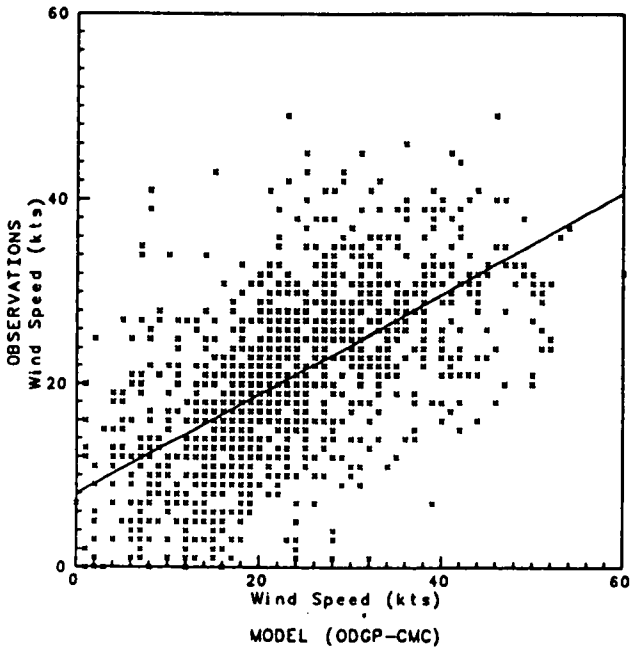

Measured Data vs. Model Predictions
January 15, 1986 to March 16, 1986
ODGP-OPR All Sites
36 Hour Forecast
Number of Points: 1312
Correlation Coeffecient: 0.576

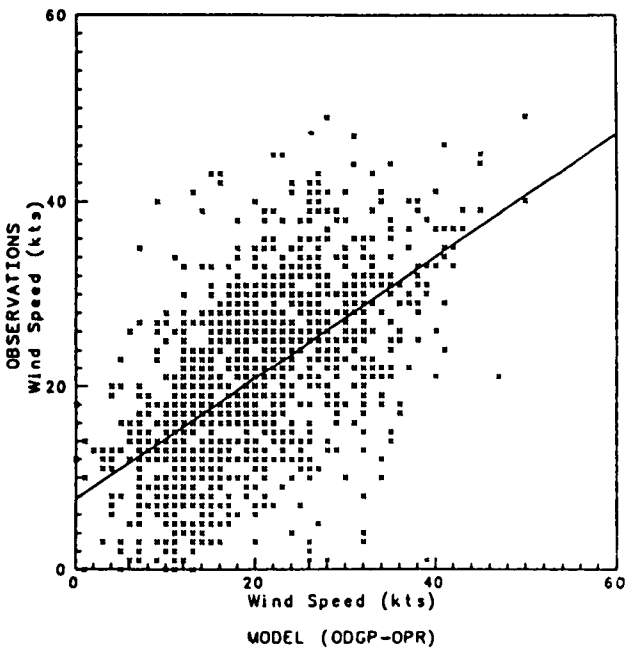

Measured Data vs. Model Predictions
January 15, 1986 to March 16, 1986
ODGP-CMC All Sites
36 Hour Forecast
Number of Points: 1285
Correlation Coeffecient: 0.660

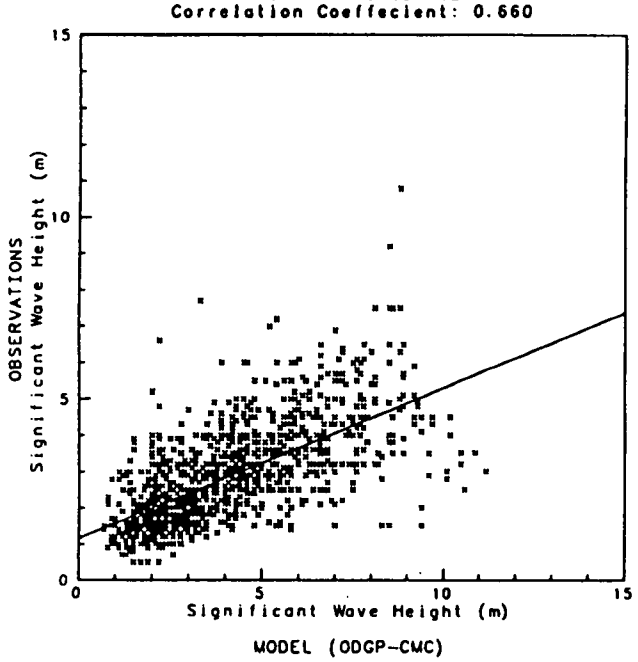

Measured Data vs. Model Predictions
January 15, 1986 to March 16, 1986
ODGP-OPR All Sites
36 Hour Forecast
Number of Points: 1344
Correlation Coeffecient: 0.720

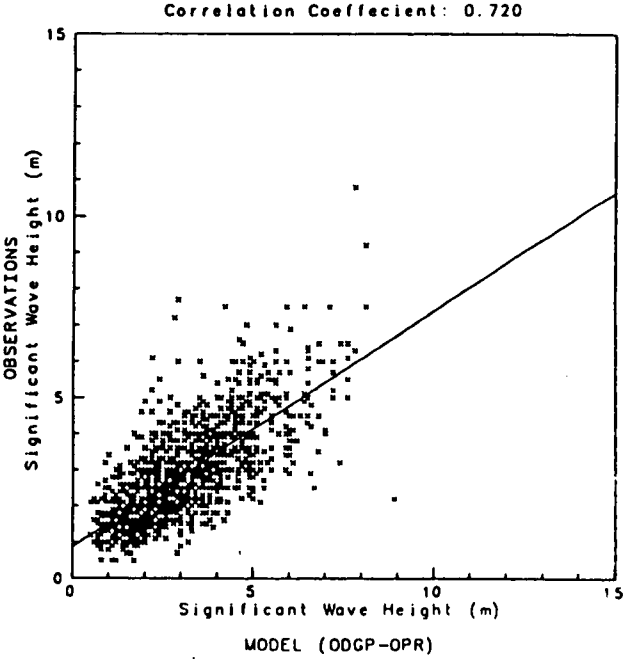

Measured Data vs. Model Predictions
January 15, 1986 to March 16, 1986
ODGP-CMC All Sites
48 Hour Forecast
Number of Points: 1228
Correlation Coeffecient: 0.564

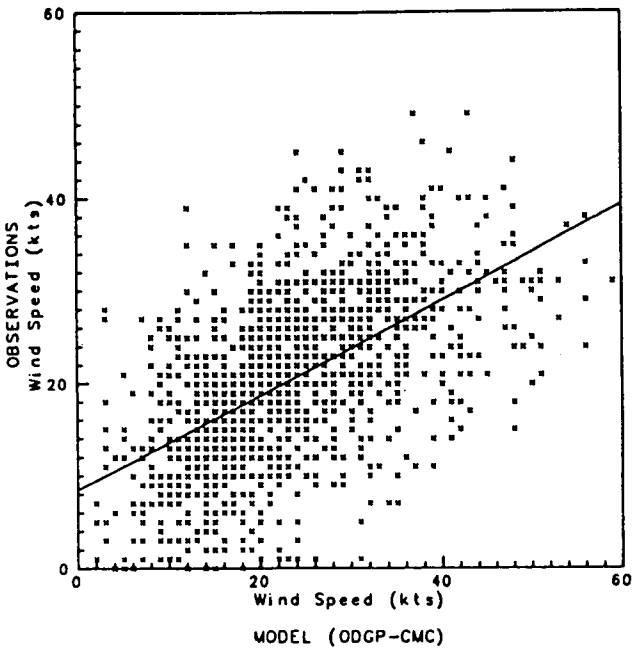

Measured Data vs. Model Predictions
January 15, 1986 to March 16, 1986
ODGP-OPR All Sites
48 Hour Forecast
Number of Points: 1312
Correlation Coeffecient: 0.482

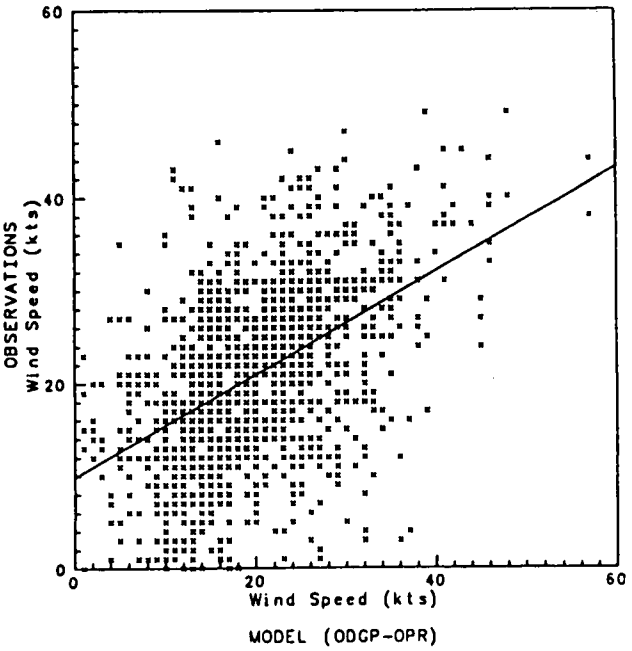

Measured Data vs. Model Predictions
January 15, 1986 to March 16, 1986
ODGP-CMC All Sites
48 Hour Forecast
Number of Points: 1275
Correlation Coeffecient: 0.637

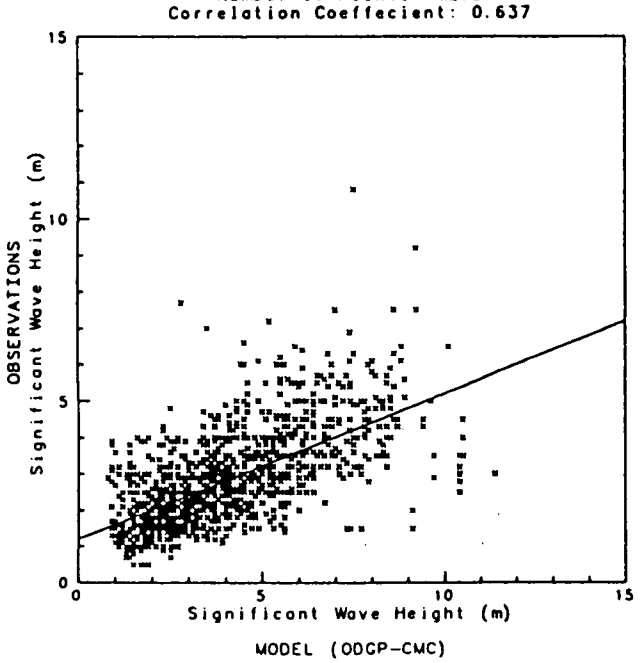

Measured Data vs. Model Predictions
January 15, 1986 to March 16, 1986
ODGP-OPR All Sites
48 Hour Forecast
Number of Points: 1344
Correlation Coeffecient: 0.688

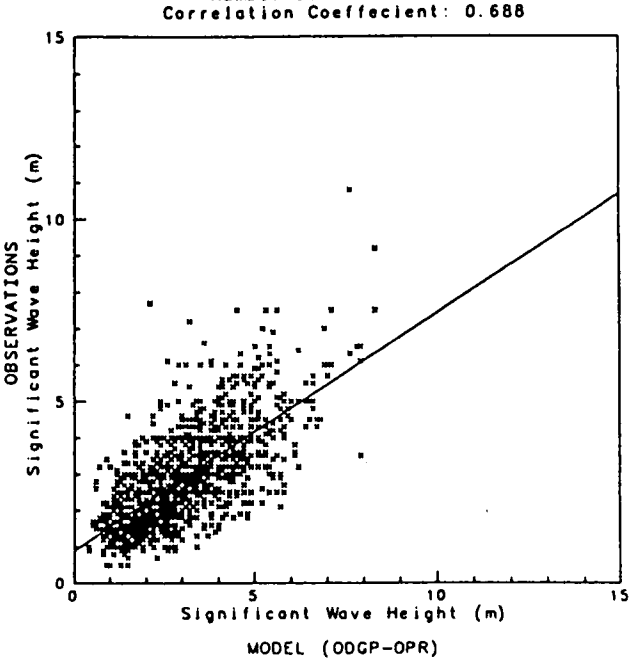

Measured Data vs. Model Predictions
January 15, 1986 to March 16, 1986
ODGP-CMC All Sites
00 Hour Analysis
Number of Points: 762
Correlation Coeffecient: 0.567

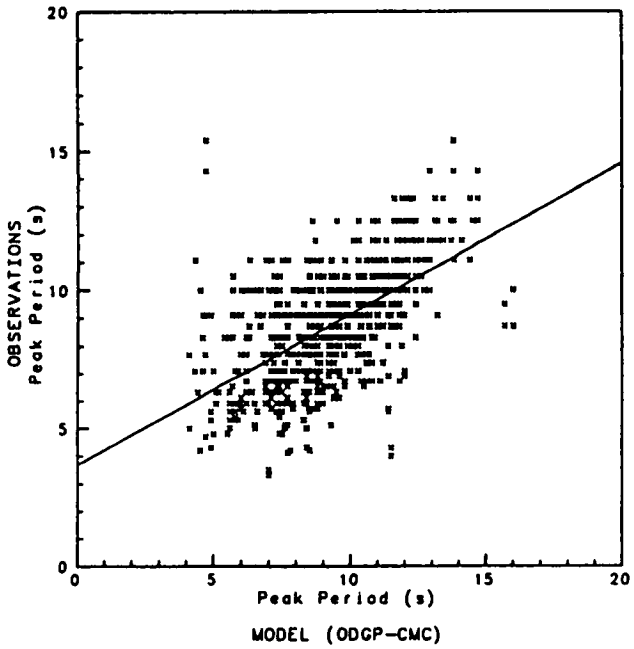

Measured Data vs. Model Predictions
January 15, 1986 to March 16, 1986
ODGP-CMC All Sites
12 Hour Forecast
Number of Points: 762
Correlation Coeffecient: 0.588

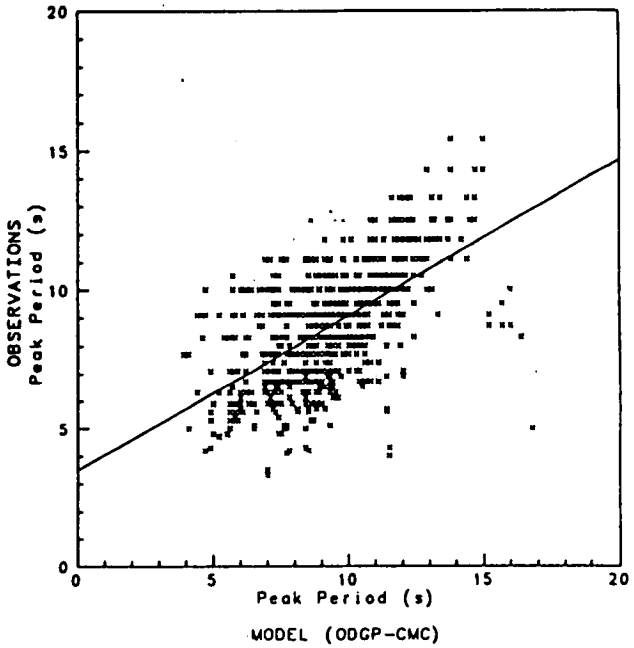

ODGP-OPR All Sites
00 Hour Analysis
Number of Points: 787
Correlation Coeffecient: 0.545

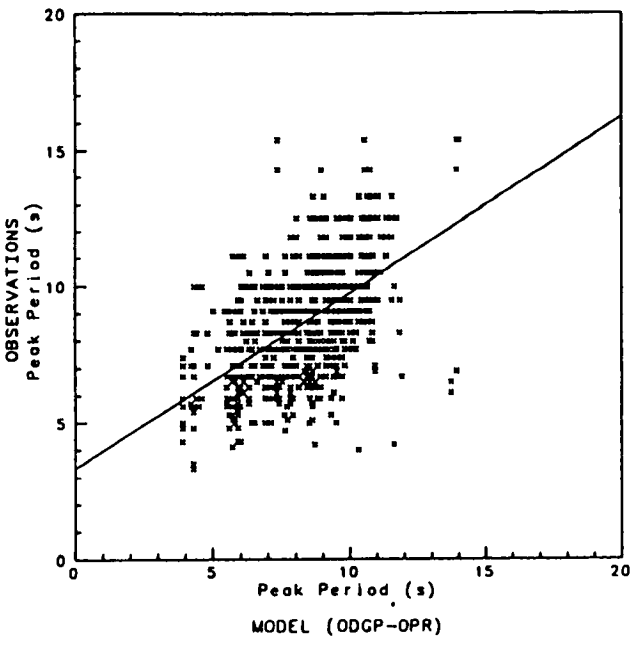

ODGP-OPR All Sites
12 Hour Forecast
Number of Points: 787
Correlation Coeffecient: 0.551

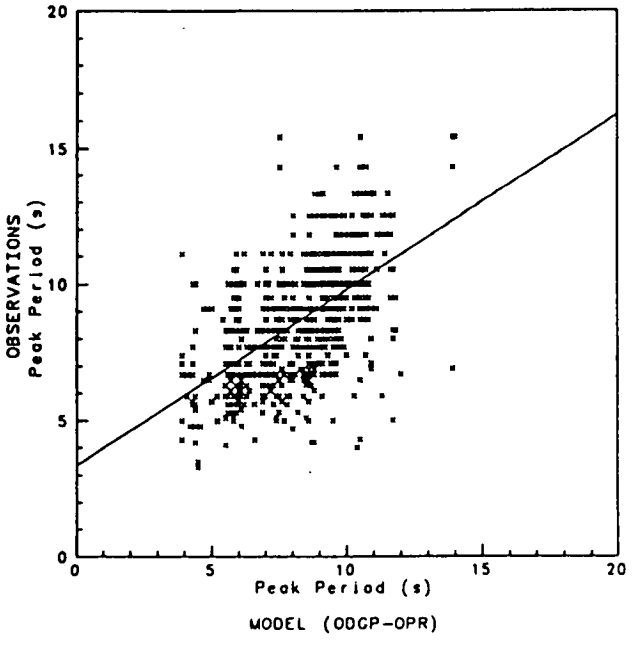

Measured Data vs. Model Predictions

January 15, 1986 to March 16, 1986

ODGP-CMC All Sites

24 Hour Forecast

Number of Points: 760

Correlation Coeffecient: 0.568

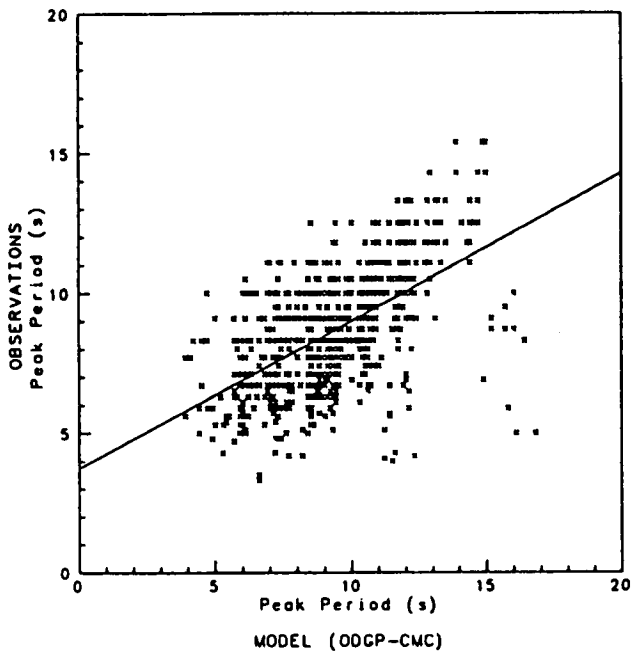

Measured Data vs. Model Predictions

January 15, 1986 to March 16, 1986

ODGP-CMC All Sites

36 Hour Forecast

Number of Points: 754

Correlation Coeffecient: 0.542

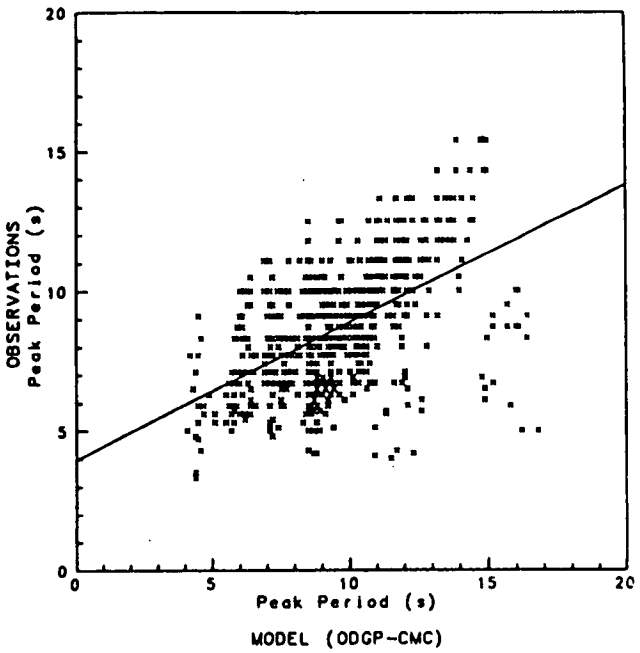

ODGP-OPR All Sites

24 Hour Forecast

Number of Points: 787

Correlation Coeffecient: 0.560

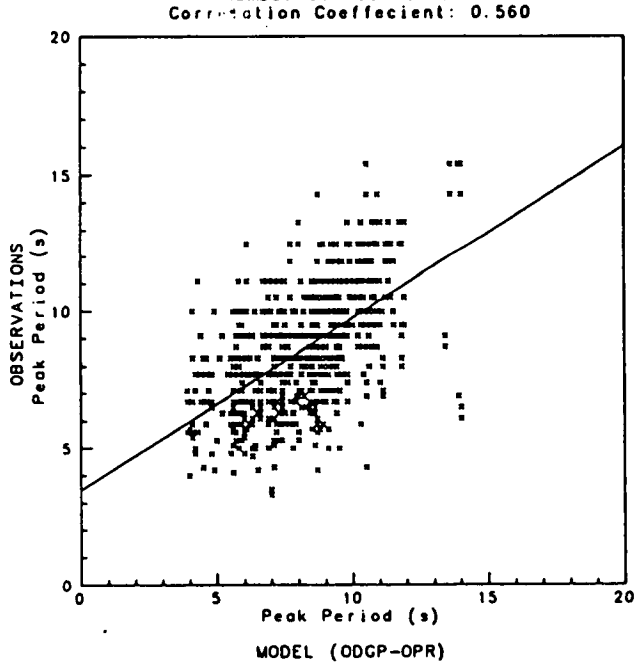

ODGP-OPR All Sites

36 Hour Forecast

Number of Points: 787

Correlation Coeffecient: 0.489

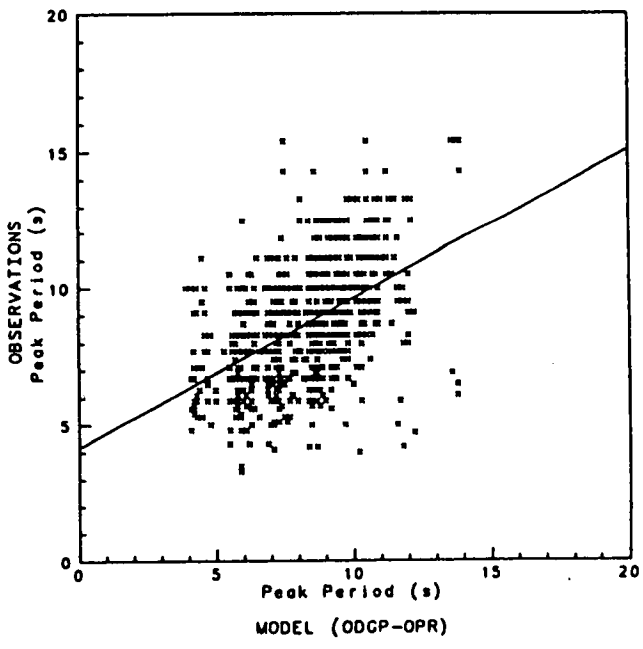

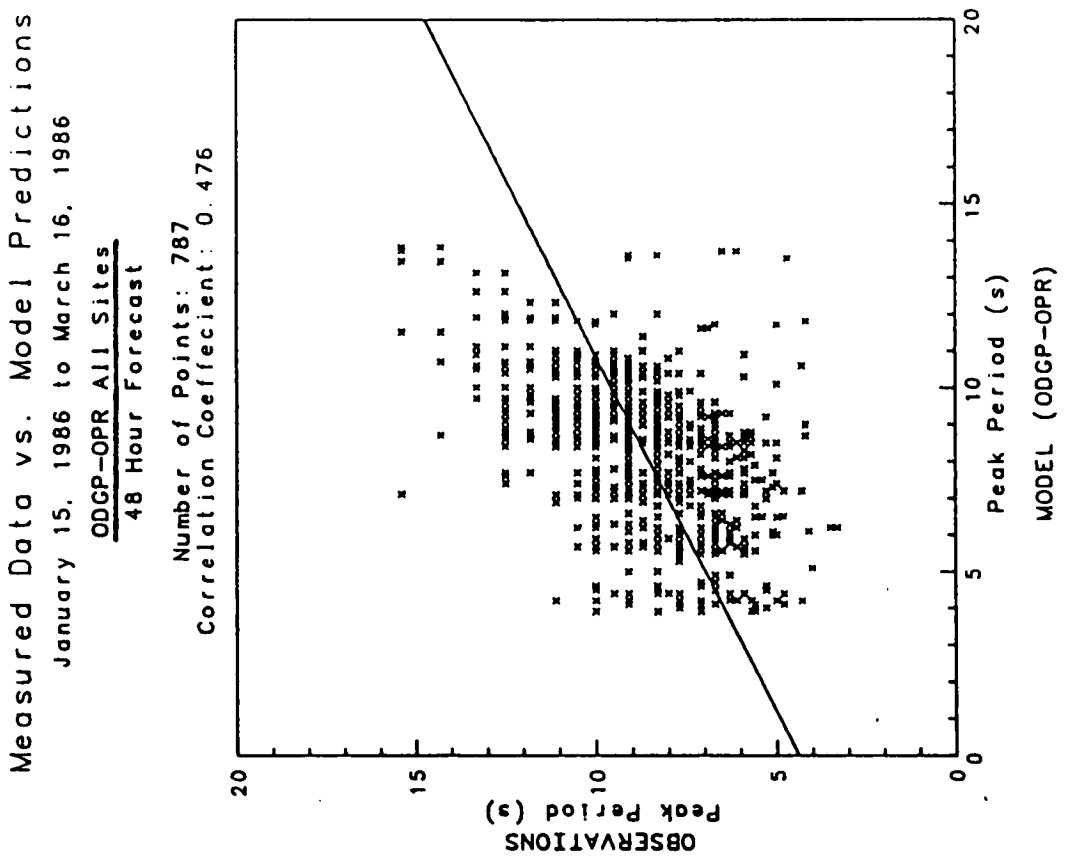
Measured Data vs. Model Predictions
January 15, 1986 to March 16, 1986
ODGP-OPR All Sites
48 Hour Forecast
Number of Points: 787
Correlation Coeffecient: 0.476
OBSERVATIONS
Peak Period (s)
MODEL (ODGP-OPR)
Peak Period (s)
0
5
10
15
20

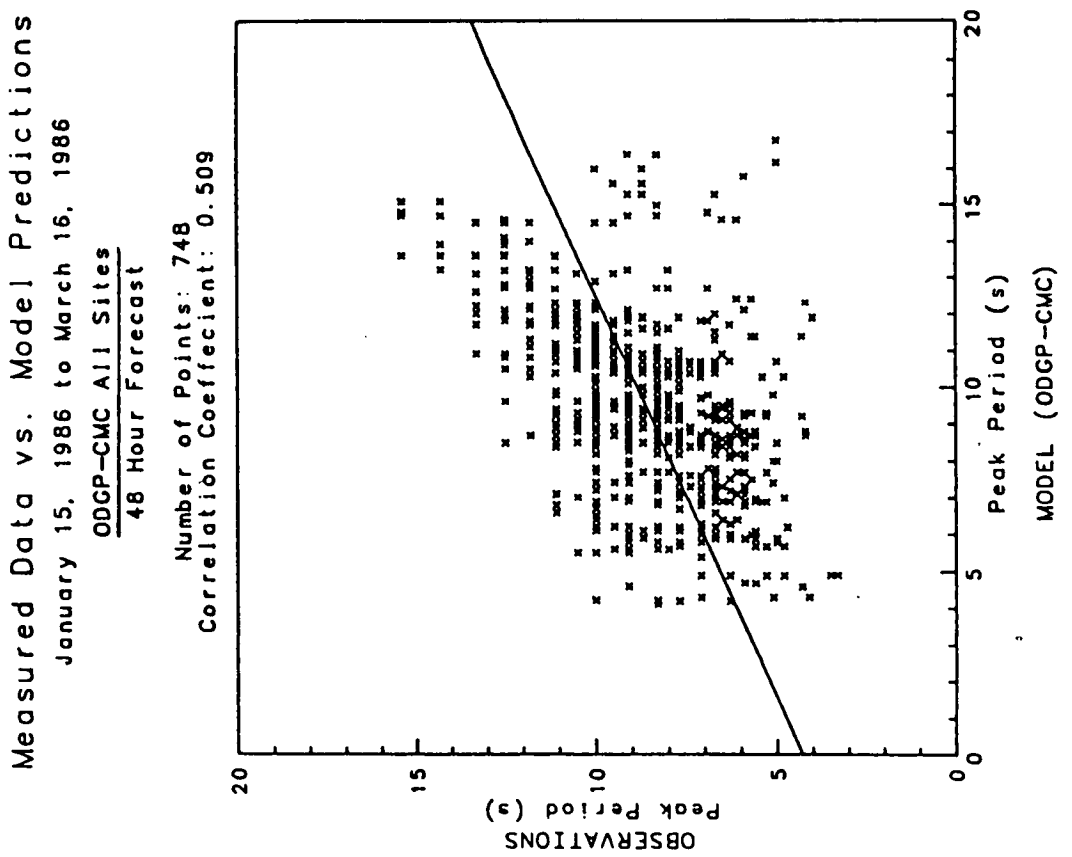
Measured Data vs. Model Predictions
January 15, 1986 to March 16, 1986
ODGP-CMC All Sites
48 Hour Forecast
Number of Points: 748
Correlation Coeffecient: 0.509
OBSERVATIONS
Peak Period (s)
MODEL (ODGP-CMC)
Peak Period (s)
0
5
10
15
20

Measured Data vs. Model Predictions

January 15, 1986 to March 16, 1986

METOC All Sites

00 Hour Analysis

Number of Points: 537
Correlation Coeffecient: 0.830

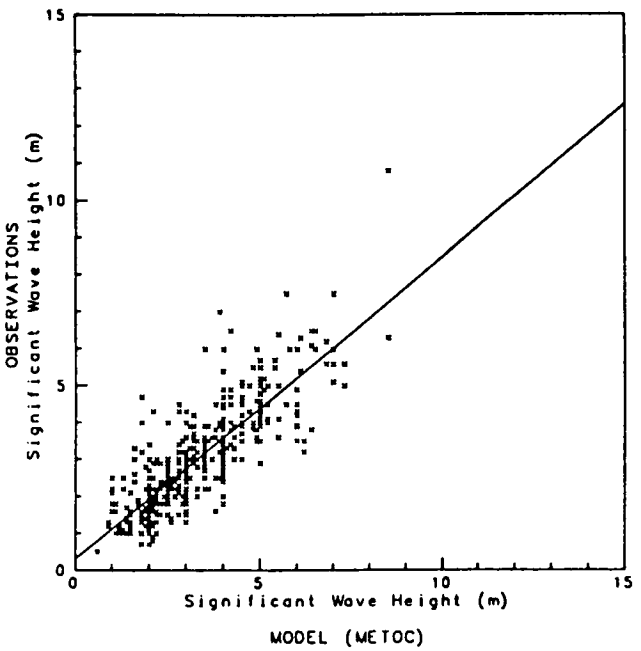

Measured Data vs. Model Predictions

January 15, 1986 to March 16, 1986

METOC All Sites

12 Hour Forecast

Number of Points: 543
Correlation Coeffecient: 0.616

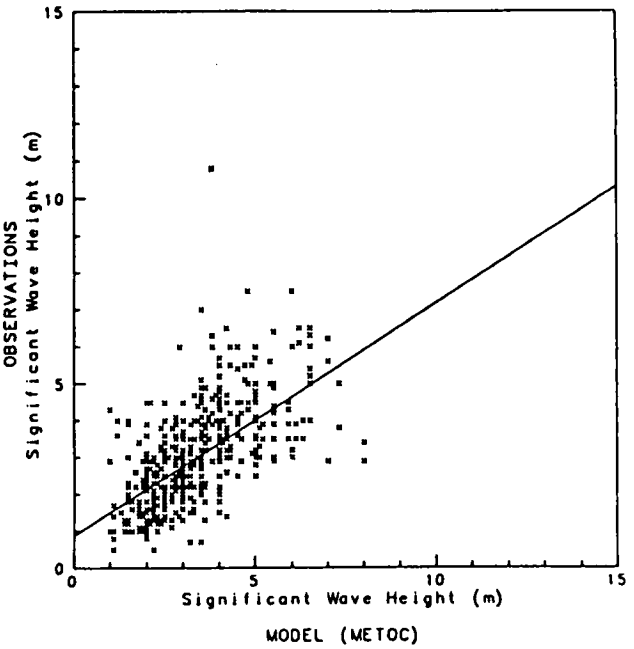

Measured Data vs. Model Predictions

January 15, 1986 to March 16, 1986

METOC All Sites

24 Hour Forecast

Number of Points: 553
Correlation Coeffecient: 0.624

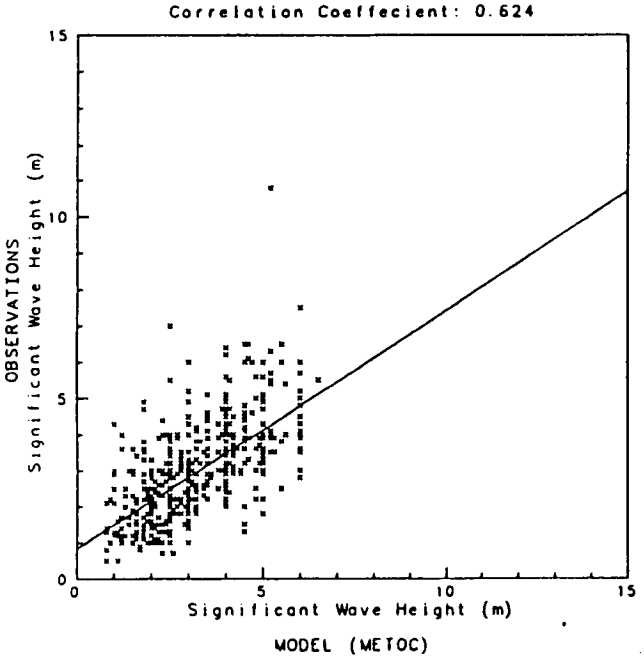

Measured Data vs. Model Predictions

January 15, 1986 to March 16, 1986

METOC All Sites

36 Hour Forecast

Number of Points: 553
Correlation Coeffecient: 0.555

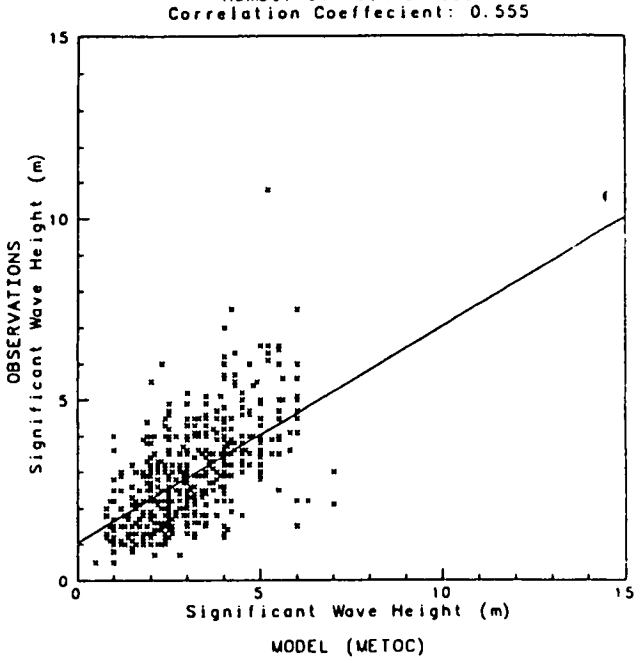

APPENDIX D

SHALLOW WATER MODEL RESULTS

- TIME SERIES PLOTS
- SCATTER DIAGRAMS & REGRESSION ANALYSIS

Measured Data vs. ODGP–CMC predictions

January 15, 1986 to February 14, 1986
Site 41 (100 m) – Shallow Water Model
00 Hour Analysis

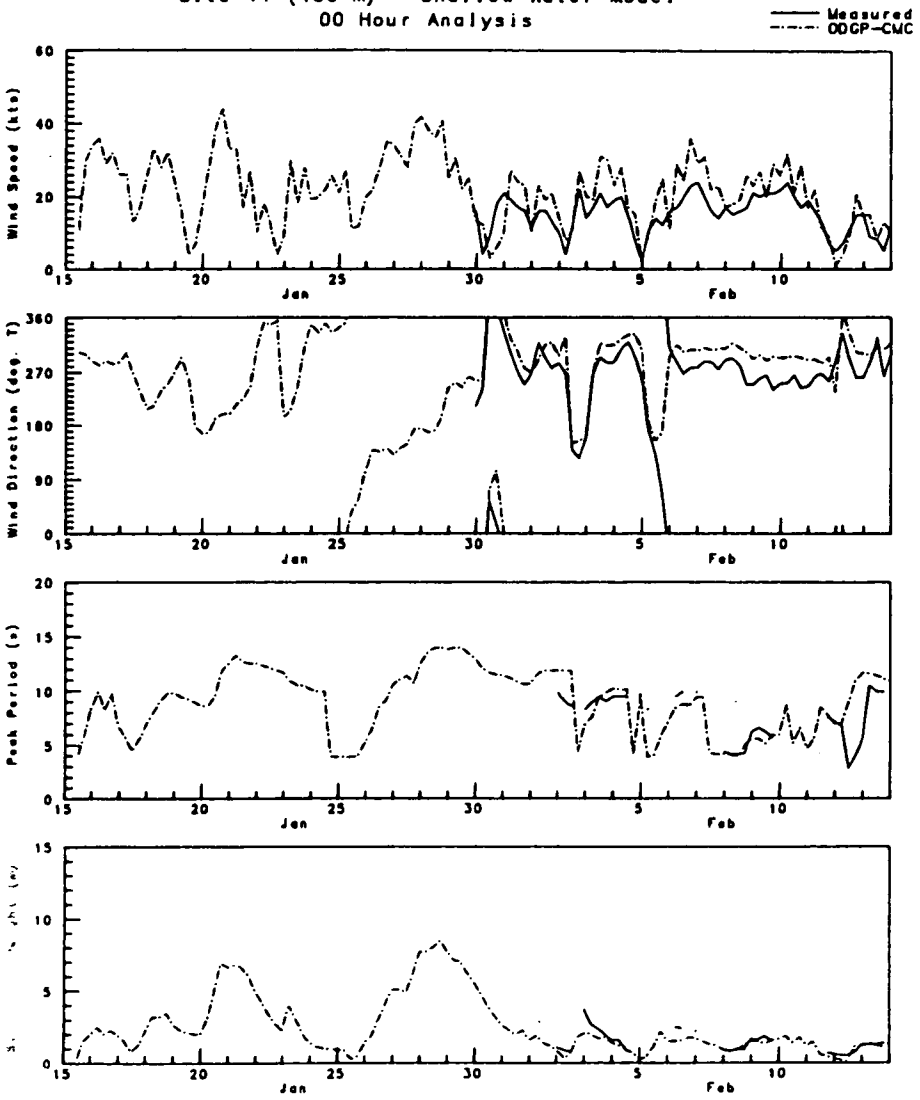

Measured Data vs. ODGP–CMC predictions

February 14, 1986 to March 16, 1986
Site 41 (100 m) – Shallow Water Model
00 Hour Analysis

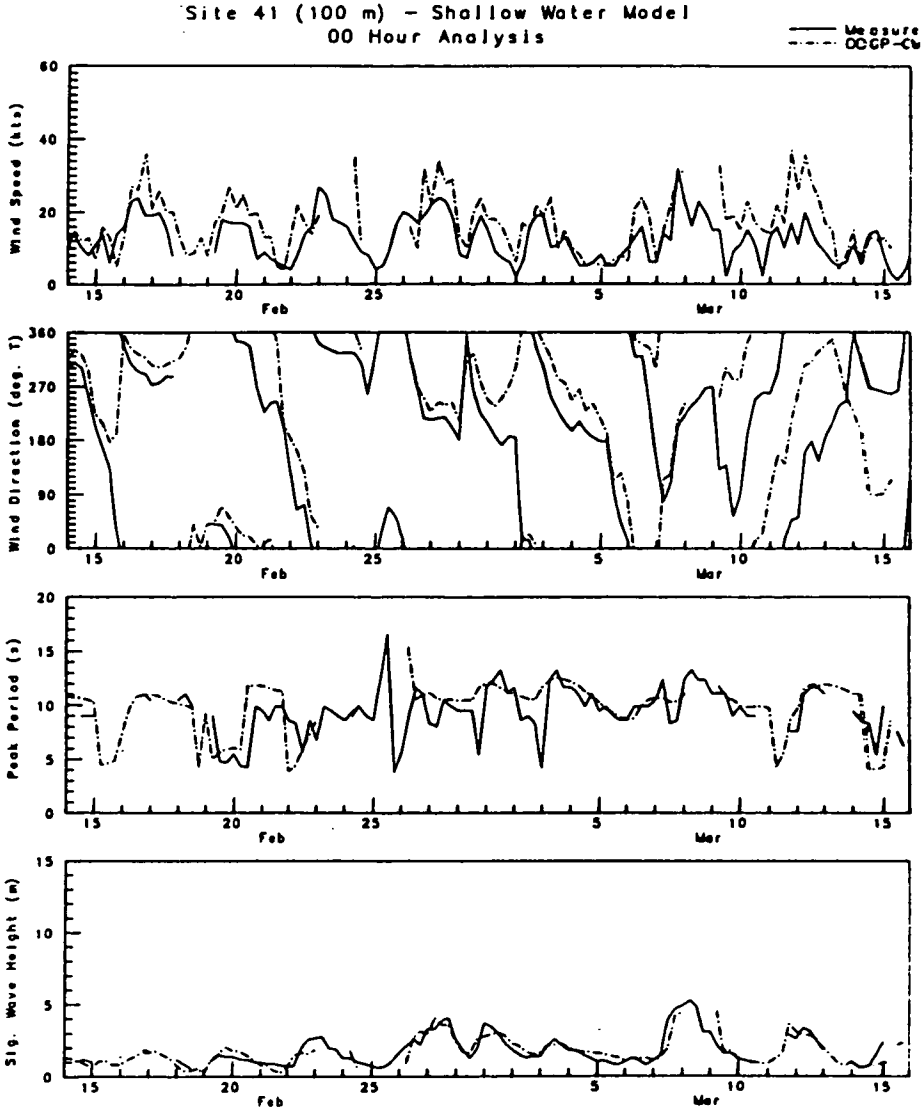

Measured Data vs. ODGP–CMC predictions

January 15, 1986 to February 14, 1986
Site 42 (50 m) – Shallow Water Model
00 Hour Analysis

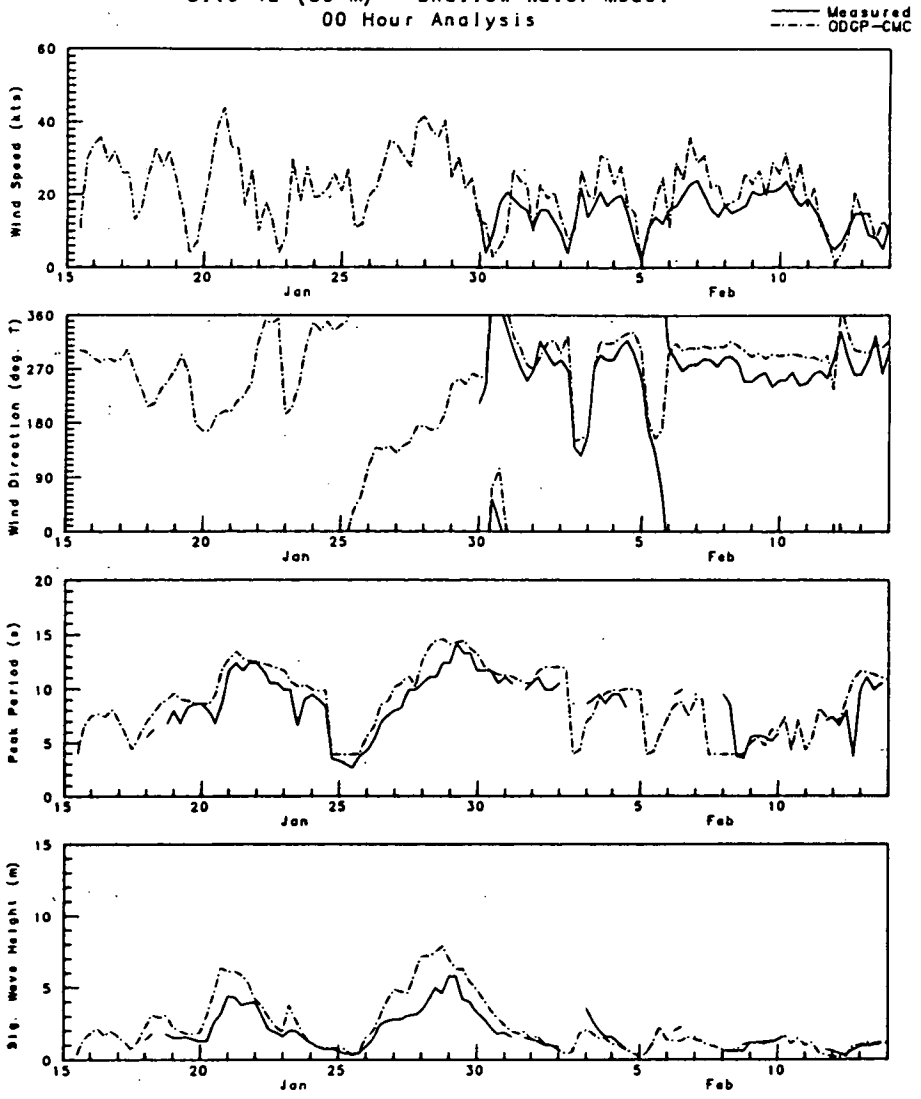

Measured Data vs. ODGP–CMC predictions

February 14, 1986 to March 16, 1986
Site 42 (50 m) – Shallow Water Model
00 Hour Analysis

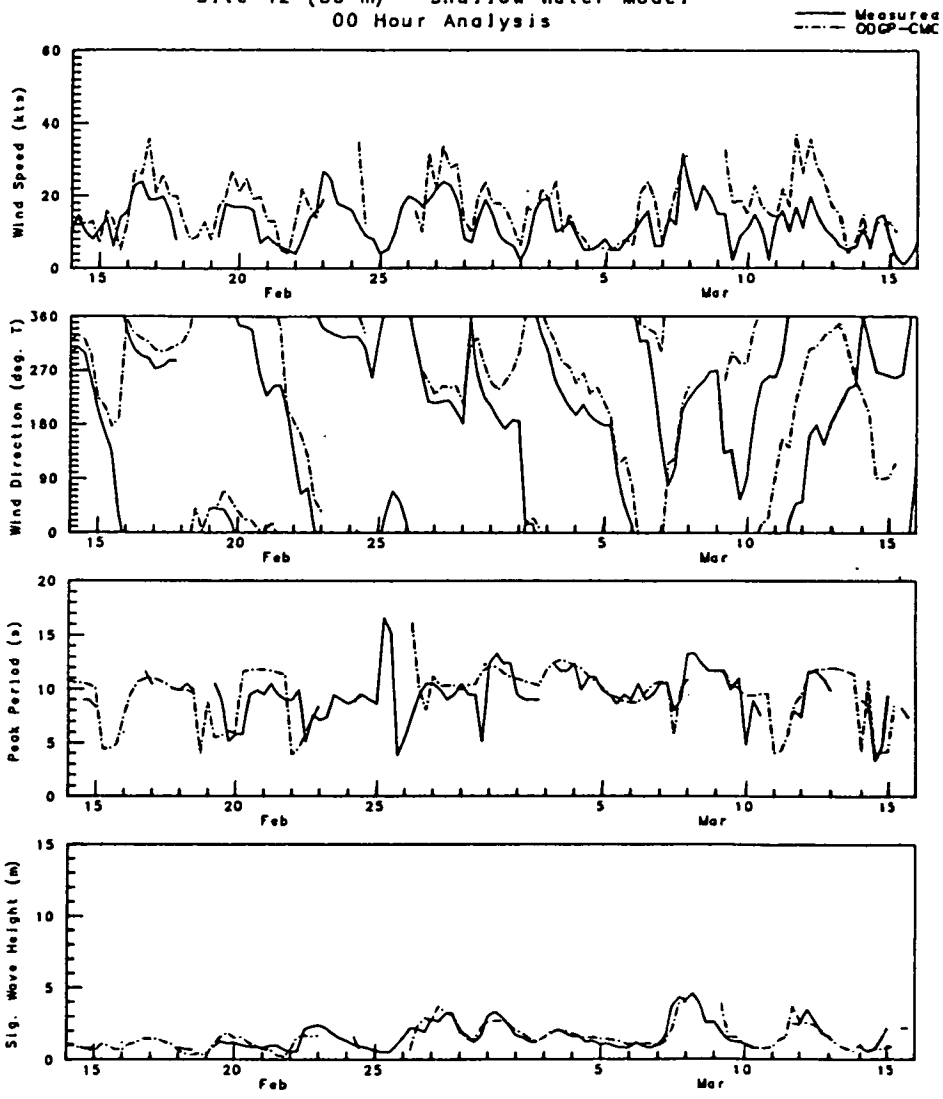

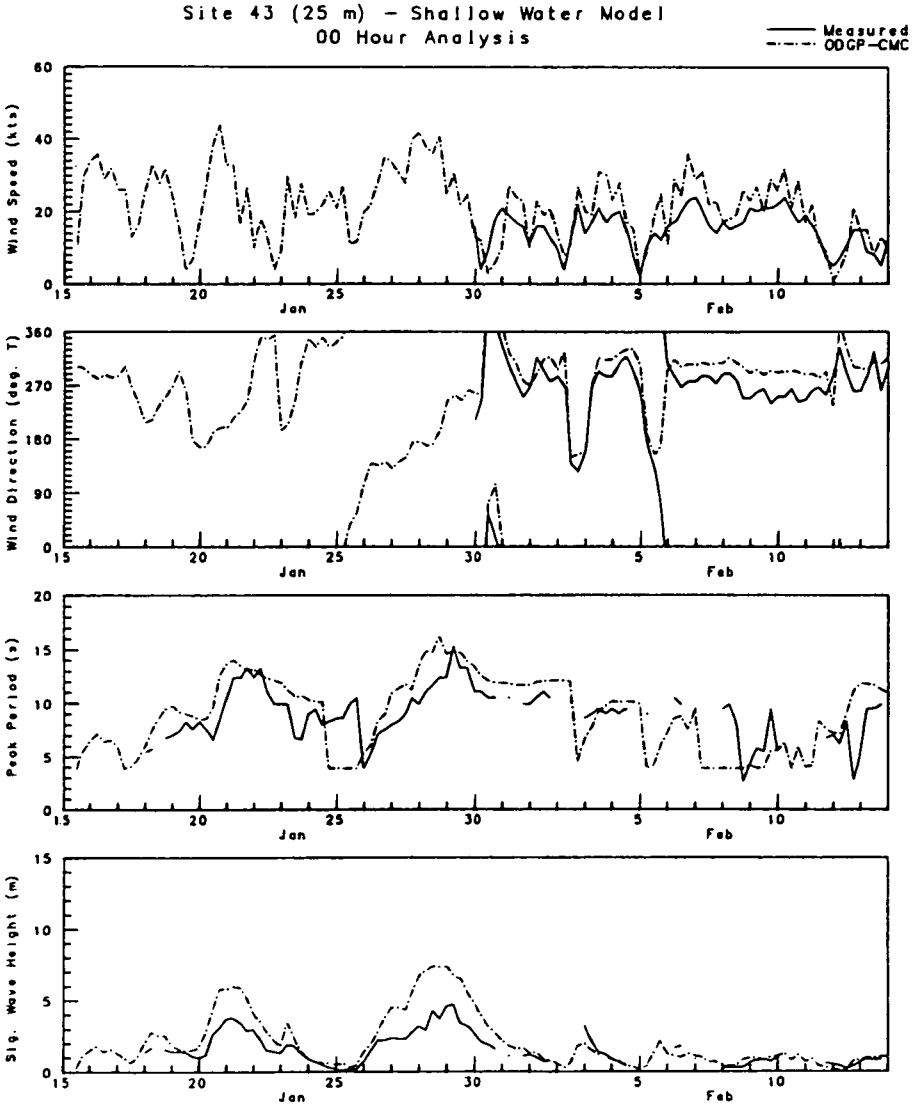
Measured Data vs. ODGP-CMC predictions
January 15, 1986 to February 14, 1986
Site 43 (25 m) - Shallow Water Model
00 Hour Analysis
Measured
ODGP-CMC
Wind Speed (kts)
Wind Direction (deg. T)
Peak Period (s)
Sig. Wave Height (m)
Jan
Feb

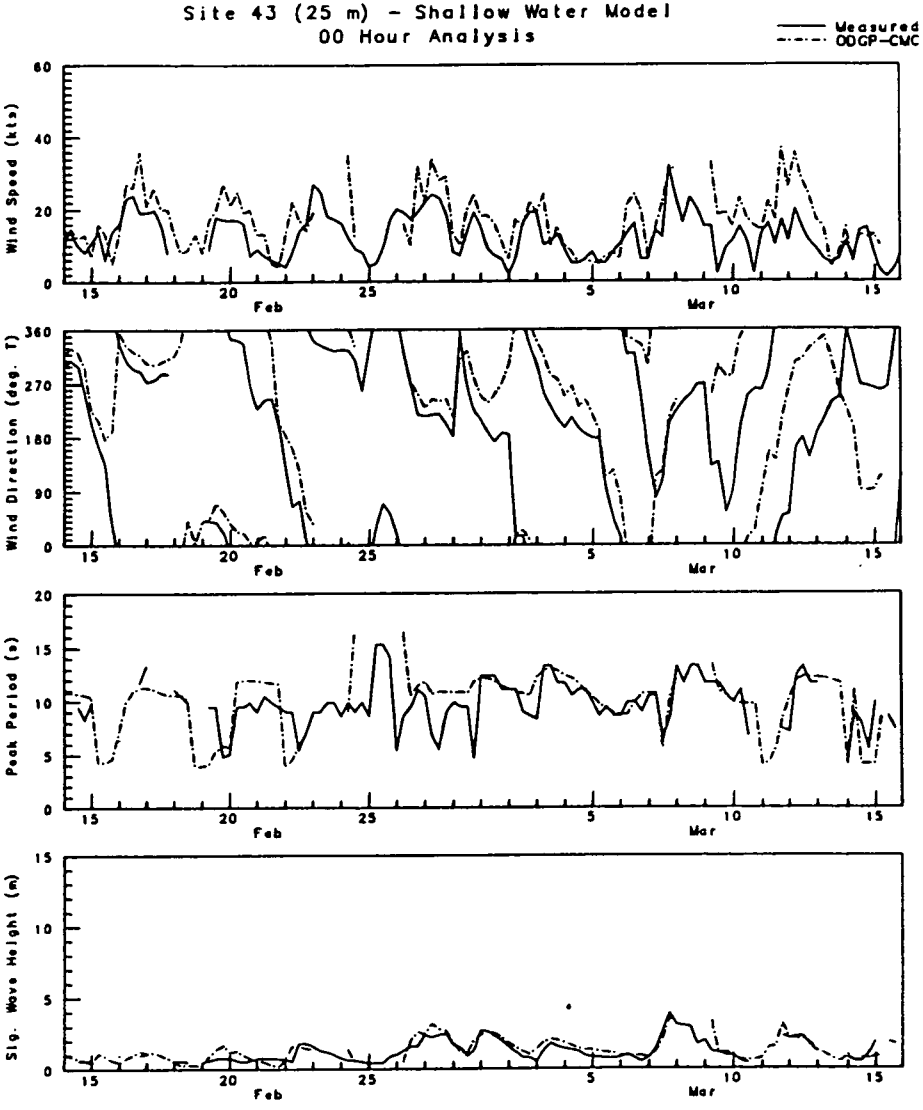
Measured Data vs. ODGP-CMC predictions
February 14, 1986 to March 16, 1986
Site 43 (25 m) - Shallow Water Model
00 Hour Analysis
Measured
ODGP-CMC
Wind Speed (kts)
Wind Direction (deg. T)
Peak Period (s)
Sig. Wave Height (m)
Feb
Mar

Measured Data vs. Model Predictions

January 15, 1986 to March 16, 1986

ODGP-CMC - All Shallow Water Sites

00 Hour Analysis

Number of Points: 477
Correlation Coeffecient: 0.697

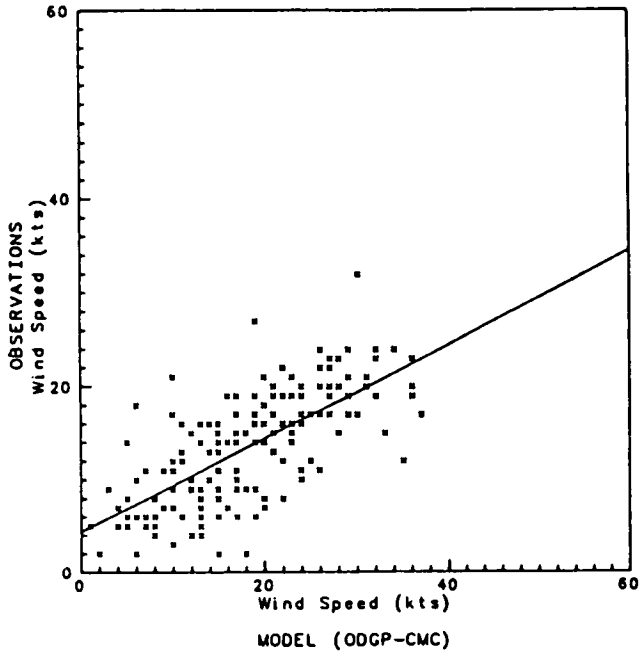

Measured Data vs. Model Predictions

January 15, 1986 to March 16, 1986

ODGP-CMC - All Shallow Water Sites

12 Hour Forecast

Number of Points: 480
Correlation Coeffecient: 0.672

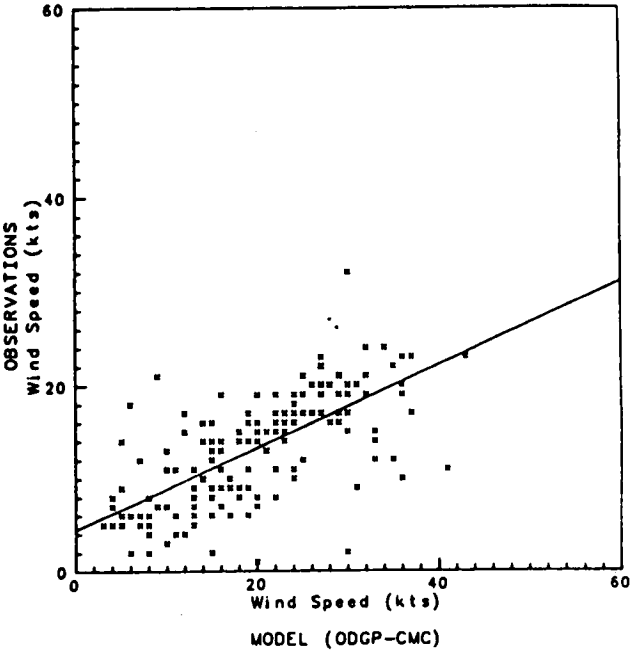

ODGP-CMC - All Shallow Water Sites

00 Hour Analysis

Number of Points: 457
Correlation Coeffecient: 0.848

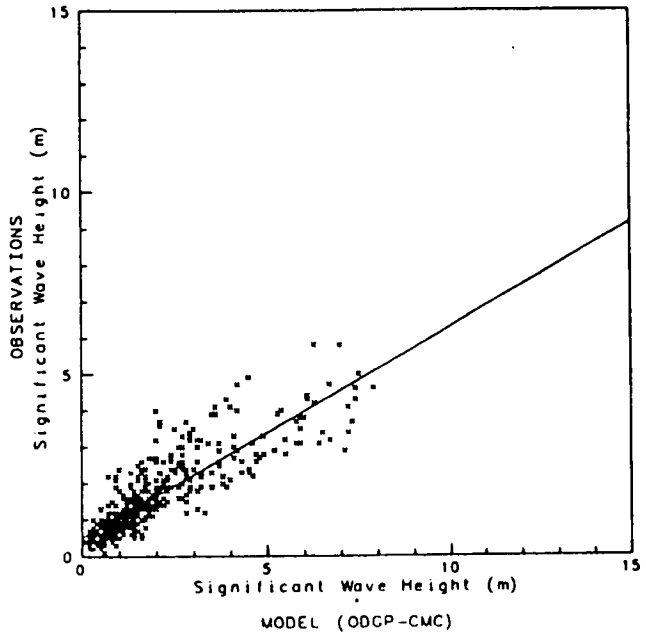

ODGP-CMC - All Shallow Water Sites

12 Hour Forecast

Number of Points: 460
Correlation Coeffecient: 0.861

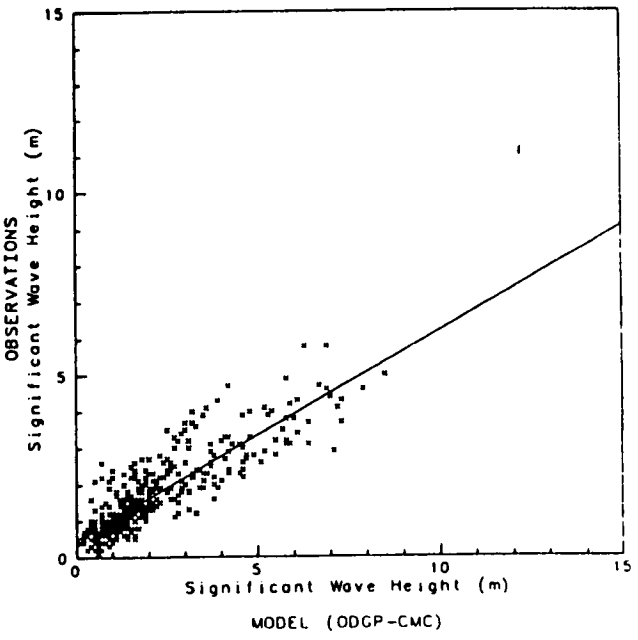

Measured Data vs. Model Predictions

January 15, 1986 to March 16, 1986

ODGP-CMC - All Shallow Water Sites

24 Hour Forecast

Number of Points: 486
Correlation Coeffecient: 0.534

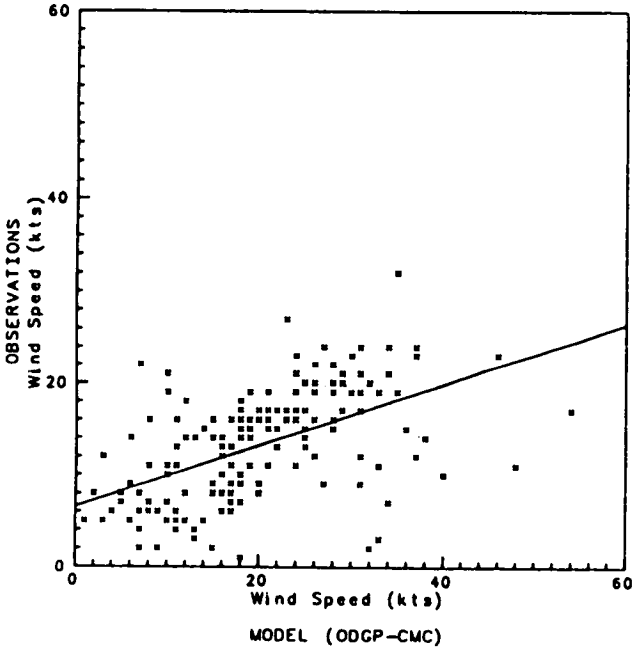

Measured Data vs. Model Predictions

January 15, 1986 to March 16, 1986

ODGP-CMC - All Shallow Water Sites

36 Hour Forecast

Number of Points: 486
Correlation Coeffecient: 0.434

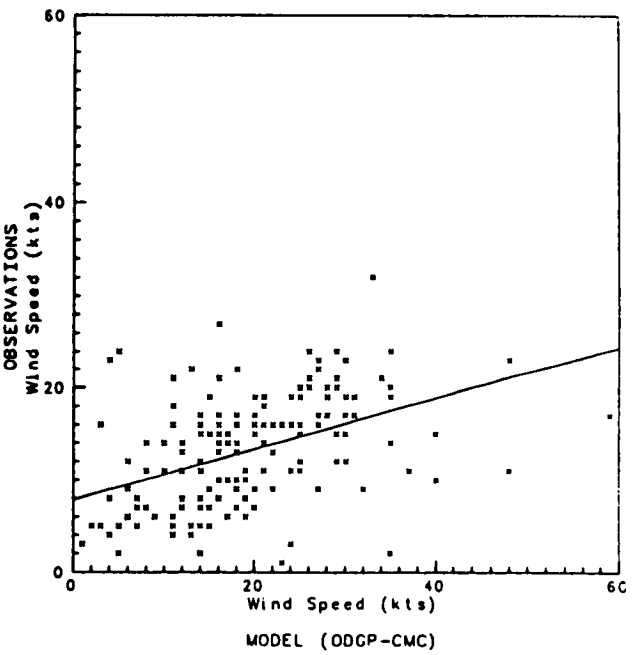

ODGP-CMC - All Shallow Water Sites

24 Hour Forecast

Number of Points: 463
Correlation Coeffecient: 0.840

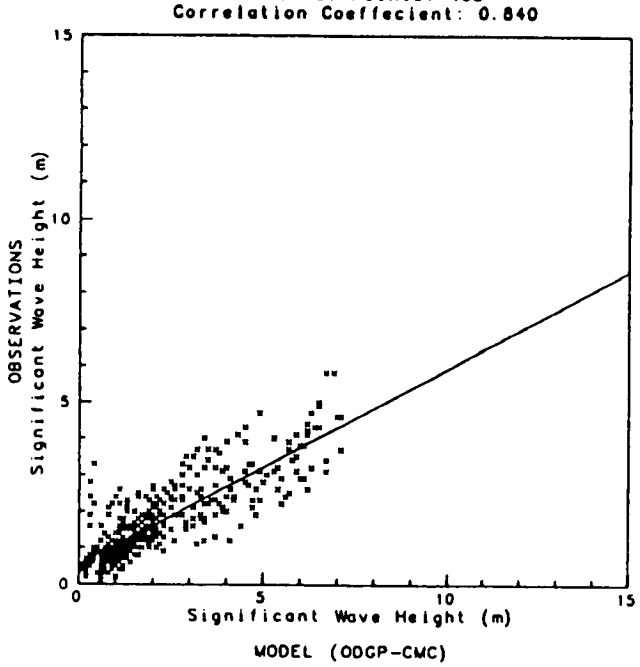

ODGP-CMC - All Shallow Water Sites

36 Hour Forecast

Number of Points: 463
Correlation Coeffecient: 0.773

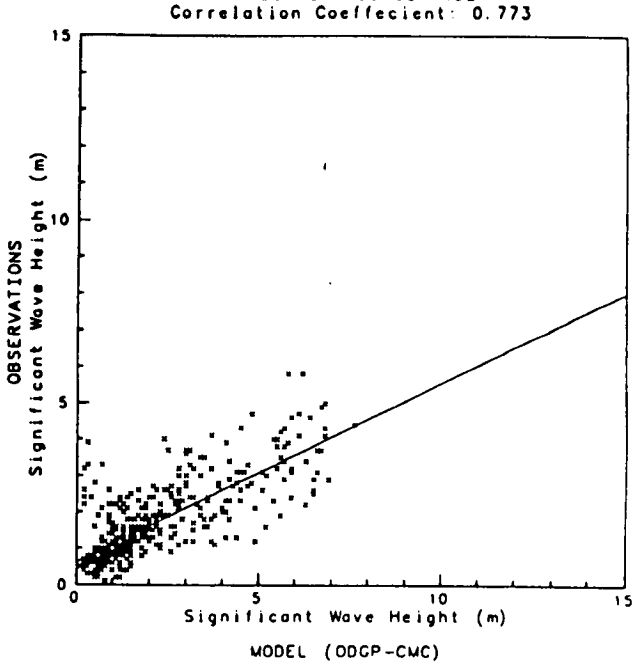

Measured Data vs. Model Predictions

January 15, 1986 to March 16, 1986

ODGP-CMC - All Shallow Water Sites

48 Hour Forecast

Number of Points: 480
Correlation Coeffecient: 0.319

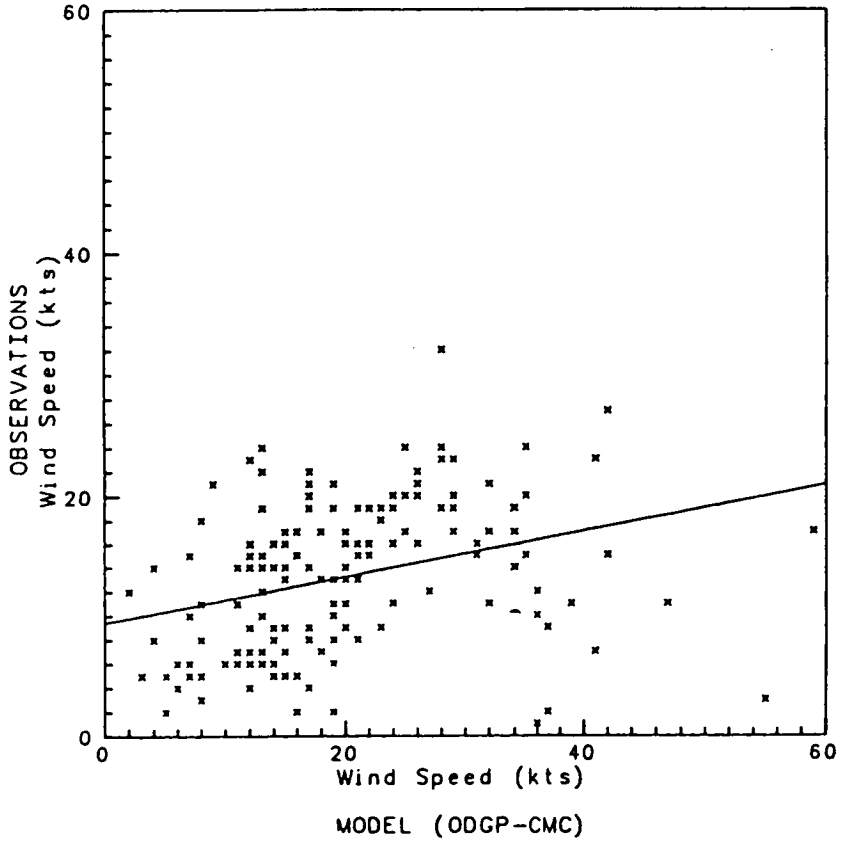

Measured Data vs. Model Predictions

January 15, 1986 to March 16, 1986

ODGP-CMC - All Shallow Water Sites

48 Hour Forecast

Number of Points: 457
Correlation Coeffecient: 0.744

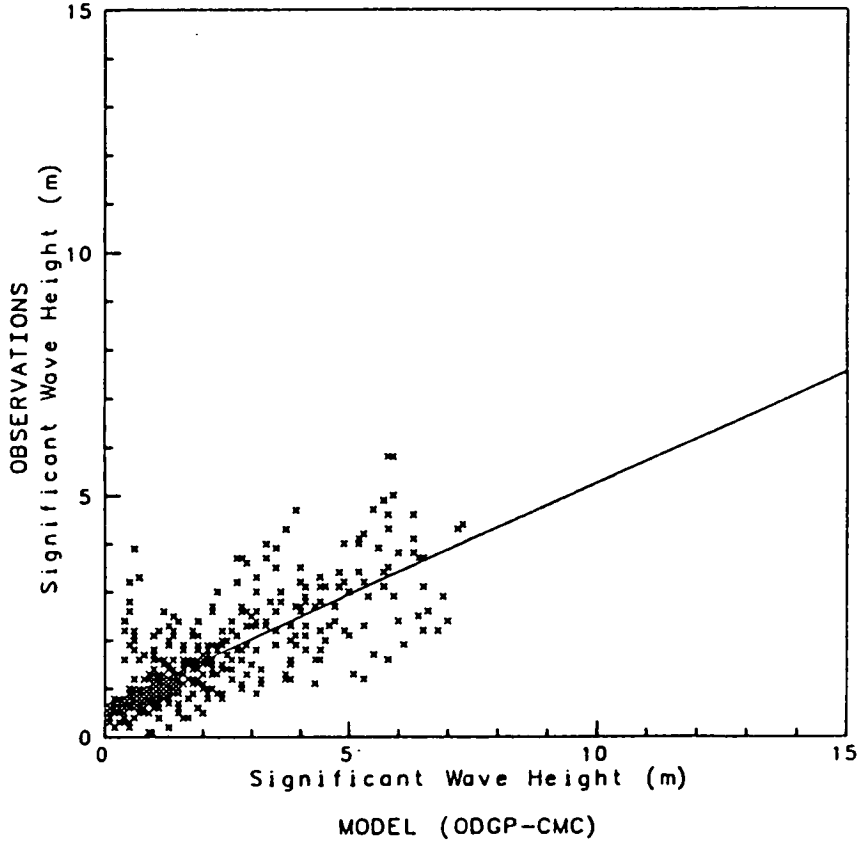

Measured Data vs. Model Predictions
January 15, 1986 to March 16, 1986
ODGP-CMC - All Shallow Water Sites
00 Hour Analysis
Number of Points: 457
Correlation Coeffecient: 0.630

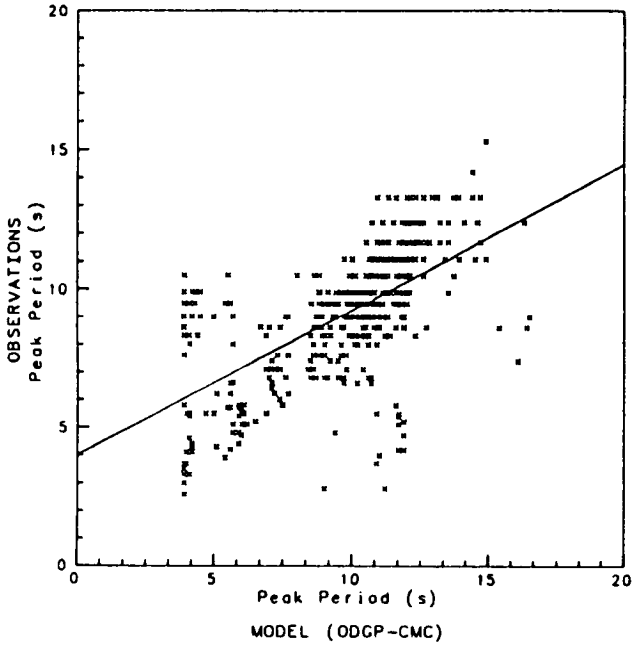

Measured Data vs. Model Predictions
January 15, 1986 to March 16, 1986
ODGP-CMC - All Shallow Water Sites
12 Hour Forecast
Number of Points: 460
Correlation Coeffecient: 0.622

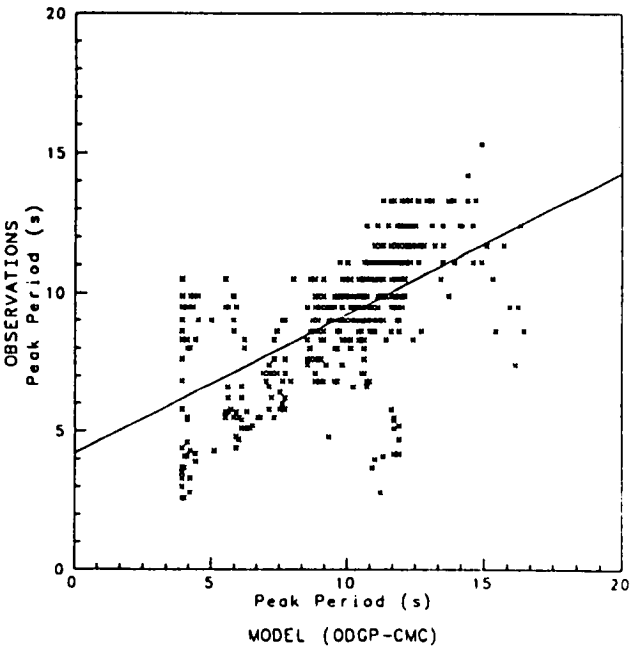

24 Hour Forecast
Number of Points: 463
Correlation Coeffecient: 0.612

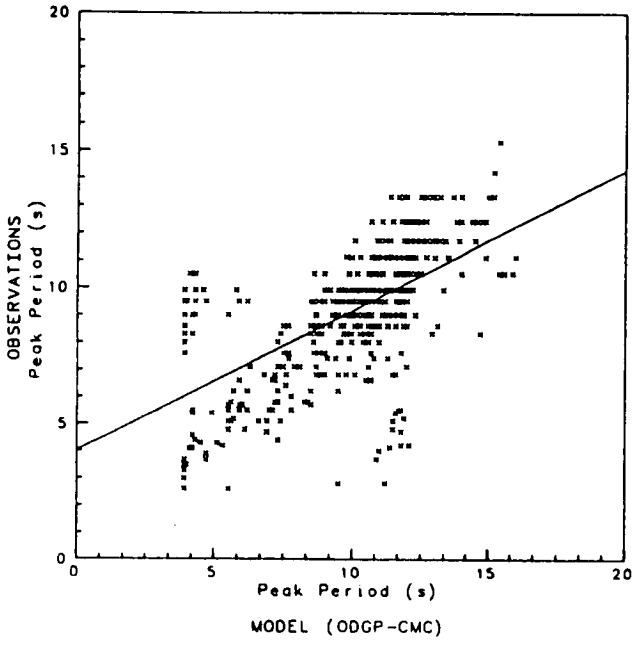

36 Hour Forecast
Number of Points: 463
Correlation Coeffecient: 0.592

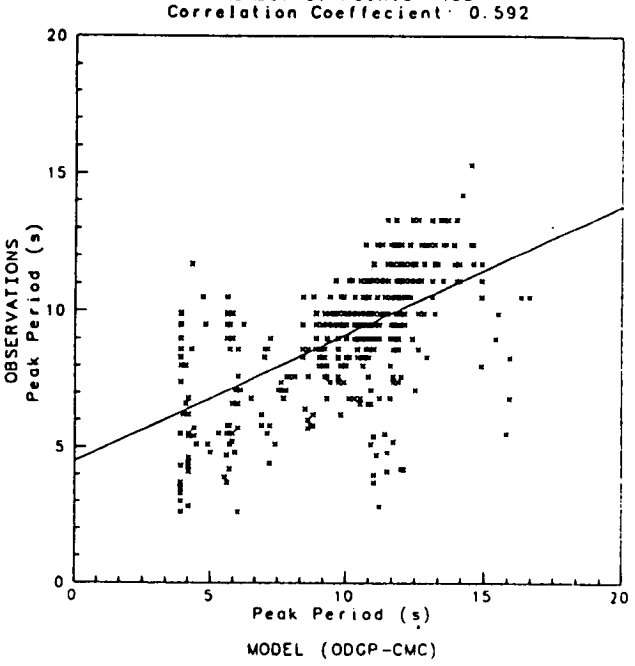

Measured Data vs. Model Predictions

January 15, 1986 to March 16, 1986

ODGP-CMC - All Shallow Water Sites

48 Hour Forecast

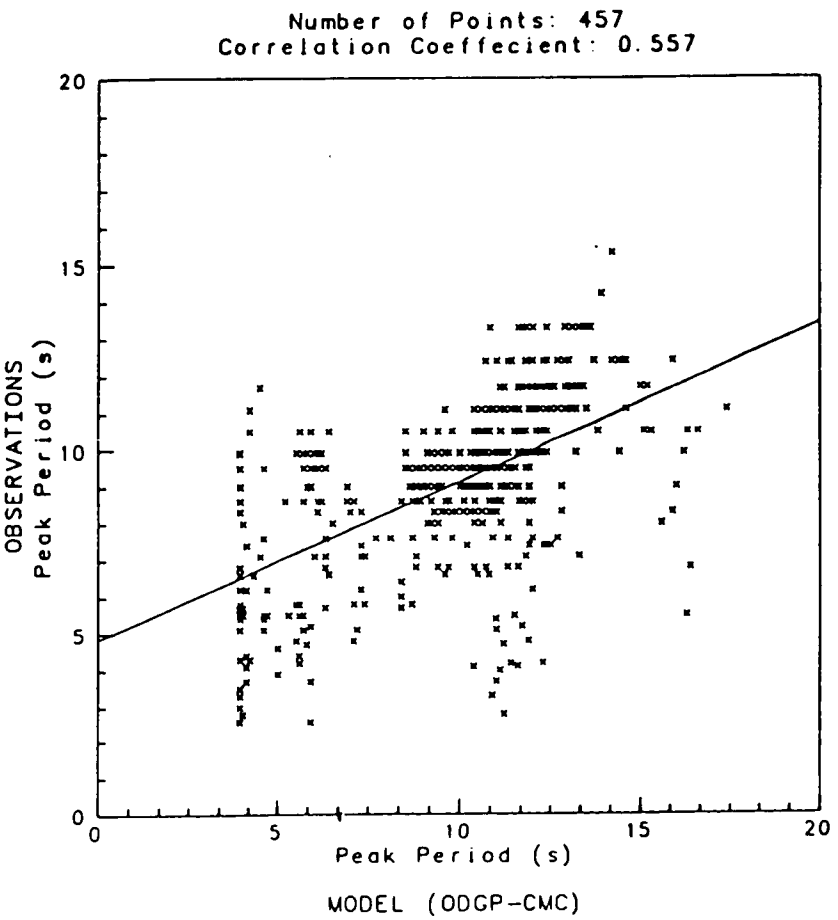

January 15 - March 15, 1986

All Shallow Water Sites (41,42,43)

PROG.	VAR	MODEL	NUMBER OF POINTS	AVERAGE OBS.VALUES	STANDARD DEVIATION	AVERAGE MODEL VAL.	STANDARD DEVIATION	MEAN ERROR	ABSOLUTE MEAN ERROR	RMSE
00 hr	HS	ODGP-CMC	457	1.62	1.04	1.92	1.53	0.30	0.57	0.90
	TP	ODGP-CMC	457	9.09	2.33	9.71	2.80	0.62	1.63	2.33
	WS	ODGP-CMC	477	13.36	5.96	17.85	8.30	4.48	5.88	7.45
	WD	ODGP-CMC	477	221.83	89.23	233.70	101.67	11.87	74.20	110.07
12 hr	HS	ODGP-CMC	460	1.63	1.03	2.00	1.55	0.37	0.61	0.93
	TP	ODGP-CMC	460	9.09	2.32	9.70	2.87	0.62	1.68	2.39
	WS	ODGP-CMC	480	13.29	6.02	19.94	9.17	6.66	7.62	9.51
	WD	ODGP-CMC	480	222.09	89.01	234.21	103.01	12.11	80.78	115.31
24 hr	HS	ODGP-CMC	463	1.63	1.03	2.04	1.62	0.41	0.68	1.02
	TP	ODGP-CMC	463	9.08	2.32	9.87	2.77	0.79	1.74	2.41
	WS	ODGP-CMC	486	13.19	6.06	20.02	9.75	6.83	8.20	10.74
	WD	ODGP-CMC	486	222.18	89.35	237.05	101.09	14.87	83.01	114.86
36 hr	HS	ODGP-CMC	463	1.63	1.03	2.04	1.62	0.41	0.74	1.13
	TP	ODGP-CMC	463	9.08	2.32	9.86	2.94	0.78	1.86	2.56
	WS	ODGP-CMC	486	13.19	6.06	19.36	9.55	6.18	8.06	10.76
	WD	ODGP-CMC	486	222.18	89.35	228.82	102.91	6.64	89.43	121.26
48 hr	HS	ODGP-CMC	457	1.61	1.03	2.10	1.66	0.49	0.82	1.23
	TP	ODGP-CMC	457	9.07	2.34	9.85	3.04	0.78	1.99	2.72
	WS	ODGP-CMC	480	13.18	6.06	19.74	10.13	6.56	8.44	11.97
	WD	ODGP-CMC	480	222.56	89.83	243.39	98.13	20.83	92.68	124.94

February 2 - March 15, 1986

Period From : Feb 2nd

All Shallow Water Sites (41,42,43)

PROG.	VAR	MODEL	NUMBER OF POINTS	AVERAGE OBS.VALUES	STANDARD DEVIATION	AVERAGE MODEL VAL.	STANDARD DEVIATION	MEAN ERROR	ABSOLUTE MEAN ERROR	RMSE
00 hr	HS	ODGP-CMC	342	1.45	0.88	1.45	0.86	0.00	0.37	0.51
	TP	ODGP-CMC	342	9.01	2.23	9.43	2.68	0.42	1.61	2.40
	WS	ODGP-CMC	441	13.26	6.05	18.01	8.33	4.75	5.81	7.46
	WD	ODGP-CMC	441	220.62	88.52	233.75	101.55	13.13	75.69	110.72
12 hr	HS	ODGP-CMC	345	1.46	0.87	1.55	0.98	0.10	0.42	0.58
	TP	ODGP-CMC	345	9.00	2.22	9.42	2.75	0.42	1.68	2.47
	WS	ODGP-CMC	444	13.18	6.11	20.11	9.28	6.94	7.60	9.60
	WD	ODGP-CMC	444	220.91	88.29	232.90	104.47	11.99	82.03	116.32
24 hr	HS	ODGP-CMC	348	1.46	0.87	1.61	1.19	0.15	0.49	0.79
	TP	ODGP-CMC	348	8.98	2.22	9.65	2.66	0.67	1.75	2.51
	WS	ODGP-CMC	450	13.07	6.15	20.21	9.98	7.15	8.36	10.99
	WD	ODGP-CMC	450	221.02	88.67	235.22	103.15	14.20	84.55	116.72
36 hr	HS	ODGP-CMC	348	1.46	0.87	1.60	1.23	0.14	0.58	0.95
	TP	ODGP-CMC	348	8.98	2.22	9.64	2.93	0.65	1.91	2.69
	WS	ODGP-CMC	450	13.07	6.15	19.43	9.75	6.36	8.12	10.97
	WD	ODGP-CMC	450	221.02	88.67	226.77	104.83	5.75	91.74	123.49
48 hr	HS	ODGP-CMC	342	1.44	0.86	1.69	1.39	0.25	0.70	1.15
	TP	ODGP-CMC	342	8.97	2.23	9.66	3.08	0.69	2.13	2.92
	WS	ODGP-CMC	444	13.06	6.16	19.81	10.39	6.75	8.49	12.20
	WD	ODGP-CMC	444	221.42	89.19	240.24	100.37	18.82	95.83	127.80

APPENDIX E

1-D SPECTRAL PLOTS

Measured V.S. Model Spectra
Storm Event 1
Noaa Buoy Data – Site 11 Noaa Bouy 44004
00 Hour Analysis

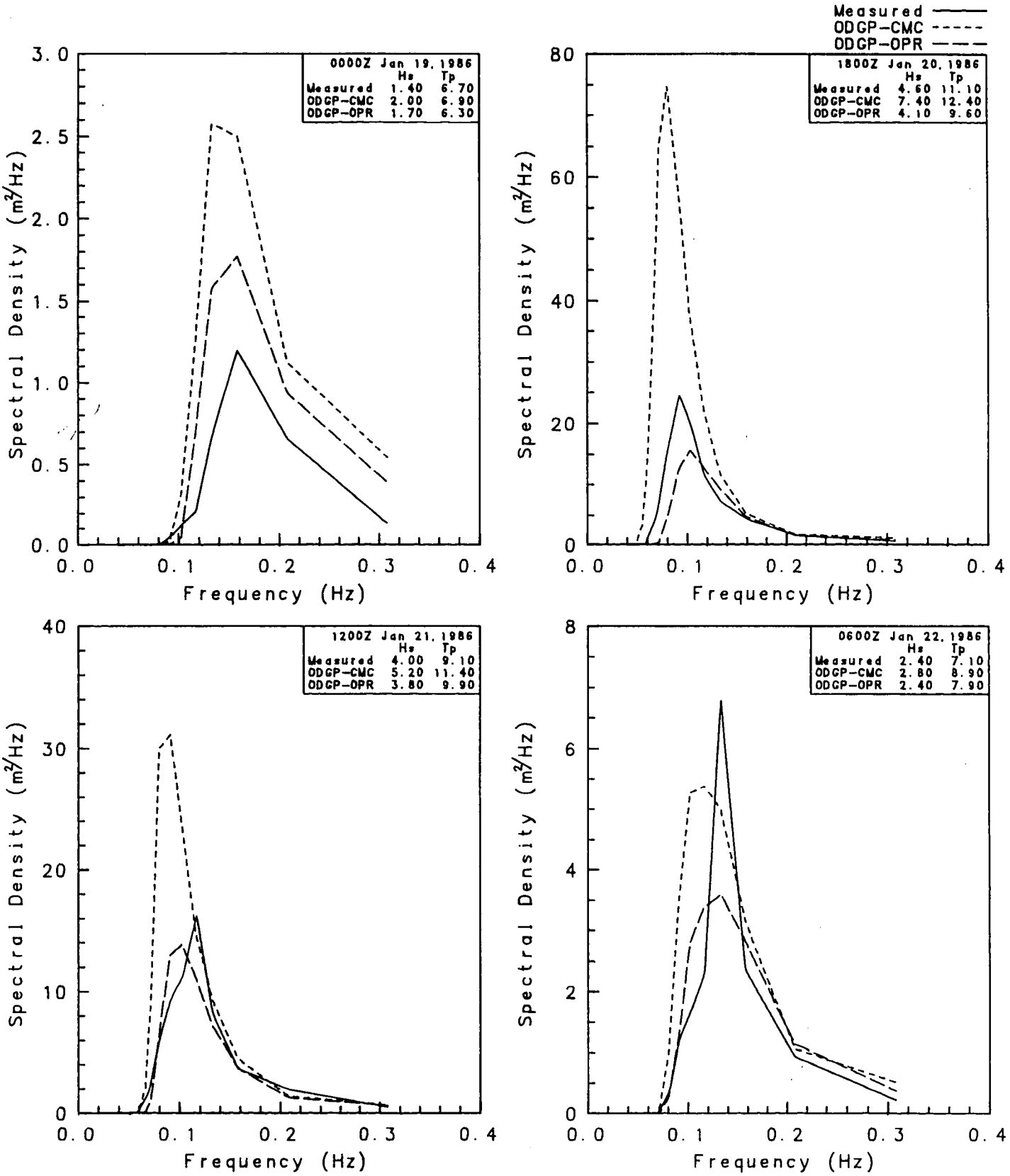

Measured V.S. Model Spectra
Storm Event 1
Waverider Data – Site 21a Rowan Gorilla 1
00 Hour Analysis

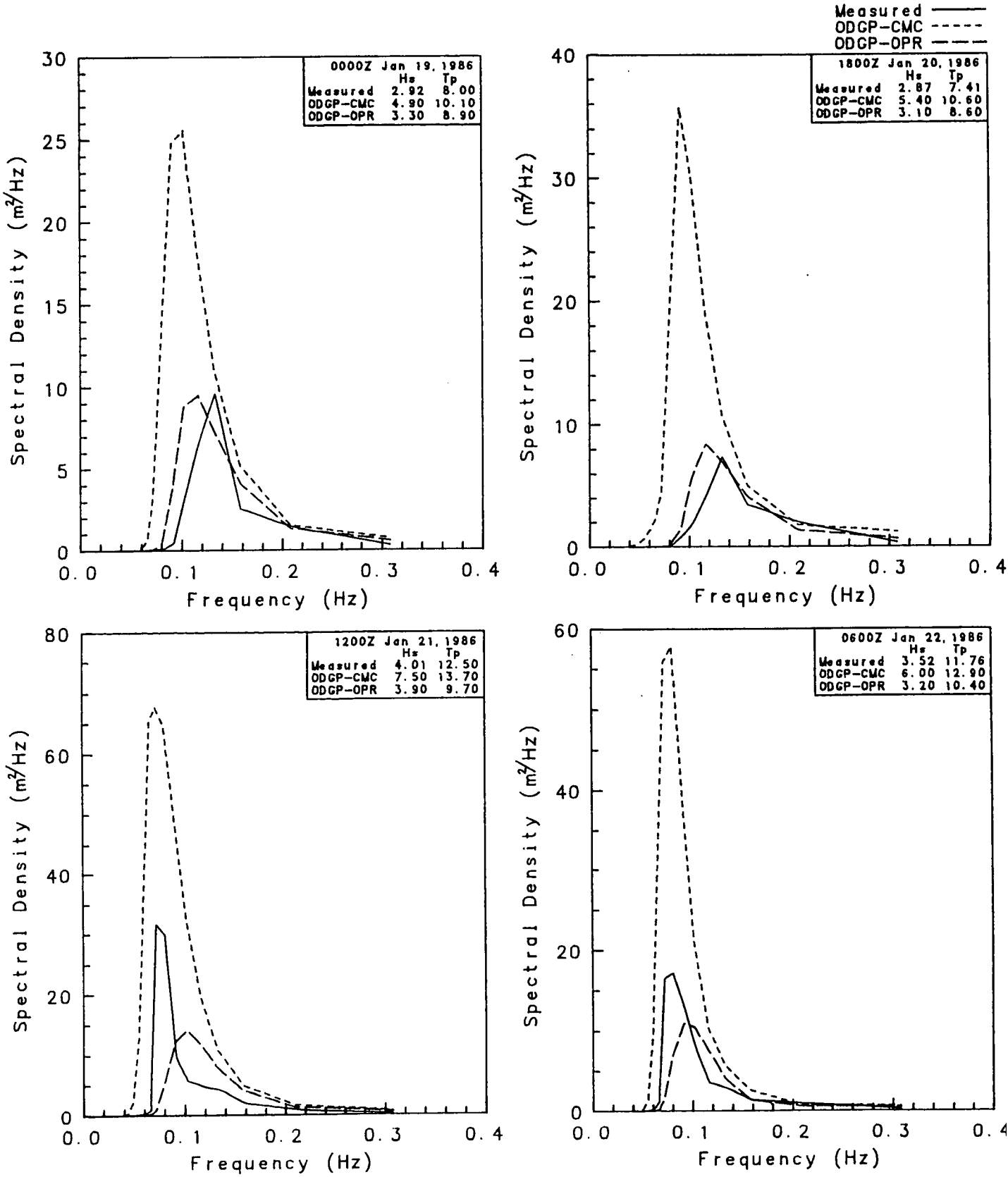

Measured V. S. Model Spectra
Storm Event 1
Waverider Data – Site 21b Sedco 709 & John Shaw
00 Hour Analysis

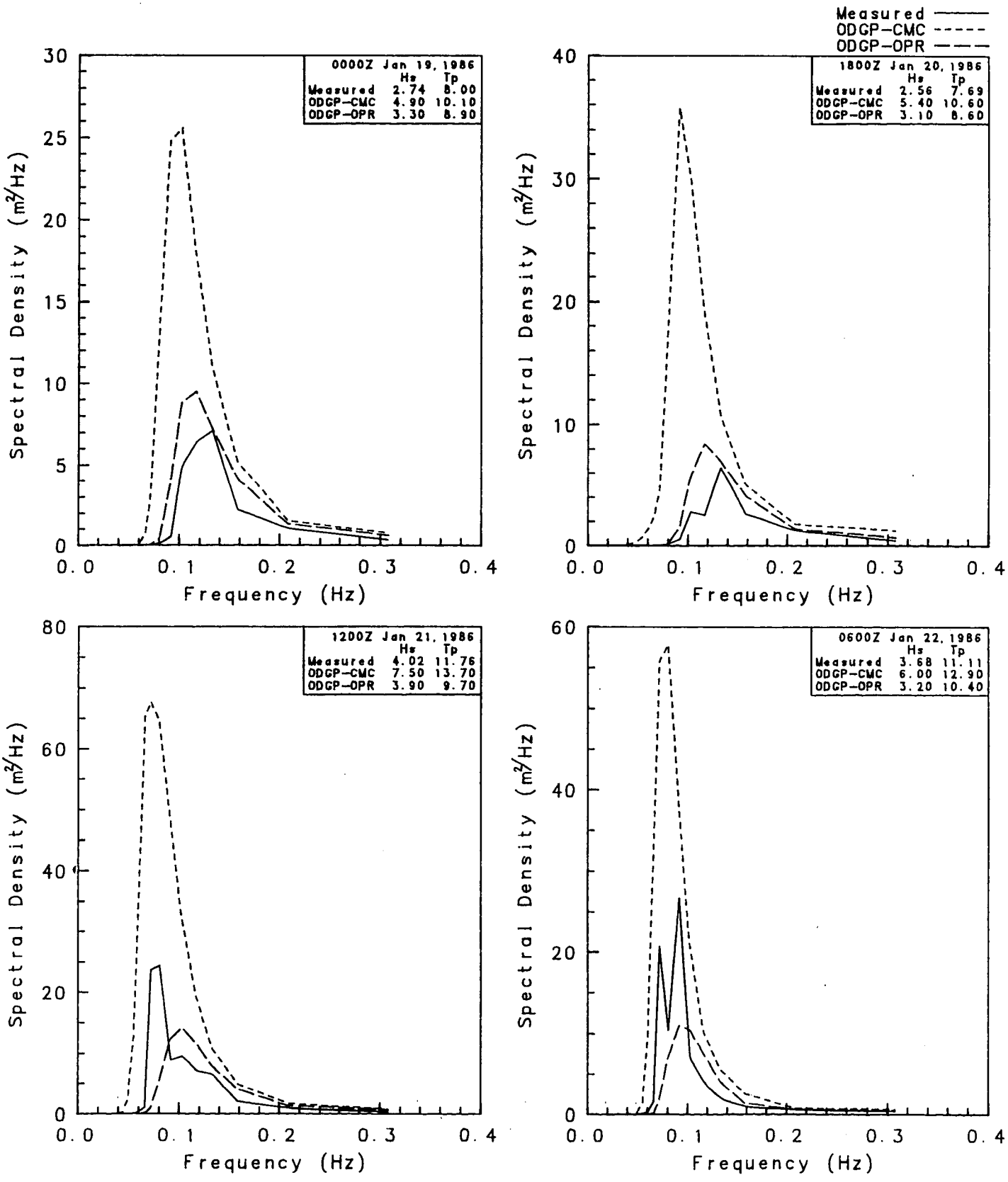

Measured V.S. Model Spectra
Storm Event 1
Waverider Data – Site 31b Bowdrill 2
00 Hour Analysis

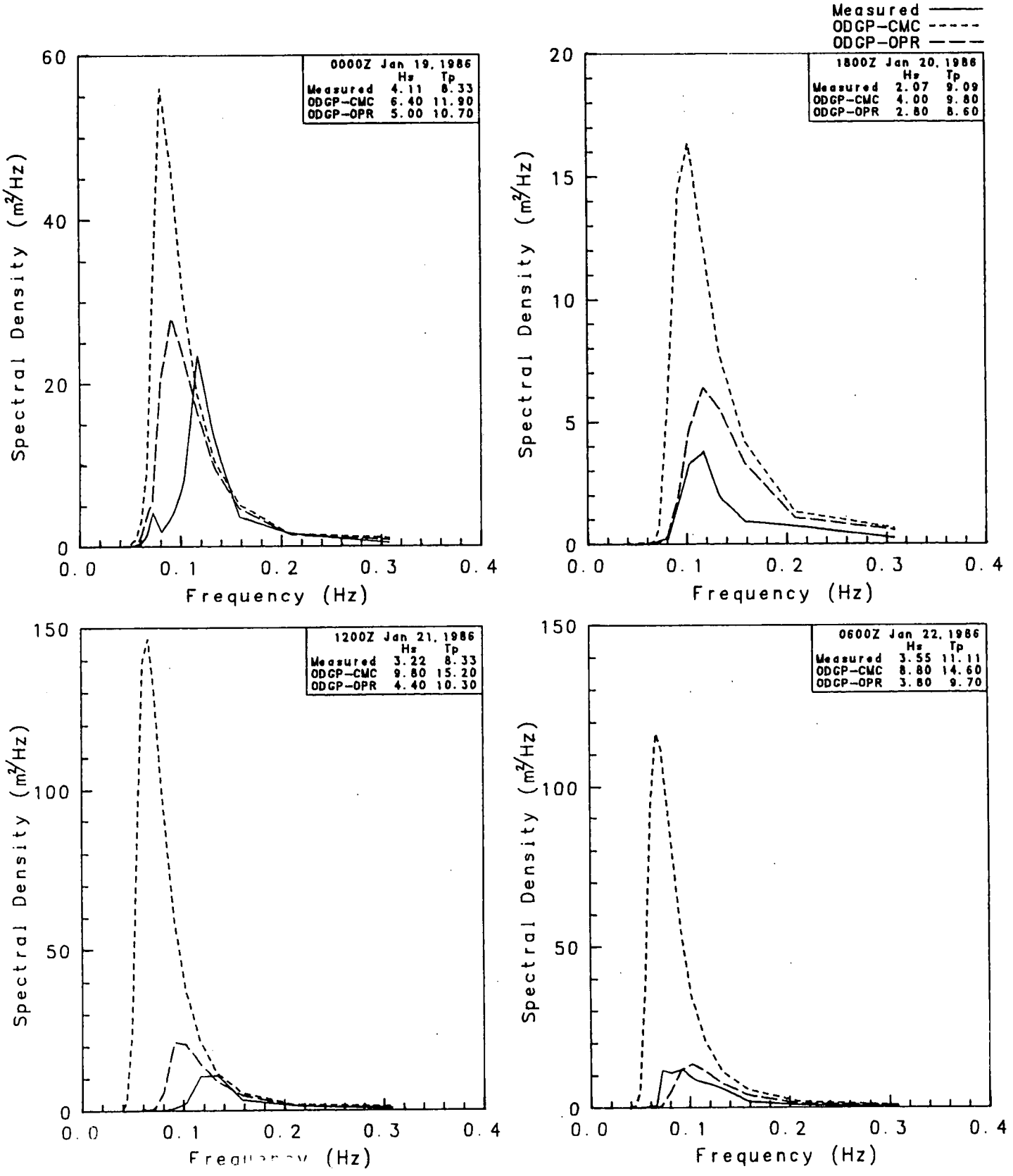

Measured V.S. Model Spectra
Storm Event 1
Waverider Data – Site 31b Sedco 710
00 Hour Analysis

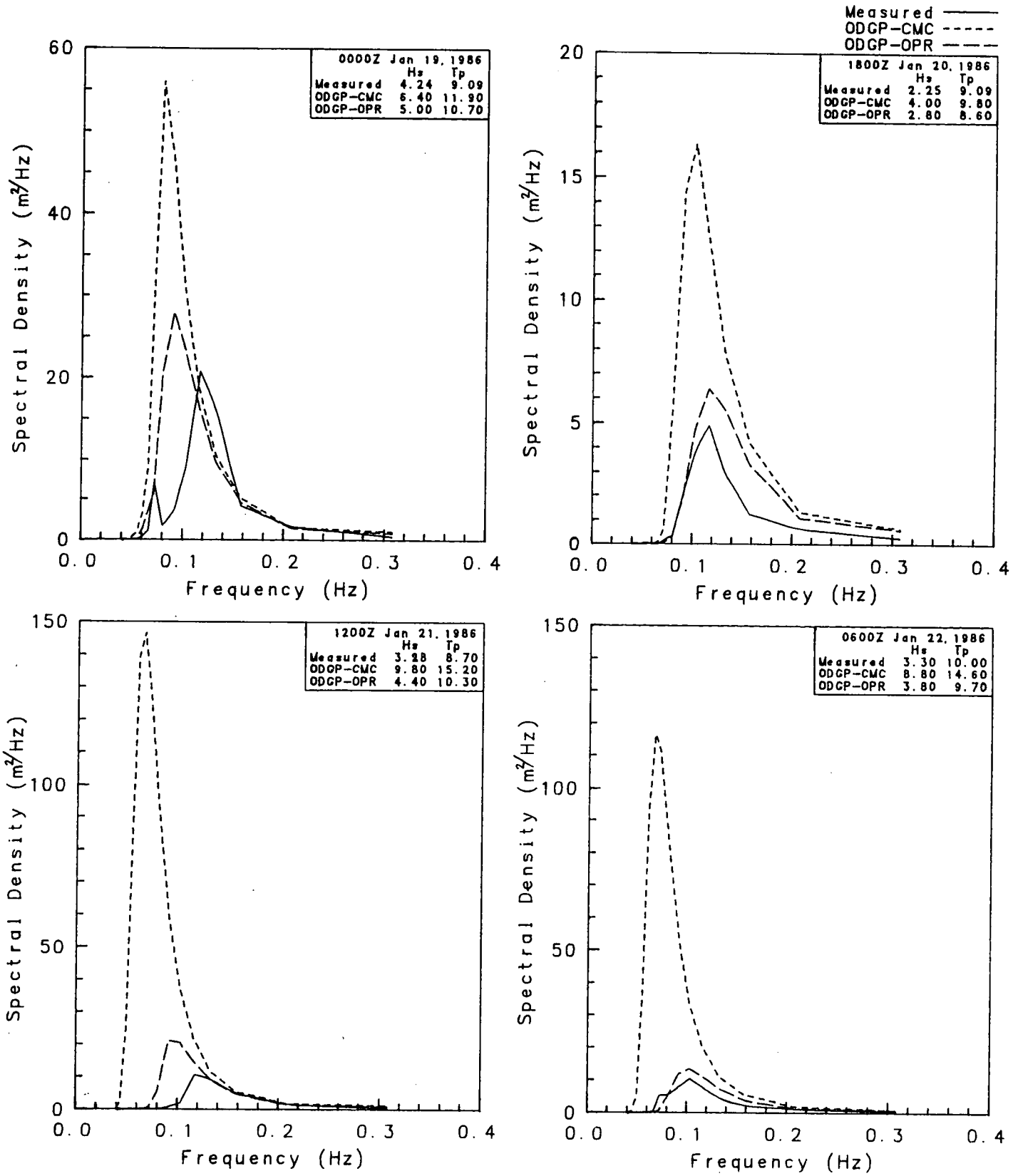

Measured V.S. Model Spectra
Storm Event 2
Noaa Buoy Data – Site 11 Noaa Bouy 44004
00 Hour Analysis

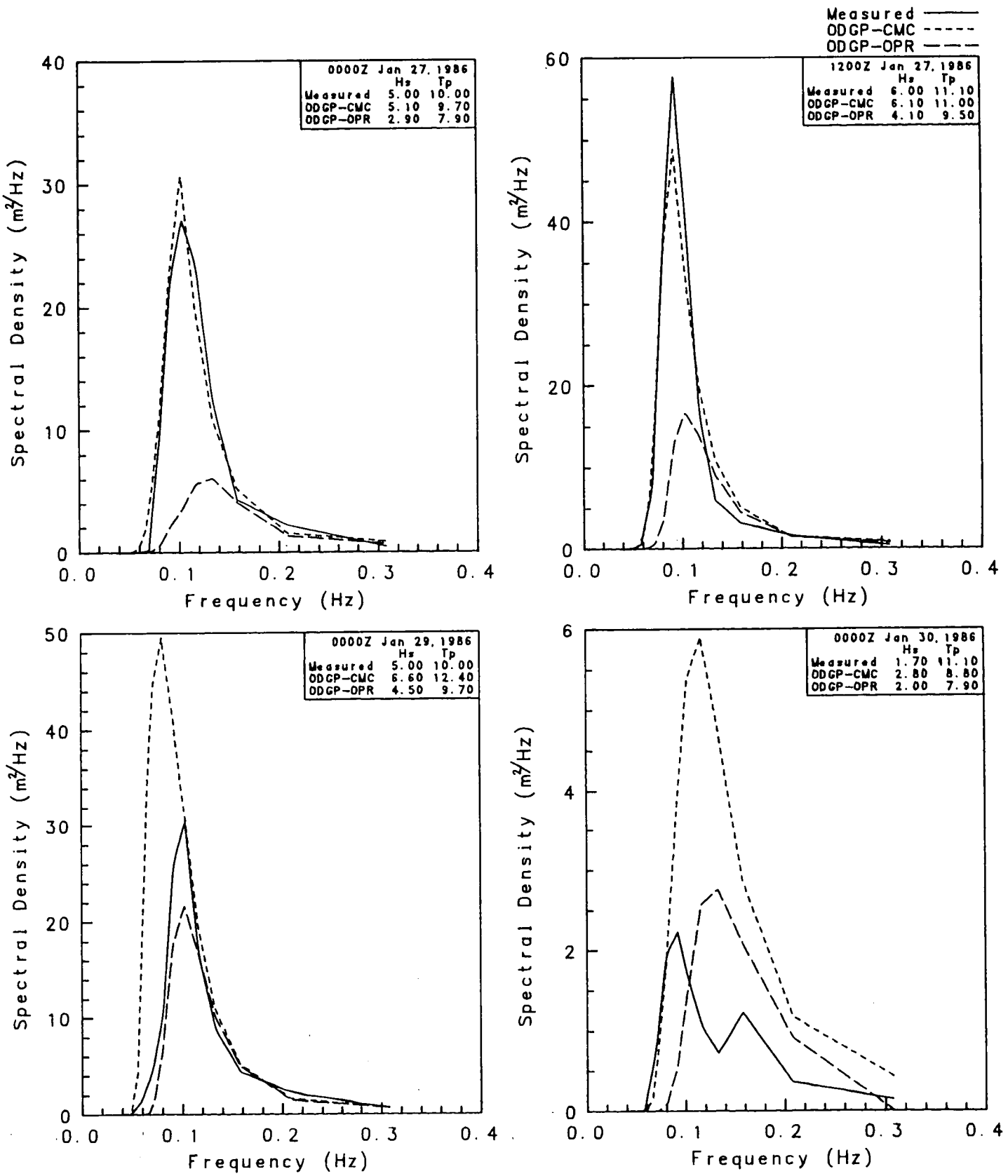

Measured V.S. Model Spectra
Storm Event 2
Waverider Data – Site 21a Rowan Gorilla 1
00 Hour Analysis

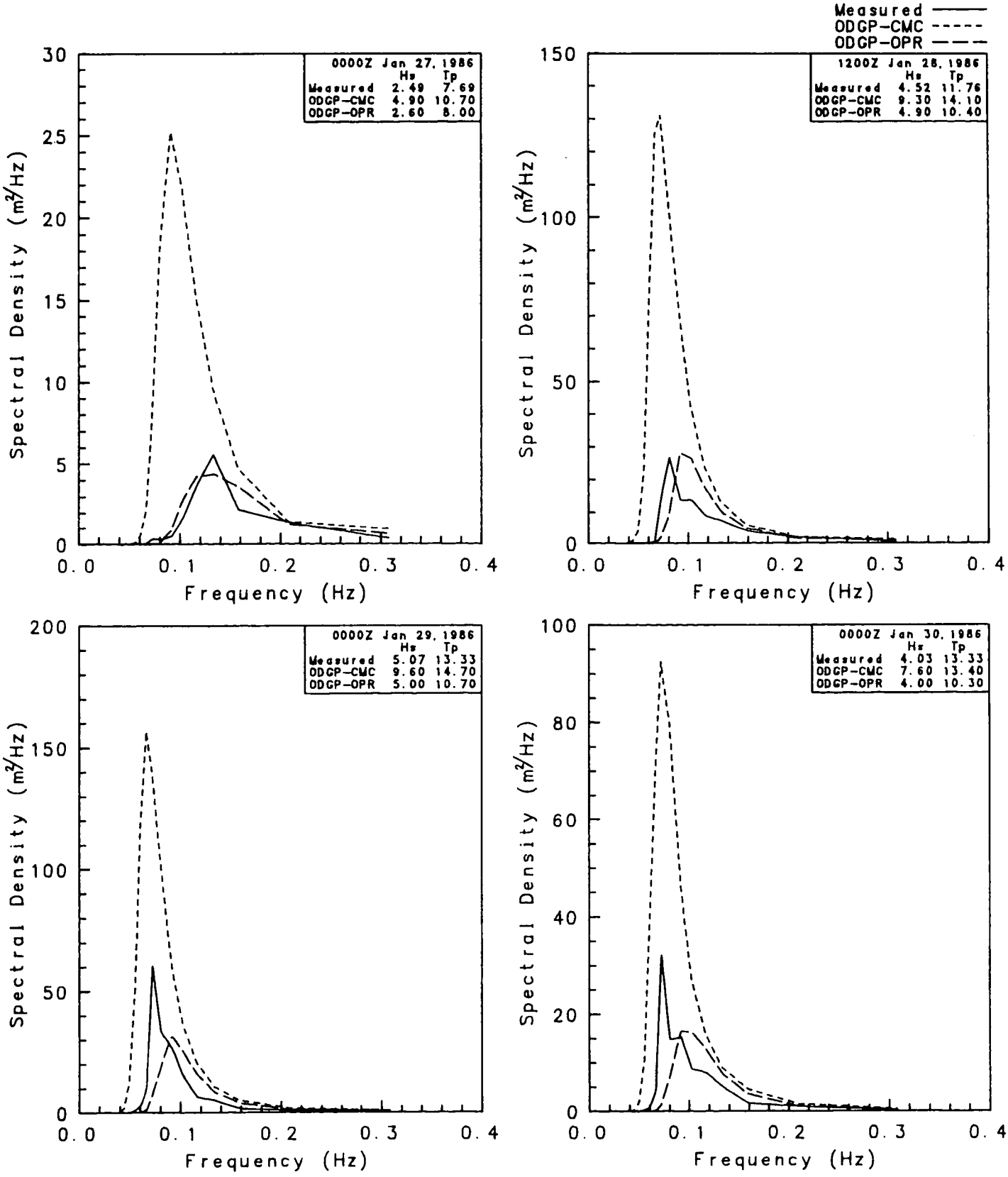

Measured V.S. Model Spectra
Storm Event 2
Waverider Data – Site 21b Sedco 709 & John Shaw
00 Hour Analysis

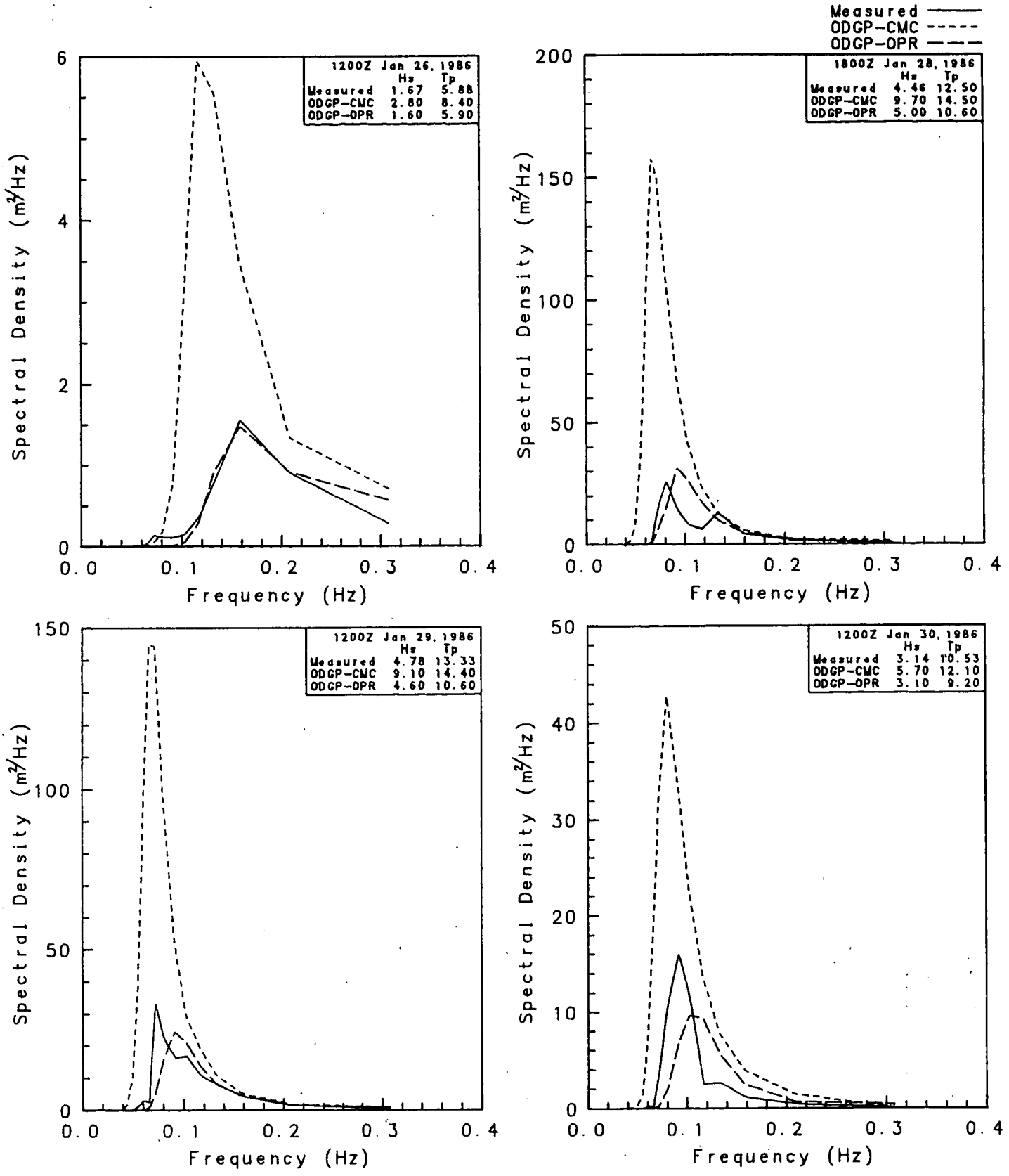

Measured V.S. Model Spectra
Storm Event 2
Waverider Data – Site 31b Bowdrill 2
00 Hour Analysis

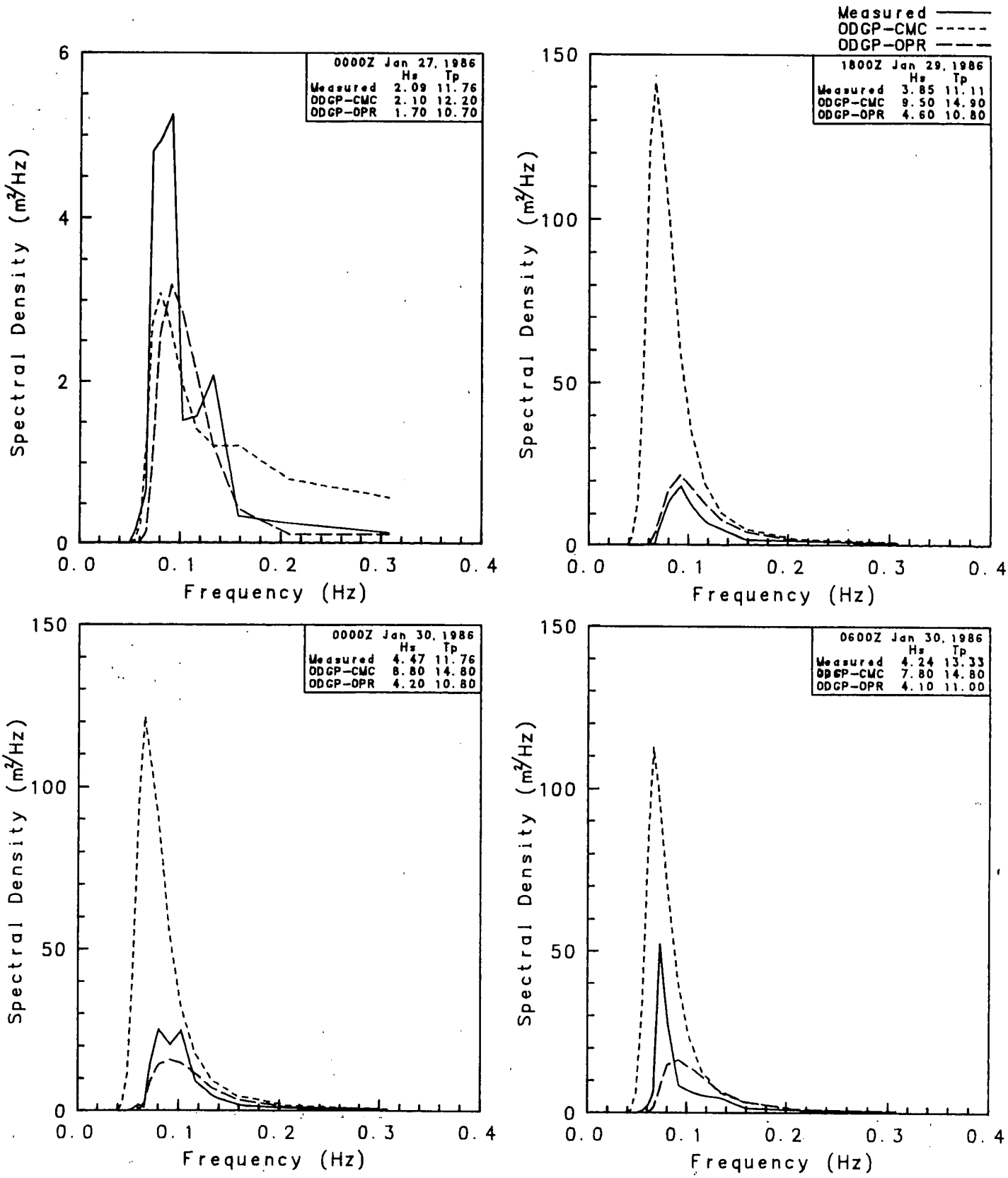

Measured V.S. Model Spectra
Storm Event 2
Waverider Data – Site 31b Sedco 710
00 Hour Analysis

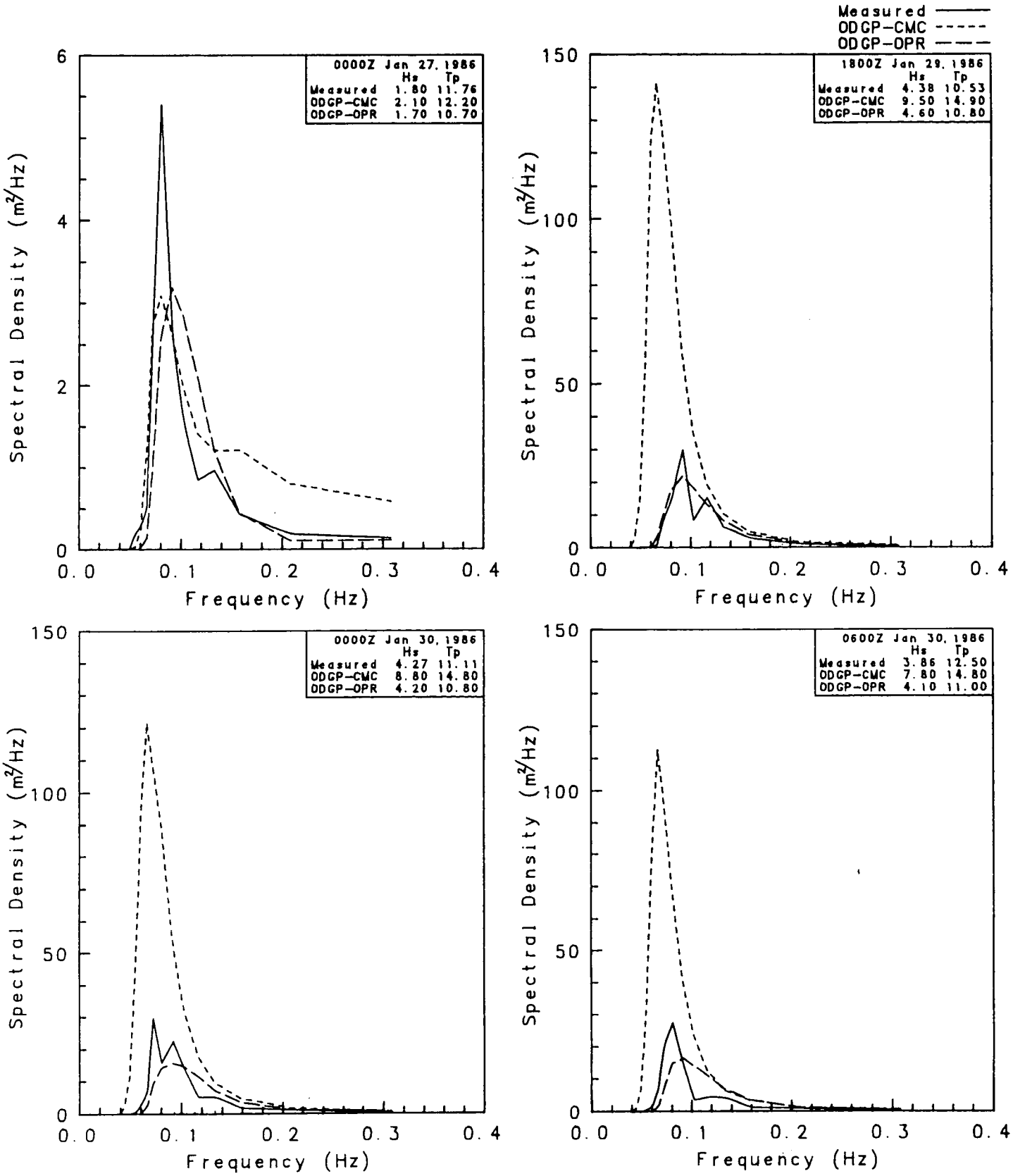

Measured V.S. Model Spectra
Storm Event 3
Noaa Buoy Data – Site 11 Noaa Bouy 44004
00 Hour Analysis

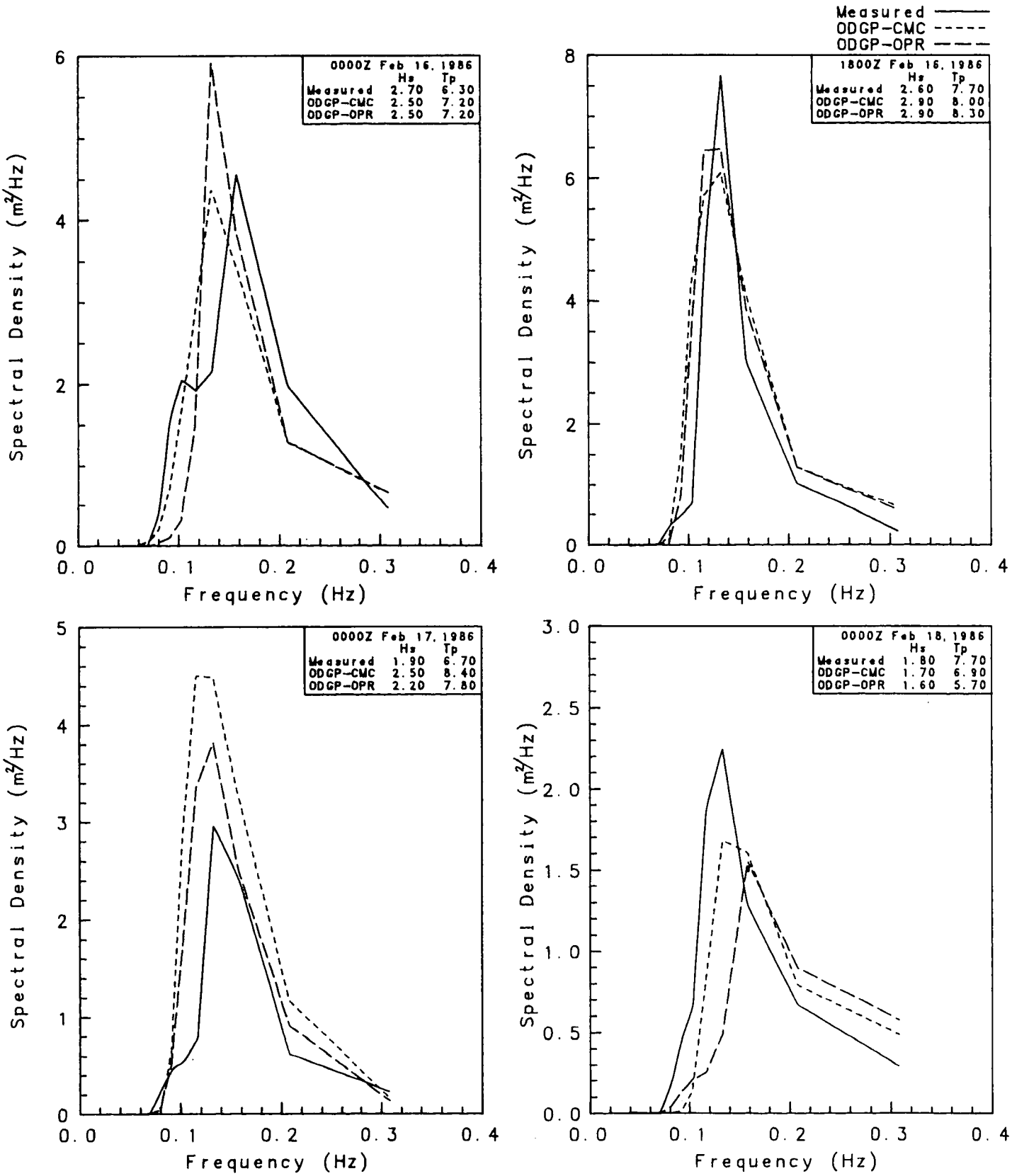

Measured V.S. Model Spectra
Storm Event 3
Waverider Data – Site 21a Rowan Gorilla 1
00 Hour Analysis

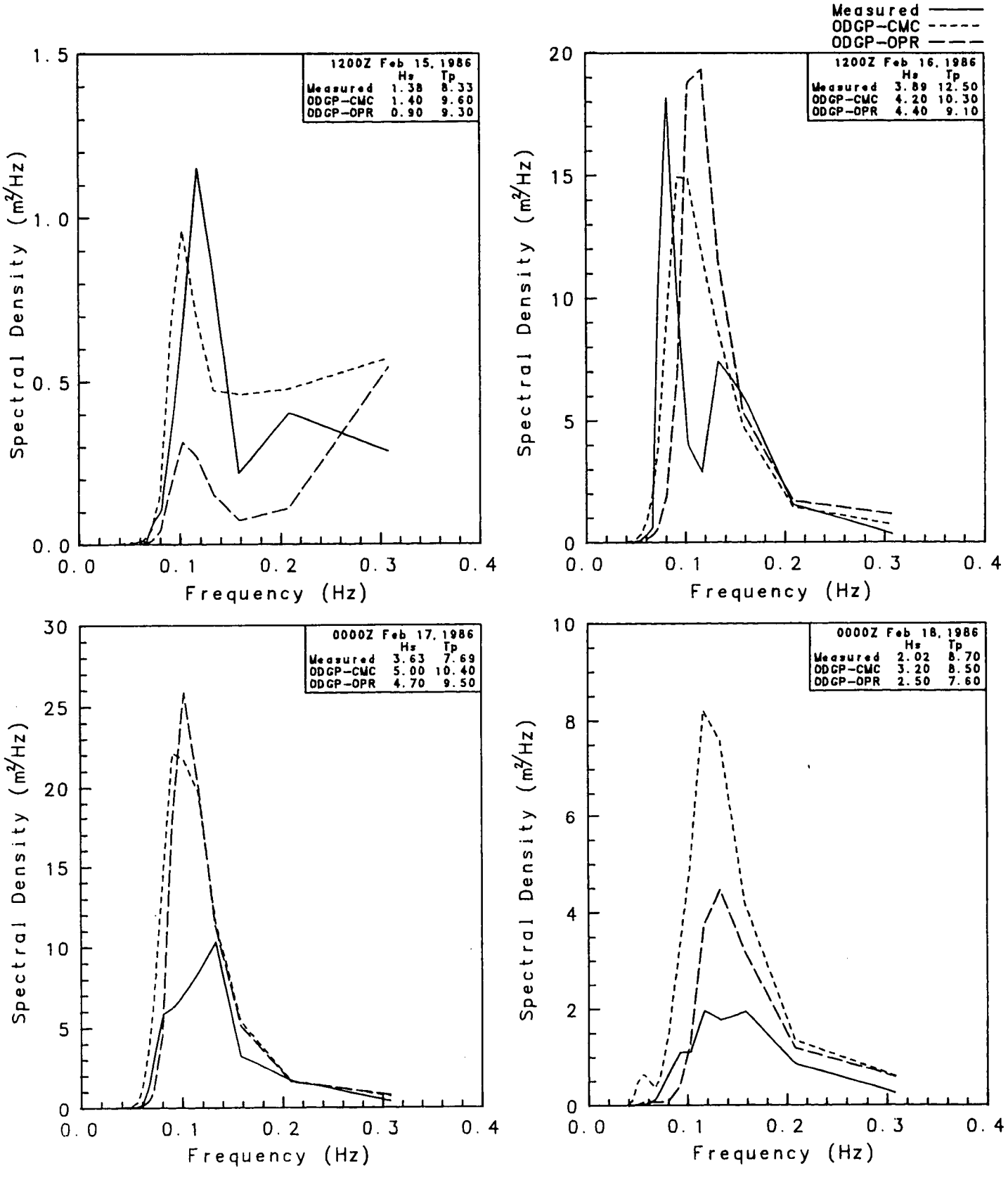

Measured V.S. Model Spectra
Storm Event 3
Waverider Data – Site 21b Sedco 709 & John Shaw
00 Hour Analysis

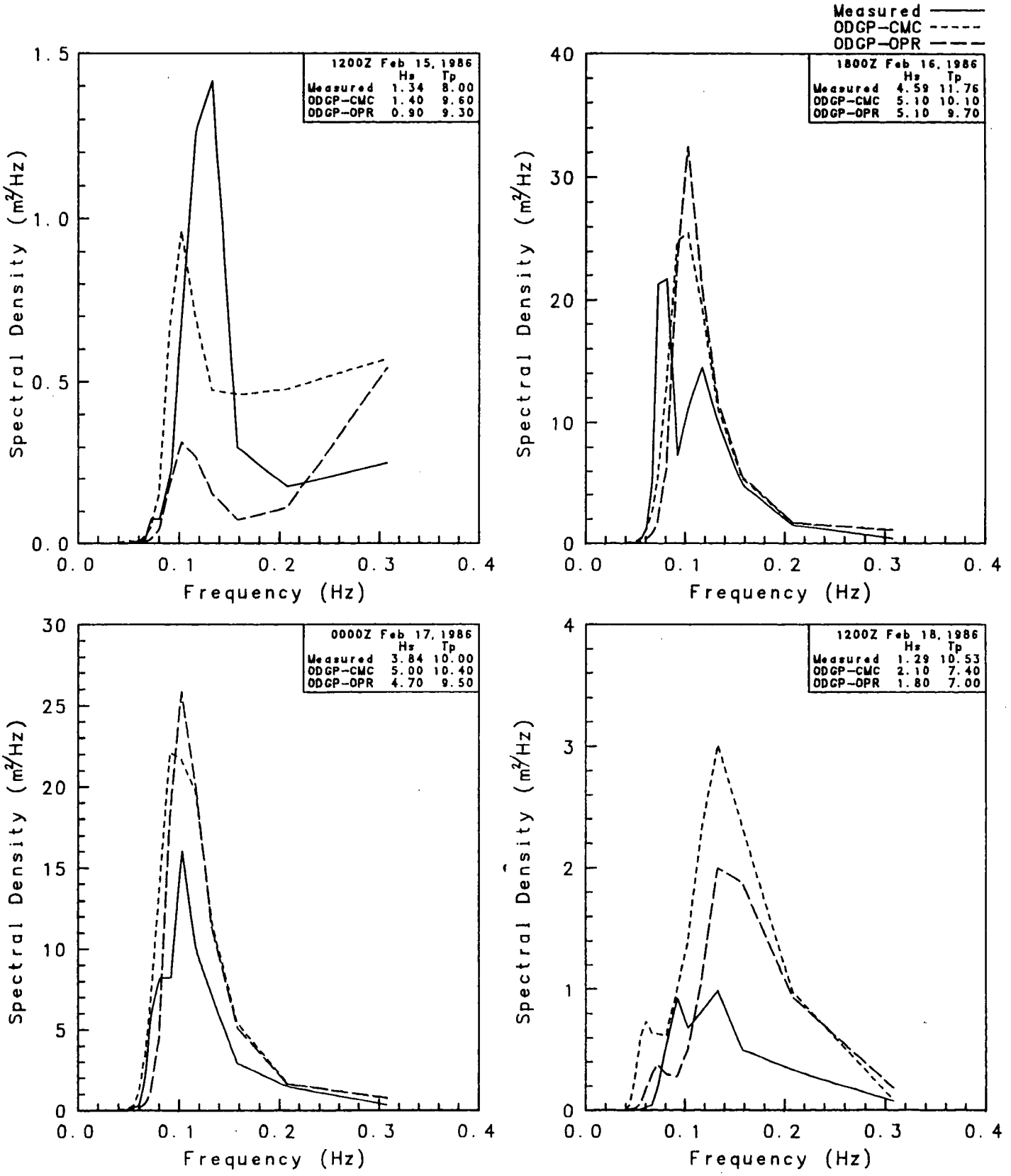

Measured V.S. Model Spectra
Storm Event 3
Waverider Data – Site 31b Models
00 Hour Analysis

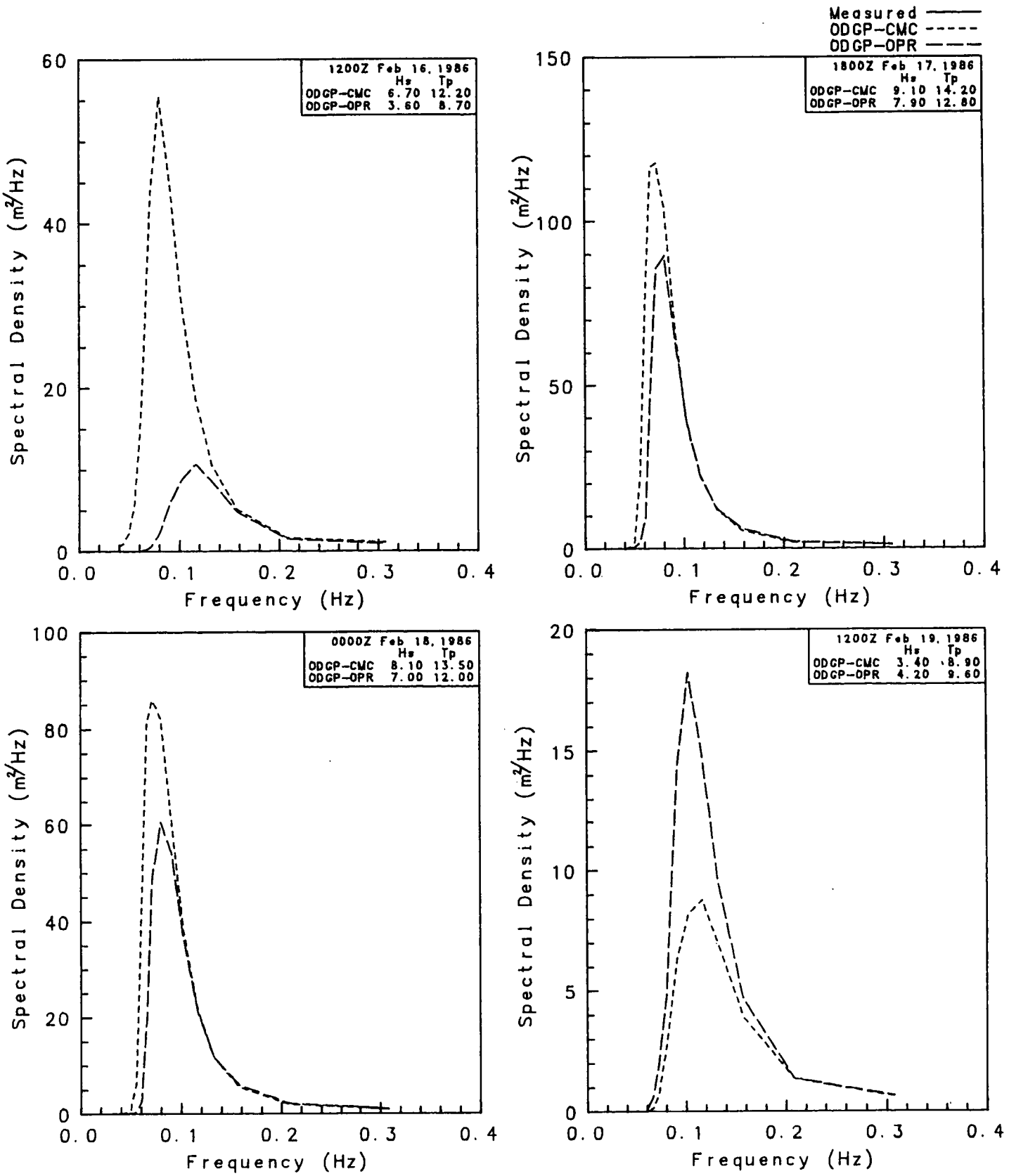

Measured V.S. Model Spectra
Storm Event 4
Noaa Buoy Data – Site 11 Noaa Bouy 44004
00 Hour Analysis

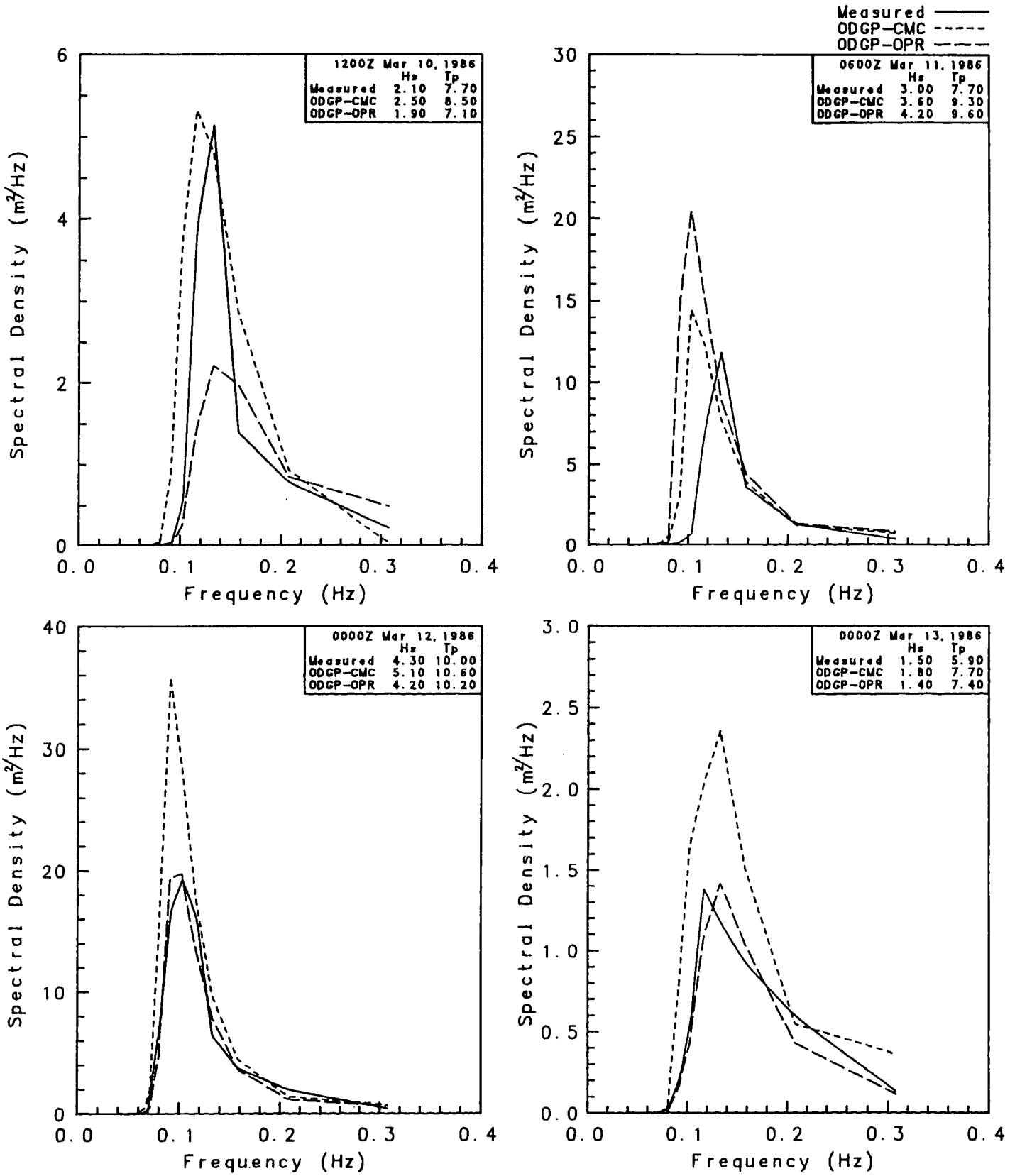

Measured V.S. Model Spectra
Storm Event 4
Waverider Data – Site 21a Rowan Gorilla 1
00 Hour Analysis

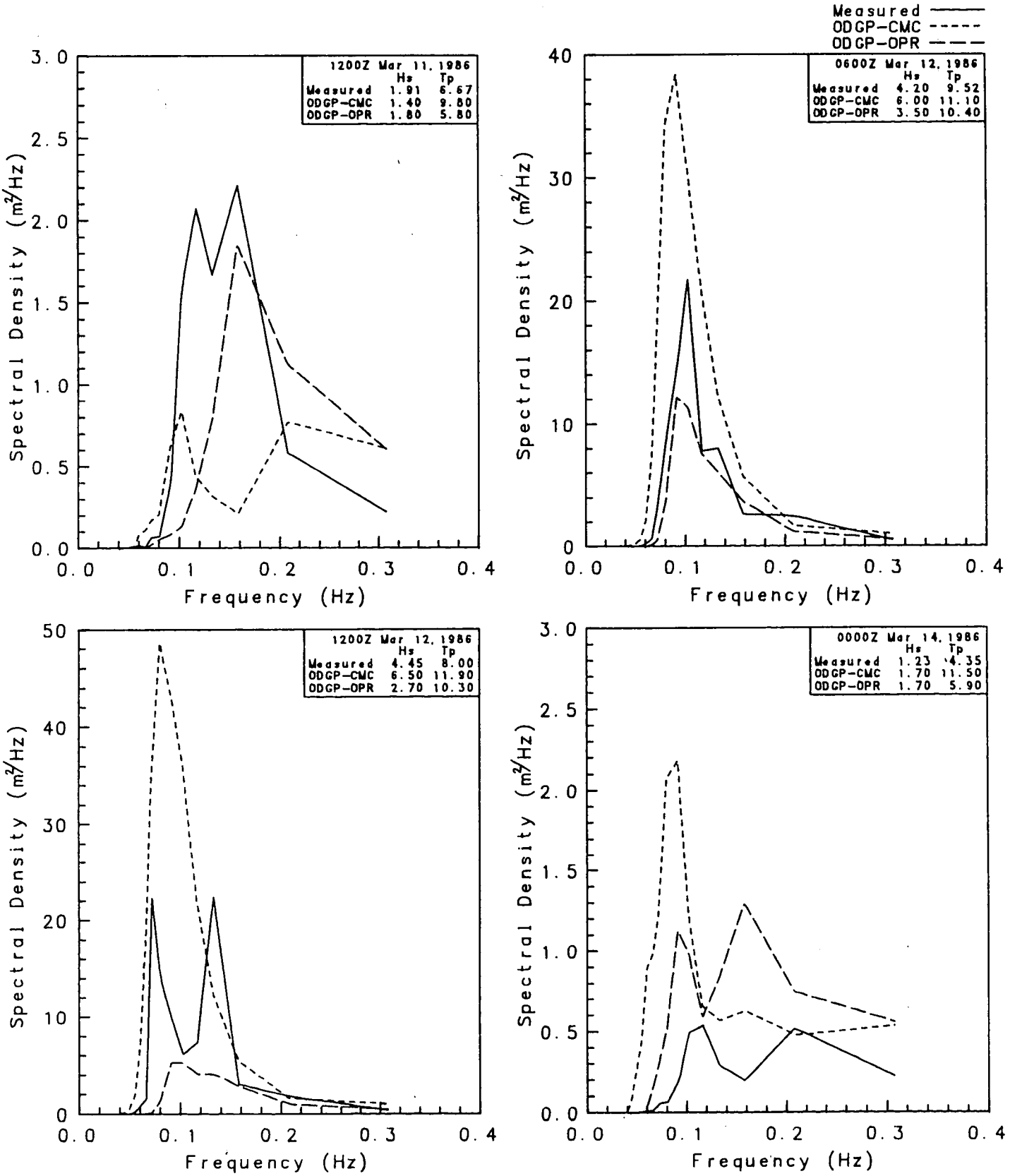

Measured V.S. Model Spectra
Storm Event 4
Waverider Data – Site 21b Sedco 709 & John Shaw
00 Hour Analysis

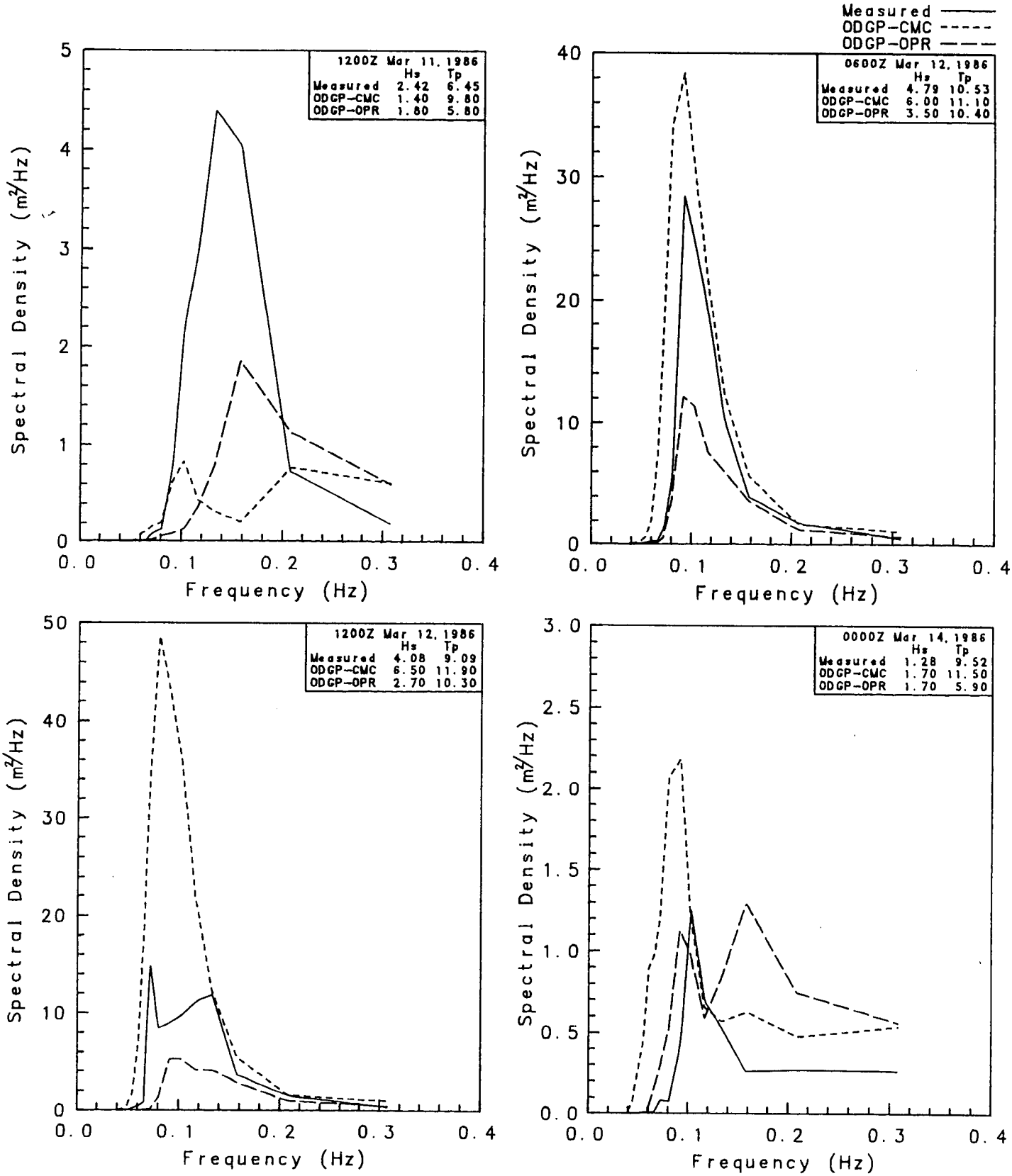

APPENDIX F

STORM CASES

- o Scatter Diagrams and Error Statistics
- o Wind Field Plots (CMC and OPR)

Measured Data vs. Model Predictions

Selected Storms - January 15, 1986 to March 16, 1986

ODGP-OPR - All Deep Water Sites

00 Hour Analysis

Number of Points: 358
Correlation Coeffecient: 0.813

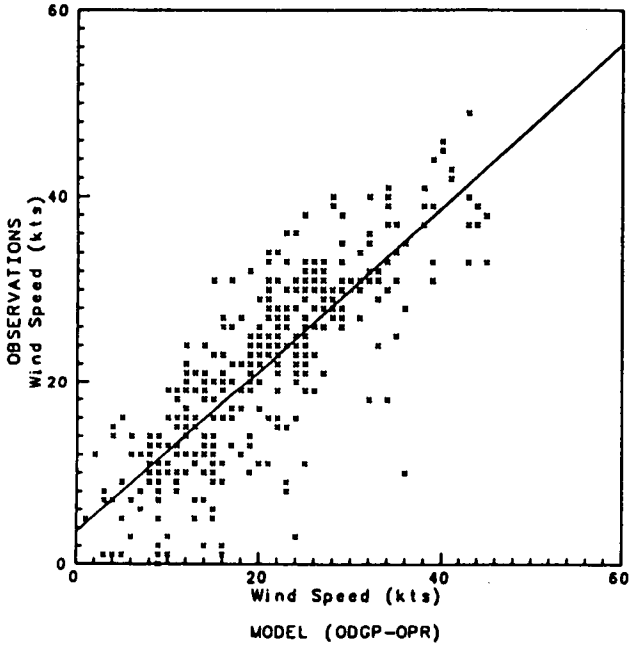

Measured Data vs. Model Predictions

Selected Storms - January 15, 1986 to March 16, 1986

ODGP-CMC - All Deep Water Sites

00 Hour Analysis

Number of Points: 358
Correlation Coeffecient: 0.781

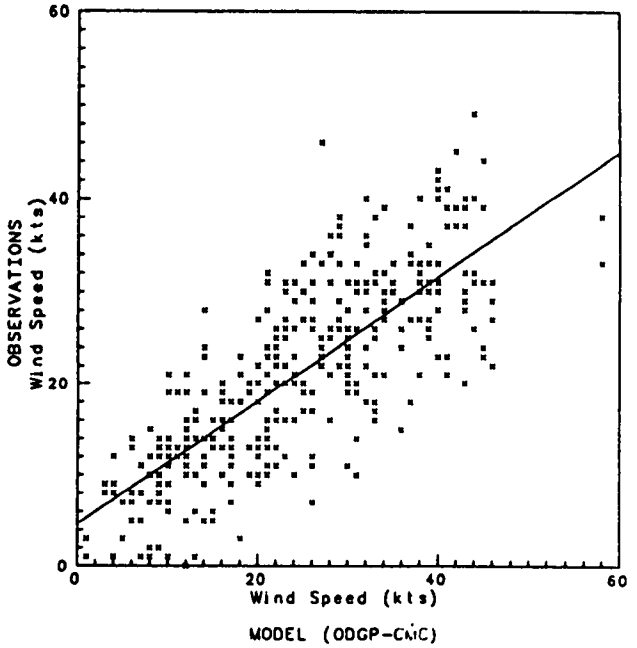

00 Hour Analysis

Number of Points: 374
Correlation Coeffecient: 0.833

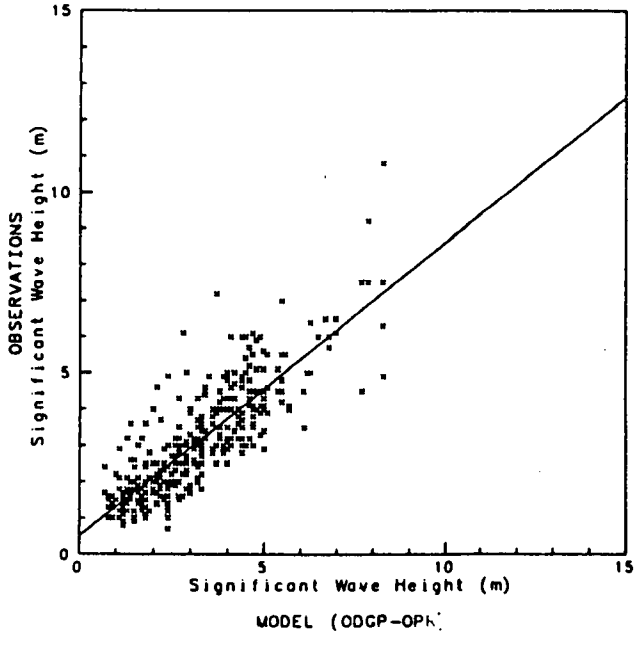

00 Hour Analysis

Number of Points: 374
Correlation Coeffecient: 0.669

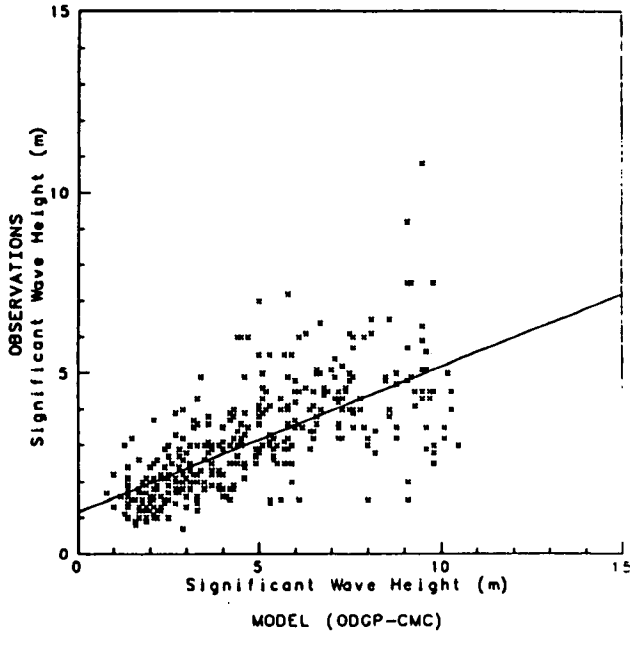

Measured Data vs. Model Predictions

Selected Storms - January 15, 1986 to March 16, 1986

ODGP-OPR - All Deep Water Sites

12 Hour Forecast

Number of Points: 358
Correlation Coeffecient: 0.720

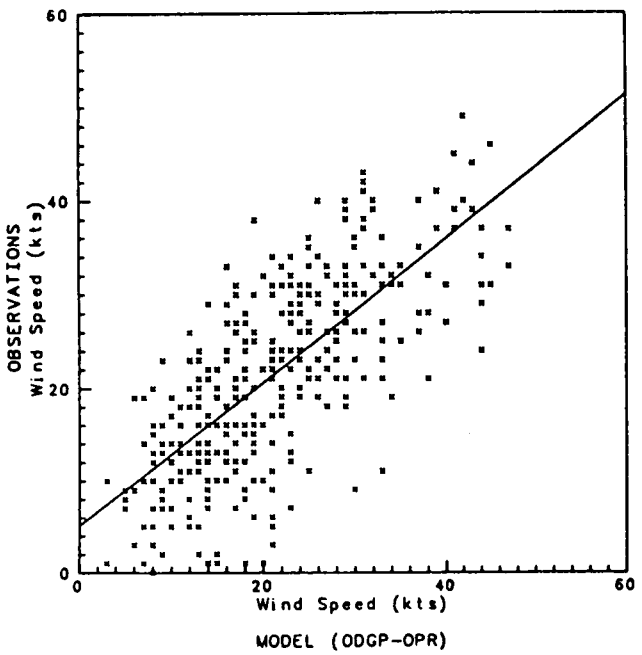

Measured Data vs. Model Predictions

Selected Storms - January 15, 1986 to March 16, 1986

ODGP-CMC - All Deep Water Sites

12 Hour Forecast

Number of Points: 358
Correlation Coeffecient: 0.766

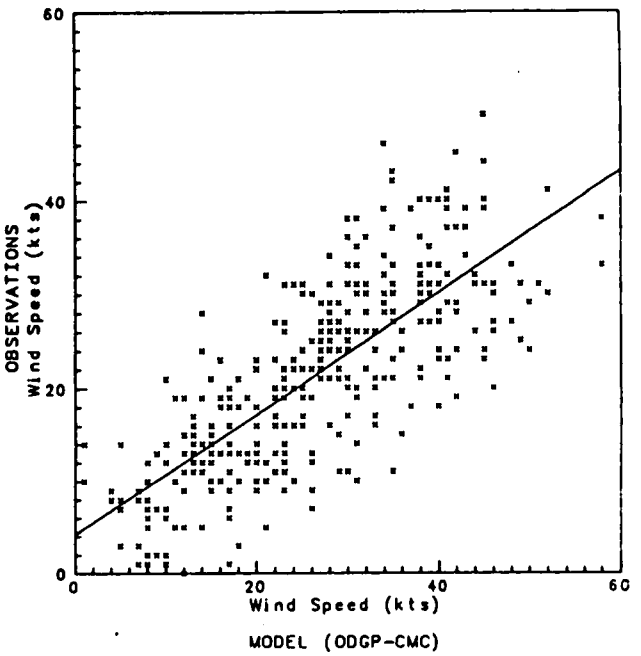

12 Hour Forecast

Number of Points: 374
Correlation Coeffecient: 0.812

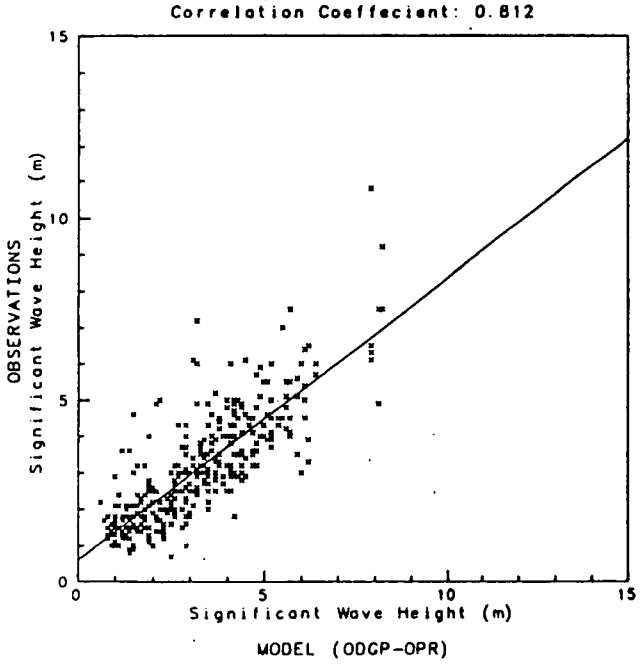

12 Hour Forecast

Number of Points: 374
Correlation Coeffecient: 0.674

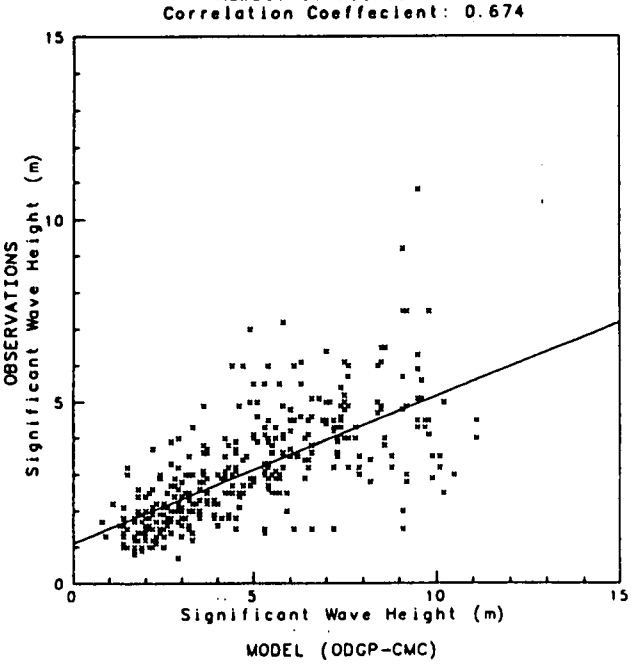

Measured Data vs. Model Predictions

Selected Storms - January 15, 1986 to March 16, 1986

ODGP-OPR - All Deep Water Sites

24 Hour Forecast

Number of Points: 358

Correlation Coeffecient: 0.725

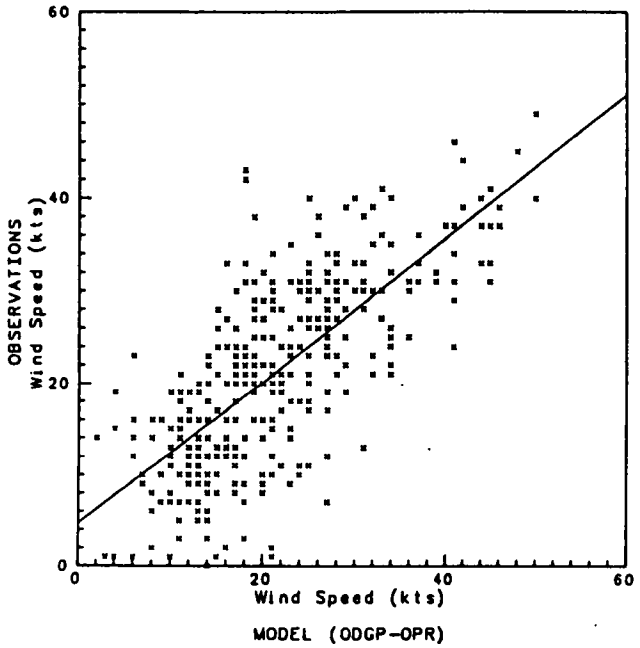

Measured Data vs. Model Predictions

Selected Storms - January 15, 1986 to March 16, 1986

ODGP-CMC - All Deep Water Sites

24 Hour Forecast

Number of Points: 358

Correlation Coeffecient: 0.702

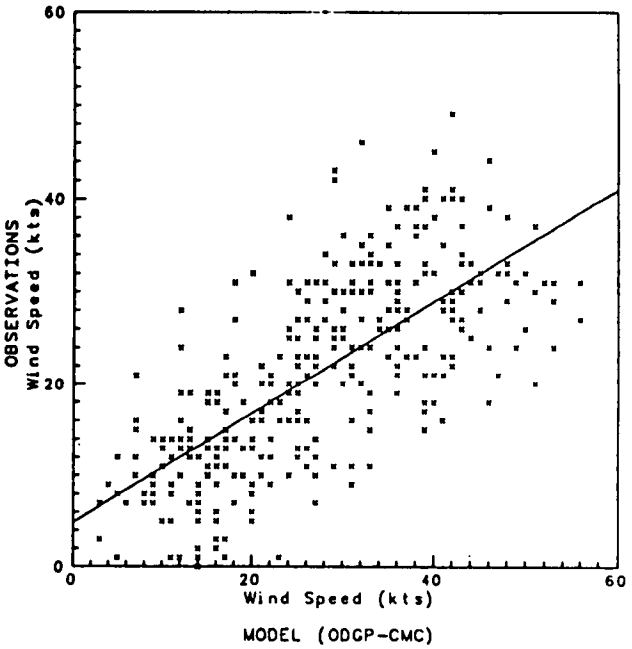

24 Hour Forecast

Number of Points: 374

Correlation Coeffecient: 0.783

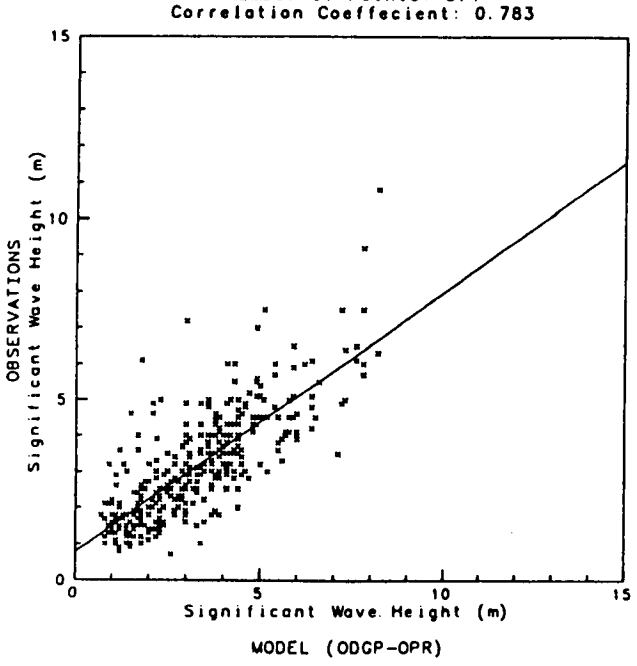

24 Hour Forecast

Number of Points: 374

Correlation Coeffecient: 0.650

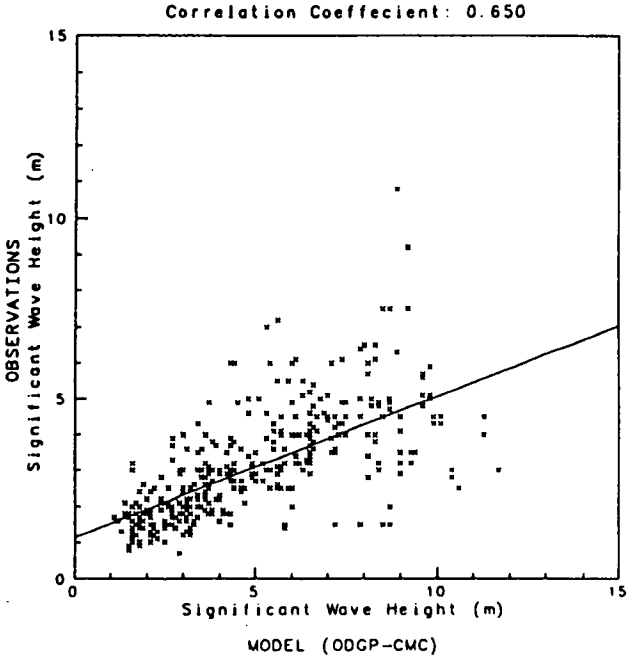

Measured Data vs. Model Predictions

Selected Storms - January 15, 1986 to March 16, 1986

ODGP-OPR - All Deep Water Sites

36 Hour Forecast

Number of Points: 358
Correlation Coeffecient: 0.658

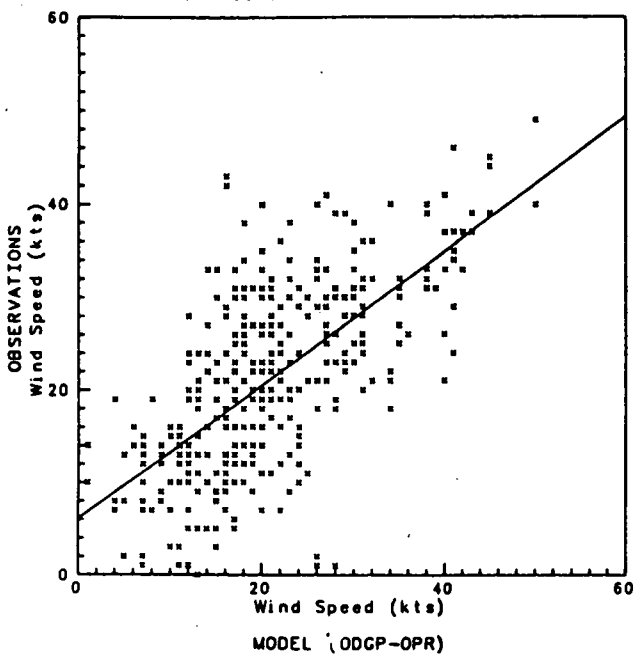

Measured Data vs. Model Predictions

Selected Storms - January 15, 1986 to March 16, 1986

ODGP-CMC - All Deep Water Sites

36 Hour Forecast

Number of Points: 358
Correlation Coeffecient: 0.647

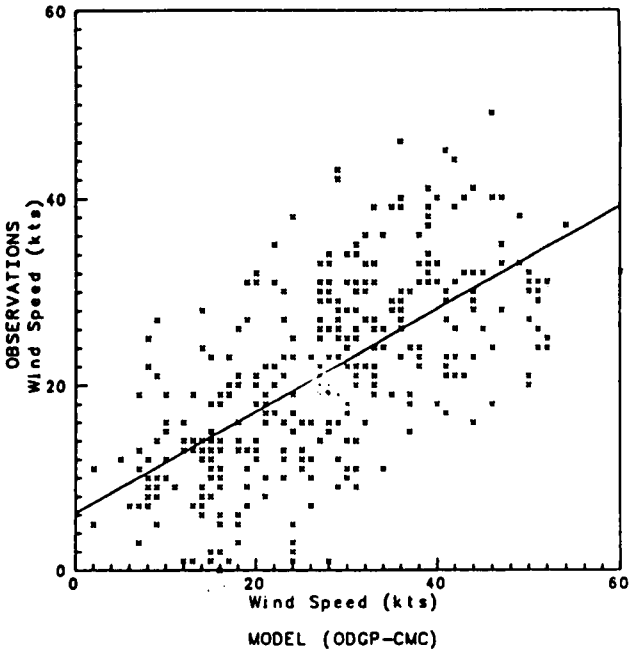

36 Hour Forecast

Number of Points: 374
Correlation Coeffecient: 0.741

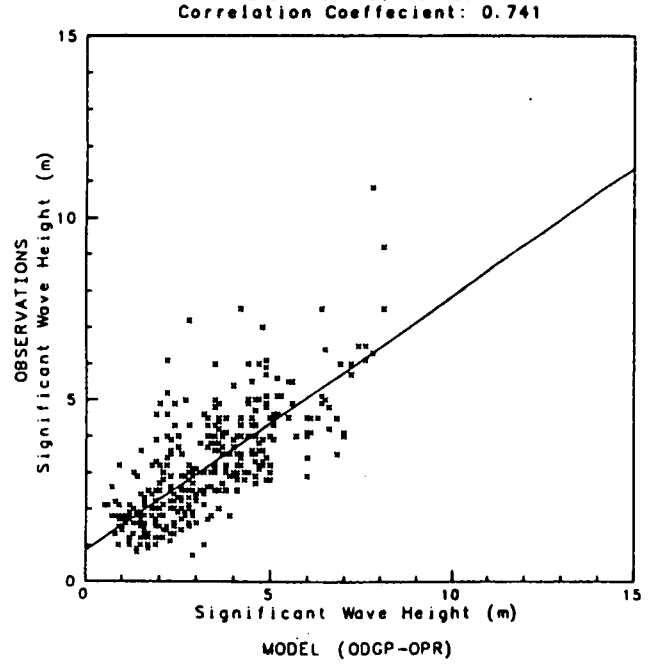

36 Hour Forecast

Number of Points: 374
Correlation Coeffecient: 0.637

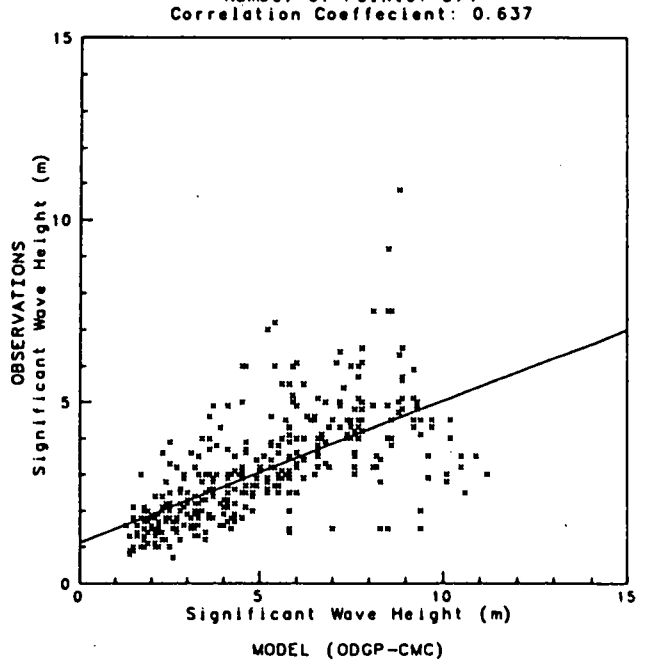

Measured Data vs. Model Predictions

Selected Storms - January 15, 1986 to March 16, 1986

ODGP-OPR - All Deep Water Sites

48 Hour Forecast

Number of Points: 358
Correlation Coeffecient: 0.583

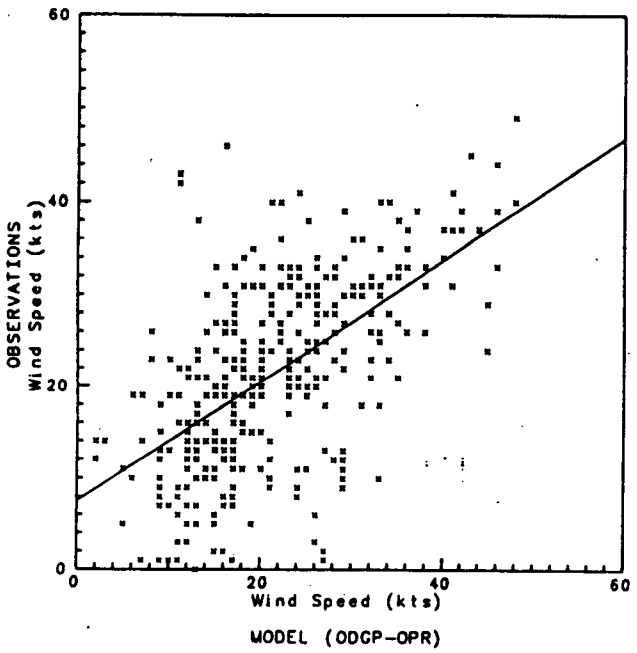

Measured Data vs. Model Predictions

Selected Storms - January 15, 1986 to March 16, 1986

ODGP-CMC - All Deep Water Sites

48 Hour Forecast

Number of Points: 358
Correlation Coeffecient: 0.589

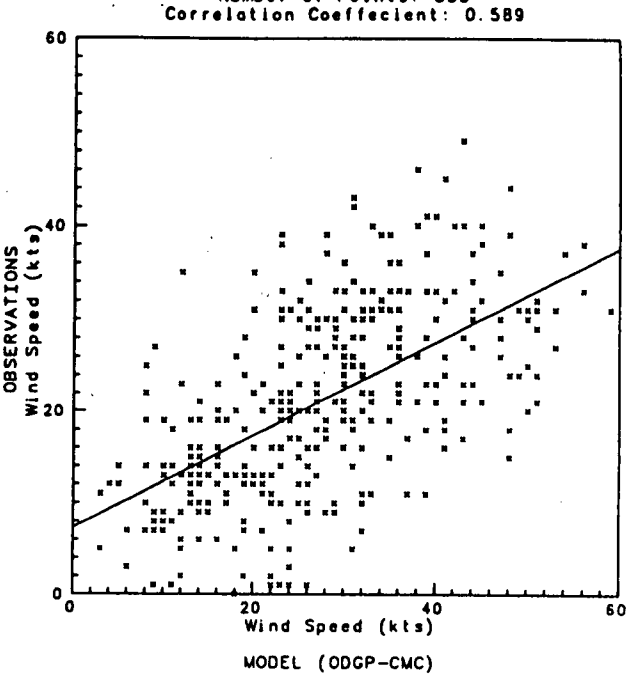

48 Hour Forecast

Number of Points: 374
Correlation Coeffecient: 0.736

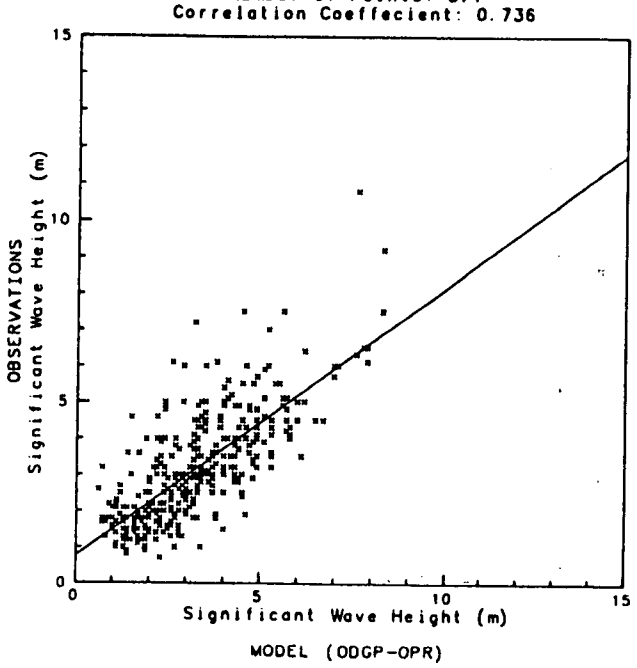

48 Hour Forecast

Number of Points: 374
Correlation Coeffecient: 0.613

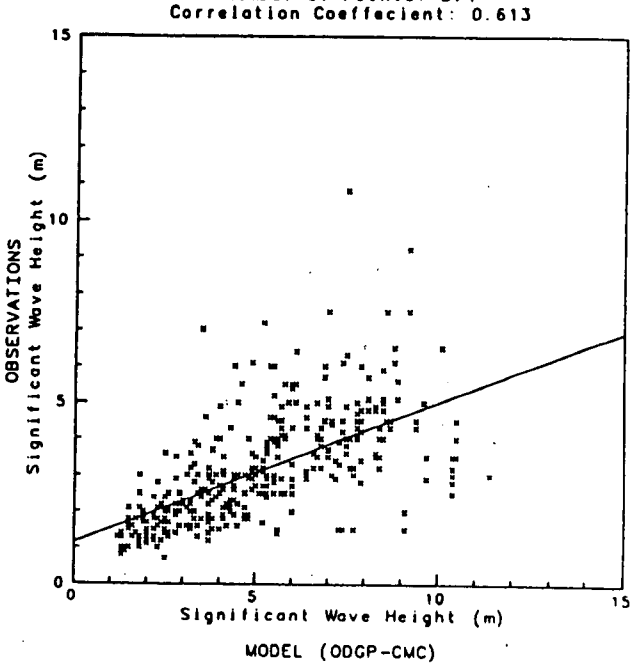

Measured Data vs. Model Predictions
Selected Storms - January 15, 1986 to March 16, 1986
ODGP-OPR - All Deep Water Sites
00 Hour Analysis
Number of Points: 221
Correlation Coeffecient: 0.635

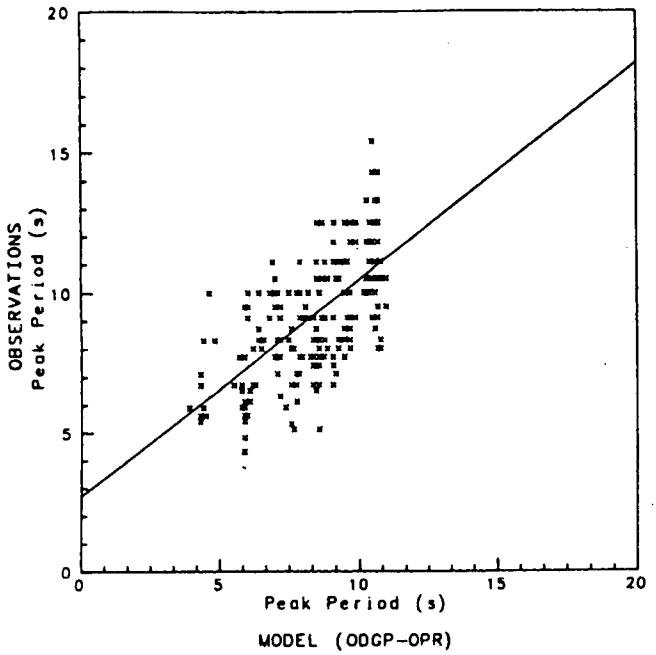

Measured Data vs. Model Predictions
Selected Storms - January 15, 1986 to March 16, 1986
ODGP-CMC - All Deep Water Sites
00 Hour Analysis
Number of Points: 221
Correlation Coeffecient: 0.716

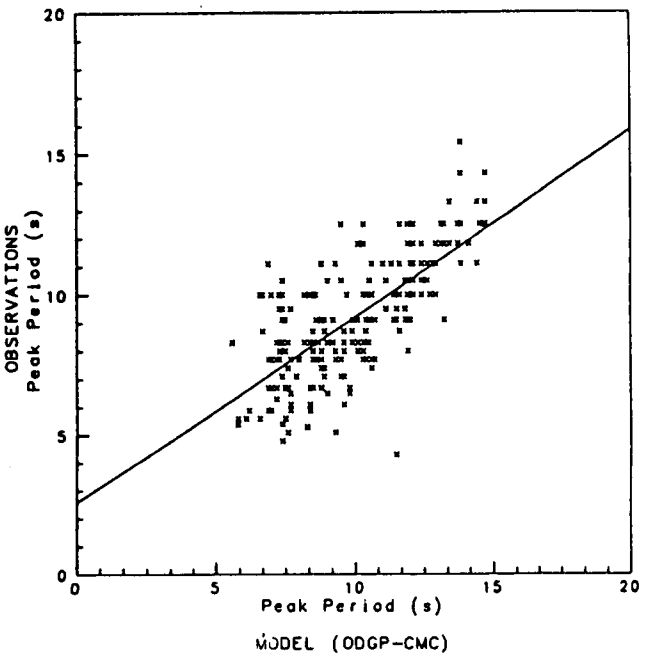

Measured Data vs. Model Predictions
Selected Storms - January 15, 1986 to March 16, 1986
ODGP-OPR - All Deep Water Sites
12 Hour Forecast
Number of Points: 221
Correlation Coeffecient: 0.608

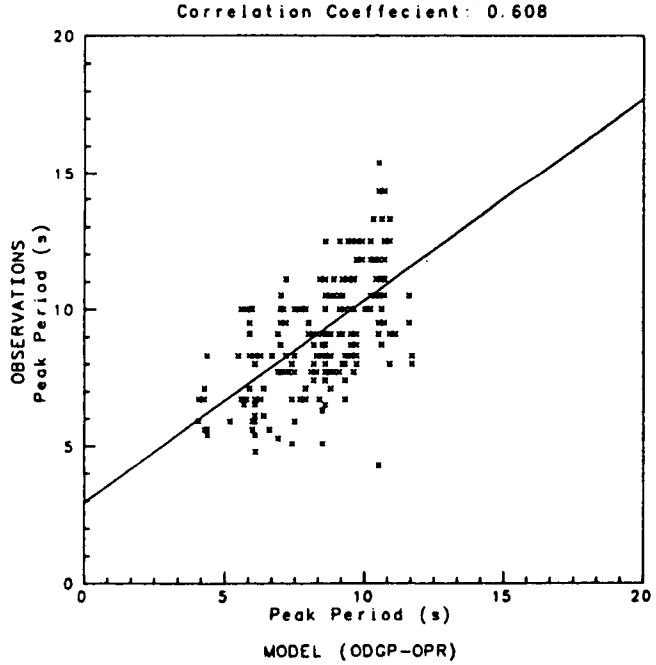

Measured Data vs. Model Predictions
Selected Storms - January 15, 1986 to March 16, 1986
ODGP-CMC - All Deep Water Sites
12 Hour Forecast
Number of Points: 221
Correlation Coeffecient: 0.708

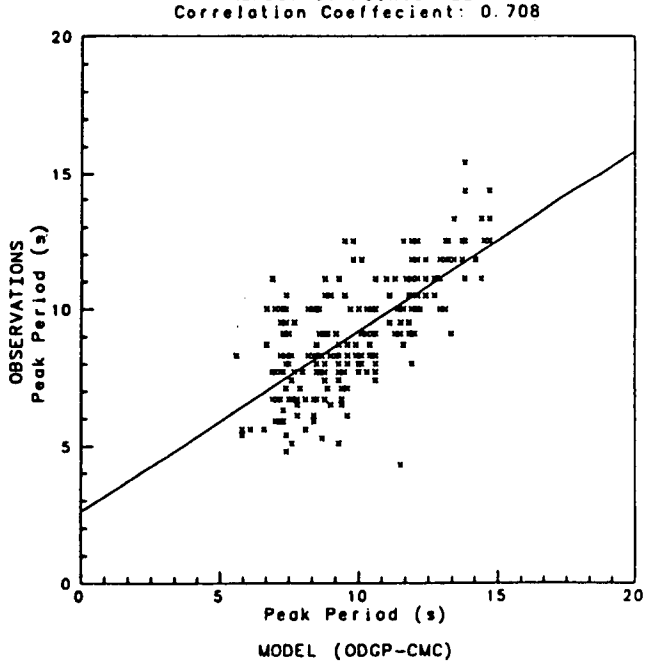

Measured Data vs. Model Predictions
Selected Storms - January 15, 1986 to March 16, 1986
ODGP-OPR - All Deep Water Sites
24 Hour Forecast
Number of Points: 221
Correlation Coeffecient: 0.552

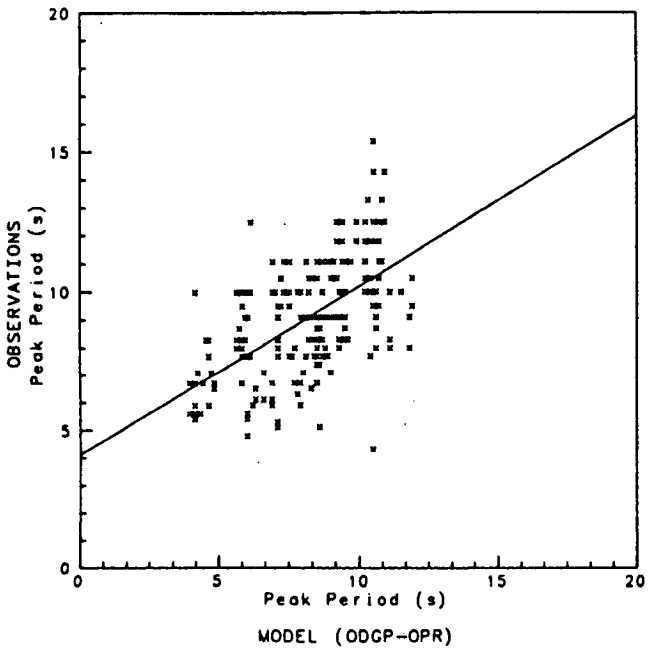

Measured Data vs. Model Predictions
Selected Storms - January 15, 1986 to March 16, 1986
ODGP-CMC - All Deep Water Sites
24 Hour Forecast
Number of Points: 221
Correlation Coeffecient: 0.696

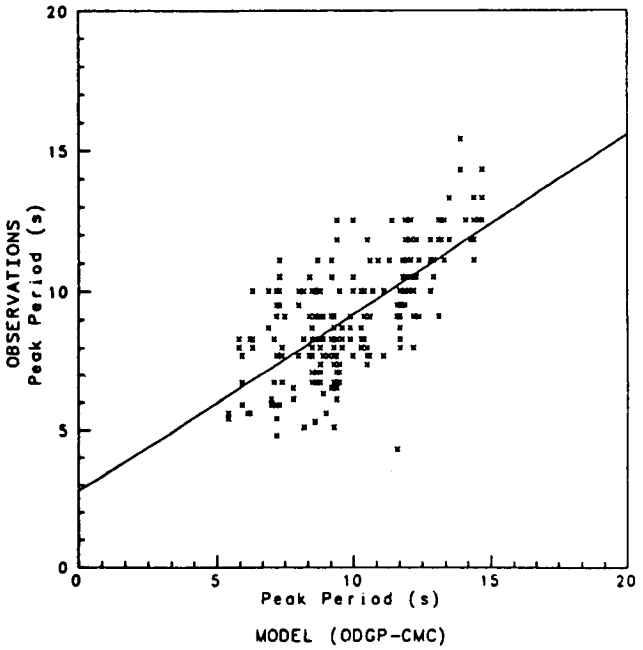

Measured Data vs. Model Predictions
Selected Storms - January 15, 1986 to March 16, 1986
ODGP-OPR - All Deep Water Sites
36 Hour Forecast
Number of Points: 221
Correlation Coeffecient: 0.556

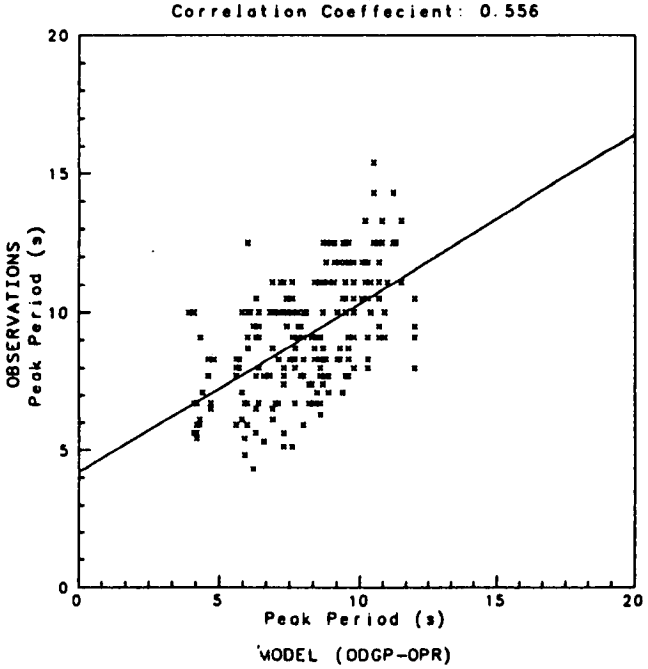

Measured Data vs. Model Predictions
Selected Storms - January 15, 1986 to March 16, 1986
ODGP-CMC - All Deep Water Sites
36 Hour Forecast
Number of Points: 221
Correlation Coeffecient: 0.672

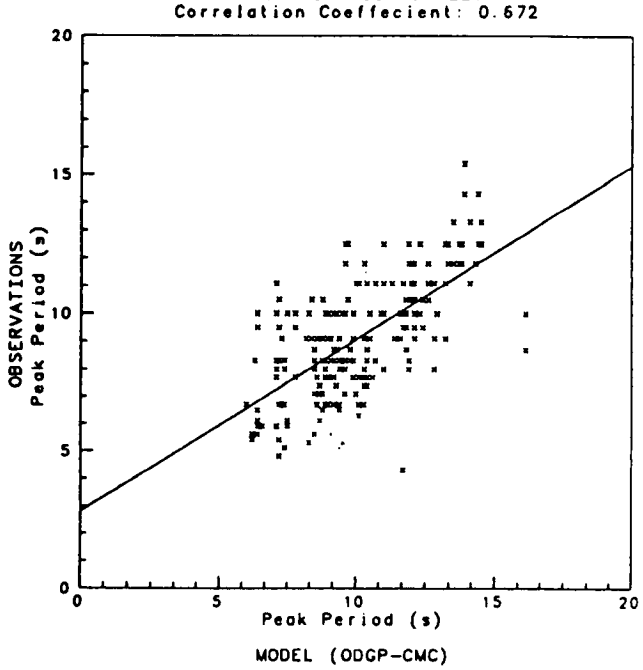

Measured Data vs. Model Predictions

Selected Storms - January 15, 1986 to March 16, 1986

ODGP-OPR - All Deep Water Sites

48 Hour Forecast

Number of Points: 221

Correlation Coeffecient: 0.473

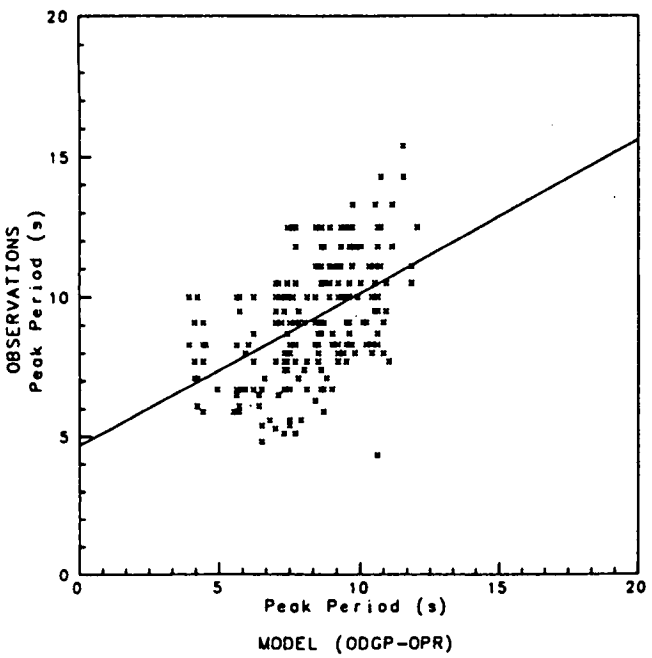

Measured Data vs. Model Predictions

Selected Storms - January 15, 1986 to March 16, 1986

ODGP-CMC - All Deep Water Sites

48 Hour Forecast

Number of Points: 221

Correlation Coeffecient: 0.637

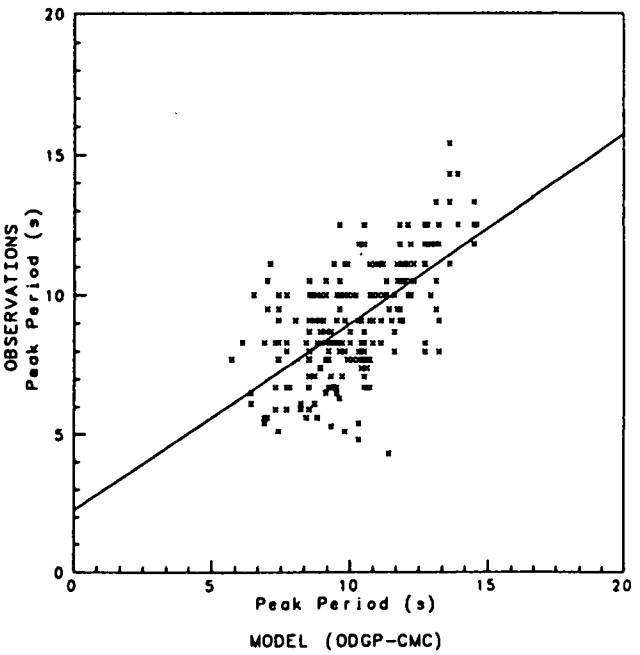

Measured Data vs. Model Predictions
Selected Storms - January 15, 1986 to March 16, 1986
METOC - All Deep Water Sites
00 Hour Analysis
Number of Points: 158
Correlation Coeffecient: 0.843

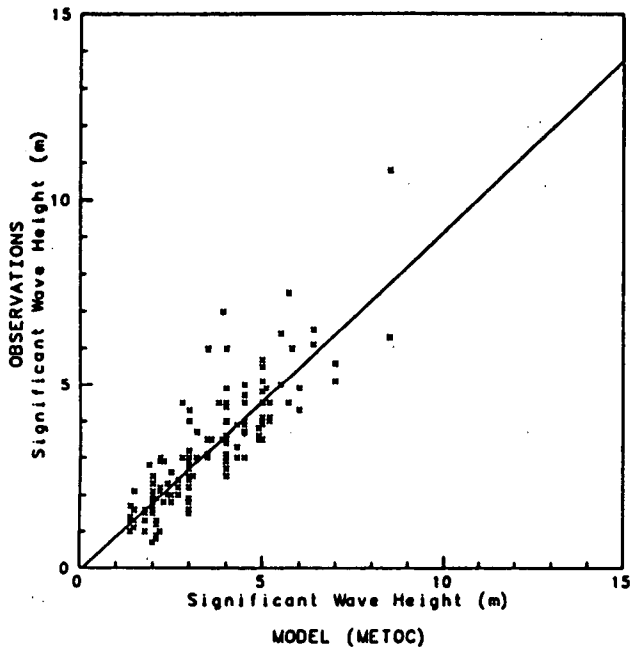

Measured Data vs. Model Predictions
Selected Storms - January 15, 1986 to March 16, 1986
METOC - All Deep Water Sites
12 Hour Forecast
Number of Points: 156
Correlation Coeffecient: 0.601

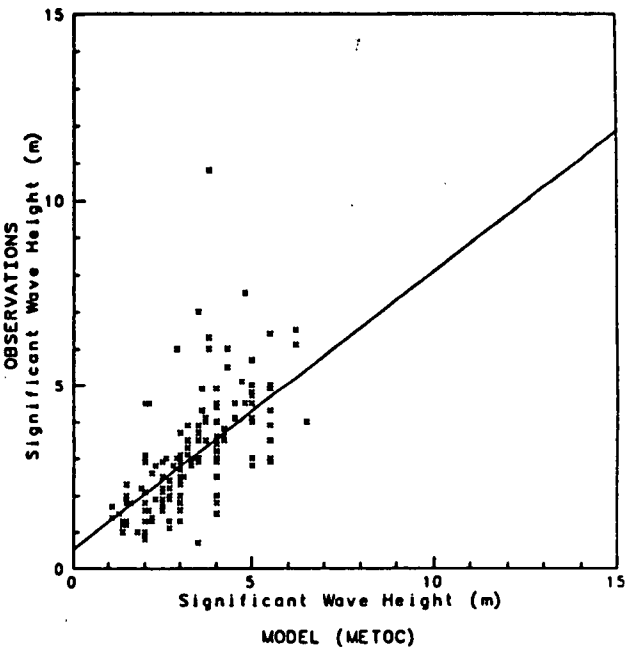

METOC - All Deep Water Sites
24 Hour Forecast
Number of Points: 162
Correlation Coeffecient: 0.609

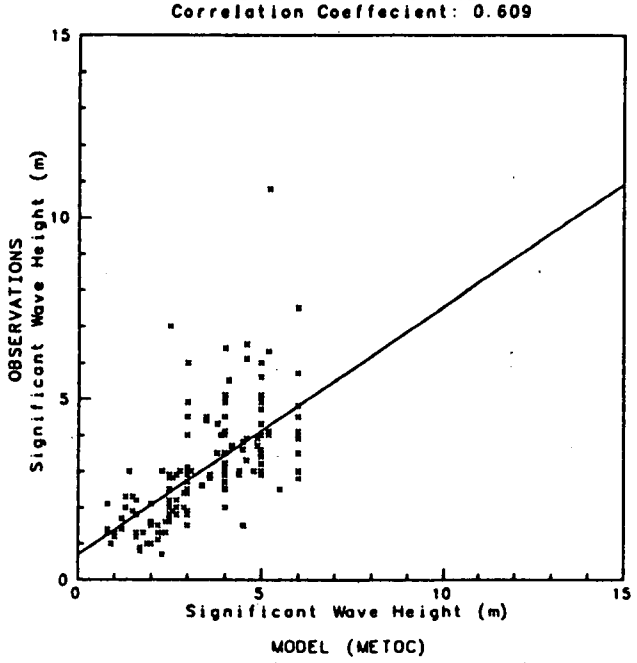

METOC - All Deep Water Sites
36 Hour Forecast
Number of Points: 162
Correlation Coeffecient: 0.571

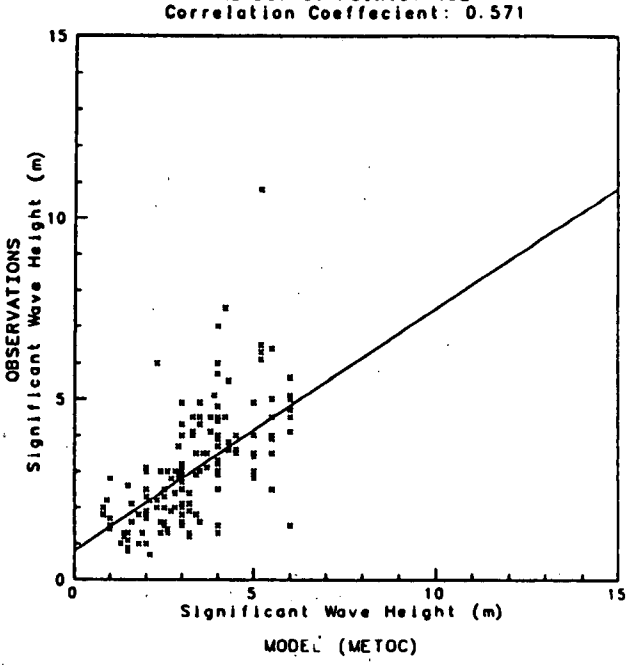

All Deep Water Sites

PROG.	VAR	MODEL	NUMBER OF POINTS	AVERAGE OBS.VALUES	STANDARD DEVIATION	AVERAGE MODEL VAL.	STANDARD DEVIATION	MEAN ERROR	ABSOLUTE MEAN ERROR	RMSE
00 hr	HS	ODGP-OPR	374	3.11	1.51	3.21	1.55	0.10	0.67	0.89
		ODGP-CMC	374	3.11	1.51	4.85	2.51	1.74	1.91	2.56
		METOC	158	3.11	1.54	3.45	1.41	0.34	0.69	0.90
	TP	ODGP-OPR	221	9.19	2.10	8.37	1.72	-0.81	1.52	1.86
		ODGP-CMC	221	9.19	2.10	9.98	2.27	0.79	1.52	1.83
	WS	ODGP-OPR	358	21.23	10.09	20.05	9.34	-1.18	4.81	6.10
		ODGP-CMC	358	21.23	10.09	24.69	11.74	3.46	6.33	8.16
	WD	ODGP-OPR	357	229.04	80.21	233.83	72.93	4.79	28.29	52.79
		ODGP-CMC	357	229.04	80.21	237.83	71.09	8.79	27.25	57.38
12 hr	HS	ODGP-OPR	374	3.11	1.51	3.23	1.58	0.12	0.72	0.96
		ODGP-CMC	374	3.11	1.51	4.91	2.51	1.80	1.96	2.59
		METOC	156	3.08	1.53	3.38	1.23	0.30	0.90	1.30
	TP	ODGP-OPR	221	9.19	2.10	8.45	1.73	-0.74	1.53	1.88
		ODGP-CMC	221	9.19	2.10	9.98	2.25	0.79	1.54	1.85
	WS	ODGP-OPR	358	21.23	10.09	20.94	9.45	-0.30	5.85	7.34
		ODGP-CMC	358	21.23	10.09	26.27	11.95	5.04	7.10	9.24
	WD	ODGP-OPR	357	229.04	80.21	231.04	74.47	2.00	37.76	73.80
		ODGP-CMC	357	229.04	80.21	240.77	70.83	11.73	28.82	58.19
24 hr	HS	ODGP-OPR	374	3.11	1.51	3.24	1.64	0.13	0.79	1.05
		ODGP-CMC	374	3.11	1.51	5.01	2.49	1.91	2.04	2.69
		METOC	162	3.08	1.54	3.48	1.37	0.40	1.03	1.36
	TP	ODGP-OPR	221	9.19	2.10	8.32	1.90	-0.87	1.71	2.09
		ODGP-CMC	221	9.19	2.10	10.02	2.29	0.83	1.61	1.91
	WS	ODGP-OPR	358	21.23	10.09	21.41	9.47	0.18	5.73	7.27
		ODGP-CMC	358	21.23	10.09	27.22	11.79	5.99	8.08	10.47
	WD	ODGP-OPR	357	229.04	80.21	233.90	75.51	4.86	35.90	63.93
		ODGP-CMC	357	229.04	80.21	243.54	68.85	14.49	37.10	72.36
36 hr	HS	ODGP-OPR	374	3.11	1.51	3.23	1.59	0.12	0.86	1.12
		ODGP-CMC	374	3.11	1.51	5.08	2.45	1.97	2.10	2.73
		METOC	162	3.08	1.54	3.40	1.31	0.33	1.03	1.37
	TP	ODGP-OPR	221	9.19	2.10	8.17	1.90	-1.02	1.77	2.15
		ODGP-CMC	221	9.19	2.10	10.18	2.26	1.00	1.65	2.03
	WS	ODGP-OPR	358	21.23	10.09	21.00	9.17	-0.23	6.40	8.04
		ODGP-CMC	358	21.23	10.09	27.38	11.93	6.15	8.68	11.23
	WD	ODGP-OPR	357	229.04	80.21	231.99	77.40	2.95	41.55	71.71
		ODGP-CMC	357	229.04	80.21	234.19	75.42	5.15	42.87	79.81
48 hr	HS	ODGP-OPR	374	3.11	1.51	3.18	1.51	0.07	0.86	1.10
		ODGP-CMC	374	3.11	1.51	5.08	2.39	1.97	2.11	2.73
	TP	ODGP-OPR	221	9.19	2.10	8.25	1.81	-0.94	1.81	2.23
		ODGP-CMC	221	9.19	2.10	10.28	1.98	1.09	1.68	2.06
	WS	ODGP-OPR	358	21.23	10.09	20.96	8.98	-0.27	6.68	8.77
		ODGP-CMC	358	21.23	10.09	27.63	11.80	6.39	9.29	11.90

All Shallow Water Sites

PROG.	VAR	MODEL	NUMBER OF POINTS	AVERAGE OBS.VALUES	STANDARD DEVIATION	AVERAGE MODEL VAL.	STANDARD DEVIATION	MEAN ERROR	ABSOLUTE MEAN ERROR	RMSE
00 hr	HS	ODGP-CMC	217	2.01	1.15	2.49	1.89	0.49	0.78	1.18
	TP	ODGP-CMC	217	9.43	2.33	10.34	2.52	0.90	1.50	2.10
	WS	ODGP-CMC	223	13.19	5.83	18.03	8.43	4.84	6.30	7.90
	WD	ODGP-CMC	223	214.03	91.58	237.44	99.64	23.41	81.64	114.81
12 hr	HS	ODGP-CMC	218	2.01	1.15	2.56	1.90	0.55	0.81	1.19
	TP	ODGP-CMC	218	9.42	2.33	10.36	2.61	0.93	1.55	2.17
	WS	ODGP-CMC	224	13.13	5.87	20.18	9.41	7.05	8.06	10.11
	WD	ODGP-CMC	224	214.25	91.43	240.70	99.48	26.45	89.28	121.03
24 hr	HS	ODGP-CMC	219	2.01	1.15	2.61	1.93	0.60	0.88	1.27
	TP	ODGP-CMC	219	9.41	2.33	10.58	2.39	1.17	1.66	2.28
	WS	ODGP-CMC	226	13.06	5.90	20.62	10.36	7.56	8.92	11.79
	WD	ODGP-CMC	226	214.38	91.66	242.74	98.01	28.36	91.02	120.78
36 hr	HS	ODGP-CMC	219	2.01	1.15	2.64	1.91	0.64	0.96	1.38
	TP	ODGP-CMC	219	9.41	2.33	10.52	2.65	1.11	1.83	2.50
	WS	ODGP-CMC	226	13.06	5.90	20.48	10.60	7.42	9.15	12.24
	WD	ODGP-CMC	226	214.38	91.66	237.51	97.17	23.12	95.73	124.55
48 hr	HS	ODGP-CMC	217	2.00	1.14	2.70	1.88	0.70	1.02	1.43
	TP	ODGP-CMC	217	9.41	2.34	10.48	2.74	1.07	1.96	2.65
	WS	ODGP-CMC	224	13.06	5.90	21.10	10.68	8.04	9.41	13.09
	WD	ODGP-CMC	224	214.59	92.03	254.72	89.03	40.13	94.93	124.59

STORM 1
WIND FIELDS

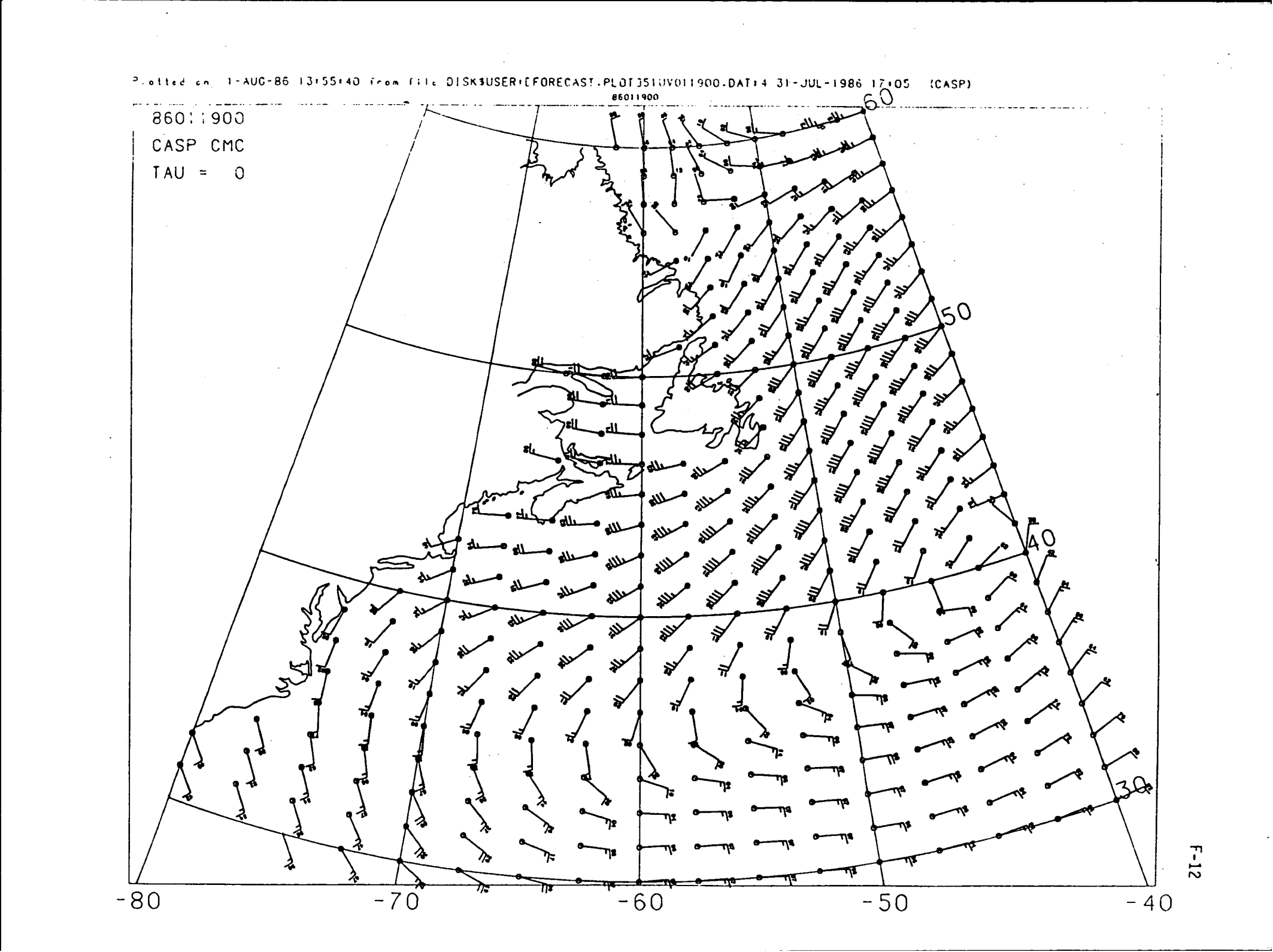
Plotted on 1-AUG-86 13:55:40 from file DISK3USER:[FORECAST.PLOT]SIUV011900.DAT;4 31-JUL-1986 17:05 (CASP)
86011900
86011900
CASP CMC
TAU = 0
60
50
40
30
-80
-70
-60
-50
-40

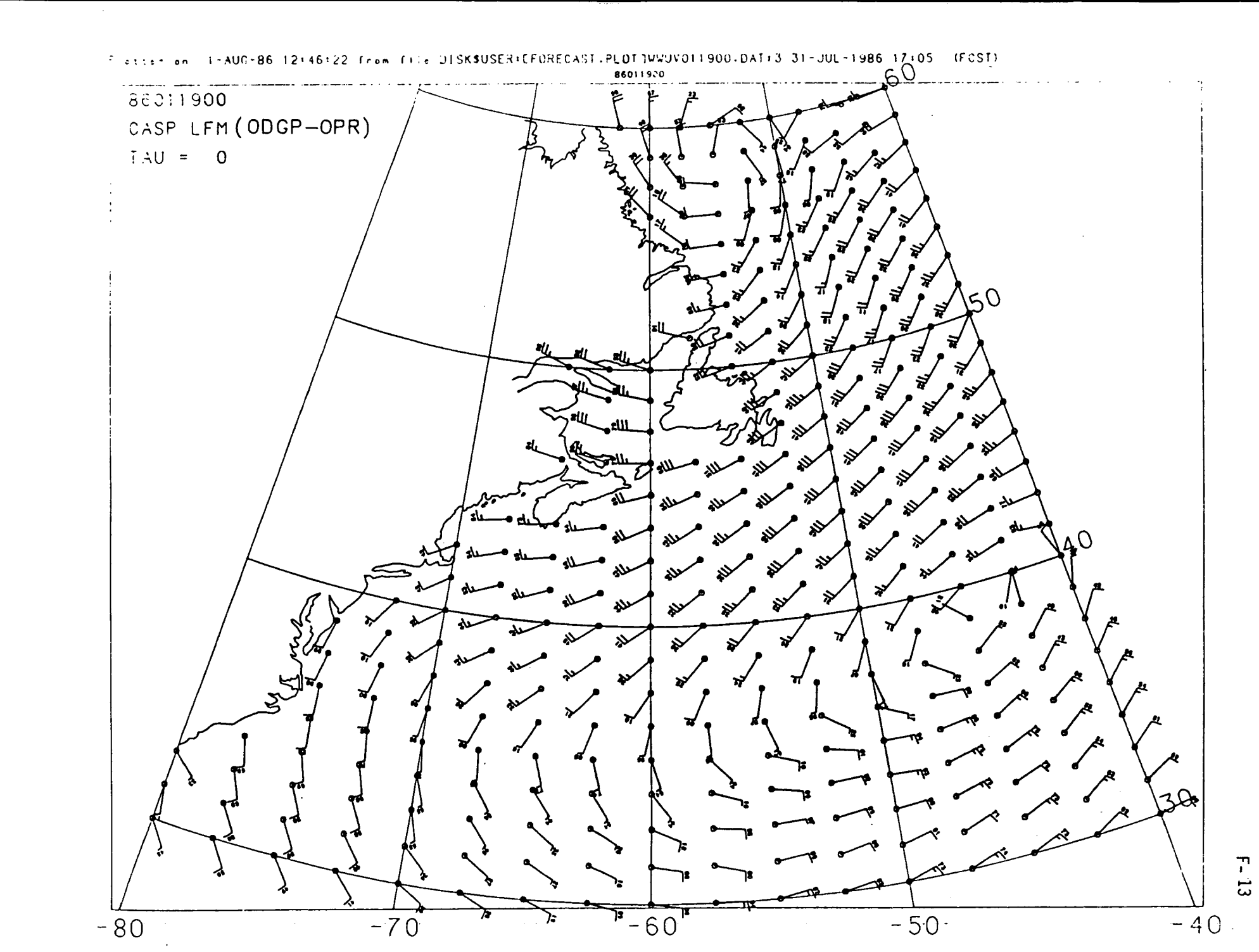
Plotted on 1-AUG-86 12:46:22 from file DISK$USER:[FORECAST.PLOT]WWOV011900.DAT;3 31-JUL-1986 17:05 (FCST)
86011900
86011900
CASP LFM (ODGP-OPR)
TAU = 0
60
50
40
30
-80
-70
-60
-50
-40

Plotted on 13-AUG-86 11:45:23 from file DISK$USER:[FORECAST.PLOT]51UV011900.DAT;4 31-JUL-1986 17:05 and WWUV011900.DAT;3

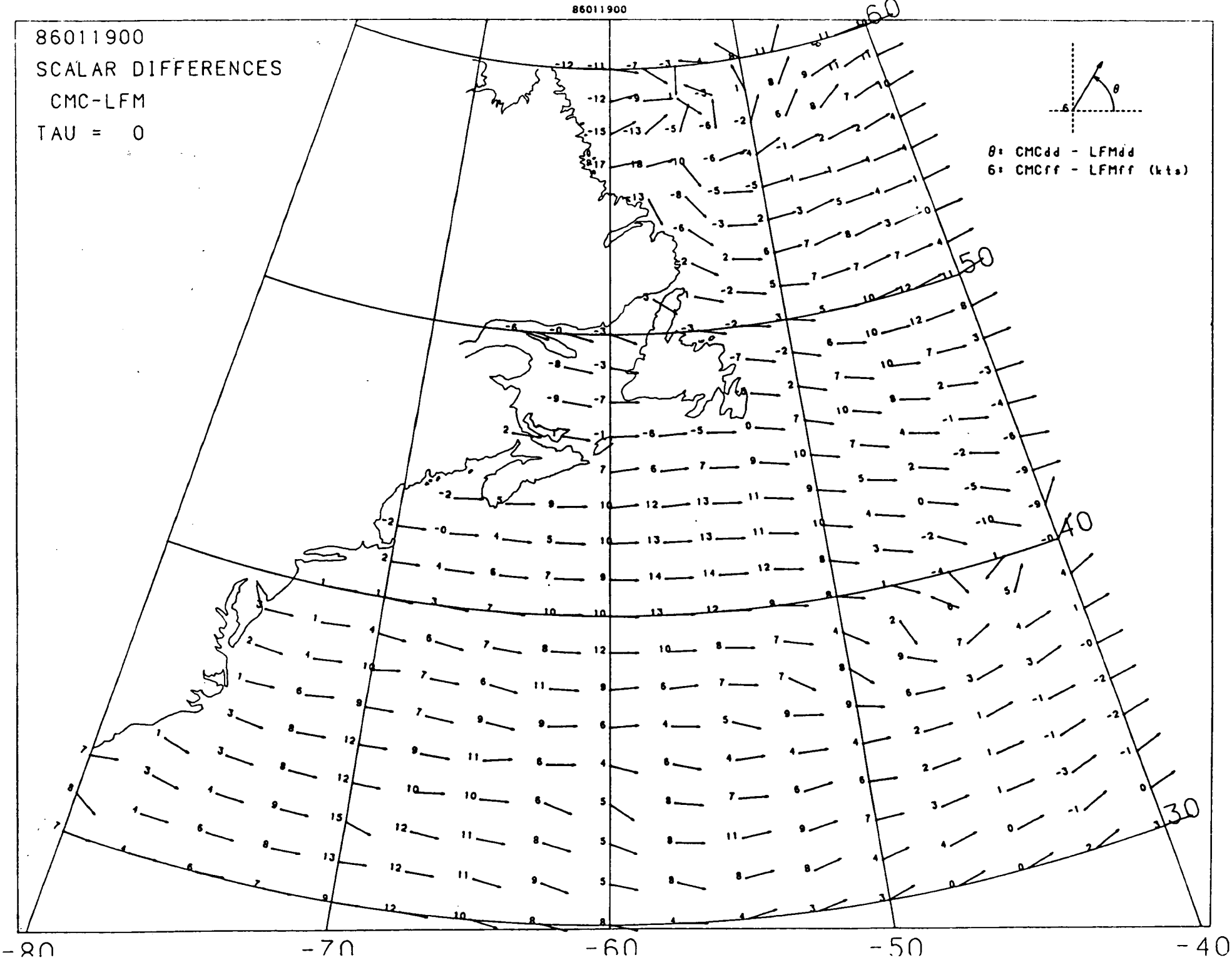

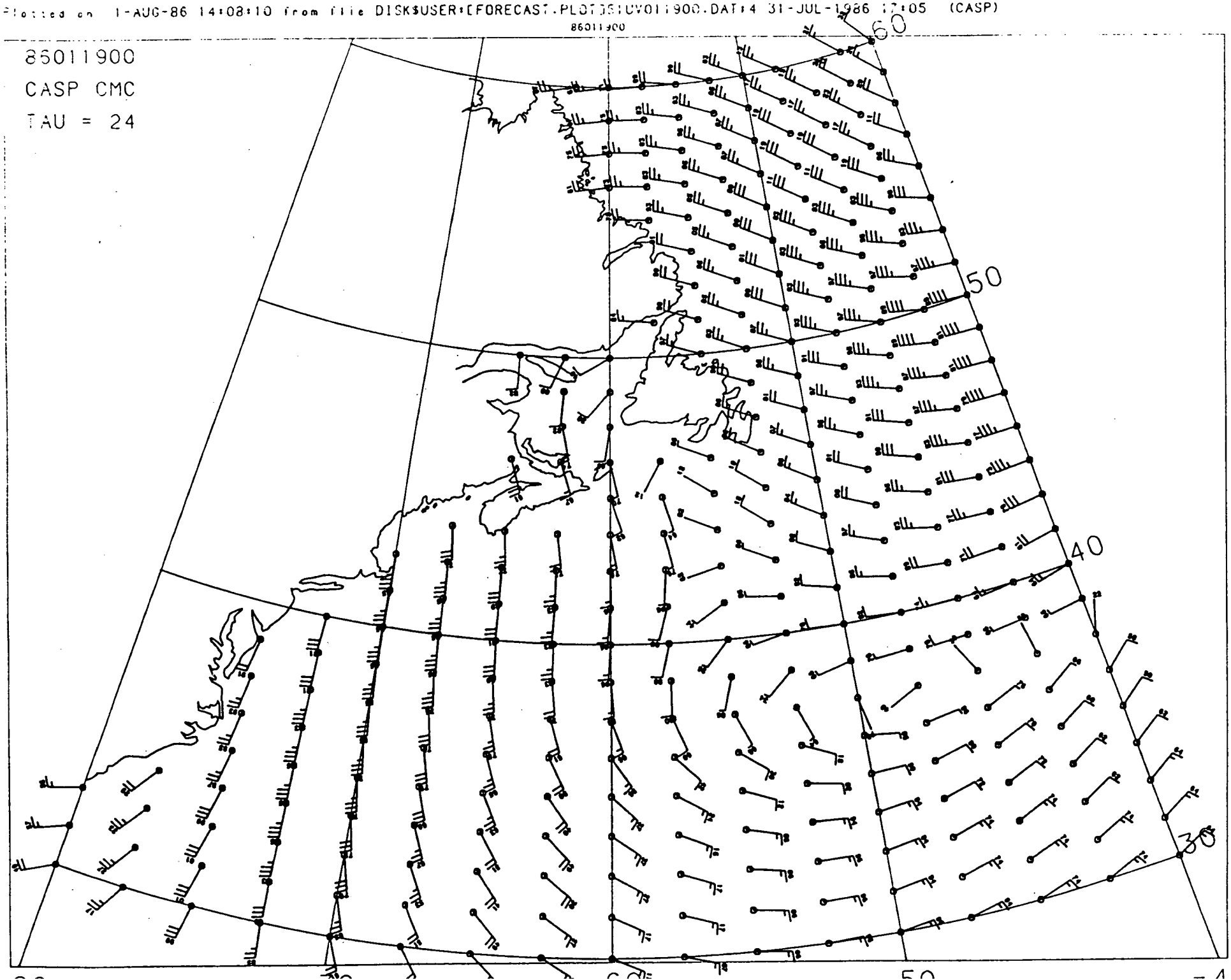
86011900
86011900
CASP CMC
TAU = 24
60
50
40
30
-40

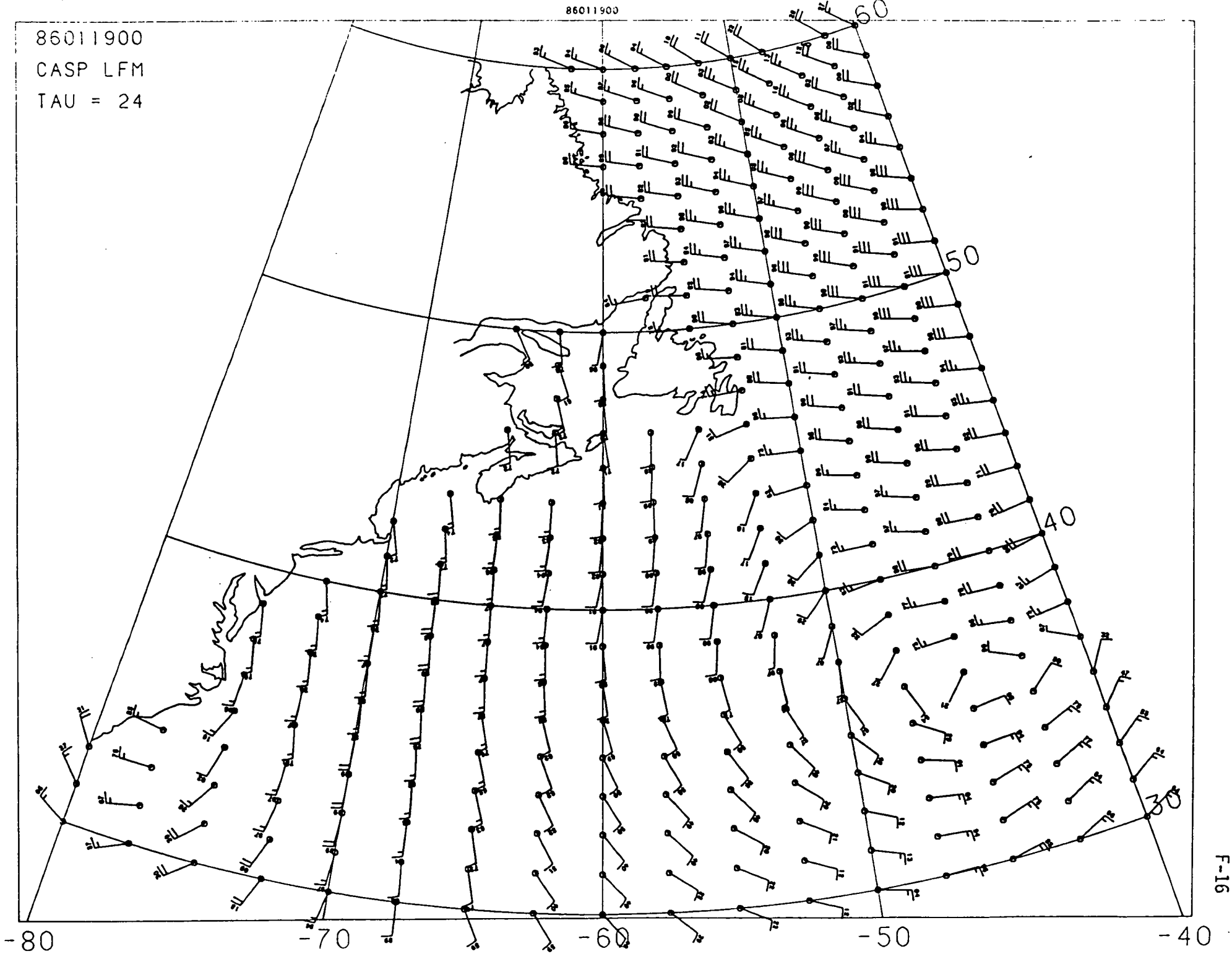
86011900
86011900
CASP LFM
TAU = 24
60
50
40
30
-80
-70
-60
-50
-40

86011900

86011900
SCALAR DIFFERENCES
CMC-LFM
TAU = 24

θ: CMCdd - LFMdd
6: CMCff - LFMff (kts)

60
50
40
30

-80 -70 -60 -50 -40

86012000

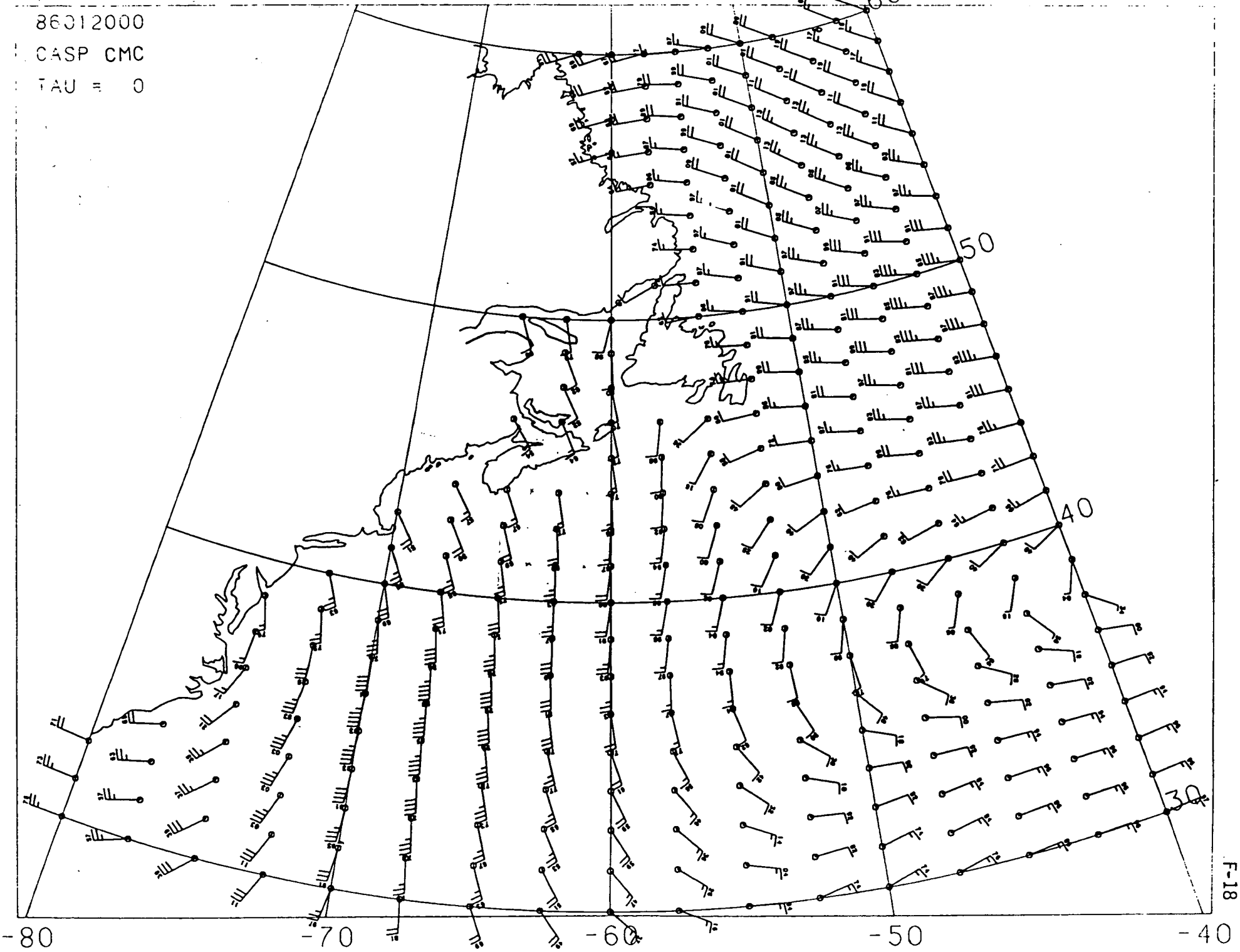

86012000

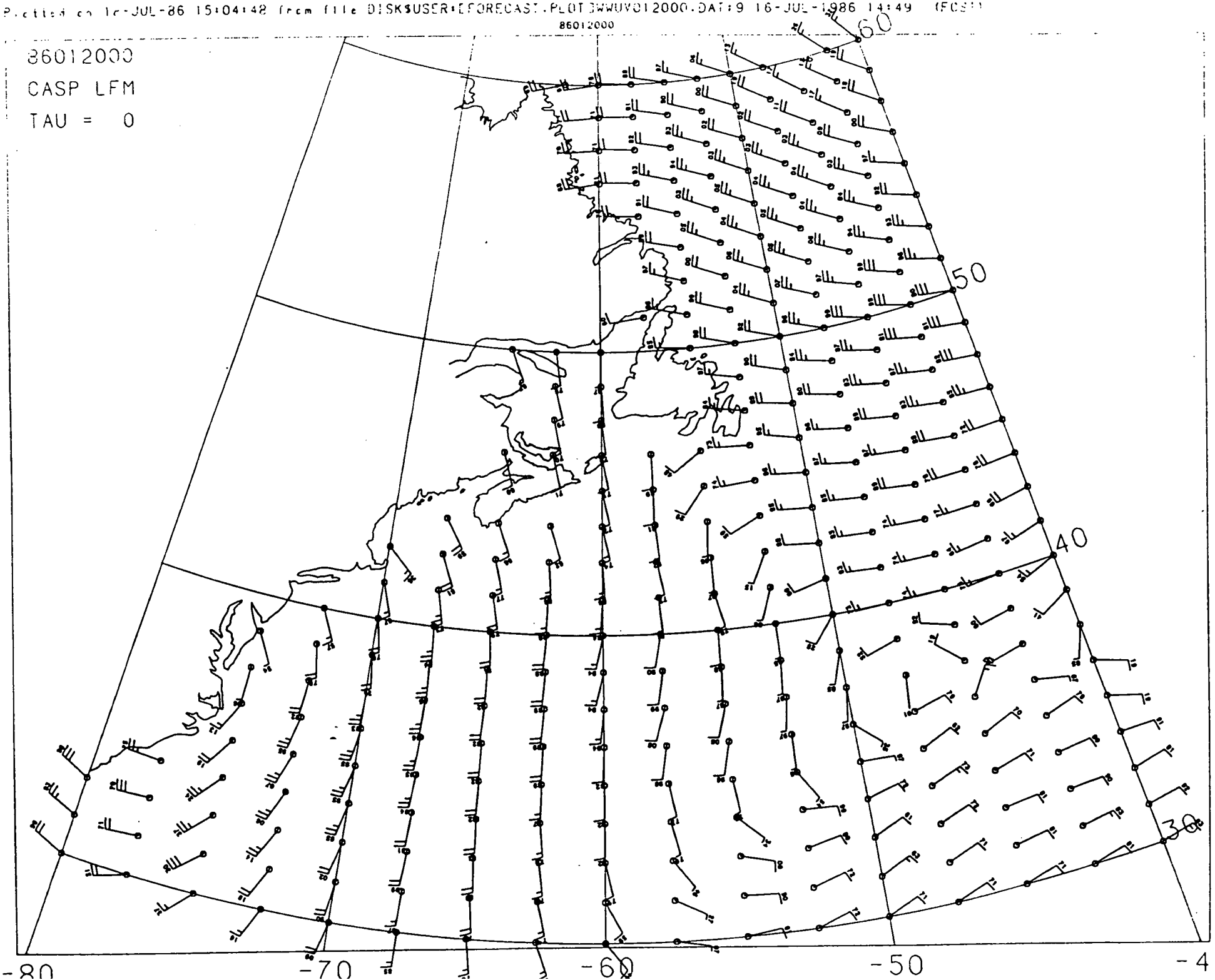

86012000

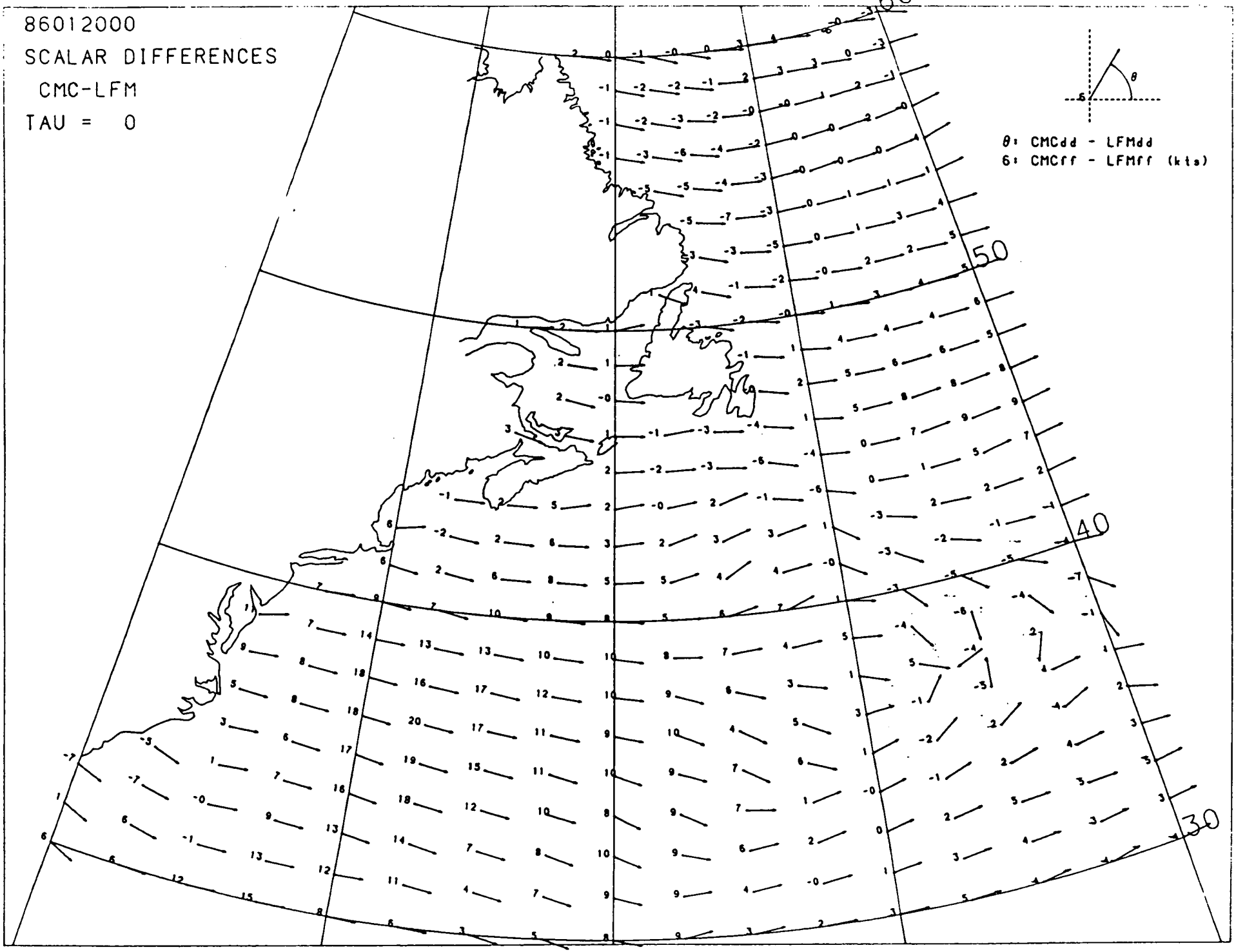
86012000
SCALAR DIFFERENCES
CMC-LFM
TAU = 0
θ: CMCdd - LFMdd
6: CMCff - LFMff (kts)
60
50
40
30
-80
-70
-60
-50
-40

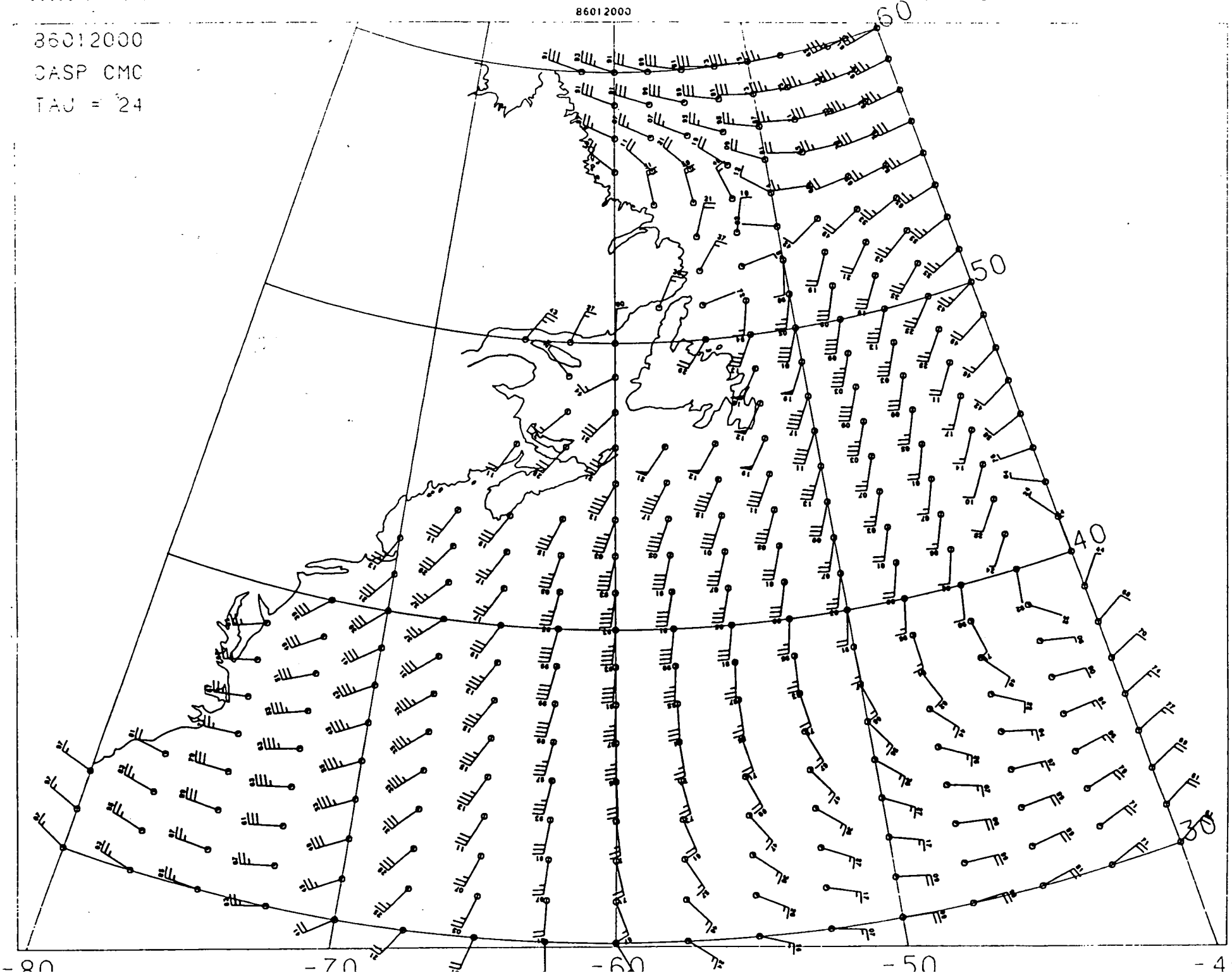
86012000
86012000
CASP CMC
TAU = 24
60
50
40
30
-80
-70
-60
-50
-40

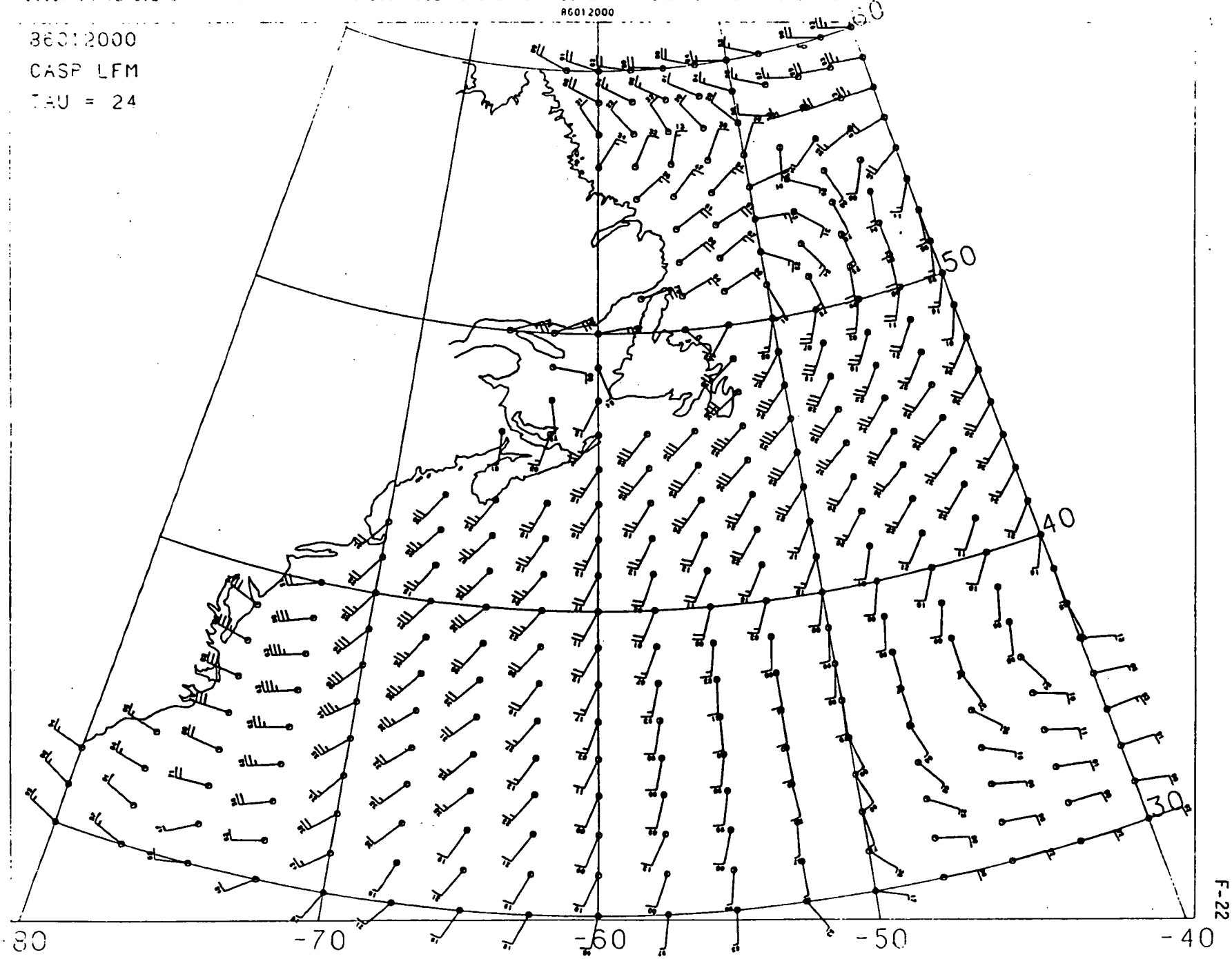
86012000
86012000
CASP LFM
TAU = 24
60
50
40
30
-80
-70
-60
-50
-40

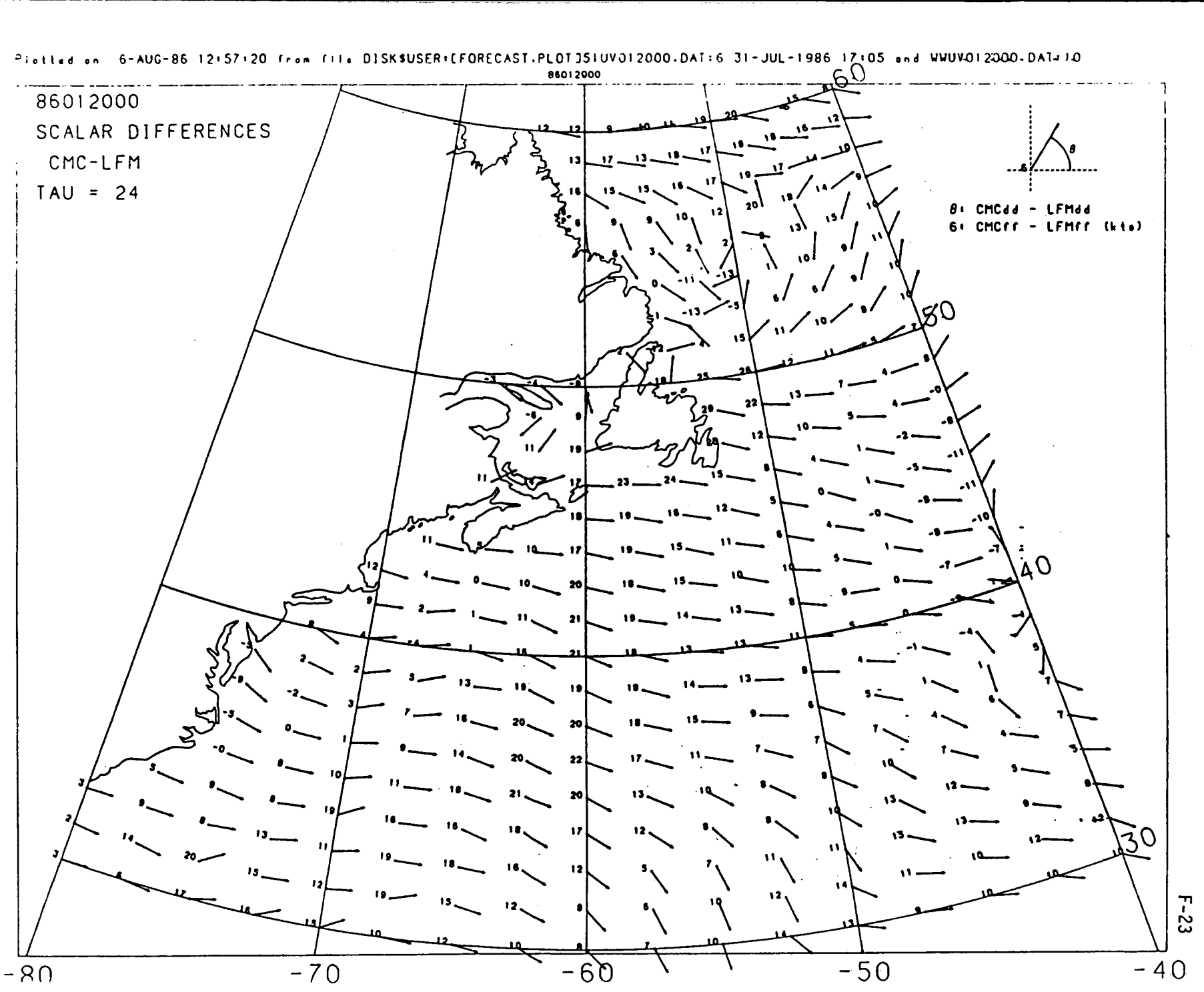
Plotted on 6-AUG-86 12:57:20 from file DISK$USER1:[FORECAST.PLOT]SIUV012000.DAT;6 31-JUL-1986 17:05 and WWUV012000.DAT;10
86012000
86012000
SCALAR DIFFERENCES
CMC-LFM
TAU = 24
θ: CMCdd - LFMdd
6: CMCff - LFMff (kts)
60
50
40
30
-80
-70
-60
-50
-40

STORM 2

86012712
CASP CMC
TAU = 0
50
40
30
-40
-50
-60
-70
-80

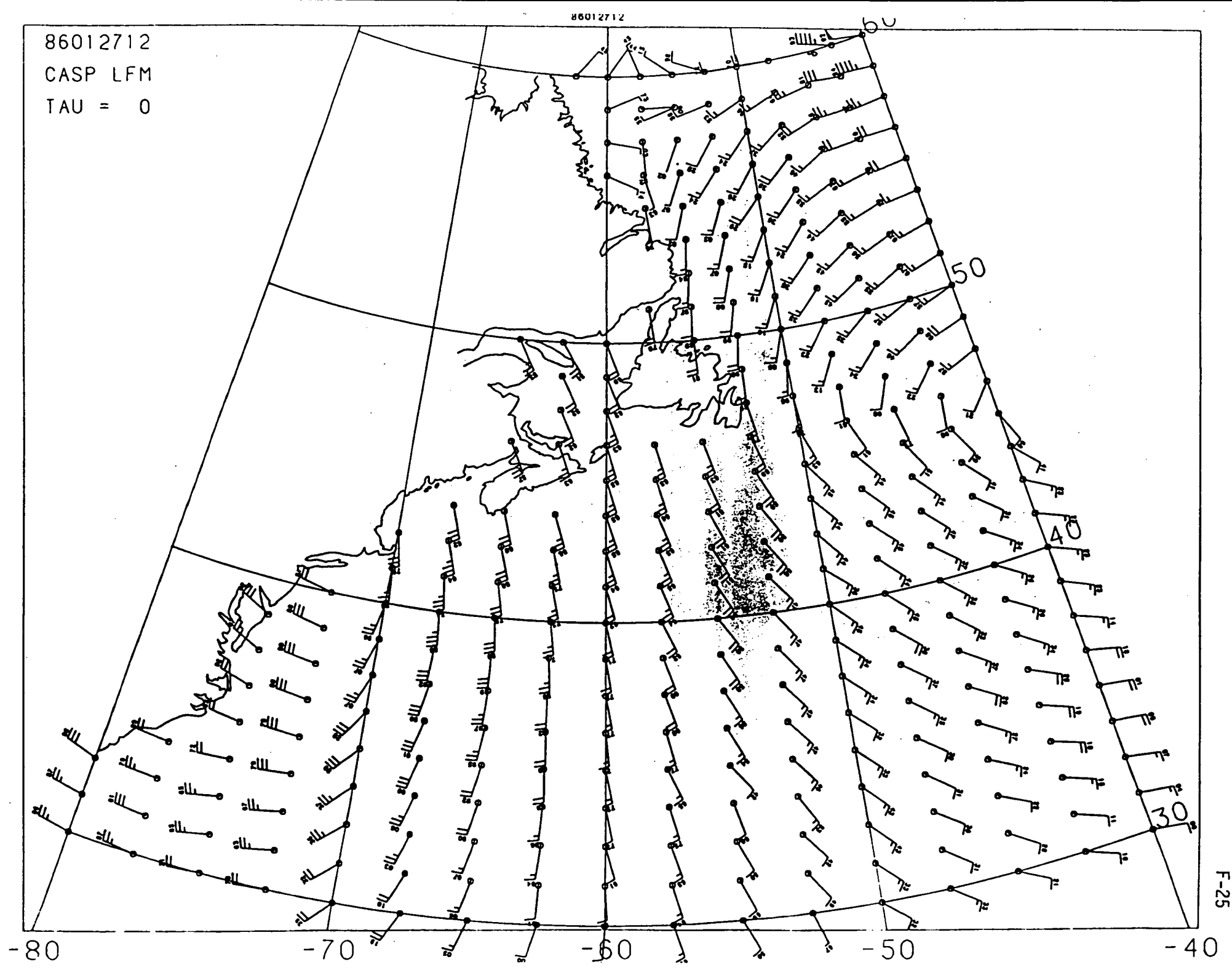
86012712
86012712
CASP LFM
TAU = 0
60
50
40
30
-80
-70
-60
-50
-40

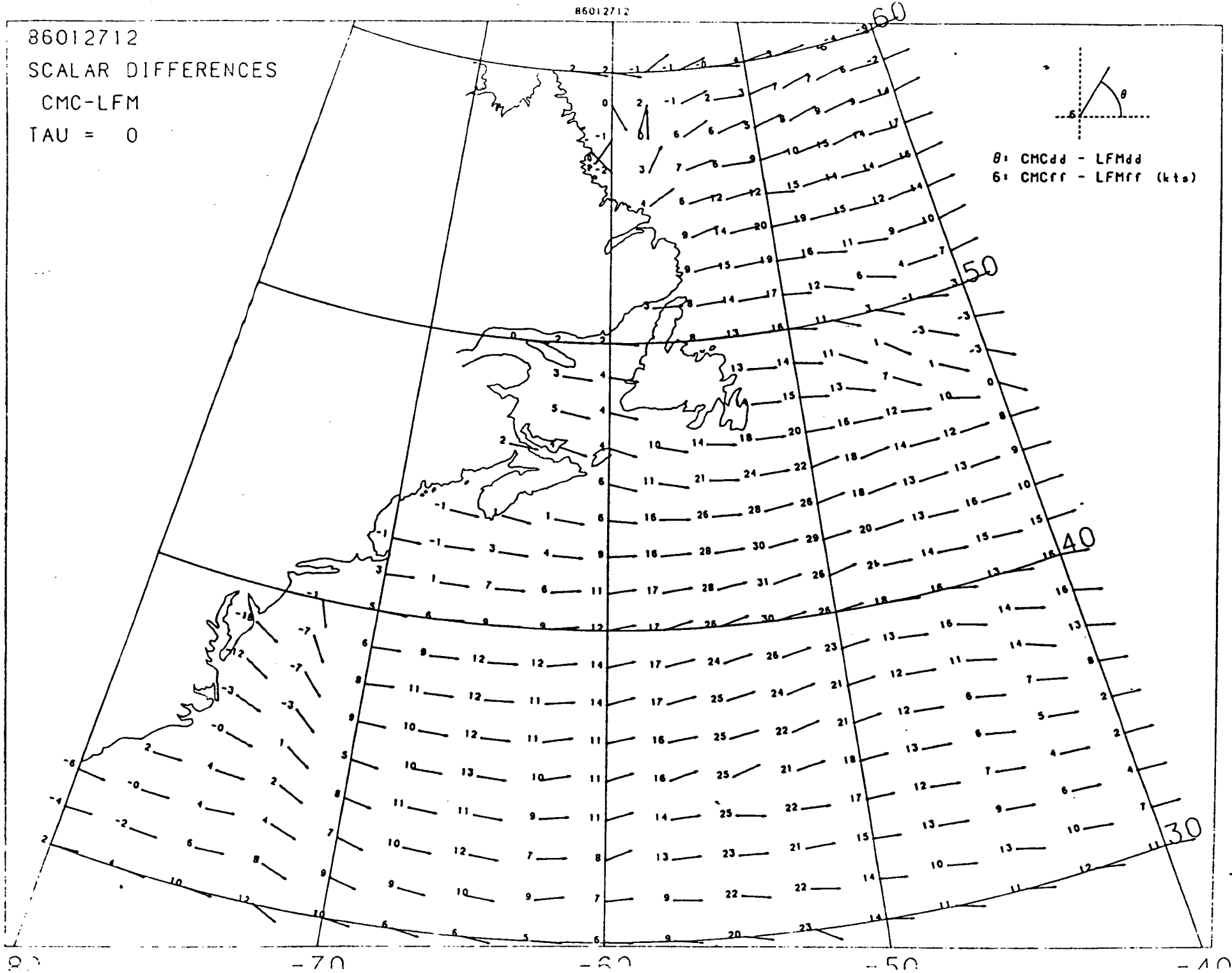
86012712
SCALAR DIFFERENCES
CMC-LFM
TAU = 0
θ: CMCdd - LFMdd
δ: CMCff - LFMff (kts)
60
50
40
30
-80
-70
-60
-50
-40

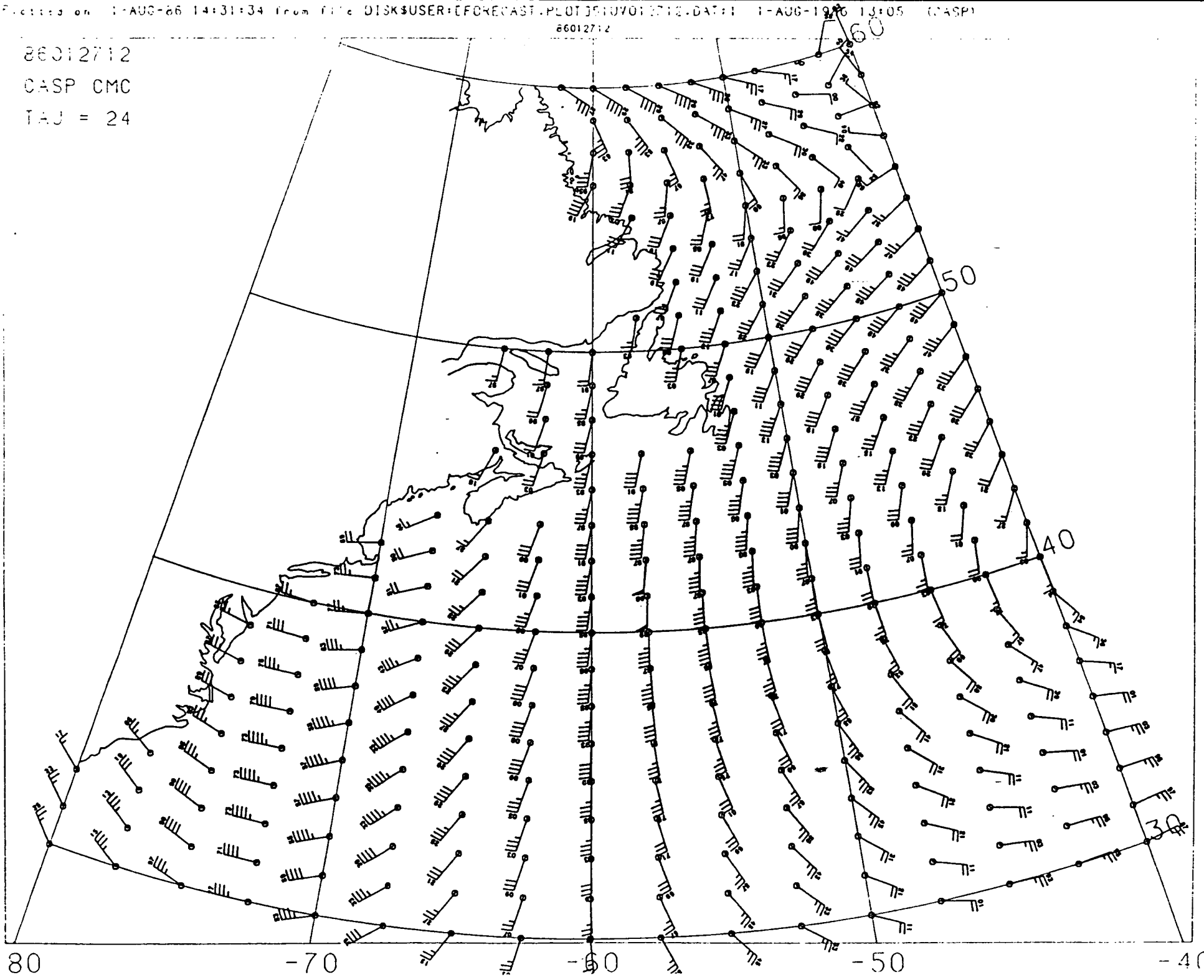
86012712
86012712
CASP CMC
TAU = 24
60
50
40
30
-80
-70
-60
-50
-40

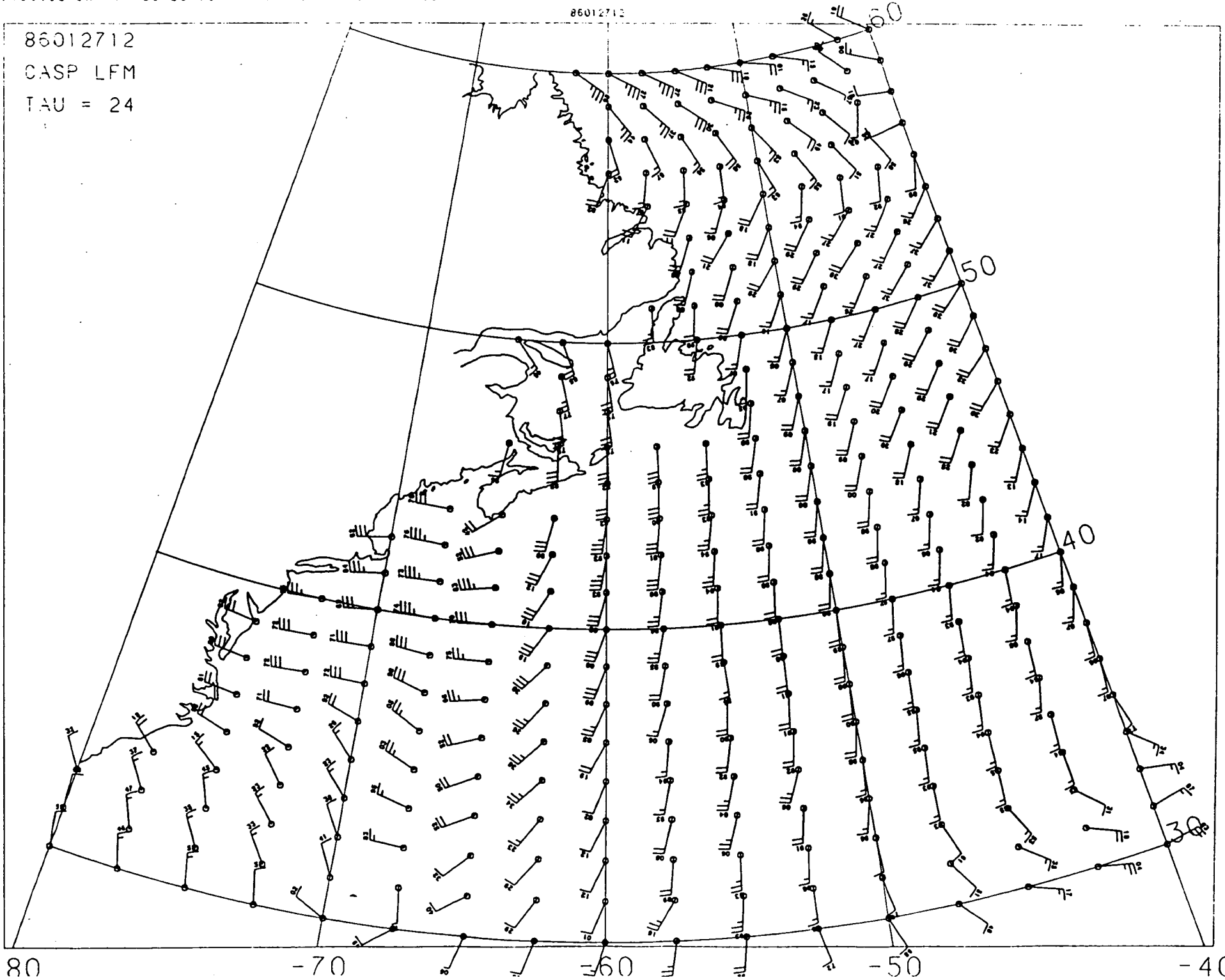
86012712
86012712
CASP LFM
TAU = 24
60
50
40
30
-80
-70
-60
-50
-40

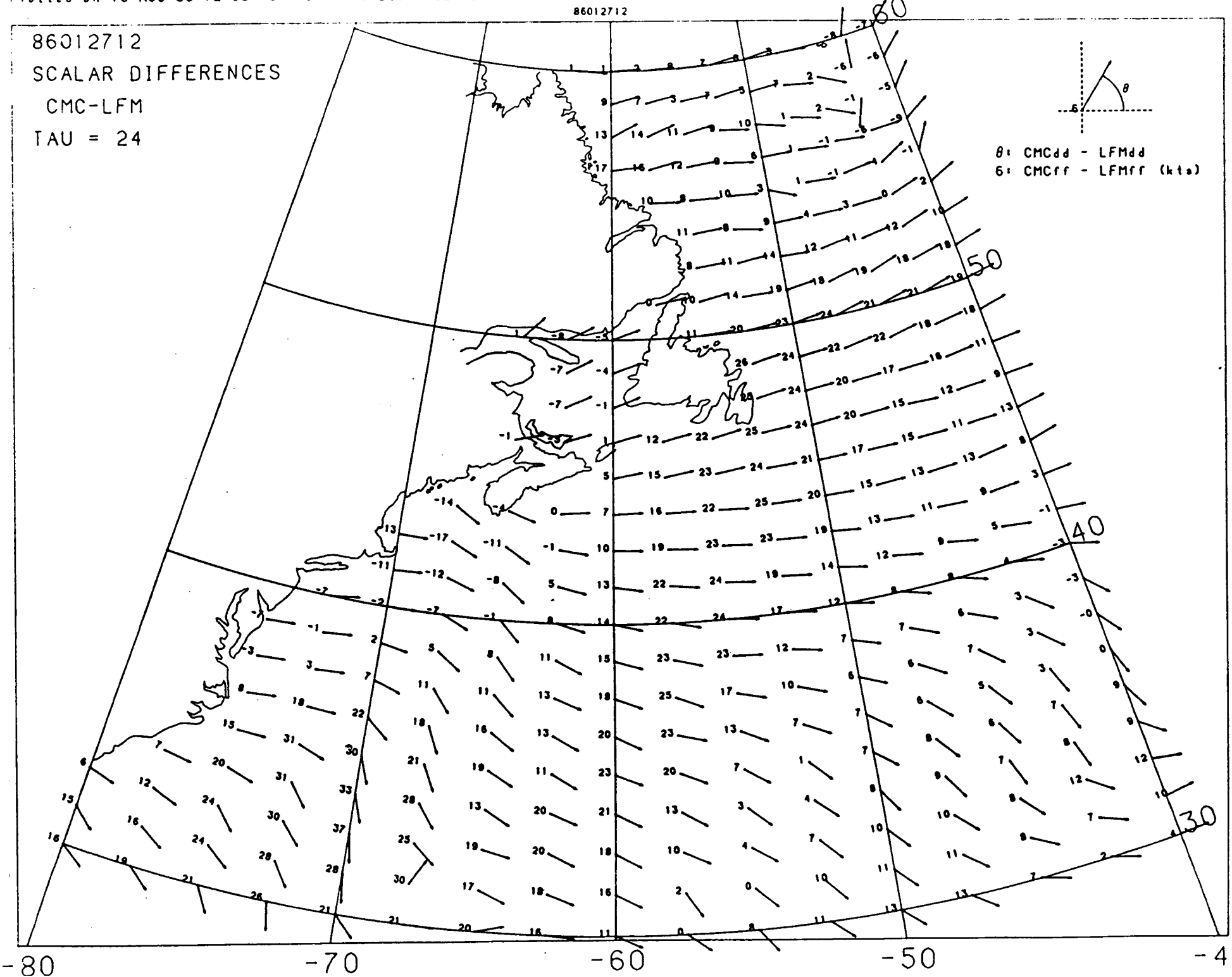
86012712
86012712
SCALAR DIFFERENCES
CMC-LFM
TAU = 24
θ: CMCdd - LFMdd
6: CMCff - LFMff (kts)
60
50
40
30
-80
-70
-60
-50
-40

STORM 3

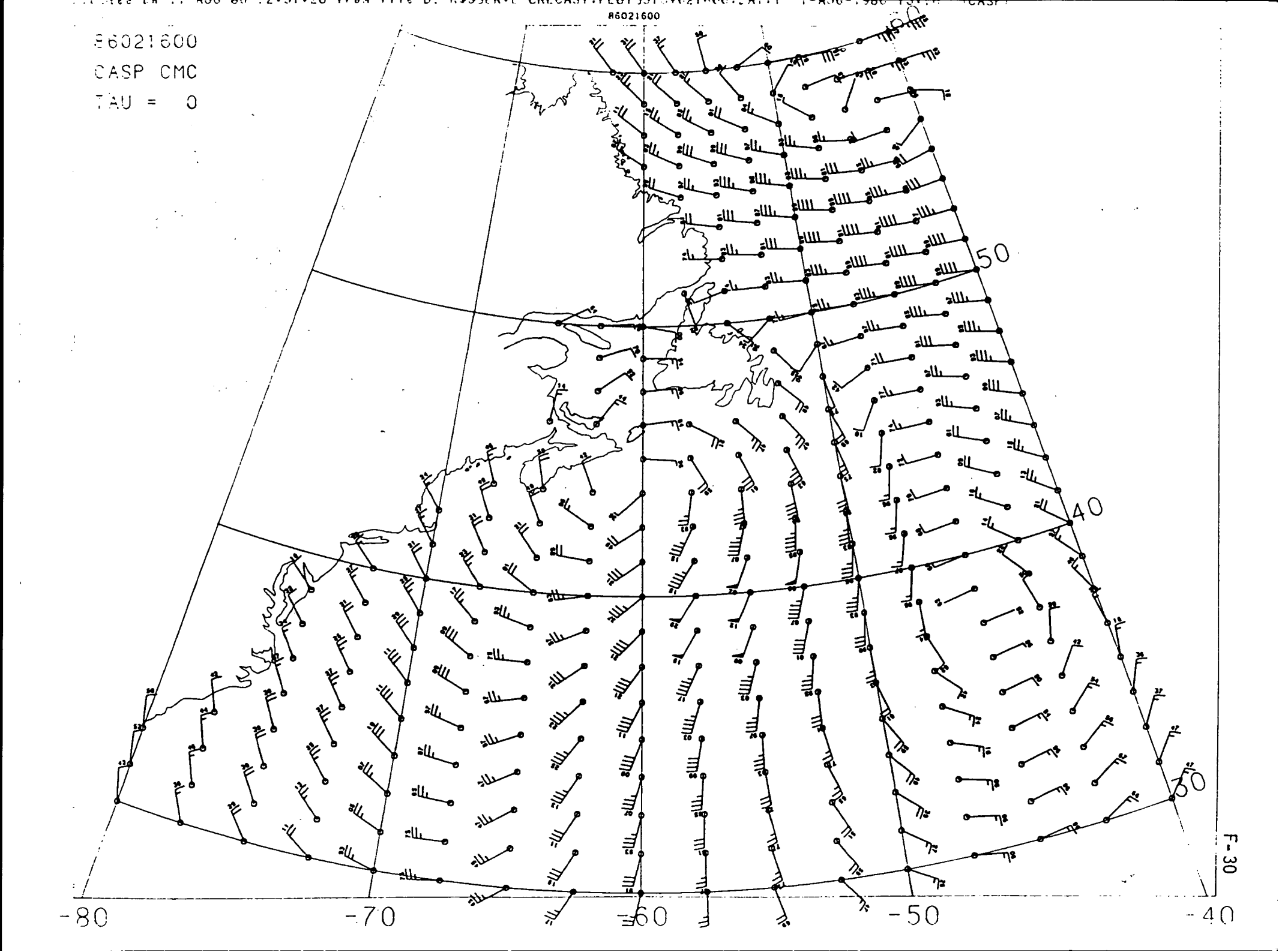
86021600
86021600
CASP CMC
TAU = 0
50
40
30
-80
-70
-60
-50
-40

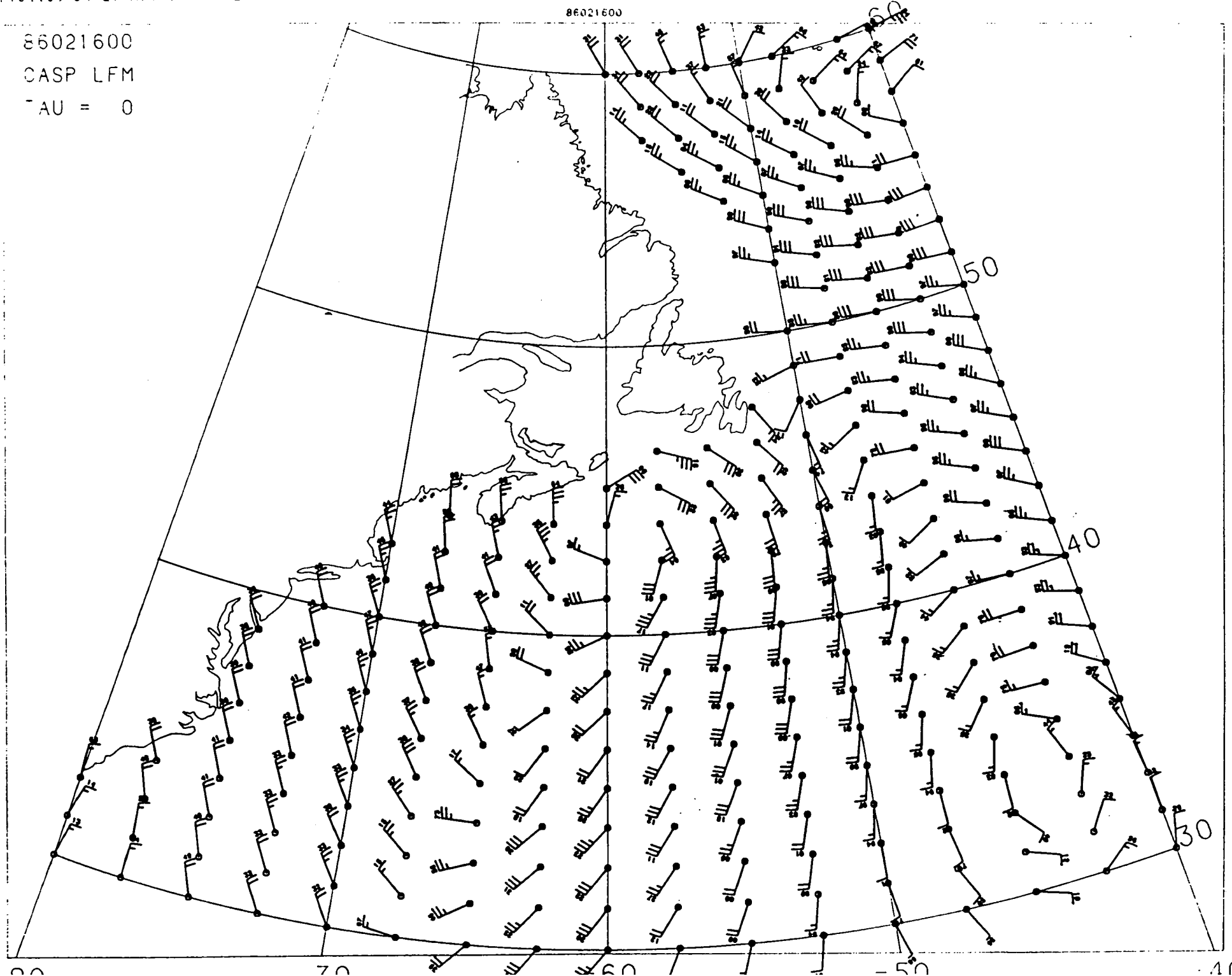
86021600
86021600
CASP LFM
TAU = 0
60
50
40
30
80
70
60
50
40

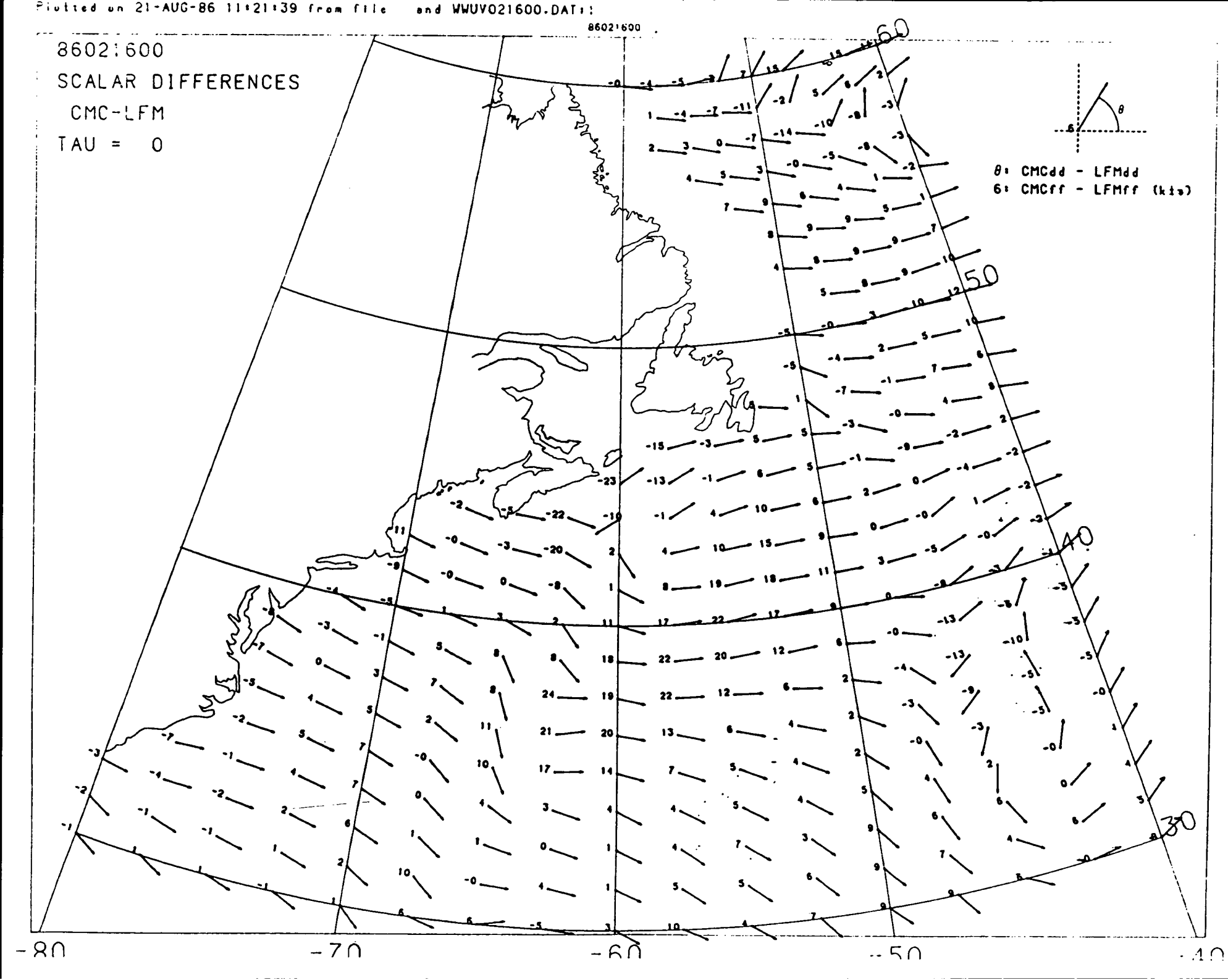
Plotted on 21-AUG-86 11:21:39 from file and WWUV021600.DAT;1
86021600
8602:600
SCALAR DIFFERENCES
CMC-LFM
TAU = 0
θ: CMCdd - LFMdd
δ: CMCff - LFMff (kts)
60
50
40
30
-80
-70
-60
-50
-40

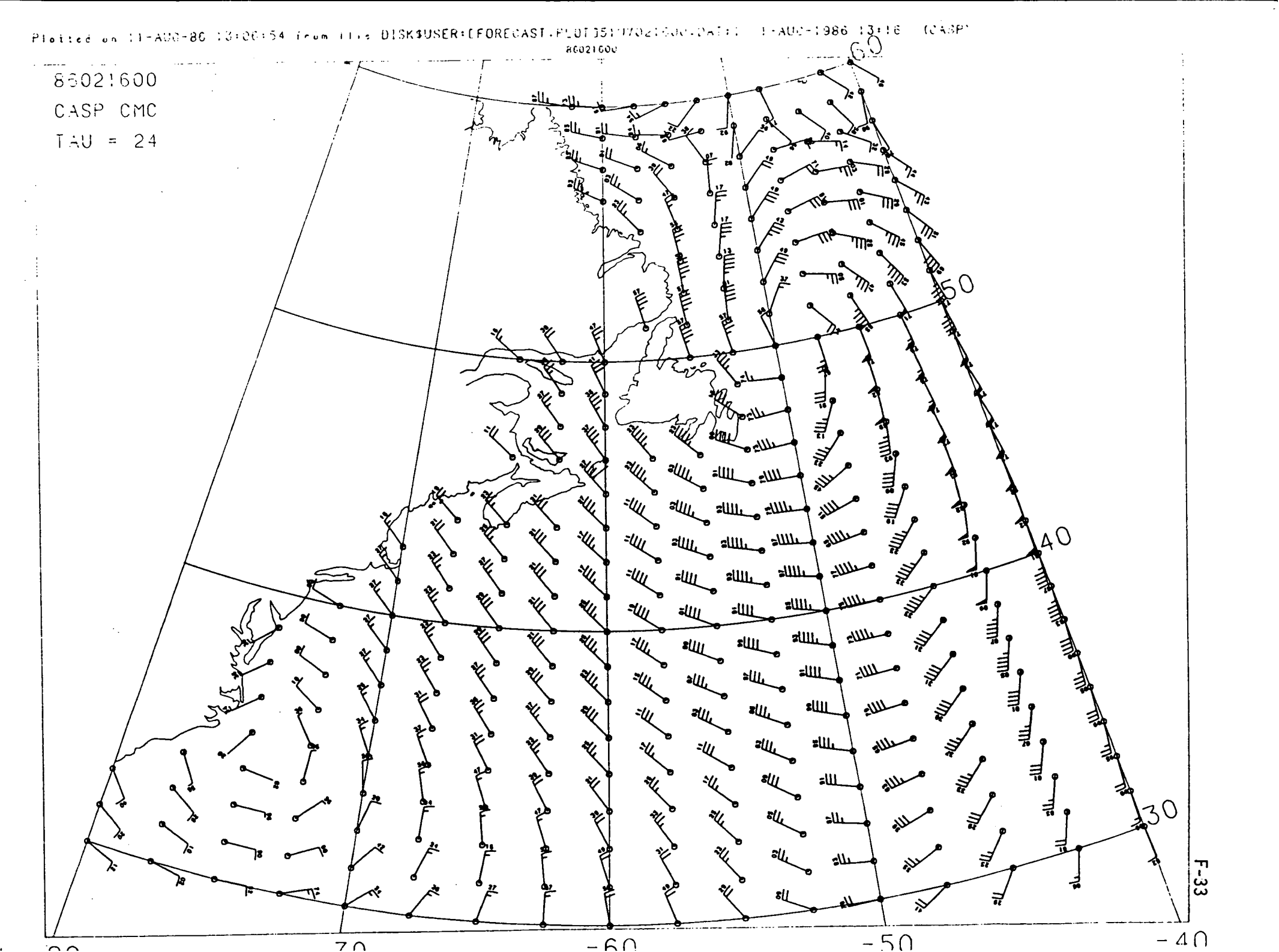
Plotted on 11-AUG-86 13:00:54 from the DISK$USER:[FORECAST.PLOT]S1170421600.DAT;1 11-AUG-1986 13:16 (CASP)
86021600
86021600
CASP CMC
TAU = 24
60
50
40
30
-70
-60
-50
-40

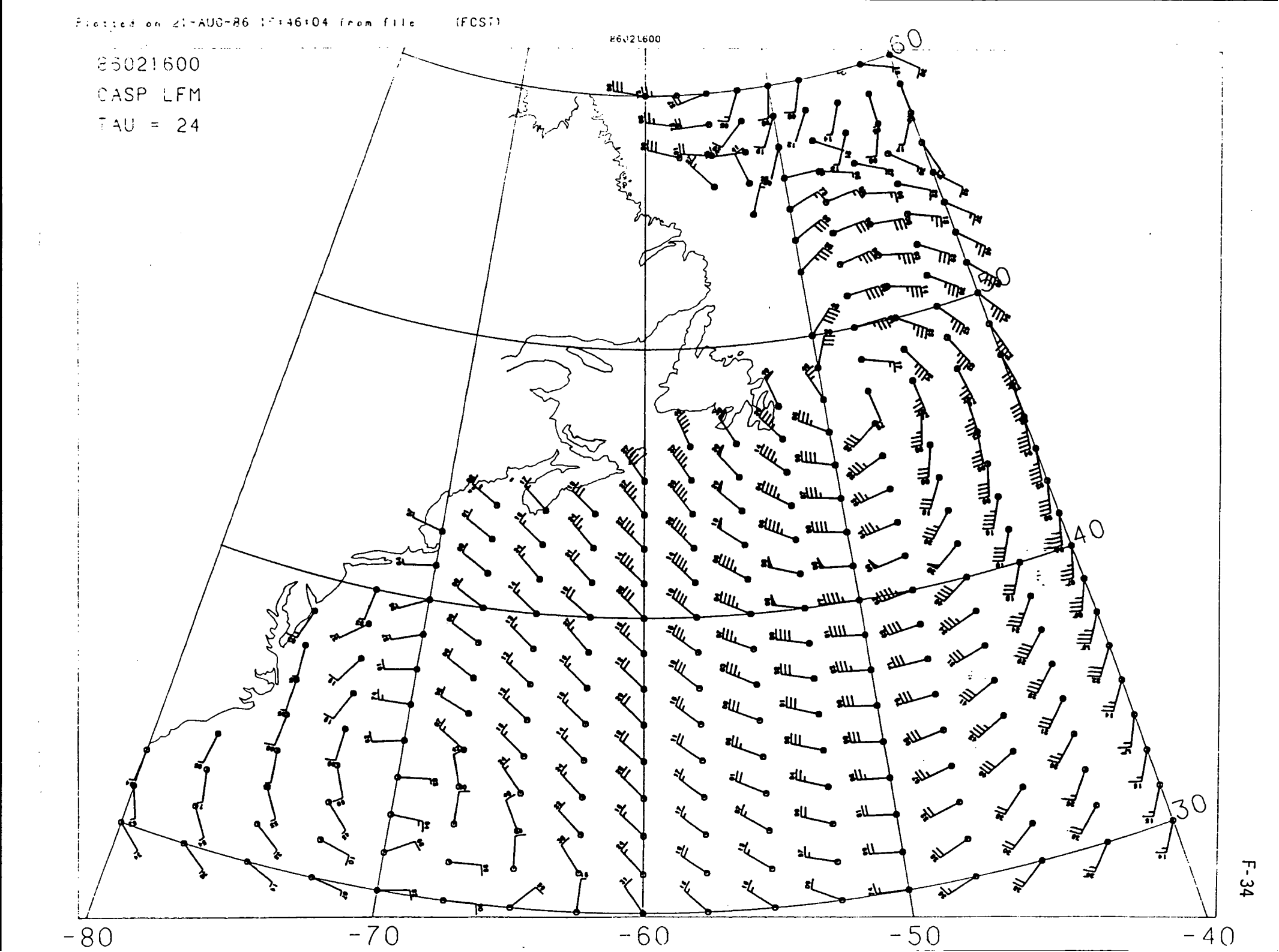
Plotted on 21-AUG-86 17:46:04 from file (FCST)
86021600
86021600
CASP LFM
TAU = 24
60
50
40
30
-80
-70
-60
-50
-40

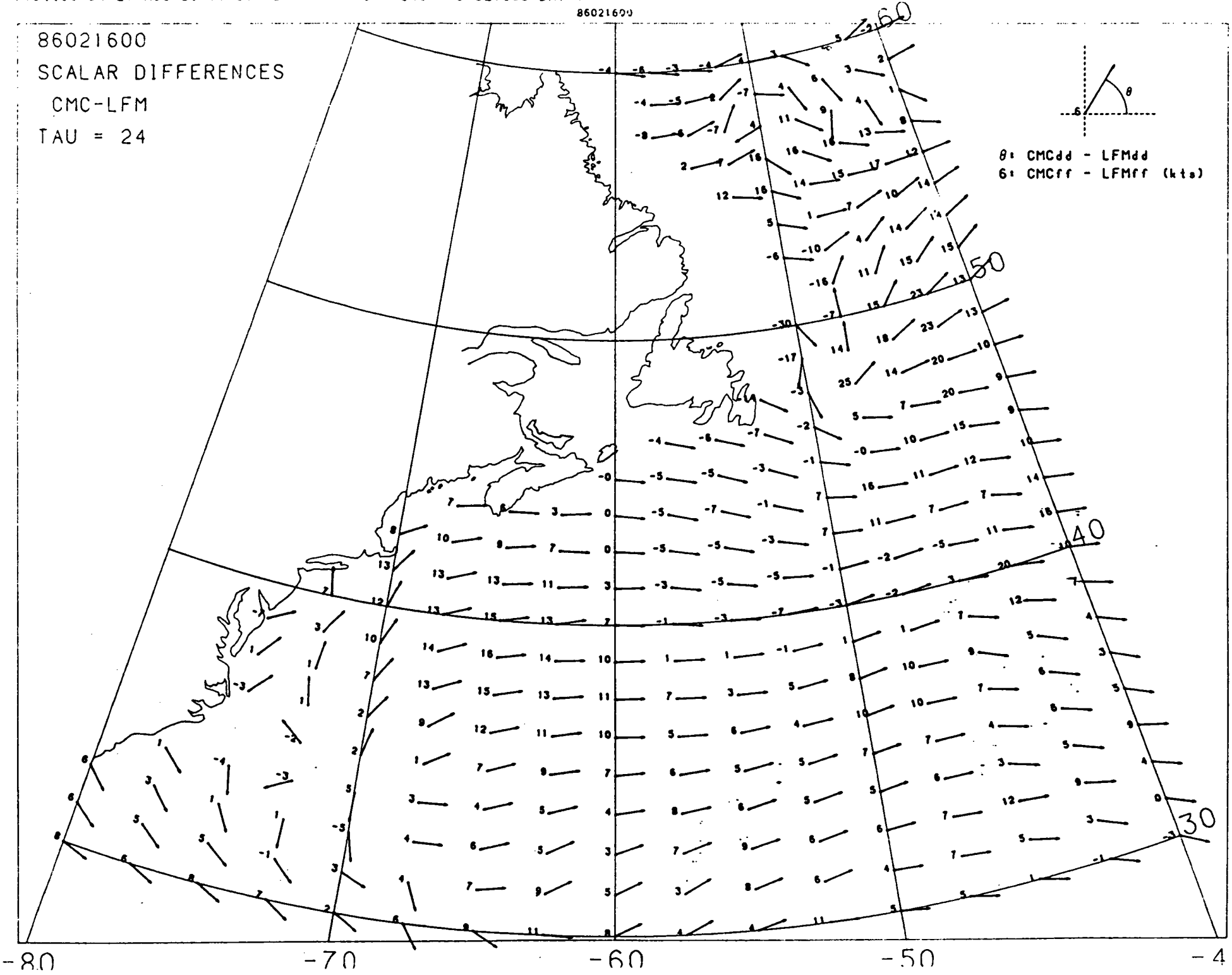
86021600
86021600
SCALAR DIFFERENCES
CMC-LFM
TAU = 24
θ: CMCdd - LFMdd
6: CMCff - LFMff (kts)
60
50
40
30
-80
-70
-60
-50
-40

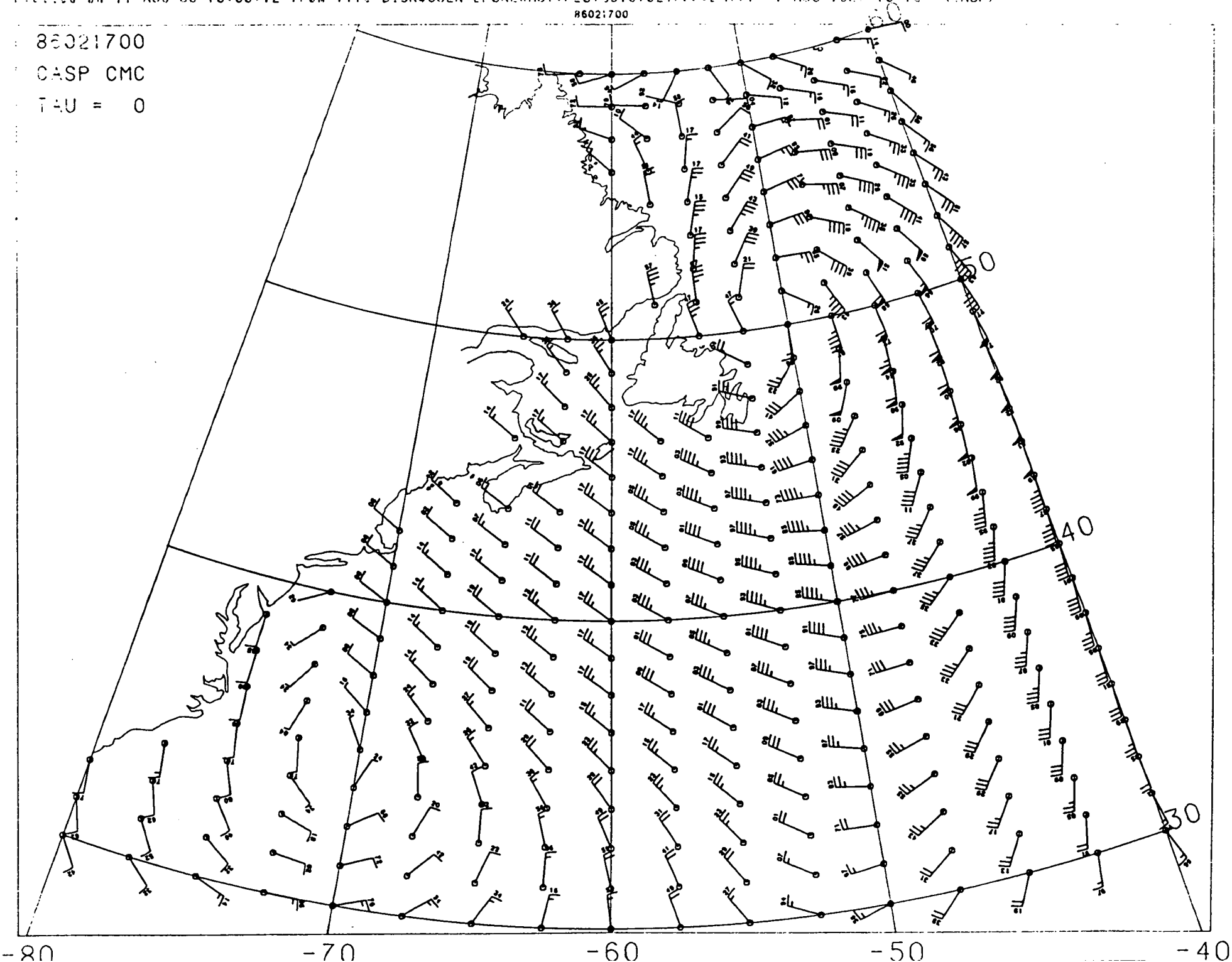
86021700
CASP CMC
TAU = 0
86021700
80
60
40
30
-80
-70
-60
-50
-40

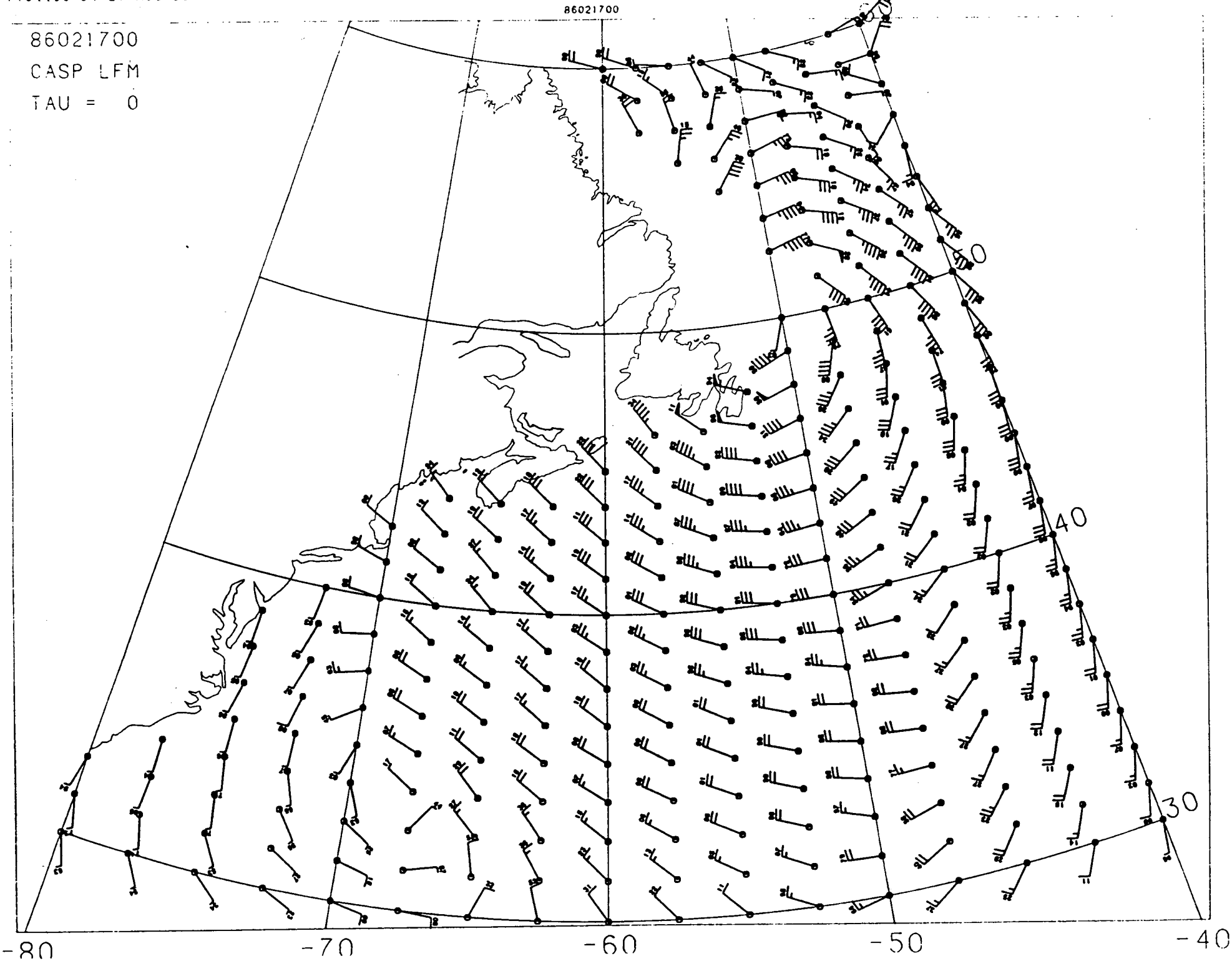
86021700
86021700
CASP LFM
TAU = 0
0
40
30
-80
-70
-60
-50
-40

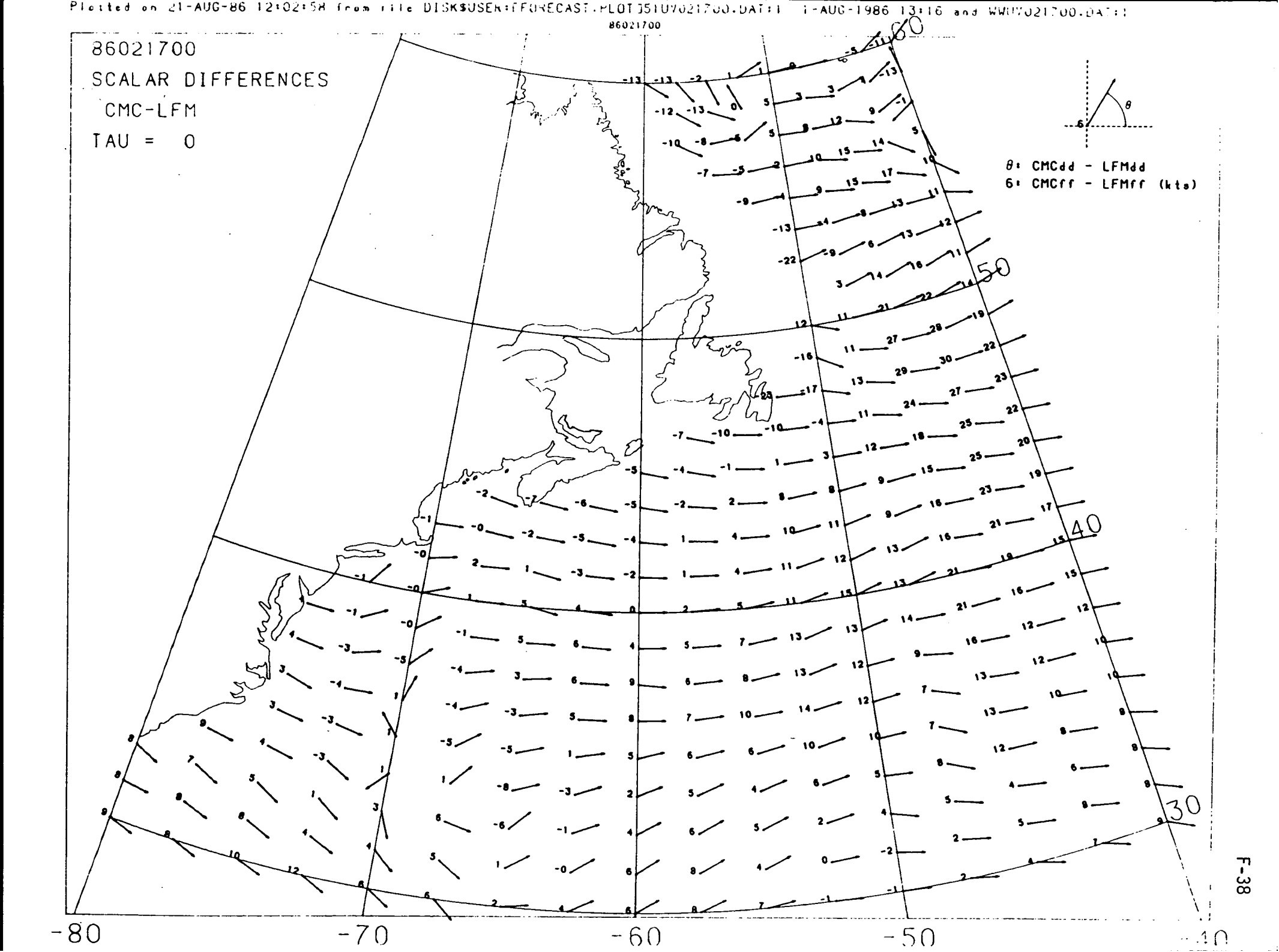
86021700
86021700
SCALAR DIFFERENCES
CMC-LFM
TAU = 0
θ: CMCdd - LFMdd
6: CMCff - LFMff (kts)
60
50
40
30
-80
-70
-60
-50
-40

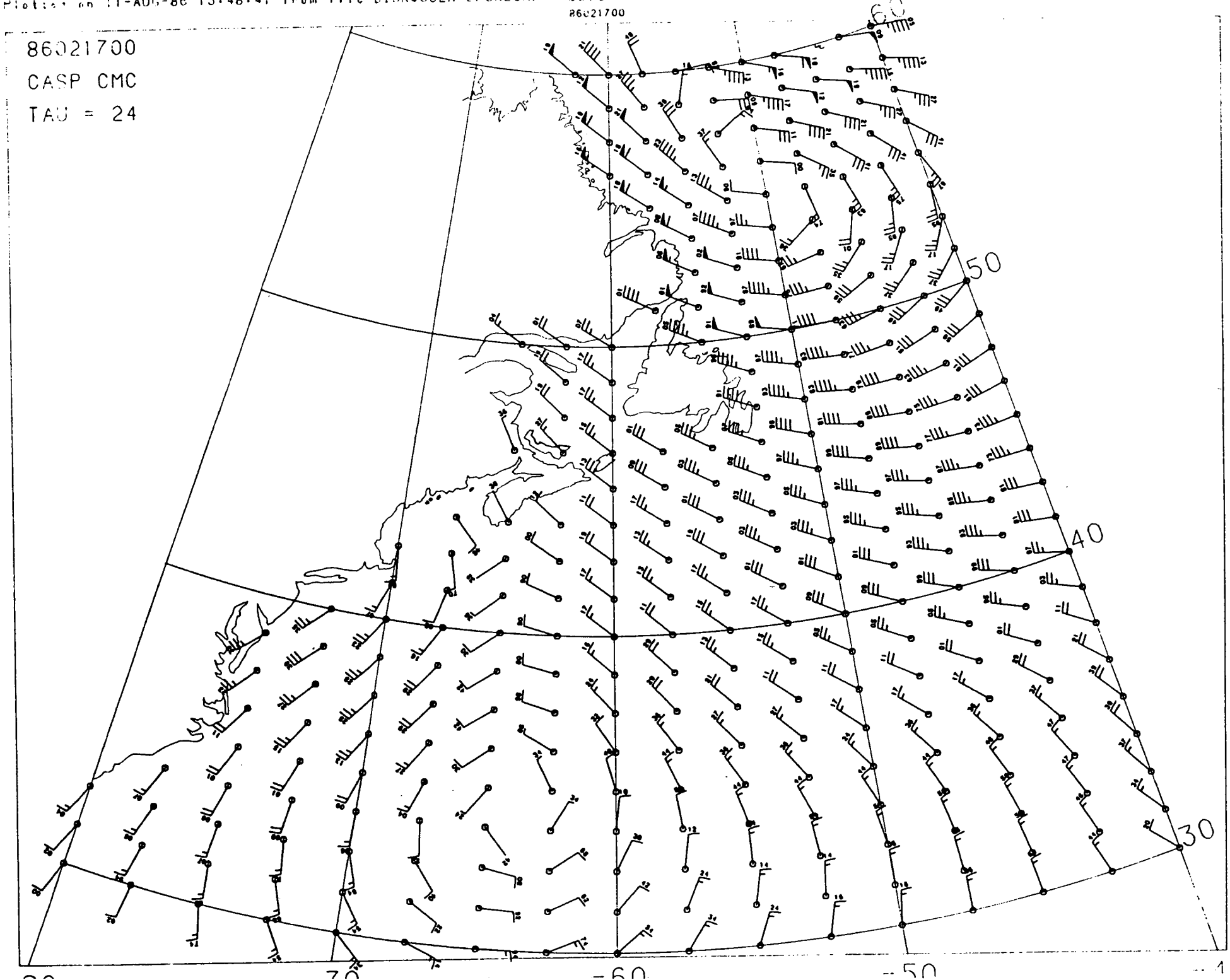
86021700
86021700
CASP CMC
TAU = 24
60
50
40
30
70
60
50
40

86021700

86021700

CASP LFM

TAU = 24

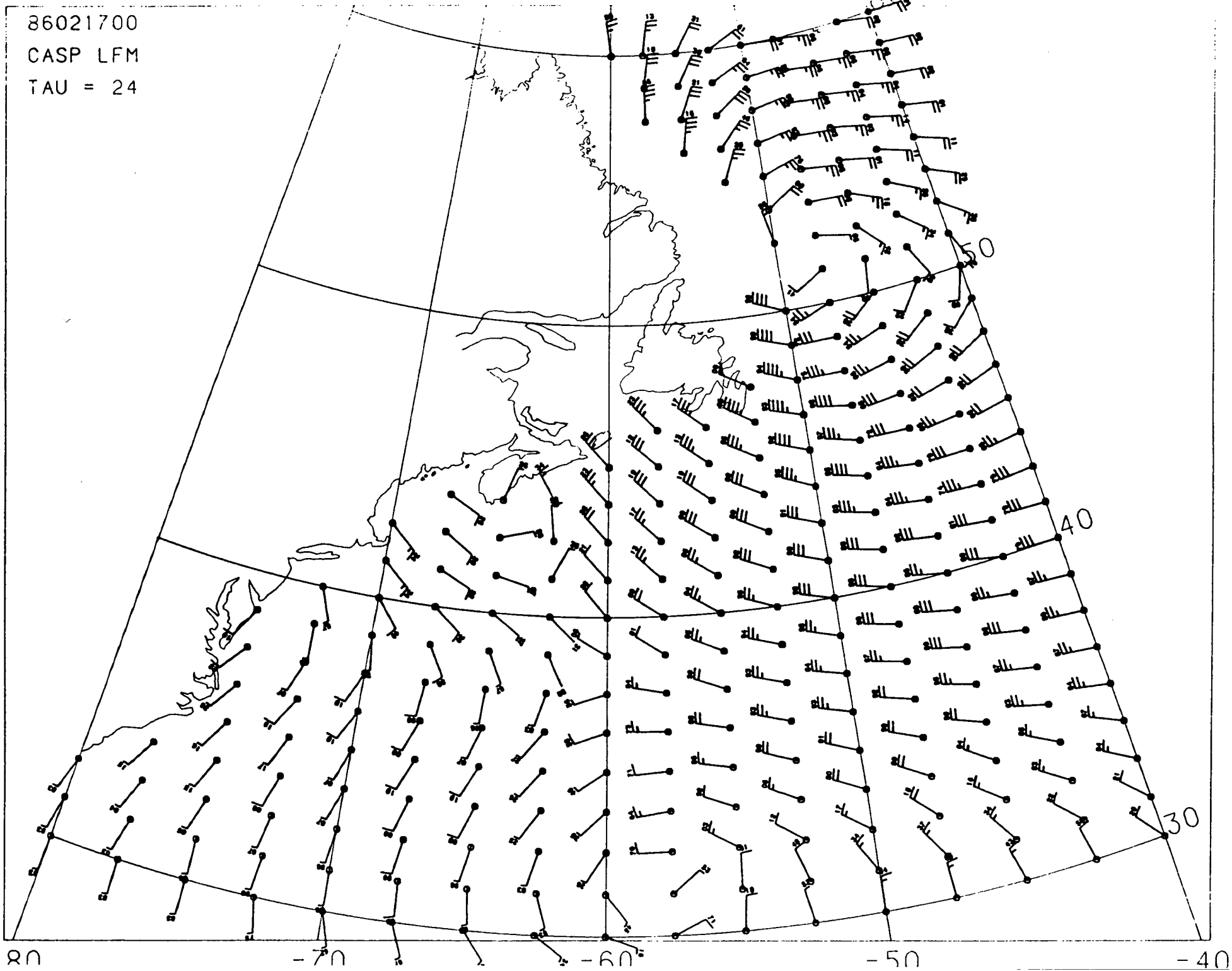

F-40

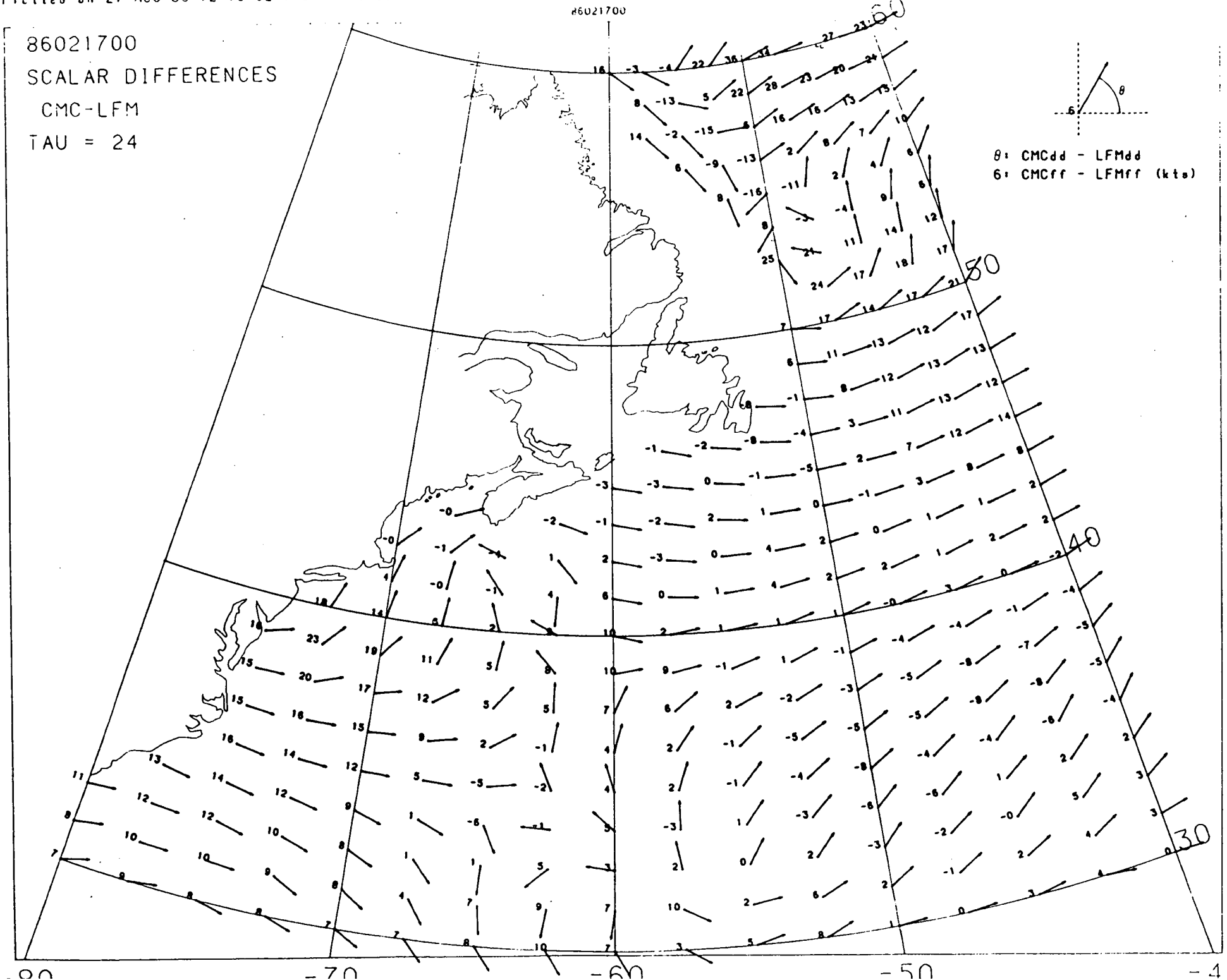
86021700
SCALAR DIFFERENCES
CMC-LFM
TAU = 24
θ: CMCdd - LFMdd
δ: CMCff - LFMff (kts)
60
50
40
30
-80
-70
-60
-50
-40

STORM 4

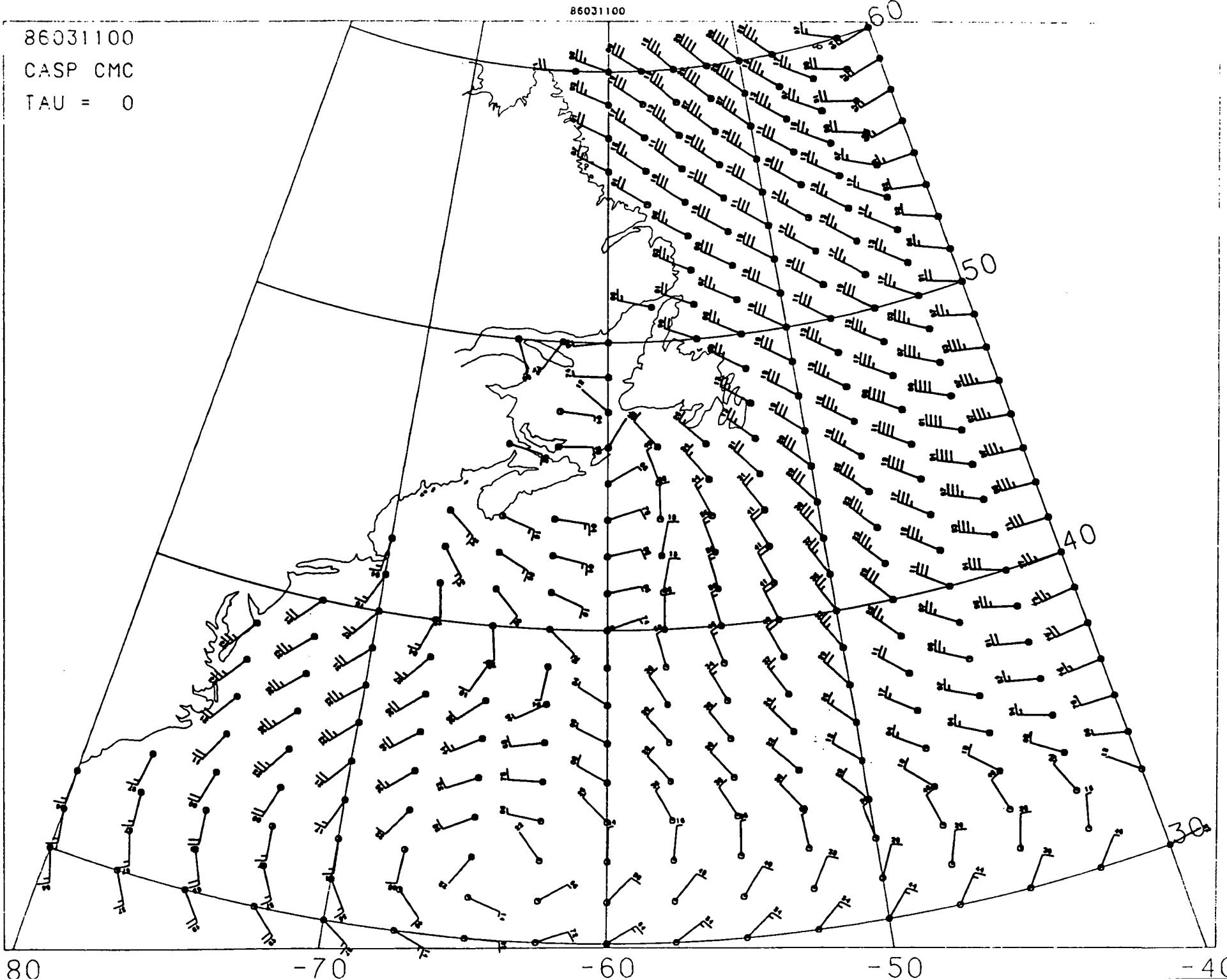
86031100
86031100
CASP CMC
TAU = 0
60
50
40
30
-80
-70
-60
-50
-40

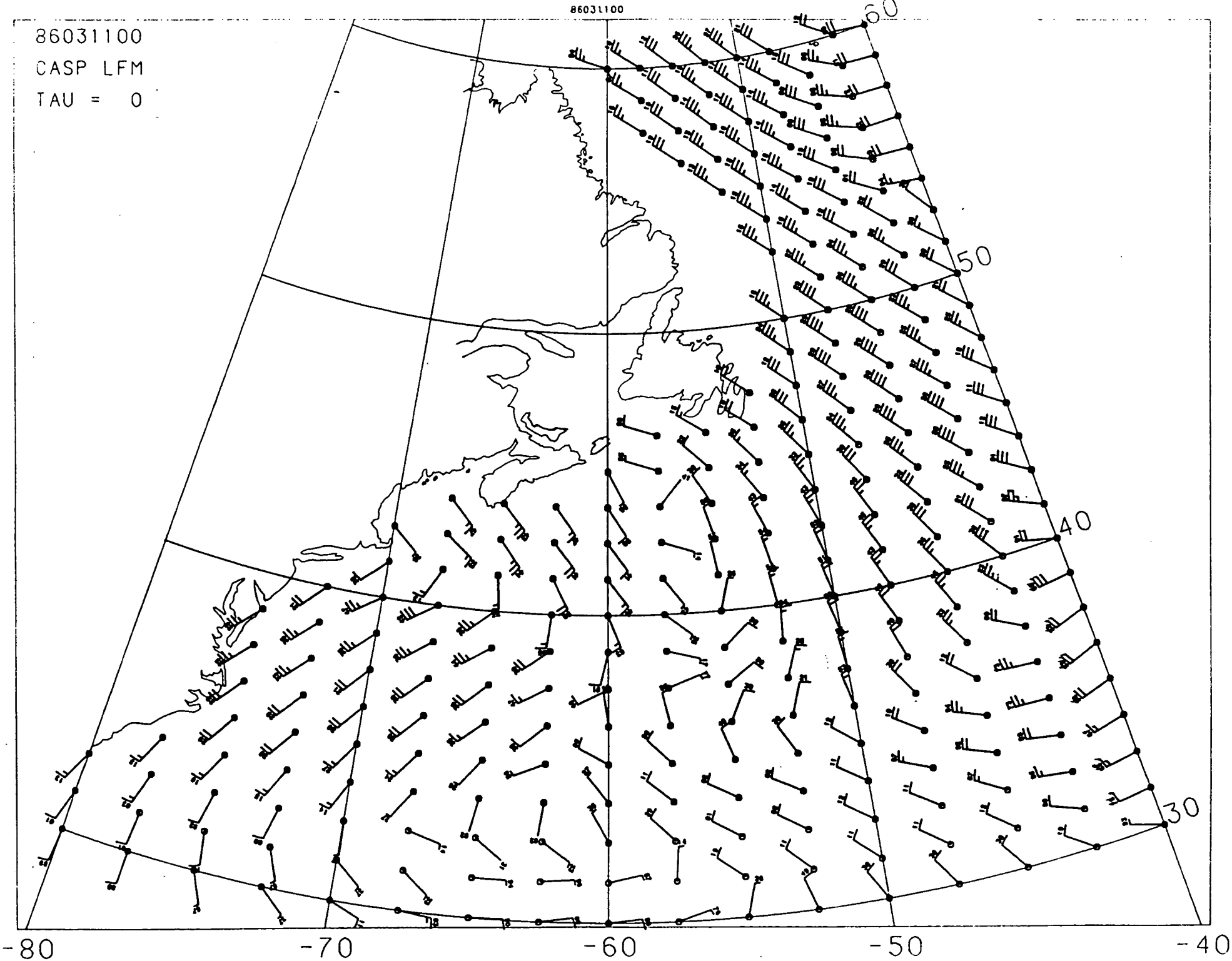
86031100
86031100
CASP LFM
TAU = 0
60
50
40
30
-80
-70
-60
-50
-40

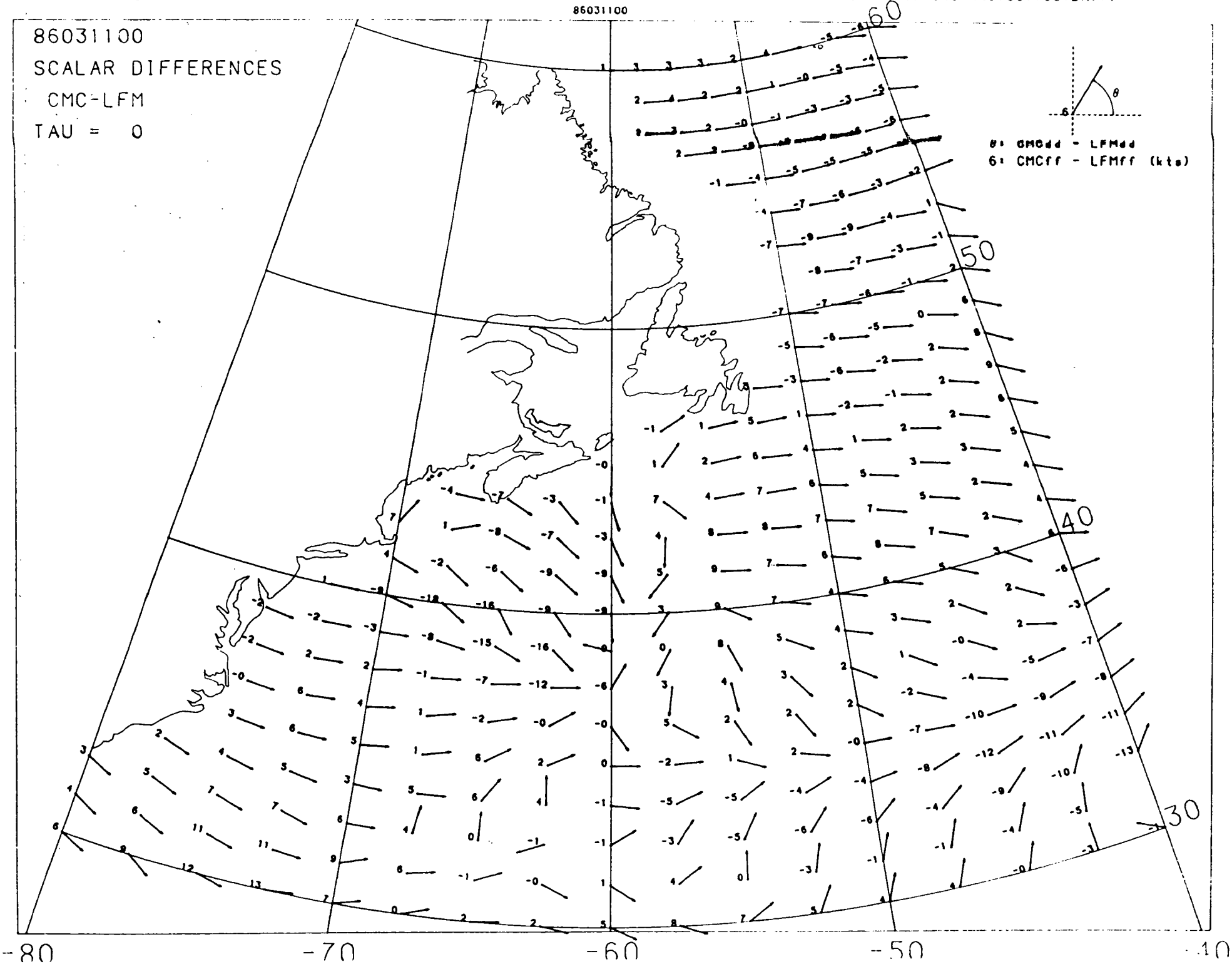
86031100
86031100
SCALAR DIFFERENCES
CMC-LFM
TAU = 0
θ: CMCdd - LFMdd
δ: CMCff - LFMff (kts)
60
50
40
30
-80
-70
-60
-50
-10

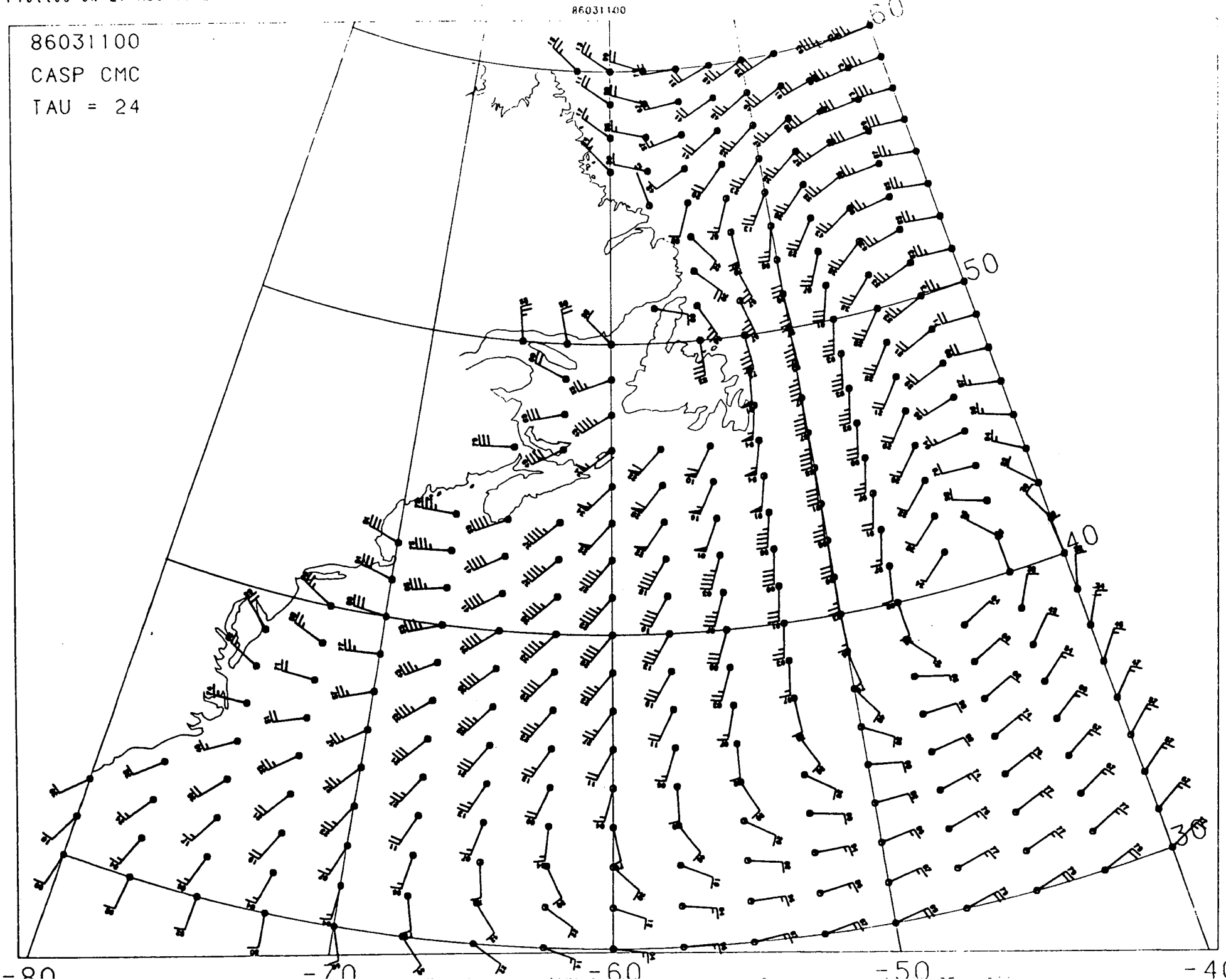
Plotted on 21-AUG-86 21:17:10 from file DISK$USER:[FORECAST.PLOTTING.DATA]
86031100
86031100
CASP CMC
TAU = 24
60
50
40
30
-80
-70
-60
-50
-40

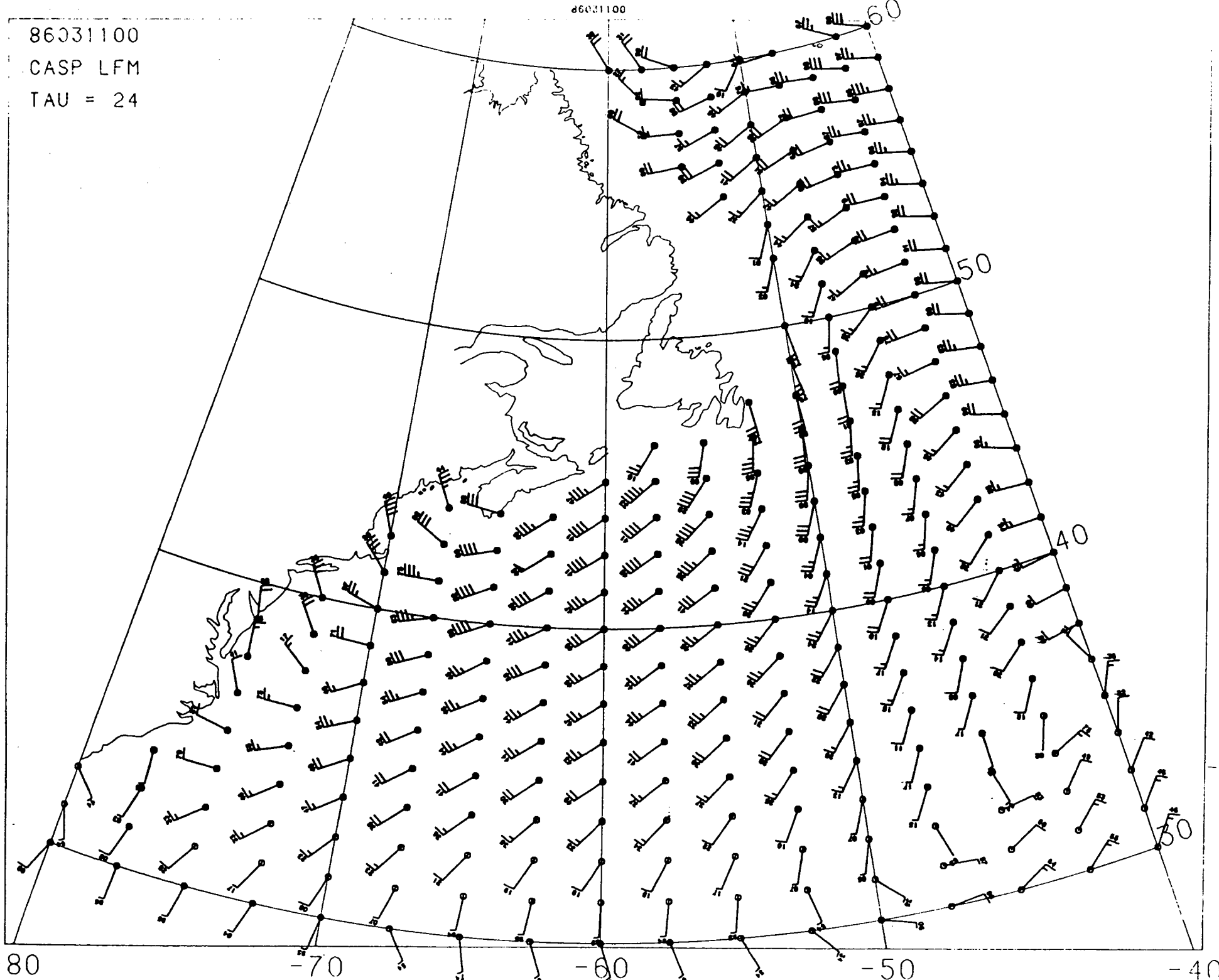
86031100
CASP LFM
TAU = 24
60
50
40
30
-80
-70
-60
-50
-40

86031100

86031100
SCALAR DIFFERENCES
CMC-LFM
TAU = 24

θ: CMCdd - LFMdd
6: CMCff - LFMff (kts)

60
50
40
30

-80 -70 -60 -50 -40